

Mechanistic Basis for Enhanced Oncolytic Potency by Mutations in Reovirus

Sigma1 and Mu2 proteins

by

Wan Kong Yip

A thesis submitted in partial fulfillment of the requirements for the degree of

Doctor of Philosophy

in

Virology

Department of Medical Microbiology and Immunology

University of Alberta

© Wan Kong Yip, 2020

ABSTRACT

Wild-type mammalian orthoreoviruses (reoviruses) are non-pathogenic viruses infecting hosts via the respiratory and enteric tracts. There are four prototype reovirus strains: the Type 1 Lang (T1L), Type 2 Jones (T2J), Type 3 Abney (T3A), Type 3 Daring (T3D) and Type 4 Ndelle (T4N). A proprietary variant of T3D has been developed as an oncolytic virotherapy under the brand name REOLYSIN® and is currently being evaluated in clinical trials. One major goal of our lab is to improve oncolytic potency of reovirus. We generated a number of reovirus variants by directed evolution that exhibited increased infectivity towards transformed cells while sparing normal cells. My thesis focused on variants that had mutations in the cell-attachment protein $\sigma 1$ and polymerase-cofactor $\mu 2$, with the overarching goal to understand how these mutations promote replication of reovirus in tumor cells.

Our lab previously showed that reduction of $\sigma 1$ levels leads to faster uncoating and it is one of the main mechanisms that augments reovirus infectivity towards transformed cells. In chapter 3 of this thesis, we characterize 6 variants with big-plaque phenotype and provide evidence that all variants have reduced levels of $\sigma 1$. Previous studies showed that the middle region of the $\sigma 1$ tail was important for virion encapsidation. I used truncations and single amino acid mutants to investigate how other regions in the $\sigma 1$ tail mediated virion association. Immunoprecipitations of transfected $\sigma 1$ showed that residues 22 and 66, as well as residues near the C-terminus of the $\sigma 1$ tail were important for virion association. Unexpectedly, data from mutant viruses showed that residues 252-286 may inhibit virion encapsidation by a mechanism yet to be identified. Our data revealed that residues 154-251 in the $\sigma 1$ tail mediate viral factory accumulation and virion association.

All documented variants to date have enhanced oncolytic potency in the binding or uncoating (entry) steps. The second goal of this thesis was to identify novel mechanisms that increased reovirus replication in transformed cells at post-entry steps. Chapter 4 describes 5 variants with mutations in different genes. One variant, named T3v10^{M1}, had a single amino acid change in the μ 2 protein. The μ 2 is a polymerase co-factor and is known to interact with reovirus non-structural protein μ NS and cellular microtubules. Data in chapter 5 demonstrates that the altered μ 2 had both infection-hindering and –promoting effects, with an overall net benefit of promoting replication in cancer cells. T3v10^{M1} bound host-cell and uncoated at similar rates relative to wild-type virus (T3wt), but *in vitro* phosphate release and RT-qPCR assays showed that T3v10^{M1} μ 2 was less efficient at hydrolyzing ribonucleotide triphosphates (rNTP) and RNA synthesis. As a consequence, T3v10^{M1} exhibited impaired ability to establish infection by 75% compared to T3wt. However, when L929 cells were exposed to equal cell-bound T3v10^{M1}, the mutant accumulated up to 4-fold more viral proteins and 3-fold more viral RNAs. Data from immunoprecipitation and far-Western blot approaches indicated that T3v10^{M1} μ 2 associated with μ NS and other viral proteins 2-fold more efficiently than T3wt μ 2, which directly enhanced progeny production by 2-fold in one replication cycle. This represents the first example of oncolytic enhancement via a post-entry mechanism. In conclusion, our findings provide insights into the mechanistic basis for enhanced oncolytic potency by mutations in reovirus σ 1 and μ 2 proteins.

PREFACE

Chapter 3 of this thesis is in preparation for publication as W.K. Yip, H. Eaton, F. Cristi and M. Shmulevitz, “Investigation of $\sigma 1$ domains and their effects on virion association and reovirus replication”. I was responsible for designing and conducting experiments, data collection and analyses, as well as manuscript composition. H. E. Eaton was responsible for transfection of cells and generating reovirus variants by reverse genetics system and manuscript editing. F. Cristi was responsible for generating mutants with single mutation and manuscript editing. X.L. Pang generously provided us reoviruses collected from the effluent. M. Shmulevitz was the supervisory author and was involved with performing experiments to characterize $\sigma 1$ levels, concept formation and manuscript editing.

Chapters 4 and 5 of this thesis are in preparation for publication as W.K. Yip, G. Trifonov, N. Narayan and M. Shmulevitz, “A reovirus $\mu 2$ C-terminal loop inversely regulates NTPase and transcription functions versus binding to factory-forming μ NS and promotes replication in tumorigenic cells”. I was responsible for the conception formation, designing and conducting experiments, data collection and analyses, as well as manuscript composition. G. Trifonov was responsible for performing the Western blots to compare reovirus variant uncoating, reassortment of T3wt and T3v10, as well as confirming the genotype of the resulting reassortants. N. Narayan was responsible for sequencing T3v6, T3v10, T3v11, T3v12 and T3v13. M. Shmulevitz was the supervisory author and was involved with concept formation and manuscript editing.

ACKNOWLEDGMENTS

First and foremost, I would like to thank my supervisor, Dr. Maya Shmulevitz, who took me to her lab 6 years ago when I had absolutely no idea what a virus was. During my time in her lab, she was always there to help and provided advice anytime I needed it. She has been a great mentor and always willing to help and encourage me to develop my professional, academic and critical thinking skills. Maya was always passionate about science and came to the lab with a positive attitude which was very encouraging when we were frustrated (P.S. the candies in her office also had a huge mood-boosting effect).

I would like to thank my supervisory committee, Dr. Debby Burshtyn and Dr. Bart Hazes for their ongoing advice and support during my studies. I would also like to thank Dr. Kevin Coombs for being my external examiner and Dr. Kathy Magor for being my internal examiner for my thesis defense. Throughout my time at the MMI department, I received so much help and support from the academic and administrative staffs within the department. I would like to especially thank Dr. Edan Foley, Dr. Troy Baldwin, Dr. Matthias Gotte, Vasquez Tabitha, Debbie Doudiet, Melissa Northmore and Anne Giles.

I would like to express my gratitude to Dr. Bart Hazes, who helped me a lot in creating the 3D model of $\mu 2$ using the Aquareovirus homolog VP5, as well as helping me to interpret results from bioinformatics analysis of this thesis. I would also like to thank Dr. Egor Tchesnokov and Brendan Todd for their valuable advice in interpreting the data of the rNTP hydrolysis assay.

During the past few years, all the members of the Shmulevitz lab were the best people I have ever met in my life. Adil was always helpful and willing to provide technical support. Ben was a very knowledgeable bacteriologist and told me great stories about *Vibrio cholerae*. Fran is my best amigo in the lab and taught me a lot of useful words in Spanish – so I may be able to talk to Messi one day. Ashley is always funny and ... hilarious at times. Heather (and the former lab tech Laura) are helpful in providing advice for experiments and ordering reagents. I also enjoyed spending time with former graduate student Kevin, we had a lot of fun in classes and soccer games. All the undergraduate project students, summer students were so great and helpful in the lab (especially Jason – who's also a huge Barcelona fan, and Tamara, my favorite student). The joint lab meetings with members from the lab of Dr. David Evans, Dr. Mary Hitt and Dr. Ronald Moore were always productive and I received a lot of insightful suggestions for my project. I would also thank members from the lab of Dr. Debby Burshtyn, Dr. David Marchant and Dr. Robert Ingham for their generosity to share reagents.

Last but not least, I would thank my family Ping Ling, Yam Yin and Ying for their unconditional emotional and financial support throughout my degree.

TABLE OF CONTENTS

ABSTRACT	ii
PREFACE.....	iv
ACKNOWLEDGMENTS.....	v
TABLE OF CONTENTS	vi
LIST OF TABLES	xii
LIST OF FIGURES	xiv
LIST OF ABBREVIATIONS	xx
CHAPTER 1: INTRODUCTION	1
1.1 Overview of cancer and oncolytic reovirus.....	1
1.1.1 Classification of reovirus	1
1.1.2 Reovirus and pathogenesis.....	3
1.1.3 Composition of reovirus genome and virion structure.....	6
1.2 Replication of T3D reovirus.....	7
1.2.1 Binding to host cells	7
1.2.2 Uncoating of reovirus	9
1.2.3 Transcription of genome	11
1.2.4 Viral progeny production and assembly	12
1.2.5 Release of reovirus.....	14
1.3 Reovirus as an oncolytic virus	16
1.3.1 Discovery of oncolytic viruses.....	16
1.3.2 Oncolytic viruses in clinical trials	17
1.3.3 Reovirus (REOLYSIN®) in clinical trials.....	18
1.3.4 Mechanisms of reovirus replication in tumor cells	20
1.4 Improving oncolytic potency of reovirus	21
1.4.1 Reovirus variants with enhanced replication in cancer cells	21

1.4.2 Reduction of $\sigma 1$ is the main mechanism for enhanced oncolytic potency of reovirus variants T3v1 and T3v2	22
1.5 Structure and functions of $\sigma 1$ protein	23
1.5.1 The N-terminal regions of $\sigma 1$ are responsible for virion anchoring and trimerization	23
1.5.2 The middle regions of the tail are important for virion association and sialic acid (SA) binding	27
1.5.3 The neck region of $\sigma 1$ is susceptible to proteolytic cleavage and the globular head mediates JAM-A binding	28
1.6 A reovirus variant has a $\mu 2$ mutation that confers replicative advantage in post-uncoating step	30
1.6.1 Mu2 may participate in genome transcription	30
1.6.2 Mu2 plays crucial roles in viral factory formation.....	33
1.6.3 Mu2 mediates cellular responses	34
1.7 Objectives of this thesis.....	36
1.7.1 Chapter 3: Characterizing domains of $\sigma 1$ involved in sigma 1- virion association ...	36
1.7.2 Chapter 4: Identifying novel mechanism that enhanced reovirus oncolytic potency	37
1.7.3 Chapter 5: Investigating how reovirus $\mu 2$ C-terminal loop regulated viral growth..	38
CHAPTER 2: METHODS AND MATERIALS	49
2.1 Cell lines and culturing conditions.....	49
2.2 Virus	51
2.2.1 Stock.....	51
2.2.2 Production and purification.....	52
2.2.3 Viral infection and plaque assay	54
2.3 Infectivity assays	55
2.3.1 Cell-based enzyme-linked immunosorbent assay (ELISA)	55
2.3.2 Immunocytochemistry	56
2.3.3 Immunofluorescence.....	56
2.4 Flow cytometry	57
2.4.1 Annexin V staining assay	58

2.5 Virus release assay	59
2.6 Binding assays	60
2.7 Coomassie Blue staining	60
2.8 Agarose gel analysis of whole reovirus.....	61
2.9 Viral core generation and rNTP hydrolysis assays	61
2.10 <i>In vitro</i> reovirus core transcription assay and in cell transcription assay	62
2.10.1 RNA extraction and detection.....	62
2.10.2 In cell transcription assay	63
2.11 Cell lysate collection and Western blot analysis	64
2.11.1 Analysis of σ 1 multimers by Western blot (Chapter 3).....	65
2.12 Far-Western blot analysis	66
2.13 Transfections and immunoprecipitations	67
2.13.1 Transfection of truncated or mutated σ 1 plasmids (Chapter 3).....	67
2.13.2 Transfection of μ 2 or μ NS (Chapter 5)	69
2.14 Plasmid and mutant constructions.....	71
2.14.1 Constructions of truncated or mutated σ 1 plasmids and mutants	71
2.14.2 Constructions of FLAG-tagged μ 2 and μ NS plasmids.....	72
2.15 Comparing dsRNA segments by SDS-PAGE	74
2.16 Collect cytoplasmic- and viral factory-associated protein	74
2.17 Growth curve	75
CHAPTER 3: INVESTIGATION OF σ1 TAIL REGIONS AND THEIR EFFECTS ON VIRION	
ASSOCIATION	84
3.1. Introduction and chapter objective.....	84
3.2 Results	85
3.2.1 Reovirus variants generated by directed evolution form larger plaques than wild-type virus on tumorigenic cells.....	85
3.2.2 Reovirus variants with enhanced replication in transformed cells have different gene mutations that ultimately lead to the reduction of σ1.....	85
3.2.3 Mutations in σ1 variants do not affect trimerization of σ1	88
3.2.4 Sigma 1 proteins with different lengths do not aggregate or form heterotrimer	91

3.2.5 σ 1 residues 155-235 are important for viral factory localization	94
3.2.6 Sigma 1 constructs with mutated amino acids 28 or 66 were able to form trimers	96
3.2.7 The length of σ 1 tail and residue 28 or 66 are important for virion association.....	99
3.2.8 Mutants generated by reverse genetics (RG) system with σ 1 truncated residues 155-251 and the L28P or S66I mutation have reduced σ 1 levels.....	100
3.3 Summary.....	102
CHAPTER 4: IDENTIFYING A NOVEL MECHANISM TO IMPROVE ONCOLYTIC REOVIRUS	124
4.1 Introduction	124
4.1.1 Chapter objective.....	124
4.1.2 Introduction to five reovirus variants that were selected for characterization in this chapter.....	124
4.2 Results	130
4.2.1 All 5 variants form bigger plaques on L929 and PanC cells relative to T3wt.....	130
4.2.2 Variants T3v11 and T3v12 had reduced levels of σ 1	131
4.2.3 All variants had similar host-cell binding and uncoating relative to T3wt.....	132
4.2.4 T3v10, T3v12 and T3v13 are less effective in establishing productive infection....	133
4.2.5 T3v10 and T3v13 release progeny earlier during infection than T3wt	134
4.2.6 T3v10 is chosen for further characterization	135
4.2.7 The A612V alteration in μ 2 is responsible for the large-plaque phenotype of T3v10	136
4.3 Summary.....	137
CHAPTER 5: A REOVIRUS μ2 C-TERMINAL LOOP INVERSELY REGULATES NTPASE AND TRANSCRIPTION FUNCTIONS VERSUS BINDING TO FACTORY-FORMING μNS AND PROMOTES REPLICATION IN TUMORIGENIC CELLS.....	156
5.1. Introduction and chapter objective.....	156
5.2 Results	157
5.2.1 The A612V mutation in μ 2 promotes reovirus replication	157
5.2.2 T3v10 ^{M1} is impaired at hydrolyzing ribonucleoside tri-phosphates (rNTPs) and RNA synthesis <i>in vitro</i>	157

5.2.3 T3v10 ^{M1} is impaired at RNA synthesis <i>in vitro</i>	159
5.2.4 Incoming T3v10 ^{M1} virion is less effective at establishing productive infection.....	161
5.2.5 Cells productively infected by T3v10 ^{M1} accumulate higher levels of viral RNAs and proteins over the course of infection relative to T3wt	162
5.2.6 T3v10 ^{M1} - μ 2 and μ NS exhibit increased association during infection and transfection relative to T3wt- μ 2	164
5.2.7 When co-transfected with μ NS, T3v10 ^{M1} μ 2 has increased association with reovirus capsid proteins relative to T3wt μ 2	168
5.2.8 Co-transfection of μ NS and T3v10 ^{M1} μ 2 promotes progeny production	169
5.2.9 T3v10 ^{M1} induces more cell-death.....	170
5.2.10 T3v10 ^{M1} has reduced induction of p-IRF3	171
5.3 Summary	172
CHAPTER 6: DISCUSSION AND FUTURE DIRECTIONS	197
6.1 Chapter 3: investigation of σ1 tail regions and their effects on virion association	197
6.1.1 Residues 28 and 66 of σ 1 are unique compared to neighboring amino acids.....	197
6.1.2 The L28P mutation may prevent proteolytic cleavage of σ 1	199
6.1.3 Sigma 1 trimers may have different conformations on SDS-PAGE in an incubation temperature-dependent manner	200
6.1.4 Assembly of σ 1 onto virion involves multiple steps.....	201
6.1.5 Major contributions and limitations of the current study	204
6.2 Chapter 4: identifying novel mechanisms to improve oncolytic reovirus.....	205
6.2.1 Oncolytic potency of T3v6 and T3v13 may be enhanced by novel mechanism(s) .	205
6.3 Chapter 5: A reovirus μ2 C-terminal loop inversely regulates NTPase and transcription functions versus binding to factory-forming μNS and promotes replication in tumorigenic cells.	207
6.3.1 Mu2 is the most conserved reovirus protein among different serotypes and field isolates.....	207
6.3.2 Effects of the μ 2 C-terminal domain on NTP hydrolysis	208
6.3.3 Effects of the μ 2 C-terminal domain on RNA transcription	209
6.3.4 Effects of the μ 2 C-terminal domain on association with μ NS and tubulin	210
6.3.5 Potential implications of the μ 2 C-terminal domain	211

6.3.6 Limitations of the current study and future directions	212
REFERENCES	226

LIST OF TABLES

Chapter 1

Table 1- 1.T3D reovirus genome segments and their encoded proteins.	39
Table 1- 2. Reovirus variants with altered replication in cancer cells.	40
Table 1- 3. The nucleoside triphosphate binding domain is well conserved in the <i>Reoviridae</i> family.....	41

Chapter 2

Table 2- 1. Volume of reagents.....	77
Table 2- 2. List of antibodies.	78
Table 2- 3. List of common buffers.	79
Table 2- 4. List of common cell culturing media.....	80
Table 2- 5. Primer sequences for $\sigma 1$ plasmids with truncations.	81
Table 2- 6. Primer sequences for $\sigma 1$ plasmids and mutants with single mutation.....	82
Table 2- 7. Primer sequences introducing stop codons into truncated $\sigma 1$ mutants.....	83

Chapter 3

Table 3- 1. Mutations in reovirus variants.....	104
---	-----

Chapter 4

Table 4- 1. Mutations in reovirus variants.....	139
---	-----

LIST OF FIGURES

Chapter 1

Figure 1- 1. Structure of T3D reovirus.	42
Figure 1- 2. Binding and entry of reovirus.	43
Figure 1- 3. Uncoating of reovirus.	44
Figure 1- 4. Structure and cleaved products of $\mu 1$	45
Figure 1- 5. Structure and known functions of $\sigma 1$	46
Figure 1- 6. Structure and known functions of $\mu 2$	47
Figure 1- 7. Replication cycle of reovirus.	48

Chapter 3

Figure 3- 1. Plaque picking of reovirus variant on L929 cells.	105
Figure 3- 2. Reovirus variants form large plaques on various mouse and human cancer cells	106
Figure 3- 3. All variants have reduced levels of $\sigma 1$	107
Figure 3- 4. Reovirus field isolates have similar levels of $s 1$ relative to lab stain T3D, and they are reassortants between T1L, T2J and T3D.	108
Figure 3- 5. Multimerization of $\sigma 1$ can be detected by altering incubation temperatures with protein sample buffer.	109

Figure 3- 6. All variants are capable of trimerization. 110

Figure 3- 7. T3v16 σ 1 migrates faster than other variants on SDS-PAGE and does not
produce detectable cleaved σ 1 product..... 111

Figure 3- 8. Associations between transfected σ 1-virion is examined by
immunoprecipitation. 112

Figure 3- 9. Different σ 1 species do not form aggregate or heteromer..... 113

Figure 3- 10. The truncated σ 1¹⁻¹⁰⁴ is not able to be co-immunoprecipitated with virion.114

Figure 3- 11. Sigma 1 residues 155-235 play crucial role in viral factory accumulation. ... 115

Figure 3- 12. Constructs with single amino acid changes at residue 28 or 66 of σ 1 protein.
..... 116

Figure 3- 13. Trimerization of σ 1 is not affected by the swapped amino acids at residue 28
or 66..... 117

Figure 3- 14. The length of σ 1 tail and residue 28 or 66 are important for virion association.
..... 118

Figure 3- 15. Sigma 1 truncations and single-site mutations are introduced to mutants
generated by the reverse genetics (RG) system. 119

Figure 3- 16. Sigma 1 levels of mutants are analyzed by Western blots..... 120

Figure 3- 17. Sigma 1 levels of mutants are analyzed by agarose gel electrophoresis 121

Figure 3- 18. Results from Western blot analysis and agarose gel electrophoresis have a very strong positive correlation.....	122
Figure 3- 19. Novel functions of $\sigma 1$ discovered by the current study.	123

Chapter 4

Figure 4- 1. Viral bands generated by Vertrel® XF-CsCl density-gradient centrifugation. .	140
Figure 4- 2. Plaque assay comparing variants with T3wt on L929 cells.....	141
Figure 4- 3. Plaque assay comparing variants with T3wt on PanC and NIH3T3 cells.	142
Figure 4- 4. Coomassie Blue staining of reovirus proteins.	143
Figure 4- 5. Western blot analysis comparing reovirus $\sigma 1$ levels.	144
Figure 4- 6. Reovirus binding assay.....	145
Figure 4- 7. Uncoating of reovirus is monitored by Western blot analysis.	146
Figure 4- 8. Immunocytochemistry staining of reovirus-infected L929 cells.	147
Figure 4- 9. Release of viral progeny is compared by plaque assay.	148
Figure 4- 10. T3v10 forms large plaques on various cancer cells.	150
Figure 4- 11. T3v10 ^{M1} is generated by co-infecting L929 with T3wt and T3v10.	151
Figure 4- 12. T3v10 ^{M1} has the same phenotype as its parental viruses T3v10 and T3wt. .	152
Figure 4- 13. Western blot analysis comparing $\sigma 1$ levels of T3wt, T3v10 and T3v10 ^{M1}	153

Figure 4- 14. Agarose gel electrophoresis comparing $\sigma 1$ levels of T3wt, T3v10 and T3v10^{M1}.
 154

Figure 4- 15. Western blot analysis comparing cell-binding of T3wt, T3v10 and T3v10^{M1}. 155

Chapter 5

Figure 5- 1. A612V mutation in $\mu 2$ enhances reovirus growth in L929 cells. 174

Figure 5- 2. Generating reovirus core by chymotrypsin (CHT) digestion. 175

Figure 5- 3. T3v10^{M1} is less effective in hydrolyzing rNTPs *in vitro*. 176

Figure 5- 4. T3v10^{M1} is less effective in synthesizing RNAs *in vitro*. 177

Figure 5- 5. Incoming T3v10^{M1} virion produces less RNAs in L929 cells. 178

Figure 5- 6. Incoming T3v10^{M1} virion is less effective at establishing productive infection.
 179

Figure 5- 7. T3v10^{M1} produces fewer reovirus antigen-positive cells relative to T3wt at the
 same multiplicity of infection (MOI). 180

Figure 5- 8. T3v10^{M1} produces 2-fold more RNAs than T3wt in L929 cells per infected cell.
 181

Figure 5- 9. T3v10^{M1} accumulates more viral proteins in infected L929 cells. 182

Figure 5- 10. T3v10^{M1} accumulates up to 3.5-fold more viral proteins in infected L929 cells
 at 15hpi. 183

Figure 5- 11. $\mu 2$ and μNS has increased association in T3v10 ^{M1} -infected L929 cells.	184
Figure 5- 12. Transfected T3v10 ^{M1} -derived $\mu 2$ ($10^{M1} \mu 2$) shows increased association with μNS in H1299 cells.	185
Figure 5- 13. Pre-transfection of T3v10 ^{M1} -derived $\mu 2$ ($10^{M1} \mu 2$) and wild-type μNS enhances association of $10^{M1} \mu 2$ and virus-expressed mNS.....	186
Figure 5- 14. Far-Western blot analysis shows T3v10 ^{M1} -derived $\mu 2$ has stronger physical interaction with μNS	188
Figure 5- 15. Increased $\mu 2$ - μNS association in T3v10 ^{M1} -infected L929 cells enhances core and outer capsid proteins recruitment.....	189
Figure 5- 16. Pre-transfection of T3v10 ^{M1} -derived $\mu 2$ and wild-type μNS enhances core and outer capsid proteins recruitment.....	190
Figure 5- 17. Pre-transfection of T3v10 ^{M1} -derived $\mu 2$ ($10^{M1} \mu 2$) and wild-type μNS promotes progeny production.....	191
Figure 5- 18. T3v10 ^{M1} infection induces more cleaved caspase-3.	192
Figure 5- 19. T3v10 ^{M1} infection induces more cell-death.....	194
Figure 5- 20. T3v10 ^{M1} has reduced of p-IRF3.....	195
Figure 5- 21. Mu2 does not self-associate on Far-Western blot.	196

Chapter 6

Figure 6- 1. Sigma 1 protein sequence comparisons of residues near the N-terminus between T1L, T2J and T3D.	215
Figure 6- 2. PDBePISA analysis of σ 1 residues 28 and 66.	216
Figure 6- 3. Residue 66 of σ 1 has unique physical properties.	217
Figure 6- 4. A model showing the effect of altered residue 66 on σ 1 cleavage.	218
Figure 6- 5. Observed σ 1 species and conformations from different incubation temperatures.	219
Figure 6- 6. Model of σ 1 assembly onto virion.	220
Figure 6- 7. Sigma 1 residues 190-232 are sensitive to mutations, suggesting they are important for σ 1 functions.	221
Figure 6- 8. Sigma 1 residues 252-286 promote association with virion but impairs assembly of σ 1.	222
Figure 6- 9. Protein sequence comparison between T3wt m2 and two homologs of VP5.	223
Figure 6- 10. The 3D model showing the transcription complex of Aquareovirus.	224
Figure 6- 11. Model: mu2 A612V promotes reovirus replication in transformed cells.	225

LIST OF ABBREVIATIONS

5FU	5-fluorouracil
AD293	Adeno 293 cells
ARV	Avian orthoreovirus
BCIP/NBT	5-bromo-4-chloro-3-indolyl phosphate/nitro blue tetrazolium
BHK-T7	Baby Hamster Kidney fibroblast containing T7 RNA polymerase Protein
BSA	Bovine serum albumi
BSC-1	Grivet kidney cell
CHO	Chinese hamster ovary
CHT	Chymotrypsin
CHX	Cycloheximide
CNS	Central nervous system
CsCl	Cesium chloride
Cyro-EM	Cyro-electron microscopy
DR	Death receptor
ELISA	Enzyme-linked immunosorbent assay
FLISA	Fluorescence-linked immunosorbent assay
GFP	Green fluorescence protein
GM-CSF	Granulocyte-macrophage colony-stimulating factor
GTase	Guanylyltransferase
H1299	Human lung carcinoma cell

HA	Hemagglutination
HEK293	Human embryonic kidney 293 cells
HEK293	Human embryonic kidney 293
HEK293T	Human embryonic kidney 293 - expressing SV40 large T antigen
HMMs	Hidden Markov models
Hpi	Hour-post-infection
HSV1	Herpes Simplex Virus 1
ICP	Infected cell protein
IF	Immunofluorescence
IRD	Interdomain region
IRF3	Interferon regulatory factor 3
ISG	Interferon-stimulated gene
ISGs	Interferon-stimulated genes
ISRE	IFN-stimulated response element
ISVP	Infectious subvirion particle
ITAM	Immunoreceptor tyrosine-based activation motif
JAM	Junctional adhesion molecules
L929	Transformed mouse fibroblast
MDA5	Melanoma differentiation-associated protein 5
MDCK	Madin-darby canine kidney
MEF	Mouse embryonic fibroblast
MHC	Major histocompatibility complex

MHC	Major histocompatibility complex
MOI	Multiplicity of infection
MRV	<i>Mammalian orthoreoviruses</i>
MT	Microtubule
MTase	M ⁷ G-methyltransferase
Ndev	Ndelle virus
NF-κB	Nuclear factor kappa-light-chain-enhancer of activated B cells
NgR1	Nogo-66 1 receptor
NH ₄ Cl	Ammonium chloride
NIH3T3	Non-transformed mouse fibroblast
NIH3T3-Ras	NIH3T3 transformed by Harvey ras oncogene
NLS	Nuclear localization signal/sequence
NTP	Nucleoside triphosphate
NTPase	Nucleoside-triphosphatase
OAS	2',5'-oligoadenylate synthetase
PanC	Human pancreatic carcinoma
PCR	Polymerase chain reaction
PFA	Paraformaldehyde
PFU	Plaque-forming unit
Phyre2	Homology/AnalogY Recognition Engine
PKR	Double-stranded RNA-activated protein kinase
PKR	Double-stranded RNA-activated protein kinase

pNPP	Para-Nitrophenylphosphate
PRRs	Pattern recognition receptors
PRV	<i>Pteropine orthoreovirus</i>
RIG-I	Retinoic acid-inducible gene 1
rNTP	Ribonucleoside tri-phosphate
RTPase	RNA 5'-triphosphatase
RT-qPCR	Quantitative reverse transcription polymerase chain reaction
SA	Sialic acid
STAT1	Signal transducer and activator of transcription 1
T1L	Type 1 Lang
T2J	Type 2 Jones
T3A	Type 3 Abney
T3D	Type 3 Dearing
T3wt	Serotype 3 Darling wild-type reovirus
T47D	Human breast cancer cell
TME	Tumor microenvironment
TRAIL	TNF-related apoptosis-inducing ligand
T-VEC	Talimogene laherparepvec

CHAPTER 1: INTRODUCTION

1.1 Overview of cancer and oncolytic reovirus

According to the Canadian Cancer Society, cancer is the leading cause of death in Canada and about 25% of Canadians will die from cancer (44). A report recently released by Health Canada concluded that the cost associated with cancer treatments and care represents about 14% of the total Canadian healthcare spending budget (110). There is an urgent need to improve cancer therapy to reduce the economic and health burden of cancer. Recently, the wild-type reovirus showed promise in treating different types of cancers as a monotherapy or in combination with chemotherapeutics and radiation. My thesis focuses on variants of reovirus that have alterations in two different viral proteins with augmented replication in transformed cells. I sought to understand how mutations in these two viral proteins affect reovirus replication and its oncolytic potency.

1.1.1 Classification of reovirus

Reovirus belongs to the *Orthoreovirus* genus and family *Reoviridae*. *Reoviridae* are subclassified into two subfamilies (*Sedoreovirinae* and *Spinareovirinae*) and 15 identified genera (1). All members of *Reoviridae* are non-enveloped, have icosahedral symmetry, possess 9-12 dsRNA genome segments and have a particle diameter of 60–85 nm (124,147,172).

Orthoreoviruses belonging to the subfamily *Spinareovirinae* infect only vertebrates, usually through the respiratory and enteric routes (1,233). Viruses in the subfamily *Spinareovirinae*

have one major distinguishing feature; they all have large turret-like-structures sitting at the 12 icosahedral vertices of the viral core while viruses from *Sedoreovirinae* have a relatively smooth and spherical appearance (1,248). *Orthoreoviruses* are subdivided into two subgroups: the fusogenic reoviruses are capable of inducing cell-cell fusion as a means to enhance spreading (83,272), and this subgroup includes *Pteropine Orthoreovirus*, *Baboon Orthoreovirus*, *Avian Orthoreoviruses*, *Reptilian Orthoreovirus* and *Piscine Orthoreovirus* (59,72,230,230). The *Mammalian orthoreoviruses* (MRV) is the only known subgroup that is non-fusogenic.

The MRV contains 10 dsRNA segments which include 4 small (S1, S2, S3, S4), 3 medium (M1, M2, M3) and 3 large (L1, L2, L3) size-class genes (72,211,225). MRV classically has three serotypes and four representative prototype strains: The serotype 1 Lang (T1L), serotype 2 Jones (T2J), serotype 3 Abney (T3A) and serotype 3 Daring (T3D) (1). The most recent edition of Virus Taxonomy listed Ndelle virus (NDEV) as the 4th serotype of MRV (1). The NDEV was first isolated in 1974 (91). Despite that NDEV cannot be neutralized by antibodies against serotypes 1,2 and 3 reoviruses (10), structural and sequence analyses suggest NDEV is related to MRV (284). Virus serotype is usually classified by divergence and antigenic properties, and for MRV, it is mainly determined by variations in sequences of the S1 gene that encodes the σ 1 cell-attachment protein (46,98). The T3D S1 gene sequence shares about 25% identity to T1L and approximately 27% to T2J (80,186). In this thesis, I will focus on the T3D strain and the term “reovirus” will refer to the wild-type T3D (T3wt) propagated in Dr. L.W. Cashdollar and sequentially in Dr. P. Lee’s laboratories, unless specified otherwise.

1.1.2 Reovirus and pathogenesis

The first human reovirus sample was obtained by rectal swab from a healthy child in Australia in 1953. Six years after its discovery, Sabin *et al.* re-classified the virus from the *Picornaviridae* family (211,240). *Mammalian orthoreovirus* infects virtually all mammals; however, its natural reservoirs or direct progenitors remain to be identified. Recently, evidence from multiple countries suggests that bats may serve as one of the reservoirs for reovirus (136,148,183,203,265). Bats are the second largest order of mammal which comprise more than 20% of all classified mammal species, they are more maneuverable than birds and capable of long flights (139). Compared to humans, bats express higher levels of interferon and interferon-stimulated genes (ISGs), and they are very effective in suppressing viral-induced pathological effects such as inflammation (14,41,190,246,289). These unique properties allow bats to spread viruses including reovirus across the globe.

Reovirus is an acronym for respiratory enteric orphan virus. The MRV is considered not pathogenic and not associated with any human disease (55). It is believed that reovirus is highly ubiquitous in nature and epidemiological studies suggest that reovirus is highly prevalent with minimal symptoms. For example, in a study conducted in Tennessee (USA), 272 healthy infants were followed from birth until the age of 5. These children were tested for the presence of reovirus antibodies using enzyme-linked immunosorbent assay (ELISA) for total IgA, IgG, and IgM levels against T3D reovirus (250). Reovirus seropositivity in 0-3 month-old infants was 75%, but 11% in 3-6 months old infants, suggesting the presence of maternal antibodies. Reovirus specific antibodies were detected in only 8.2% of 1-2-year-old children, 32% of 4-year-olds, and 50% of 5-year-olds. The authors stated that most tested children did not show any

symptoms from the infection, but a few of them had signs of mild respiratory infections. They further concluded that an antibody response against reovirus was acquired during early childhood and reovirus infection was common among young children. In a study focused on adults with idiopathic cholestatic liver disease, 91% of patients and up to 100% of volunteers tested positive for antibodies against serotype 3 reovirus (178). In summary, these epidemiological studies suggested that almost all adults have been infected with reovirus, but severe symptoms are rarely reported.

Prevalence of reovirus infections among children and adults were investigated by studies described above. Another study directly tested the pathogenesis of reovirus in adults by dividing 27 male volunteers into 3 groups, with 9 participants in each group that would receive one dose of reovirus serotype 1, 2 or 3 by intranasal inoculation (209). Three out of 9 participants received types 1 and 2 viruses showed symptoms normally associated with common colds such as malaise, rhinorrhea, cough, pharyngitis and headache. Only 2 out of 9 participants had rhinitis. However, all symptoms were mild and only lasted 4-7 days. Reovirus was recovered in less than 8% of participants (authors did not specify serotype) by throat swabs, and type 1 and type 3 viruses could be recovered in 8 out of 9 participants in fecal samples. Note that all participants were healthy and seropositive for reovirus. The authors were not able to find participants that were seronegative for the virus. It is possible that these volunteers were able to mount a rapid immune response against reovirus infections which minimized the associated symptoms. I should also note that this study would not be allowed today due to ethical issues.

Although reovirus is regarded as non-pathogenic and the wild-type T3D is being evaluated in clinical trials (see section 1.3.3), isolated incidents associated with reovirus infection have been reported. In Melaka of Malaysia, a previously unknown virus ('Melaka virus') was isolated from a 39 years old male (58). The patient developed acute respiratory symptoms with high fever at the time of virus isolation. One week later, two family members of the patients were infected with the same virus and developed similar symptoms. Epidemiological tracing revealed that the family was exposed to a bat about one week before the male patient's onset of symptoms, suggesting the virus was bat-borne and transmitted to humans. Sequencing data of the virus showed a close genetic relationship to the Pulau virus, a reovirus isolated from fruit bat in Malaysia. Pulau virus belongs to the *Pteropine orthoreovirus* (it is formerly known as *Nelson Bay orthoreovirus*), a fusogenic orthoreovirus with no previous record of human infection. A recently published review article summarized a number of reports about human infections with 12 isolates from *Pteropine orthoreovirus* (PRV) (251). The viruses mostly originated from Southeast Asia and evidence suggested that some viruses from PRV were capable of human-to-human transmission. Although no death was reported, PRV and MRV are the two members from orthoreovirus that can infect humans to date. Several recent studies also reported bat-borne viruses with reovirus genes; these viruses were more likely to be associated with spillover infections (i.e. pathogens from a reservoir which gains the ability to infect a novel host). In addition, sequence data suggested that events of reassortment have occurred which altered the tropism and enhanced virulence of reovirus and other viruses (116,143,256,266,270,275). In conclusion, more studies are needed to understand the mechanisms of how viruses acquired the ability for cross-species transmissions. In 2018, the

Department of the Defense, Defense Threat Reduction Agency (USA) has funded and established the Western Asia Bat Research Network in Western Asia. This is the first coordinated research effort to track and identify bat-associated viruses in hope of understanding the mechanisms of spillover infections (198).

1.1.3 Composition of reovirus genome and virion structure

As discussed earlier, reovirus has 10 linear dsRNA segments that encode for 13 proteins, including proteins produced by leaky scanning. Eight of the reovirus proteins fulfill structural roles, while 3 are nonstructural proteins expressed in infected cells that aid reovirus replication (1). Reovirus proteins are designated in terms of relative sizes and the genes encoding them; for example, all proteins encoded by S genes (S1, S2, S3, S4) are named “Sigma”. Reovirus gene designations can be confusing, for example the M1 gene encodes μ_2 , so please refer to Table 1-1 while reading the thesis.

Structure of the reovirus virion is depicted in Figure 1- 1. The outer capsid is composed of 600 copies each of σ_3 and μ_1 . These two outer capsid proteins form an interlocking σ_3 - μ_1 heterohexamer and this gives the virus an icosahedral shape (68,226,286). The surface of reovirus is not smooth, because the pentameric subunits of λ_2 sit at each of 12 vertices, forming the flower-like turret structures that span from the inner core to the outer capsid (35). There is an opening in the middle of the λ_2 pentamer, which anchors the cell-attachment σ_1 protein (97,154,165,206). λ_2 possesses enzymatic activities that are involved in capping the nascent viral mRNA (40,155).

Beneath the outer capsid is the main structural core (inner capsid) composed of 120 copies of $\lambda 1$ and 150 copies of $\sigma 2$ (1). The reovirus polymerase $\lambda 3$ and its co-factor $\mu 2$ are located inside the core and at the base of each vertex. The $\lambda 3$ - $\mu 2$ complex is suggested to hold one of ten genome segments, with 2 vertices therefore empty of dsRNA genome. Some research suggests a 1:1 $\lambda 3$ -to- $\mu 2$ ratio (82,215), while other researchers argue that one $\lambda 3$ associates with two $\mu 2$ (68,147,287). The known functions of each reovirus protein are summarized in Table 1- 1 and will be described in the context of virus replication stages in section 1.2.

1.2 Replication of T3D reovirus

1.2.1 Binding to host cells

Reovirus naturally infects intestinal epithelial cells in the small intestine and the respiratory tract (1,194,210,271). The steps of reovirus binding and internalization are summarized in Figure 1- 2. Reovirus-cell attachment is a multi-step process mediated by the viral cell-attachment protein $\sigma 1$. Sigma1 has a lollipop shape, with an N-terminal stem “tail” domain, and a globular C-terminal “head” domain (142,186). The tail domain contains the binding regions that bind sialic acids (SA) on the cell surface with low affinity (18). SA is an acidic sugar with a nine-carbon backbone that is commonly expressed on all cell-surfaces and most secreted proteins of vertebrates and some invertebrates (214,258,259). SA plays important roles in many biological processes such as stabilizing interactions between cells and membranes, transport of ions and drugs, maintaining conformations of enzymes and enhancing

neurotransmission between neurons (213,253). SAs are also exploited by many toxins and pathogens, including reovirus, as binding targets (260).

After low-affinity SA binding, reovirus particles initiate high-affinity interactions with junctional adhesion molecule-A (JAM-A) via the $\sigma 1$ head (19,43,131,134). JAMs are cell-cell adhesion molecules from the immunoglobulin superfamily that are widely expressed on hematopoietic, endothelial, and epithelial cells (247). JAMs are enriched and localized at cell-cell junctions. Their functions are not well understood, but it's believed that JAMs promote monocytes and other immune cells to transmigrate across endothelial cells effectively (7,22,56,87). There are three closely related isoforms of JAMs: JAM-A, JAM-B and JAM-C, but reovirus only binds JAM-A (43,204).

Following attachment to the host cell, reovirus needs to internalize into the cytoplasm. The $\lambda 2$ protein at reovirus vertices is involved in reovirus internalization (163). Lambda 2 protein contains integrin-binding motifs RGD and KGE (35,220) that mediate integrin binding and internalization. Maginnis *et al.* showed that reovirus infection was dramatically attenuated when they depleted integrin availability with $\beta 1$ -integrin-specific antibodies in HeLa cells (163). A follow-up study by the same group of researchers showed that $\beta 1$ integrin cytoplasmic NPXY motifs were required for the proper sorting and transport of reovirus to lysosomal compartments post-internalization (164). In conclusion, the entry of reovirus involves 3 major processes, SA-mediated binding, JAM-A-mediated binding, and $\beta 1$ integrin-mediated internalization (Figure 1- 2).

1.2.2 Uncoating of reovirus

Following internalization into the host cell, reovirus sheds its outer capsid (uncoating) to produce transcriptionally-active core particles (233). Reovirus naturally infects the intestine and early studies showed that reovirus uncoats in the intestinal lumen of neonatal mice (20,28). A study pretreating mice intragastrically with protease inhibitors before intragastric inoculation of reovirus suggested that trypsin and chymotrypsin are likely the main proteolytic enzymes for reovirus uncoating in animals (20). Reovirus can also uncoat inside cells as happens in our *in vitro* experiments. Here I will further describe reovirus uncoating in cells. Reovirus uncoats in endosomes. Endosomes are membrane-bound compartments that sort, degrade and recycle internal or external cellular materials such as lipids, proteins and toxins (173). Studies showed that reovirus utilizes microtubule motor dynein 1 to traverse the endocytic pathway (168). Reovirus can be found in early, late, and recycling endosomal compartments. However, only reovirus that moves across early and late endosomes are capable of establishing infection (166,167). The fate of viral particles in the recycling endosomes is not clear, but it is believed that they can be re-directed to the cell surface where they may re-enter the same cell or disengage.

Late endosome containing reovirus ultimately fuse with lysosomes, forming a hybrid structure called “endo-lysosome”. The real distinction between such hybrid structures and lysosomes is not clear. In this section, I will refer to endo-lysosomes and lysosomes synonymously as lysosomes. Lysosomes are vesicles containing various soluble acid-dependent hydrolytic enzymes (hydrolases). They serve as a major degradative compartment

in eukaryotic cells that degrade both endogenous and exogenous materials (73,156,157). Inside the lysosome, reovirus undergoes uncoating. In general, uncoating involves a series of proteolytic events that cause conformational and structural changes to reovirus outer-capsid proteins, ultimately leading to removal of the outer capsid (Figure 1- 3). First, the outer capsid $\sigma 3$ is completely disassembled by proteolysis, which triggers the cleavage of $\mu 1$ to $\mu 1N$, δ and ϕ (Figure 1- 4), generating an infectious subviral particle (ISVP) (4,31,32). Eventually, $\mu 1N$, ϕ and $\sigma 1$ from ISVPs are released and δ is remained with the viral structure known as ISVP*. $\mu 1N$ and ϕ are capable of forming pores in cell or lysosomal membranes, but whether the two fragments work cooperatively or independently remains to be investigated (3,238,285). It was proposed that pore formation allows ISVP* to pass through membranes, but direct evidence for pore formation remains lacking. Nevertheless, δ is the only $\mu 1$ fragment remaining on ISVP*, and allows the ISVP* to penetrate the lysosomal membrane to deliver the transcriptionally active core particles into the cytoplasm (49,50,191).

Proteolytic disassembly of reovirus may be performed by different proteases in an environment with a range of different acidity (105). Uncoating of reovirus is well characterized in L929 (transformed mouse fibroblasts) cells. Researchers treated L929 cells with cysteine protease inhibitor E64 which inhibited reovirus replication (12,86), but aspartic protease inhibitor pepstatin A had no effect on reovirus growth in L929 and MDCK (Madin-Darby Canine Kidney) cells (138). A separate study used L929 and MEF (mouse embryonic fibroblast) to confirm that Cathepsins B and L were responsible for reovirus uncoating (85). Both enzymes were found to work optimally in acidic pH as cells treated with the lysosomotropic agent ammonium chloride (NH_4Cl) inhibited reovirus replication. *In vitro* studies also showed that full

virions, but not ISVPs, were sensitive to NH_4Cl ; this provided evidence that uncoating of reovirus takes place in an acidic environment (169,245). Furthermore, uncoating of reovirus can be mimicked *in vitro*; treatment of full virions with chymotrypsin or trypsin generates ISVPs. Prolonged *in vitro* digestion of reovirions with these proteolytic enzymes completely removes the outer capsid, producing transcriptionally active cores (31,93,125,277). Taken together, these studies demonstrated that reovirus outer capsids are uncoated either by extracellular gut proteases or intracellular lysosomal cathepsins.

1.2.3 Transcription of genome

Once uncoated, reovirus is completely devoid of its outer capsid and the core remains highly stable and resistant to proteolytic digestion (223,233). Genome transcription is performed by the RNA-dependent RNA polymerase $\lambda 3$ and its co-factor $\mu 2$; both proteins are proposed to locate at the base of a capsid vertex (132,255). Genome transcription begins as $\lambda 3$ uses the negative-sense strands of the dsRNA as templates to synthesize mRNA (2,217,224,234). $\mu 2$ is considered the polymerase co-factor because it was found to possess nucleoside-triphosphatase (NTPase) activity and capable of hydrolyzing ribonucleoside triphosphates (rNTPs) (132,188). Since $\mu 2$ is one of the main focuses of this thesis, section 1.6 will provide further details about $\mu 2$ functions and structure. Nascent mRNA molecules then exit the core particle through the $\lambda 2$ turrets, and are capped by the capping enzymatic functions of $\lambda 2$ during export (63,154). Uncapped viral mRNA is more likely to be detected by cytoplasmic pattern recognition receptors (PRRs) such as melanoma differentiation-associated protein 5

(MDA5) and retinoic acid-inducible gene I (RIG-I) (95,216,218,292); capping of viral mRNA significantly diminishes its detection by PRRs and enhances its stability in host cells (34,121,205). Some early studies suggested that cap synthesis may be inactivated or masked at the later stages of reovirus infection (235,236,283), but their findings were not supported by further studies. The mechanisms of reovirus mRNA capping at different replicative stages remained to be elucidated by future studies.

Reovirus mRNA capping is a multiple-step process and involves sequential actions of three enzymatic activities: RNA 5'-triphosphatase (RTPase), guanylyltransferase (GTase), and m⁷G-methyltransferase (MTase) (205). The current model proposes that the core protein λ 1 possesses RTPase activity, generating a 5'-diphosphate mRNA terminus as a precursor for the final processing step by the λ 2 GTase and MTase (24,25,40,154). Ultimately it is important to remember that for reoviruses, mRNA is synthesized within the core particles and released through λ 2 channels into the cytoplasm.

1.2.4 Viral progeny production and assembly

Mature reovirus mRNAs serve two functions. They are either packaged into newly assembled virions and used for progeny dsRNA generation as they act as templates for negative-sense RNA synthesis, or they serve as templates for translation of viral proteins (233). As reovirus proteins are synthesized, they traffic to virus inclusion bodies (also known as virus factories) for assembly into progeny virus cores. The traffic of reovirus proteins and production of factories is coordinated by the non-structural protein μ NS and non-virion associated μ 2 that

interacts with cellular microtubules (MT) (36,37,39). More specifically, transfected μ NS was shown to be sufficient for forming viral factory-like structures, but the expression of μ 2 was required to properly develop the structure of viral factories anchored to microtubules (45,176). Formation of viral factories plays a crucial role in determining whether reovirus can establish productive infection, as viral factories are the main sites of reovirus mRNA transcription, protein translation and virion assembly (184,189). Newly assembled progeny virus cores then participate in sequential rounds of genome transcription and protein synthesis. Important to note for this thesis is that there are two phases of reovirus transcription; the 'first phase' is when incoming cores transcribe RNAs that establish the infection, while the 'second phase' is when newly assembled cores within viral factories transcribe RNAs to amplify and accelerate the infection (233).

In addition to its well-characterized roles in virus replication, recent studies showed that viral factories are capable of sequestering factors from the host cells that could otherwise inhibit the replication of reovirus. Ivanovic and colleagues demonstrated that reovirus was able to recruit cellular clathrin to T1L viral factory in BSC-1 (grivet kidney) cells (119). The authors further showed that clathrin was co-immunoprecipitated with μ NS. Clathrin is well known to play main functions in packing proteins and cellular materials into vesicles and transfer them between the membrane and the *trans*-Golgi network (182,197). It is not clear whether sequestration of clathrin into viral factories provides the virus any direct replication benefits. The authors speculated that inhibition of clathrin-dependent membrane trafficking may prevent host cells from presenting viral antigens to its major histocompatibility complex (MHC); innate immune signaling may be also affected by impaired intracellular trafficking of cellular

factors. A recent study provided direct evidence of reovirus modulating antiviral response through sequestration of cellular transcription factors into viral factories. Using immunofluorescence (IF) staining, Stanifer *et al.* showed that interferon regulatory factor 3 (IRF3), a main interferon regulatory factor induced by T3D reovirus infection (128,227), was recruited to virus factories of infected A549 (human lung cancer) cells (239). When T3D μ NS was transiently transfected into A549 cells, IRF3 was not able to translocate into the nucleus, and induction of interferon (IFN) response was repressed. Furthermore, the authors showed that mutant μ NS that could not form factory-like structure was not able to inhibit the IFN response, and concluded that the viral factory was responsible for IRF3 sequestering. In conclusion, μ NS cooperates with μ 2 in the formation of viral factories. The viral factory not only serves as the site for reovirus replication but also represses antiviral responses.

1.2.5 Release of reovirus

Reovirus progenies are assembled in the viral factory and mature virions need to be released to spread the infection. Release of reovirus is one of the least understood processes compared to other replicative steps discussed earlier. The current view believes that reovirus induces different forms of cell-death to enhance progeny release (107). Importantly, reovirus-induced cell-death is exploited as a means to kill a wide variety of cancer cells and tumors (199). Cell-death is not the main focus of this thesis, but I will briefly describe a few well established and documented cell-death pathways that affect reovirus replication.

The nuclear factor kappa-light-chain-enhancer of activated B cells (NF- κ B) is one of the major signaling pathways activated by reovirus to induce cell death. Activation of the NF- κ B can either potentiate or inhibit apoptosis, depending on the presence of various apoptotic stimuli and expression of other cellular factors (126,127). Inhibition of NF- κ B activation following reovirus exposure significantly decreased apoptosis (66). Reovirus induced-apoptosis was also substantially decreased in mouse embryonic fibroblasts (MEFs) with NF- κ B subunit p50 or p65 knockdown compared to wild-type MEFs (66). The μ 2 protein has the immunoreceptor tyrosine-based activation motifs (ITAMs) that were showed to induce NF- κ B in AD-293 cells by reporter assay, and mutation in the ITAMs significantly reduced viral titer in the same cell line (241). Another study showed reovirus induced 10-fold more apoptotic cells and produced 9-fold more titer in NIH3T3-Ras (transformed with Harvey Ras oncogene) compared to non-transformed cells at 24 hour-post-infection (hpi) (170). The same study showed that reovirus induced cell-death is caspase-dependent as cells treated with caspase inhibitor greatly reduced cell-death and viral spreading. Caspase-dependent cell-death also promotes reovirus spreading in mice (170). In conclusion, various studies suggested that reovirus induces cell-death to enhance progeny release.

Reovirus was shown to induce other cell-death pathways, but whether these pathways promote viral replication is not clear. For example, studies demonstrated that reovirus induces TNF-related apoptosis-inducing ligand (TRAIL) in HEK293 and L929 (60,61). Mitochondrial signaling pathways (208), and the c-Jun N-terminal kinase (JNK) are also implicated in reovirus-induced cell-death (62). In L929 cells, reovirus was shown to induce necroptosis (23). Taken

together, the pathways described above are associated with reovirus-induced cell-death, but many studies did not directly examine viral replication.

1.3 Reovirus as an oncolytic virus

1.3.1 Discovery of oncolytic viruses

The use of viruses as an oncolytic agent was first reported in 1912 (268). An Italian physician administered rabies vaccine to female patients who had cervical carcinoma and regression of the tumor was observed. The rabies vaccine was first developed by Louis Pasteur in France during 1885. Rabies virus is a neurotropic single-stranded RNA virus that infects humans and mammals. In the 19th century, humans bitten by rabid dogs often developed fatal conditions. Pasteur planned to use the same but attenuated virus to immunize humans before they were exposed to the virus originating from dogs. He injected the virus into rabbits and collected the live virus from dried nerve tissues repeatedly. After 50 serial passages, the virus accumulated multiple mutations and it was much more adapted to infect rabbits, but its virulence for dogs and humans was greatly weakened (112,273). The use and development of rabies vaccine marked a milestone in oncolytic virus research. First, the attenuated rabies virus was the first identified virus possessing oncolytic properties, and second, Pasteur showed that the properties and virulence of a virus could be altered by directed evolution; an approach utilized by our lab for improving oncolytic potency of wild-type reovirus (will be discussed in details later).

1.3.2 Oncolytic viruses in clinical trials

Nowadays, rabies virus is still being used in treating cancer patients, but almost all reported findings are from pilot clinical studies or anecdotal case reports. The virus was mainly used for melanoma, glioblastoma, and cervical cancer. However, it is not clear if the treatments were effective as standard procedures or guidelines for the administration of the virus were lacking, and many physicians were inconsistent in reporting their findings (5,77,100). At the time of writing this thesis, 7 major groups of oncolytic viruses are currently being evaluated in clinical trials: Herpes Simplex Virus 1 (Herpesvirus), Adenovirus, Vaccinia Virus, Coxsackie Virus, Polio Virus, Adenovirus, and Reovirus (T3D) (13,96,141,171).

Among the 7 viruses mentioned above, two of them have been clinically approved for cancer therapy. Oncorine (H101) is one of the adenovirus variants being tested in clinical trials. Oncorine was developed by Shanghai Sunway Biotech. It has been approved by the Chinese State Food and Drug Administration for the treatment of late-stage refractory nasopharyngeal cancer in 2005 (149,269). The virus has its E1B-55-kDa region deleted, so it cannot express the E1B55K protein. The E1B55K protein interacts with another adenovirus protein E4orf6 in the formation of an E3 ubiquitin ligase complex that targets p53 for proteasomal degradation. This will block p53-mediated cell cycle arrest and apoptosis, allowing adenovirus to keep replicating in host cell (26). With the E1B-55-kDa region deletion, Oncorine replicates selectively in p53-deficient tumor cells. In October of 2015, the US Food and Drug Administration (FDA) officially approved talimogene laherparepvec (OncoVEXGM-CSF or commonly known as T-VEC) for patients with advanced melanoma that cannot be completely removed by surgery (201). T-VEC

belongs to the Herpes Simplex Virus 1 (HSV1) group and its genes were extensively modified: 1. The infected cell protein (ICP)34.5 gene was deleted to prevent infection of healthy cells, 2. Deletion of the ICP47 gene allowed the virus to present its antigens on the surface of infect cell (to encourage immune clearance), 3. Translocation of US11 to increase cancer cell-specific lytic activity, and 4. Two copies of human granulocyte-macrophage colony-stimulating factor (GM-CSF) were inserted into the deleted ICP34.5 genomic site to enhance induction of anti-tumoral immunity (6,67,115,201,221).

1.3.3 Reovirus (REOLYSIN®) in clinical trials

Among the 7 oncolytic viruses that are currently in clinical trials (discussed above), coxsackievirus (CVA21 – a natural occurring strain) and reovirus are the only two viruses that are not genetically modified. Both viruses are RNA viruses and have very compact genomes, this makes manipulation of their genes very challenging. Coxsackievirus belongs to the *Enterovirus* genus of the *Picornaviridae* family. Members of coxsackievirus have positive-sense single-stranded RNA genomes that are about 7.4-8.8kb in size (1,111,117).

A proprietary isolate of the unmodified T3D Reovirus (REOLYSIN®; pelareorep) was developed by Oncolytics Biotech Inc in Calgary of Canada. Dr. Adil Mohamed (former PhD student) compared sequence of REOLYSIN® with the wild-type (T3wt) in our lab and found no amino acid differences between the two viruses (personal communication). The virus has been extensively evaluated in phase I and II clinical trials regarding its safety; reovirus was evaluated as a single agent or in combination with traditional therapy such as radiation, chemotherapy

and other standard drug treatments. The virus was injected intralesionally, intravenously intraperitoneally or intratumorally, and the typical dose levels ranging from a single injection of 10^7 to 3×10^{10} plaque-forming units (pfu) (64,130,262). Most patients experienced grade I (mild or no symptoms) or grade II toxicities (moderate; minimal intervention indicated). Commonly reported side effects include nausea, vomiting, headache, fatigue and flu-like illness with no dose-limiting toxicities (75,106,212,242,252,262).

Regarding reovirus' efficacy in treating cancer, some promising results have been observed and multiple reviews have been published recently (108,212,219,249,288). I will focus on a few recent phase II/III clinical studies here. In one study, 26 patients with head and neck cancer received reovirus by intravenous injection combined with chemotherapy drugs paclitaxel and carboplatin. One patient showed complete response, 6 patients had partial response and 9 patients had stable disease (defined as the tumor had <20% enlargement to <30% reduction). The clinical benefit rate was 61.5% (25% higher than patients that received only drug treatment). In another study, 16 patients with various advanced or refractory solid malignancies received reovirus by intratumoral injection and local irradiation. Ninety-three percent of patients had stable disease. In one phase I study, 12 patients with brain tumors received reovirus intravenously prior to the planned surgery. The objective of the study was to determine whether reovirus could bypass the blood-brain area, as no oncolytic virus has been shown to infect brain tumor. Reovirus RNA and proteins were detected from resected brain tissues from 3 patients. These results suggested that reovirus may be tested for treating brain cancers. In 2015, REOLYSIN® received orphan drug designation from FDA for malignant glioma, ovarian cancer and pancreatic cancer (181), and two years later, the FDA granted Fast Track

Designation for REOLYSIN in treating metastatic breast cancer (47). In conclusion, although wild-type reovirus shows promise as a cancer therapy, reovirus monotherapy is less effective and not all patients respond to the treatment. One of the main goals of my project was to identify mutations that augmented reovirus infectivity towards cancer cells.

1.3.4 Mechanisms of reovirus replication in tumor cells

The application of using reovirus in cancer therapy was discovered by Patrick Lee and colleagues; they observed that cells that expressed epidermal growth factor receptor (EGFR) support the growth and replication of reovirus (244). The same study concluded that reovirus did not bind EGFR directly, but the infection was facilitated by EGFR-mediated signaling pathways. One major downstream target of EGFR is the Ras signaling pathway (92,263). The Ras signaling pathway is controlled by the active GTP-bound or inactive GDP-bound state (130,263). Many types of cancers are associated with mutations in the Ras pathway (and its downstream targets). Ras-transformation continuously promotes cell survival and differentiation, even in the absence of growth stimuli (33).

Ras transformation confers reovirus permissiveness to host cells and studies suggest that reovirus exploits the following mechanisms: Ras transformation leads to increased production of lysosomal cathepsin, an enzyme that aids the uncoating of reovirus (170). Ras-transformation also enhances apoptosis in viral-infected cells, which results in the increase of viral progeny release (17,65,66,200). Tumor cells may have evolved mechanisms to escape from immune surveillance. For example, several major antiviral pathways such as MDA5, RIG-I

and interferon-induced, double-stranded RNA-activated protein kinase (PKR) are downregulated (227,232). These three dsRNA sensors activate downstream transcription factors interferon regulatory factors IRF3 and IRF7, which in turn activate the IFN- β response (113,114). When the antiviral response is impaired or downregulated, reovirus is able to replicate and disseminate. In addition, several multiple myeloma cell lines have been found to overexpress JAM-A which enhances reovirus-mediated apoptosis and sensitivity (131). In summary, there are several processes in cancer cells, that when deregulated, support reovirus replication which would otherwise be controlled in non-transformed cells. It is important to note that it is not essential that the Ras oncogene itself be mutated for susceptibility to reovirus, but rather that these processes needed by reovirus are dysregulated.

1.4 Improving oncolytic potency of reovirus

1.4.1 Reovirus variants with enhanced replication in cancer cells

As discussed earlier, although reovirus showed promise in cancer therapy, the virus was not effective as a monotherapy and not all patients responded to the virotherapy. Our lab has successfully created various variants with augmented infectivity towards cancer cells in *vitro* and in *vivo* by directed evolution. The rationale for using directed evolution to generate reovirus variants is that virus adaptation to new niches is documented in nature and in experimental systems. For example, as discussed earlier, the approach Pasteur used to produce the rabies vaccine by infecting rabbits using naturally occurring rabies virus from dogs was a good example of directed evolution. Compared to DNA viruses, RNA viruses tend to have

higher mutation rates, the viruses are associated with shorter replication times and yield more progeny per replicative cycle (79,81,123); therefore utilization of directed evolution is a convenient and useful approach to create reovirus mutants with desired phenotypes, so long as a positive selection strategy is possible.

A number of studies generated or discovered reovirus variants with enhanced infectivity towards cancer cells (179). Table 1- 2. Reovirus variants with altered replication in cancer cells. In our laboratory, reovirus variants with enhanced tumor cell infection were positively selected based on their ability to produce larger plaques on tumorigenic cells. Large plaque-forming viruses were subjected to two additional rounds of positive selection. Using this approach, two variants, T3v1 and T3v2, were generated (231). Both variants exhibited increased infectivity specifically towards tumorigenic cells as they formed bigger plaques on various types of cancer cells relative to T3wt. Importantly, these variants significantly prolonged survival of mice with subcutaneously grafted B16 melanoma and this study showed that reoviruses with big-plaque phenotype might be more effective than T3wt in suppressing tumor *in vivo*.

1.4.2 Reduction of σ 1 is the main mechanism for enhanced oncolytic potency of reovirus variants T3v1 and T3v2

T3v1 and T3v2, the variants that were described in the previous section, were shown to possess fewer cell-attachment protein σ 1 (231). T3v2 had an S18I mutation in the σ 1 protein that reduced σ 1 levels by 5-fold compared to T3wt. The altered residue is located in the anchoring domain of σ 1 (165); this mutation directly impaired σ 1-virion association. The T3v1 had a single M110I mutation in the λ 2 protein, and Shmulevitz *et al.* concluded that the

mutated residue belongs to the flap domain of $\lambda 2$ which impaired its interaction with $\sigma 1$ (82,165,175,186). T3v1 has 2.5-fold lower levels of $\sigma 1$ relative to T3wt. Since both variants shared a common phenotype of $\sigma 1$ reduction despite that their mutations were in distinct proteins, the authors hypothesized that having fewer $\sigma 1$ may be the mechanistic basis for enhanced oncolytic potency. To test this hypothesis, Dr. Adil Mohamed generated T3wt with reduced $\sigma 1$ by using RNA interference (180). His Western blot analysis showed that reduction of $\sigma 1$ conferred reovirus up to a 5-fold increase in infectivity towards cancer cells. Based on the observed results, he proposed the following model: the microenvironment of the intestinal tract is highly acidic and it has a large amount of trypsin and chymotrypsin (103,104,177). Reovirus does not require full amount of $\sigma 1$ proteins to bind cells, but having more $\sigma 1$ on the outer capsid allow the virus to withstand the proteolytic digestion in the intestinal tract. The tumor microenvironment (TME) is less harsh relative to the intestinal tract. Reovirus particles with fewer $\sigma 1$ molecules have the advantage of uncoating faster and consequently complete the rest of the replication cycle more rapidly. In conclusion, reduction of $\sigma 1$ directly enhances reovirus oncolytic potency.

1.5 Structure and functions of $\sigma 1$ protein

1.5.1 The N-terminal regions of $\sigma 1$ are responsible for virion anchoring and trimerization

Having learned that levels of sigma 1 can vary and that reduced sigma 1 promotes infectivity towards tumor cells, we became curious about how sigma 1 was assembled on

virions. Previous studies documented that $\sigma 1$ has multiple domains associated with different functions; however, little is known about which domains of $\sigma 1$ are important for virion association. Chapter 1 of my thesis explores sigma1 domains and their roles in assembly, and therefore a comprehensive introduction to sigma1 is provided in this section.

As described in section 1.2.1, $\sigma 1$ is the reovirus cell-attachment protein and it is anchored at the 12 vertices of virus particles by the $\lambda 2$ turret-like protein (82,97,142). The T3D $\sigma 1$ has 455 amino acids and it is composed of an N-terminal elongated tail and a globular head at the C terminus (186). The N-terminal tail has 4 regions that are classified by different physical properties and functions associated with each region (186). The structure of $\sigma 1$ and the identified functions of each region is summarized in Figure 1- 5.

The first region T(i) contains 25 residues at the N-terminus that make up the anchoring domain with unique morphological properties. The first 16 residues are highly hydrophobic and residues 17 to 24 are hydrophilic (94). T(i) is proposed to bury into $\lambda 2$ and directly anchors $\sigma 1$ into the virion (146,165). Although clearly the anchoring domain is involved in sigma1 assembly, it is unknown whether this domain is sufficient.

The next ~ 150 residues belong to the T(ii) region which accounts for half the length of the tail and is predicted to form a long and continuous α -helical coiled-coil domain with heptad repeats that is important for the stability of $\sigma 1$ (94,186). A study reported that $\sigma 1$ existed as multimer by SDS-PAGE analysis (21). To determine the region that was important for multimerization, Banerjea and Joklik created a series of $\sigma 1$ constructs with truncations from the C-terminus by using expression vector system (15). The authors incubated these constructs with SDS-containing protein sample buffer at 37°C or 100°C before subjecting the samples to

SDS-PAGE. They concluded that the first 161 amino acids were important for multimer formation.

A similar study was conducted by another group of researchers. Stronger *et al.* used the *in vitro* rabbit reticulocyte lysate translation system to produce full-length $\sigma 1$ (243). They used two different methods to determine the oligomeric state of $\sigma 1$. First, they used the column filtration and sucrose gradient sedimentation analysis to determine the sedimentation coefficient of $\sigma 1$ which allowed them to calculate and compare molecular weight of $\sigma 1$ to the $\sigma 1$ monomer (145), and they concluded that $\sigma 1$ existed as trimer. Secondly, they treated full-length $\sigma 1$ with trypsin that cleaved the protein into the N-terminal and C-terminal fragments. They incubated the two fragments with SDS-containing protein sample buffer at 37°C or 100°C, followed by SDS-PAGE analysis. They concluded that both fragments were capable of forming homotrimers. The same group also performed a follow-up study to investigate whether the $\sigma 1$ monomer or trimer was capable of binding L929 cells (144). They stopped the *in vitro* translation reactions at various time points and applied the reaction mixtures directly to monolayers of L929 cells to assay for cell binding. They concluded that $\sigma 1$ monomers were precursors of trimers and only $\sigma 1$ trimers were able to bind L929 cells. In conclusion, the $\sigma 1$ tail and head can form trimers independently. The T(ii) region in $\sigma 1$ tail is responsible for trimerization but it is not clear which region in the head is responsible for trimerization. The $\sigma 1$ trimer is the functional form that binds to the host cell.

It was shown that reovirus $\sigma 1$ undergoes conformational changes and adopts a more extended form during cell attachment and on ISVPs compared to virions (82,97). It was proposed that the extended conformation may facilitate cell binding and membrane

penetration. Electron microscopy analyses suggest that the σ 1 tail has two main flexible regions that may enable its conformational changes (94). One flexible region is composed of residues 155-164 in the T(ii) region named the interdomain region (IRD) 1. The IRD2 is near the globular head and made of residues 291-294 in the T(iv) region (30,94). Bokiej and colleagues designed 4 mutants to test if the length of σ 1 tail and the two IRDs were important for reovirus replication (30): mutant Δ 51-100, mutant Δ 83-155, mutant (IRD1) Δ 155-164 and mutant (IRD2) Δ 291-294. The symbol Δ indicates deletion. They concluded that truncation of reovirus σ 1 residues 51-100 or 83-155 decreased L929 cells binding by unidentified mechanism(s). Truncation of residues 155-164 (IRD1) impaired σ 1-virion association and this consequently decreased L929 cell-binding and replication of the virus.

Although crystal structure of σ 1 is available, the roles of σ 1 tail in virion association and reovirus replication are not well understood. Recently, Dietrich and her colleagues examined the coiled-coil-to-body transition region in the midpoint (residues 161-182) of σ 1 tail using X-ray crystallography (78). The authors observed that this transition region is highly conserved among all three serotypes of reovirus. They predicted that residues 161 and 182 are especially important in maintaining the stability of σ 1. At 48 hpi, mutant R161A and mutant N182A had a 100-fold reduction in viral titer and titer of mutant R161A & N182A was 1000 times lower than the wild-type virus in L929 cells. Both mutations did not affect cell binding or uncoating. However, each mutation reduced σ 1 levels by 50% and mutant R161A & N182A retained only 30% of σ 1 compared to the wild-type virus. Taken together, this study provided evidence that residues 161 and 182 played key roles in σ 1 encapsidation into the virion.

In summary, the $\sigma 1$ N-terminal regions of the tail are involved in multiple functions. The first 25 amino acids belong to the T(i) region and this region is known as the anchoring domain and it is connected to the virion via $\lambda 2$ -turret protein. The T(ii) regions is made of ~ 150 residues that form a long domain of α -helical coiled-coil. This region is responsible for $\sigma 1$ trimerization and coiled-coil-to-body transition region (residues 155-182) near the end of T(ii) is crucial to virion encapsidation.

1.5.2 The middle regions of the tail are important for virion association and sialic acid (SA) binding

The T(iii) region of reovirus $\sigma 1$ tail is composed of residues ~ 175 -240 that are rich in β -sheets and β -turns (186). This region shares structural similarity with the adenovirus fiber protein (94). However, it is unclear whether the two viruses evolved divergently from the same ancestor (53,134,186,257). The T(iii) region has a well-documented role in binding SA on host cell surface (52,76,196,207). SA (the name is used interchangeably with N-acetylneuraminic acid) is a general term for a family of neuraminic acids and they are one of the most diverse sugars found on glycan chains of mammalian cells (8,214). SA has nine carbons and is often linked to other sugars or glycan chains via the carbon at the 2-position (207,261). A study generated reovirus mutants with point mutations and showed that SA binding was completely abolished when any residue of 198, 202, 203 or 204 was altered. Residue 205 might also play roles in SA binding and the same study demonstrated that reovirus was capable of binding α -2,3-, α -2,6-, and α -2,8-sialic acid (207). In conclusion, the transition region (residues 161-182)

overlaps with the coiled-coil domain in T(ii), and the transition region was shown to play a pivotal role in virion association (especially residue 161 or 182, please refer to section 1.5.1). Residues 198, 202-204 may cooperate with each other in binding SA, as replacement of any of these residues leads to little or no agglutination with red blood cells *in vitro*.

1.5.3 The neck region of σ 1 is susceptible to proteolytic cleavage and the globular head mediates JAM-A binding

The T(iv) region is on the C-terminus of σ 1 tail which connects to the globular head. The region is also known as the “neck” region and consists of residues ~240-311. A mixed composition of α -helical coiled-coils and β -spiral repeats were identified in this region (186). From a study conducted in 1995, Nibert *et al.* observed that T3D, but not T1L ISVPs was sensitive to chymotrypsin (CHT) digestion (185). By exposing L929 cells with CHT-treated purified T3D virions, they showed that binding and titer of T3D were greatly impaired. Western blot analysis revealed that σ 1 was the sole protein that was cleaved by CHT. In a separate study, Chappell *et al.* subjected 8 T3D field isolates to Western blot analysis and observed that the viruses exhibited different sensitivity to CHT treatment (51). The authors proceed to compare their σ 1 sequences and concluded that residue 249 was the proteolytic cleavage site. Another group of researchers subjected σ 1 expressed by the baculovirus expression vector system to CHT digestion (84), and they separated the cleaved σ 1 fragments by SDS-PAGE. To determine the amino acid sequences that are susceptible to the proteolytic cleavage, they performed Edman degradation on σ 1 excised from SDS-PAGE and subjected the fragments for

high-performance liquid chromatography-mass spectrometry (88). Their data suggested that residues 245, 250 and 261 were susceptible to CHT cleavage. Residues 291-294 from the T(iv) region are thought to be more flexible compared to their region. However, removal of these residues did not seem to affect reovirus binding and replication in L929 cells (78). Taken together, these studies showed that the T3D σ 1 is susceptible to proteolytic cleavage in the intestine or *in vitro*. Multiple lines of evidence suggested that residues 245-261 in the T(iii) region are targets for such cleavage.

The globular head of σ 1 is at the C-terminus of σ 1 tail. The σ 1 head has a very compact structure and it is composed of eight-stranded β -barrel. The σ 1 head is known to bind JAM-A (described in section 1.2.1). JAM-A is a member of the immunoglobulin (Ig) superfamily and it is proposed to play roles in forming tight junctions (152). Crystal structures of the extracellular region of human (h) JAM-A revealed that JAM-A has two Ig-like domains that form a symmetrical dimer (D1 and D2) (204). Previously, it was thought that JAM-A bound reovirus only in dimer form, but Guglielmi and colleagues showed that JAM-A monomers were also able to bind σ 1 (109), and the residues that were important for σ 1 binding have been identified. A separate study examined crystal structure of σ 1-JAM-A complex and identified several amino acids on the σ 1 head that might be important for JAM-A binding (134). The authors evaluated their contributions of JAM-A binding by using a plasmid-based reverse genetics system to introduce single residue replacements in T3D virus. They concluded that residues 369, 380, 381, and 423 were important for JAM-A engagement. In addition to its well-documented role in binding JAM-A, σ 1 head is implicated in pathogenesis of the mouse CNS. However, its binding partner on the neuron remained to be elucidated. In conclusion, the head of σ 1 is

responsible for JAM-A binding and receptor binding in the mouse brain. This thesis will focus on the structure of $\sigma 1$ and its association with the virion.

1.6 A reovirus variant has a $\mu 2$ mutation that confers replicative advantage in post-uncoating step

The second main goal of this thesis was to identify mutation that augments reovirus oncolytic potency in post-uncoating step. During my screening of multiple variants, a variant was found to have a single amino acid change in the $\mu 2$ protein. A thorough introduction to $\mu 2$ structure and function is provided below, with a main focus on information relevant to this thesis. The linear protein structure and known functional domains of $\mu 2$ are depicted in Figure 1- 6.

1.6.1 $\mu 2$ may participate in genome transcription

In section 1.2.3, I briefly described $\mu 2$ as the polymerase co-factor, but how $\mu 2$ contributes to genome transcription is still not well-understood. Noble and Nibert were the first researchers to show $\mu 2$ possessed NTPase activities based on genetic analysis (188). Their discovery began with the characterization of ATPase activity from multiple T1L x T3D reassortants. They observed that the cores of reassortants exhibited different effectiveness in hydrolyzing ATP and GTP, and they mapped the differences contributed by the $\mu 2$ -encoding M1 gene. However, they failed to show that $\mu 2$ possessed NTPase activity. They first expressed $\mu 2$

by recombinant baculovirus and purified it by an immunoaffinity column. They measured the NTPase activity of purified $\mu 2$ and concluded it did not show NTPase activity (they didn't publish the methods and results of the experiment). The authors argued that maybe the protein was inactivated or misfolded during the purification process. Another genetic study suggested $\mu 2$ played roles in reovirus transcription (278). Yin and colleagues purified T1L, T3D and several T1L x T3D reassortants by cesium chloride gradients (their method is similar to procedures described in section 2.2.2). Purified virions were incubated with CHT to generate viral cores (a similar procedure is described in section 2.8). The cores were used to perform *in vitro* transcription assay (a similar procedure is described in section 2.9). Their results suggested that transcription activities of T1L and T3D cores were associated with different temperature optimum, and therefore, these unique properties allowed the researchers to use T1L x T3D reassortants to determine which gene was responsible for the phenotypic differences. By performing *in vitro* transcription assay with the core of reassortants, they concluded the M1 gene was involved in transcription and this was the first study to suggest that $\mu 2$ was involved in genome transcription by genetic analysis. In summary, early genetic analyses implicated that $\mu 2$ was an NTPase, but direct support from experimental data was lacking.

The first report provided biochemical evidence that $\mu 2$ had both NTPase and RTPase activities was published in 2004 by Kim and colleagues (132). They used baculovirus vector expression system to generate the wild-type T1L $\mu 2$ and another construct expressed the K415A/K419A $\mu 2$. $\mu 2$ has the nucleoside triphosphate (NTP) binding domain with motif A and motif B (Table 1- 3). The K415A/K419A $\mu 2$ had the lysine to alanine mutations for residues 415 and 419 was predicted to abolish NTPase activity. Purification of $\mu 2$ was done using a series of

ion-exchange and affinity columns. SDS-PAGE and immunoblotting with $\mu 2$ -specific polyclonal antiserum was performed to confirm the purified protein was $\mu 2$. ATPase activity of purified $\mu 2$ was measured by incubating $\mu 2$ with ATP and the release of free phosphate ion was determined by a colorimetric assay (please refer to a similar procedure described in section 2.8). The T1L $\mu 2$ was shown to hydrolyze ATP in a protein concentration-dependent manner, while the K415A/K419A $\mu 2$ failed to hydrolyze ATP. Furthermore, given that $\mu 2$ also has a second role in virus factory formation (described in section 1.2.4), the authors use IF staining to show both T1L $\mu 2$ and K415A/K419A $\mu 2$ could bind microtubules and μ NS; this suggested that the K415A/K419A mutation specifically abrogated ATPase activity and other functions of $\mu 2$ were spared. The study also provided evidence that $\lambda 3$ (reovirus polymerase) directly associated with wild-type or mutant $\mu 2$, as $\mu 2$ -specific polyclonal antibodies were able to pull down $\lambda 3$. To test the RTPase activity of $\mu 2$, wild-type or mutant $\mu 2$ were incubated with γ -labeled 45-nucleotide RNA substrates and thin-layer chromatography showed that only the wild-type $\mu 2$ was able to release the γ -phosphate from RNA molecules. This suggested that $\mu 2$ might be involved in the mRNA capping process (described in section 1.2.3), and importantly, the putative NTP binding domain was indispensable for both ATPase and RTPase activities. In conclusion, many members from *Reoviridae* were shown to encode for protein with highly conserved NTP binding domain. The NTP binding domain is involved in both ATPase and RTPase activities. Mutations in this domain do not affect $\mu 2$ -microtubule association nor the association of $\mu 2$ with $\lambda 3$.

1.6.2 Mu2 plays crucial roles in viral factory formation

Reovirus replicates in highly-specialized structures termed viral factories (also known as inclusion bodies). Functions of viral factories were briefly described in section 1.2.4. Broering *et al.* demonstrated that transfected μ NS itself was able to form viral factory-like structures in the absence of actual viral infection (39). However, these structures had globular shape and did not resemble the filamentous viral factories that were formed by reovirus infection (195). The same study further showed that when μ 2 is co-expressed, μ 2 and μ NS colocalized to microtubules (MT) by immunofluorescence microscopy analysis. The authors believed that μ 2 was responsible for redistributing μ NS to MT, because another study expressed μ 2 from reovirus-derived M1 gene and concluded that μ 2 colocalized with MT (195). Recently, a study identified μ 2 residues 283-325 were important for MT, μ NS and self-association by expressing truncated μ 2 in cells and co-localization of μ 2 and other proteins were visualized by IF staining (90). Residues 3-5 and 257-282 were found to be important for MT association. In summary, the soluble μ 2 protein is one of the main components of the viral factory and μ 2 also determines the morphology of viral factory.

Studies described so far showed μ 2 associated with μ NS in viral factory formation. However, it was not clear how μ 2 affected reovirus replication and why μ 2-MT and μ 2- μ NS associations were important. To answer those questions, Carvalho and colleagues transfected CV1 cells with M1-siRNA to knockdown T3D- μ 2 24 hours prior to exposing cells to T3D infection. The cells were harvested at 24 and 48 hpi and titered on L929 cells. Their results showed that viral titers were reduced to the input level at both time points (45). Next, they tested whether viral titer could be rescued by constructing a rescue plasmid that contained 3

silent mutations in the target sequence of M1-siRNA. In cells co-transfected with M1-siRNA and the rescue plasmid, yield of viral titer was rescued by greater than 100-fold at both 24 and 48 hpi. Results from this study suggested that protein expression of $\mu 2$ is required in cell for viral replication, and importantly, this study demonstrated that transfected $\mu 2$ could dramatically aid progeny yield. The authors further concluded that the rescue was microtubule-dependent by repeating the rescue experiment in CV1 cells. The microtubule-depolymerizing drug nocodazole at 6 hpi and rescue plasmid failed to restore viral yield. Taken together, $\mu 2$ has a well-defined role in associations with both MT and μNS in the formation of the viral factory. The current model proposes that that $\mu 2$ directly interacts with μNS and redistributes μNS to MT. μNS acts as a scaffold protein to recruit other reovirus proteins to the replication site for progeny assemble and synthesis (36-38,90,176).

1.6.3 $\mu 2$ mediates cellular responses

The reovirus $\mu 2$ protein is a multifunctional protein. In sections 1.6.1 and 1.6.2, I discussed its potential involvements in genome transcription and its crucial roles in the formation of the viral factory. It was observed that T3D reovirus was a strong IFN inducer, but also highly sensitive to the antiviral effects of IFN response, and therefore did not induce myocarditis in neonatal mice (229). On the other hand, T1L was shown to be a weak inducer of IFN response and the virus was able to induce myocarditis in mice. By using a panel of reassortant viruses, the $\mu 2$ -encoding M1 gene was mapped to be responsible for the phenotypic difference (228). To identify the residue of $\mu 2$ that was responsible for the

phenotypic difference, a study generated a panel of T1L-T3D chimeric viruses containing mutations in the M1 gene, and tested their induction of IFN signaling in L929 (118). Expression levels of IFN- β and IRF7 in mouse cardiac fibroblasts were monitored by performing quantitative reverse transcription polymerase chain reaction (RT-qPCR), the authors showed that a single amino acid change at residue 208 was solely responsible for the differences in IFN induction. The T1L virus had a proline, while their reported T3D had a serine. When residue 208 was occupied by a serine, gene expression of both IFN- β and IRF7 had a 2-fold increase at 24 hpi. Note that findings of this study are not relevant to our T3D lab strain, since our T3D strain has a proline at residue 208. Nevertheless, it is important to note that these studies implicate μ 2 in IFN repression or induction.

The role of μ 2 in mediating IFN response was documented by another study. Zurney and her colleagues infected L929 cells with T1L and T3D and at 20hpi, infected cells were exposed to IFN α/β treatment (291). By performing RT-qPCR and Western blot analysis, they observed that T1L infection was associated with reduced induction of downstream targets of IFN α/β including interferon-stimulated gene (ISG)-56, IRF7 and signal transducer and activator of transcription 1 (STAT1). They generate a panel of reassortants containing a mixture of genes derived from T1L and T3D, and identified that the M1 gene was responsible for the differences in IFN induction. By performing immunoblotting analysis of cytoplasmic- and nuclear-associated proteins, IRF9 was shown to accumulate in the nucleus in T1L infected L929 cells. IRF9 normally binds to STAT1 and STAT2 to form a functional complex to activate the IFN-stimulated response elements (ISRE) in the promoters of genes that encode proteins with antiviral effects (57). It is not clear why IRF9 is sequestered in the nucleus by T1L virus and how

this aids reovirus replication. The authors proposed that accumulation of IRF9 in the nucleus may prevent other activators from binding to the ISER, and thus sequestration of IRF9 in the nucleus may reduce antiviral effects. In conclusion, $\mu 2$ has been shown to mediate antiviral responses and aids reovirus replication.

The N-terminal residues 99-110 of $\mu 2$ are proposed to be the nuclear localization sequence (NLS) that is highly conserved among all 3 serotypes (135). Immunofluorescence analysis showed that transfected $\mu 2$ with truncated or altered residues in the NLS distributed exclusively in the cytoplasm, while the wild-type protein was found in both the nucleus and cytoplasm of HEK293T cells. To test the importance of NLS on viral replication, the authors generated HEK293T that stably expressed M1 shRNA to knockdown expression of $\mu 2$. The cells were first exposed to reovirus and then transfected with either wild-type $\mu 2$ or mutant with alterations in the NLS. Viral titers were decreased up to 100-fold. Taken together, the NLS of $\mu 2$ is essential for viral replication but its precise functions are not identified yet. Also, the C-terminal region of $\mu 2$ has not been characterized and this thesis will investigate its biological functions in the genome transcription and late stages of reovirus infection.

1.7 Objectives of this thesis

1.7.1 Chapter 3: Characterizing domains of $\sigma 1$ involved in sigma 1- virion association

We knew from our published data that reduced levels of $\sigma 1$ on virions directly enhanced reovirus oncolytic potency in the entry step (180).

In addition to the two published variants (T3v1 and T3v2), we also accumulated 6 additional variants that had enhanced replication on tumor cells owing to reduced $\sigma 1$ levels on virions. What was striking, was that the mutations spanned unique domains of $\sigma 1$, as well as other viral proteins. These variants raised an important question; how is $\sigma 1$ assembled onto virions and what domains, aside from the well-characterized “anchoring domain”, are involved in the assembly of $\sigma 1$? With the variants at hand, as well as additional $\sigma 1$ truncations and mutations that we generated, chapter 3 aimed to discover the contribution of $\sigma 1$ domains to various stages of $\sigma 1$ assembly.

Aim 1: To identify the mutations associated with each variant and whether they affect $\sigma 1$ levels.

Aim 2: To determine which regions in $\sigma 1$ are important for virion association.

Aim 3: To determine the contribution of $\sigma 1$ domains and $\sigma 1$ levels to virus infectivity.

1.7.2 Chapter 4: Identifying novel mechanism that enhanced reovirus oncolytic potency

With the knowledge that entry steps of reovirus infection in tumor cells can be enhanced by reduced sigma1 levels, we wondered if other steps of virus replication in tumor cells could also be enhanced by adaptation of reovirus. The second main goal of my project was therefore to identify a novel mechanism that enhanced reovirus replication at a post-entry step and independent from reduction of $\sigma 1$. To this end, five reovirus variants were generated

by directed evolution and screening tests were performed to assess $\sigma 1$ levels, cell binding and late steps of replication such as protein synthesis and progeny release.

Aim 1: To select a candidate variant of reovirus that replicates more efficiently in tumor cells (relative to wild-type T3D) due to post-entry and sigma1-level-independent mechanisms.

Aim 2: To isolate the mutation(s) responsible for enhanced replication of the candidate virus.

1.7.3 Chapter 5: Investigating how reovirus $\mu 2$ C-terminal loop regulated viral growth

I successfully identified a variant named T3v10^{M1} that possessed a mutation in the $\mu 2$ -encoding M1 gene. The $\mu 2$ protein is multifunctional, with roles in virus transcription, factory formation, and IFN regulation. Interestingly, the mutation is located in a previously-uncharacterized domain of $\mu 2$, and therefore the aim of Chapter 5 was to determine how the $\mu 2$ mutation promotes reovirus replication in tumorigenic cells. This thesis focuses on the post-uncoating step. An overview of reovirus replication and replicative steps investigated by this chapter is depicted in Figure 1- 7.

Aim 1: To investigate the effect of $\mu 2$ A612V mutation on core-associated functions such as transcription and onset of infection.

Aim 2: To determine the impact of $\mu 2$ A612V mutation on factory-forming functions such as μ NS and microtubule associations.

Gene	Size (bp)	Encoded Protein	Approximate Size (kDa)	Copies per virion	Location	Functions
S1	1416	$\sigma 1/\sigma 1s$	49	36/0	outer capsid	Cell attachment Cell tropism Apoptosis Cell cycle arrest
S2	1331	$\sigma 2$	46	150	Core	Weak dsRNA binding Interact with μ NS in viral factory
S3	1189	σ NS	41	0	Cell	ssRNA binding Viral factory development
S4	1196	$\sigma 3$	41	600	outer capsid	ssRNA binding Modulate cellular antiviral response Metal ion binding
M1	2304	$\mu 2$	83	20-24	core	NTPase RTPase Cell tropism Modulate cellular antiviral response Viral factory formation
M2	2203	$\mu 1/\mu 1c$ (Structural protein) $\mu 1N/\delta/\phi$ (cleaved from $\mu 1$ during cell entry)	75	600	outer capsid	Cell entry – membrane penetration Apoptosis
M3	2235	μ NS	80/75	0	cell	Viral factory formation
L1	3854	$\lambda 3$	142	10-12	core	RNA-dependent-RNA Polymerase
L2	3916	$\lambda 2$	143	60	core spike	Guanylyltransferase Methyltransferase Nascent mRNA exit site Interact with $\sigma 1$
L3	3896	$\lambda 1$	142	120	core	Helicase NTPase RTPase Bind ssRNA Bind dsRNA

Table 1- 1.T3D reovirus genome segments and their encoded proteins.

This table shows the 10 genes of reovirus and their protein products. The confirmed protein functions are also included.

Step	Variant Name	Mutations (Amino Acid Change) ¹	Domain Function	Phenotype	
Improving Potency	Attachment	T3DSA ⁻	<u>σ1</u> (R202W)	Sialic-binding	Reduced infection in some cells (e.g., HeLa) and <i>in vivo</i> pathogenesis in neonatal immunocompromised mice
		VeroAV	<u>σ1</u> (Q78P; N198K) <u>μ1</u> (E89G; A114V)	Trimerization; Sialic-binding	Enhanced binding to Vero Cells
		Jin-1	<u>σ1</u> (T193M; Q336R)	Sialic-binding; JAM-A binding	Infectious towards JAM-A deficient cells
		Jin-2	<u>σ1</u> (G187R; Q336R)	Sialic-binding; JAM-A binding	
		Jin-3	<u>σ1</u> (G196R)	Sialic-binding	
	Uncoating and Onset of Infection	T3D-S1His	<u>σ1</u> ((His) ₆ tag @ C-terminus)	Additional binding domain added	Ability to replicate in JAM-A-deficient U118 cells that express (His) ₆ -specific antibody fragment
		NA	<u>μ1</u> (A305L), (A276V), (D371N), (Q456R), (P497S), (L185S), or (E89Q)	μ1-μ1 interactions	Altered rates of ISVP → ISVP* and core production
		Y354H	<u>σ3</u> (Y354H)	C-terminal surface exposed domain	Enhanced disassembly and resistance to E64 protease inhibitor. Enhanced replication, dissemination and pathogenesis in immunocompromised mice
		T3v1	<u>λ1</u> (N138D)	Inner face of virion core	Enhanced particle infectivity and oncolytic activity <i>in vivo</i>
			<u>λ2</u> (M1101I) <u>λ3</u> (P400S)	Flap domain that open/close Core-facing surface	
T3v2	<u>σ1</u> (S18I)	Virion-anchoring domain			
Improving Specificity/Safety	Attachment	HTR1 (AV-Reo)	<u>σ1</u> (L116P; V127A; Q251STOP; I300M) <u>σ3</u> (S177E; H251L)	Trimerization; JAM-A binding	Reduced toxicity <i>in vivo</i>
		Antiviral Response	P4L-12	<u>σ3</u> (G198E; M221I) <u>μ1</u> (P315S; T449A) <u>μNS</u> (V705A)	
	NA		<u>μ2</u> (P208)	Methyltransferase domain	
	NA		<u>σ3</u> (R236), (R239), (K291), or (K293)	Unknown	Important in repression of interferon signaling
	ts453		<u>σ3</u> (N16K)	dsRNA binding domain	
			<u>μ1</u> association domain	Increased dsRNA binding and IFN resistance	

¹ Mutated residues in bold underline are suggested to play a dominant role in the variant phenotype.

Table 1- 2. Reovirus variants with altered replication in cancer cells.

Infectivity towards cancer cells was altered by previously published reovirus variants in two ways: 1. The entry step (cell-attachment and uncoating) of the replication cycle and 2. Modulation of antiviral response of the host cells. This figure is adapted from Mohamed *et al.* (180)

genpept	motif A		motif B		virus	protein	size	genus
	@xxxKgsGKsx@xxxL		@dSDxyGxxL					
AAL99936	411-AVLPKGSFKSTIMRVL--16aa--VDSDEVGEQM-452		mORV1	μ2	736aa	<i>Orthoreovirus</i>		
AAK54467	411-AVLPKGSFKSTIMRVL--16aa--VDSDEVGERM-452		mORV2	μ2	736aa	<i>Orthoreovirus</i>		
AAL99937	411-AVLPKGSFKSTIMRVL--16aa--VDSDEVGEQM-452		mORV3	μ2	736aa	<i>Orthoreovirus</i>		
AAM92736	406-LTLPKGSYKSTIIDTL--15aa--IDSDALGDSL-446		GCRV	VP5	728aa	<i>Aquareovirus</i>		
AAM93416	406-LTLPKGSFKSTIMIDTL--15aa--VSDHLGDSL-446		GIRV	VP5	728aa	<i>Aquareovirus</i>		
AAM92748	406-LTLPKGSYKSTIIDTL--15aa--IDSDALGDSL-446		GSRV	VP5	728aa	<i>Aquareovirus</i>		
BAA92426	351-VYAEKGGKTSFSLSTY--14aa--LSSDAYGRWL-390		BmCPV1	VSP4	561aa	<i>Cypovirus</i>		
AAN84546	351-VYAEKGGKTSFSLSTY--14aa--LSSDAYGRWL-390		DpCPV1	VP4	561aa	<i>Cypovirus</i>		
AAK73525	351-VYAEKGGKTSFSLSTY--14aa--LSSDAYGRWL-390		LdCPV1	unknown	561aa	<i>Cypovirus</i>		
AAP57257	353-VIGNKICIGKTRLTAEEL--09aa--IDSDYGFIF-387		FDV	hypoth.	594aa	<i>Fijivirus</i>		
AAN07092	353-VIGNKGVGKTEIGRMM--09aa--IDSDYGRFL-387		MRCV	P-S8	583aa	<i>Fijivirus</i>		
AAK77198	353-IIGNKGVGKSEIGAML--09aa--VSDYGRFL-387		RBSDV	core	591aa	<i>Fijivirus</i>		
BAA25151	358-LIGNKGGKSTLIRGM--09aa--VSDYGFIFL-392		OSDV	P9	583aa	<i>Fijivirus</i>		
BAA08548	399-VVANKGSGKTVLRKEL--07aa--IDSDYGFIF-431		NLRV	73.5KD	629aa	<i>Fijivirus</i>		
AAB63567	392-LIGPKASSKSFVTQRL--18aa--VSDAFGKVV-435		RRSV	Pns7	608aa	<i>Oryzavirus</i>		
AAG00074	383-LLGRKGGKSRSLKIF--07aa--LSDTYGKVL-415		CTFV	VP10	605aa	<i>Coltivirus</i>		
AAM18352	383-LLGRKGGKSRSLKTF--07aa--LSDTYGKVL-415		EYAV	VP10	605aa	<i>Coltivirus</i>		
BAC07519	416-MVGKKNKGKGMIGKLI--07aa--IDSDYGRVL-448		RArV	P6	634aa	<i>Mycoreovirus</i>		

Table 1- 3. The nucleoside triphosphate binding domain is well conserved in the *Reoviridae* family.

The above table shows a list of viruses from *Reoviridae* that are known to possess protein with NTPase activity. The table is adapted from (187).

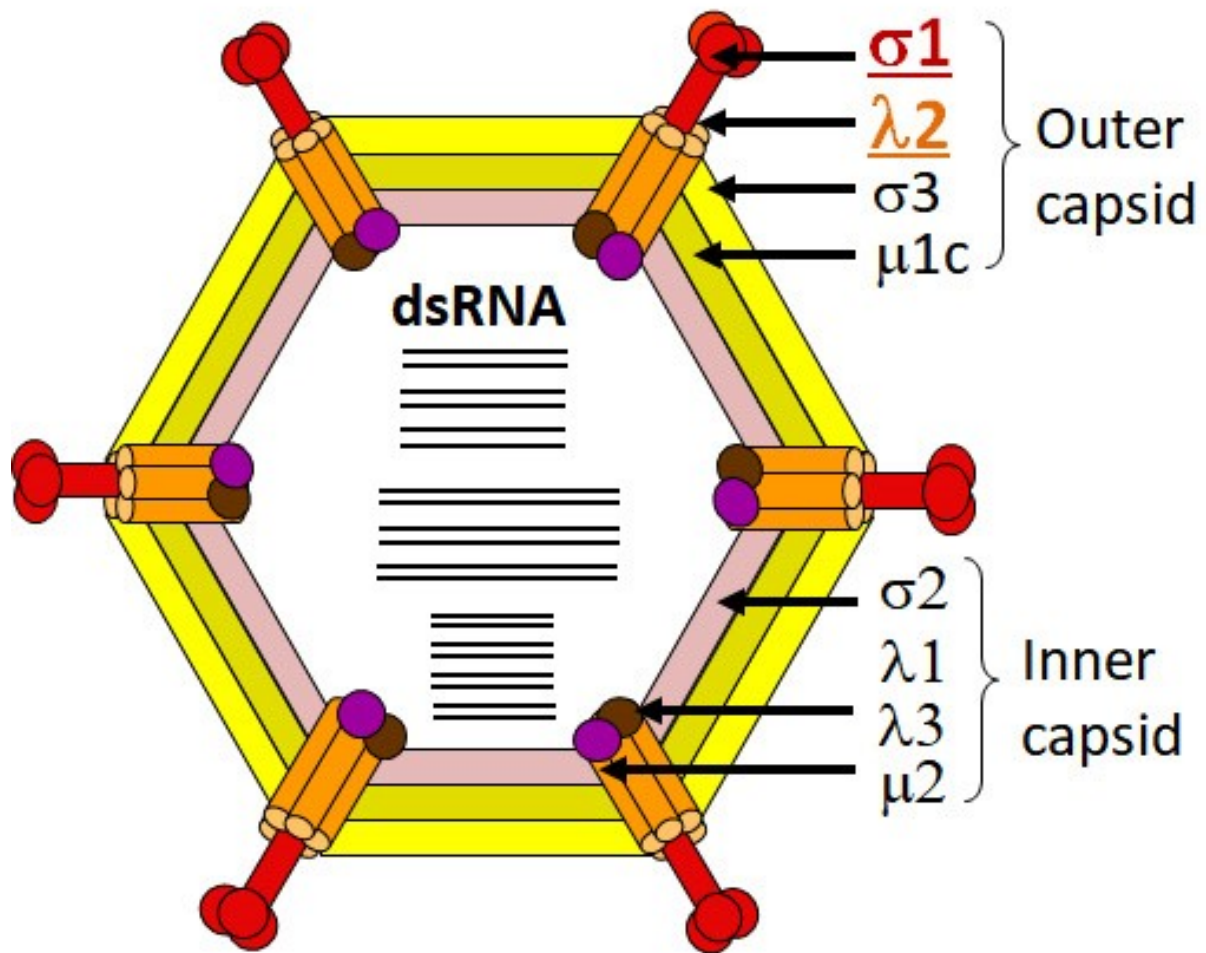


Figure 1- 1. Structure of T3D reovirus.

Reovirus is composed of the outer capsid and inner capsid (core). 10 linear dsRNA segments are enclosed by the core (figure courtesy of Dr. Shmulevitz).

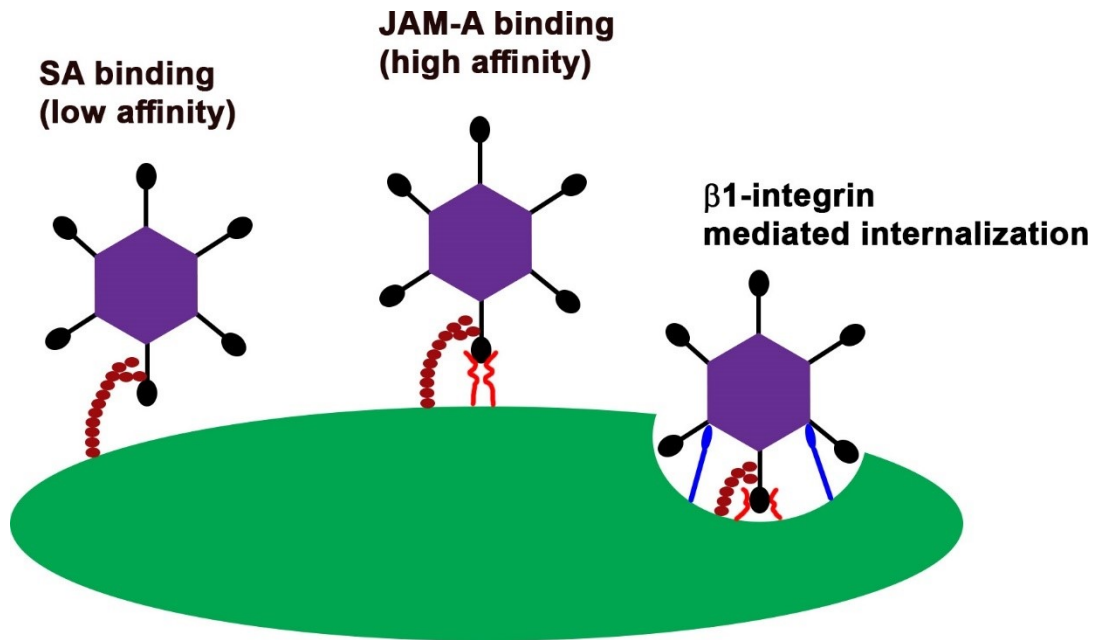


Figure 1- 2. Binding and entry of reovirus.

Reovirus enters host cell via three major steps. First, SA binding domain in the tail region of σ 1 initiates low-affinity interactions with SA on cell surfaces, followed by high-affinity binding between cellular JAM-A and the σ 1 head. Lastly, β 1-integrin interacts with the virion (probably via λ 2) to aid reovirus internalization.

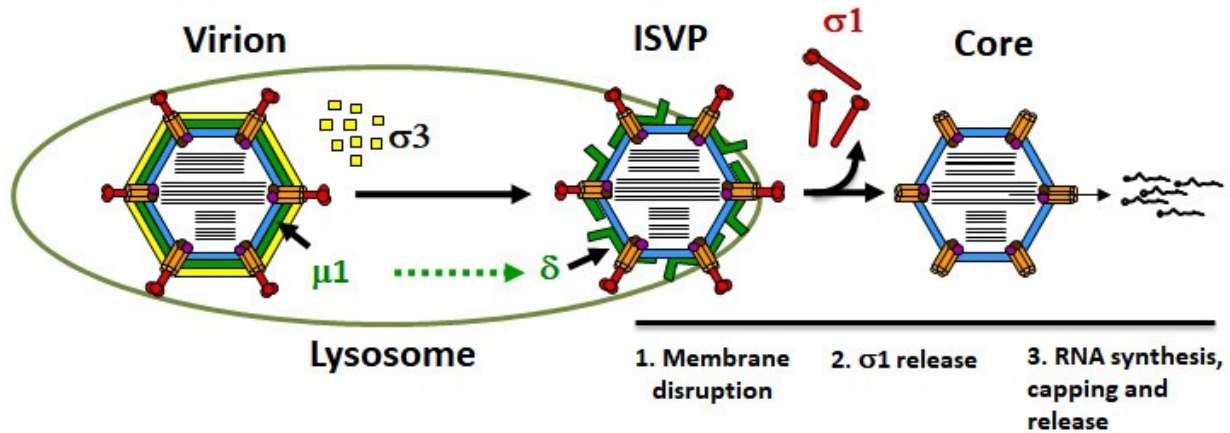


Figure 1- 3. Uncoating of reovirus.

Reovirus uncoats in the lysosome. Outer capsid protein $\sigma 3$ is completely degraded by proteases, exposing $\mu 1$ which is then cleaved to generate $\mu 1N$, δ and ϕ . ϕ and $\sigma 1$ remain on the virion creating the infectious subvirion particle (ISVP). Sustained proteolysis completely removes $\sigma 1$, $\mu 1N$ and ϕ , leaving δ on the viral structure known as ISVP*. ISVP* can penetrate the lysosomal membrane and translocate into the cytoplasm. ϕ is released or degraded by an unidentified mechanism. Once the outer capsid is completely removed, the core (inner capsid) can initiate genome transcription (figure courtesy of Dr. Shmulevitz).



Figure 1- 4. Structure and cleaved products of $\mu 1$.

During the uncoating step in the reovirus replicative cycle, $\mu 1$ is cleaved into 4 major fragments. The proposed functions of each fragment are shown on the right. The $\mu 1N$, δ and ϕ fragments are proposed to aid membrane penetration during reovirus infection. It is unclear whether $\mu 1$ or $\mu 1C$ is the dominant structural protein associated with the virion. Cleavage of $\mu 1$ to $\mu 1C$ can be an artifact associated with electrophoresis in denaturing conditions (191).

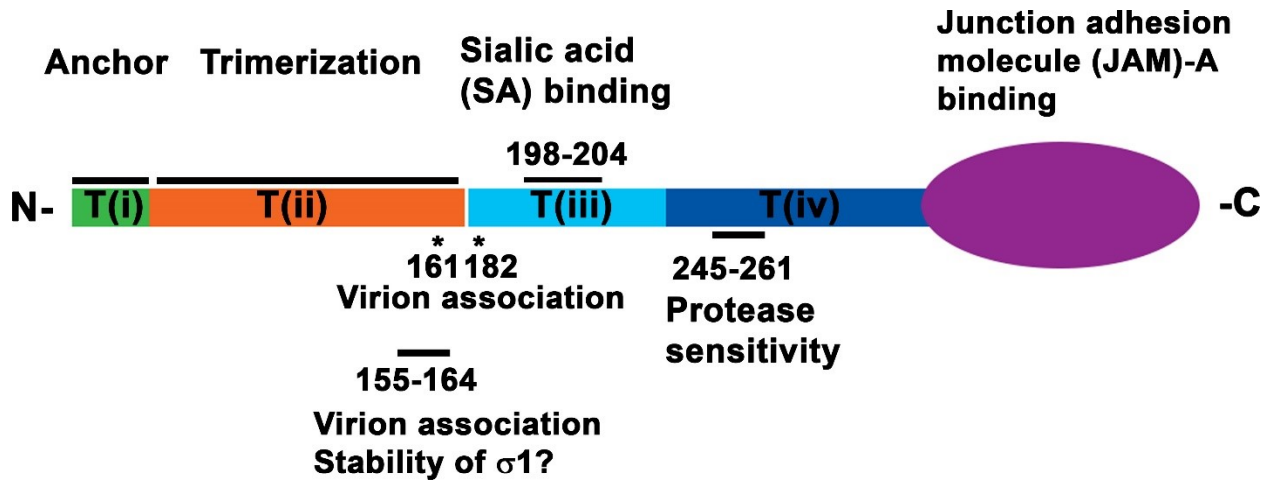


Figure 1- 5. Structure and known functions of $\sigma 1$.

The reovirus cell-attachment protein $\sigma 1$ is composed of 455 amino acids. It has the tail and globular head domains. Known functions of distinct domains or residues are indicated.

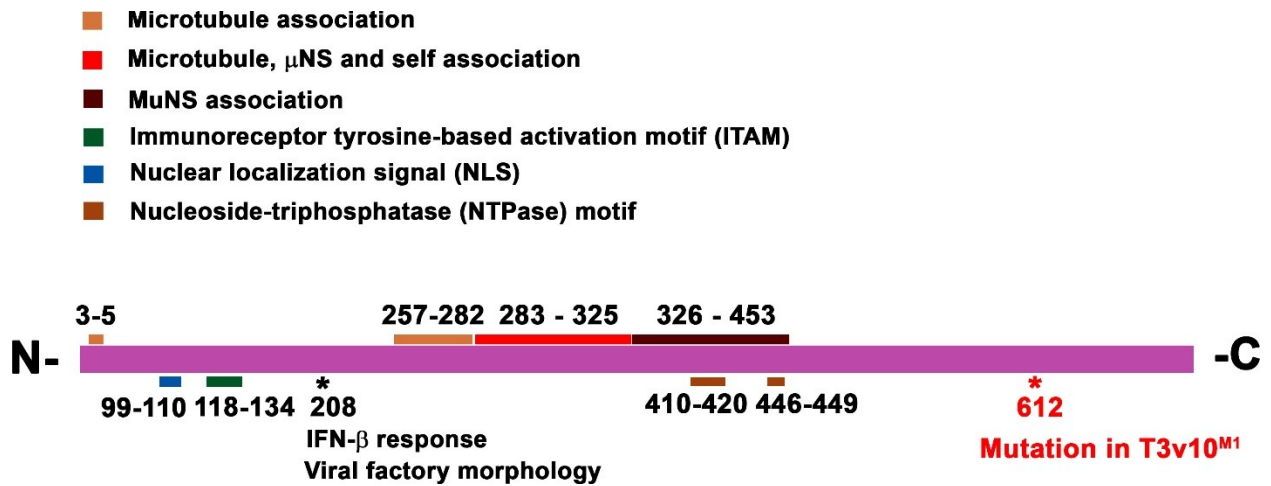


Figure 1- 6. Structure and known functions of μ 2.

The T3D μ 2 is 736-amino-acid long. The crystal structure of μ 2 is currently not available and a linear protein structure is shown. Variant T3v10^{M1} is the focus of chapter 5 of this thesis and it has an altered 612 residue.

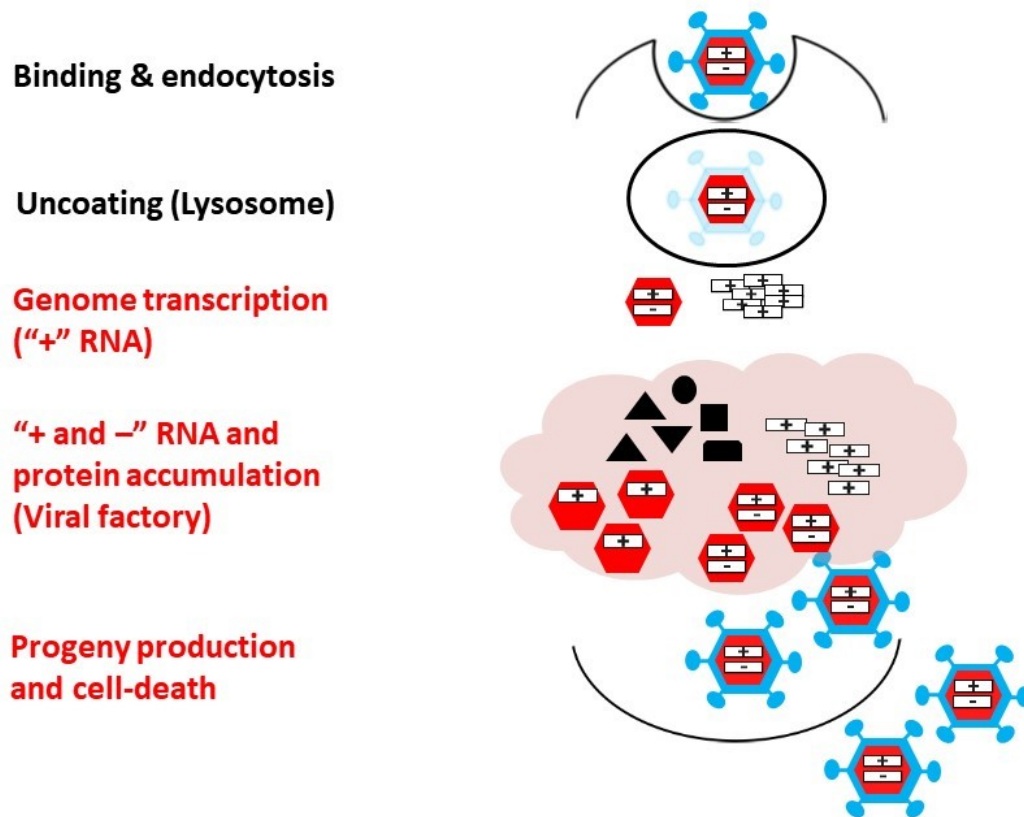


Figure 1- 7. Replication cycle of reovirus.

Reovirus takes an average of 24 hours to complete one replication cycle. Variant T3v10^{M1} forms bigger plaques on L929 cells and its sole mutation in $\mu 2$ does not promote the entry steps. Chapter 5 focuses on replicative steps in red text. The $\mu 2$ is also known to cooperate with μNS and microtubule; their interactions are explored.

CHAPTER 2: METHODS AND MATERIALS

2.1 Cell lines and culturing conditions

Please refer to Table 2- 4 for product numbers and manufacturers.

Cells:

L929 (Transformed mouse fibroblast)

NIH3T3 (Non-transformed mouse fibroblast)

NIH3T3-Ras (NIH3T3 transformed by Harvey ras oncogene)

Culture medium (adherent culture):

MEM supplemented with 2mM L-glutamine (Sigma), 10% fetal bovine serum (Sigma/Gibco), 1x

MEM non-essential amino acids (Gibco), 1x antibiotic antimycotics (Thermo Fisher) and 1mM

sodium pyruvate (Thermo Fisher)

Subculture routine:

When cells reach 90-100% confluency, remove medium and rinse twice with 1x PBS

(Gibco/Focus Biosciences), incubate with Trypsin-EDTA (0.25%)(Gibco) at 37°C with 5% CO₂ until

cell detach. Dilute cells with fresh culture medium at 1:8-1:10 ratio when cells reach 90-100%

confluency.

Cells:

H1299 (Human lung carcinoma cell)

Culture medium (adherent culture):

RPMI 1640 (Thermo Fisher) supplemented with 2mM L-glutamine (Sigma), 10% fetal bovine serum (Sigma/Gibco), 1x MEM non-essential amino acids (Gibco), 1x antibiotic antimycotics (Thermo Fisher) and 1mM sodium pyruvate (Thermo Fisher)

Subculture routine:

When cells reach 90-100% confluency, remove medium and rinse twice with 1x PBS (Gibco/Focus Biosciences), incubate with Trypsin-EDTA (0.25%)(Gibco) at 37°C with 5% CO₂ until cell detach. Dilute cells with fresh culture medium at 1:5-1:8 ratio when cells reach 90-95% confluency.

Cells:

T47D (Human breast cancer cell)

MDA-MB-231 (Human breast cancer cell)

HEK 293T (Human embryonic kidney 293 cell expressing SV40 large T antigen)

BHK-T7 (Baby Hamster Kidney fibroblast containing T7 RNA polymerase)

Culture medium (adherent culture):

DMEM (Sigma) supplemented with 2mM L-glutamine (Sigma), 10% fetal bovine serum (Sigma /Gibco), 1x MEM non-essential amino acids (Gibco), 1x antibiotic antimycotics (Thermo Fisher) and 1mM sodium pyruvate (Thermo Fisher)

For BHK-T7 cells, they were further maintained in 1 mg/ml Geneticin (InvivoGen, San Diego, CA) every second passage.

Subculture routine:

When cells reach 90-100% confluency, remove medium and rinse twice with 1x PBS (Gibco/Focus Biosciences), incubate with Trypsin-EDTA (0.25%)(Gibco) at 37°C with 5% CO₂ until cell detach. Dilute cells with fresh culture medium at 1:8-1:10 ratio when cells reach 90-100% confluency.

Cells:

L929 (Transformed mouse fibroblast isolated from subcutaneous connective tissues)

Culture medium (free-float culture):

Culture medium was made from powder of Minimum Essential Medium Joklik's Modification (JMEM, Sigma), 1 Litre of medium (JMEM powder 11 g, NaHCO₃ 2.2 g, HEPES Sodium Salt 1.3 g, Glucose 1g, in 1 L of H₂O at pH 7.2) was supplemented with 5% fetal bovine serum (Sigma/Gibco), 1x MEM non-essential amino acids (Gibco), 1x antibiotic antimycotics (Thermo Fisher) and 1mM sodium pyruvate (Thermo Fisher). The final medium is known as "JMEM medium"

Subculture routine:

When confluency reaches 10⁶ cells/ml, dilute cells with fresh culture at 1:4-1:5 ratio.

2.2 Virus

2.2.1 Stock

Lab strain of T3D (referred as T3wt in this thesis) was given as a gift from Dr. Patrick Lee (Dalhousie University). The virus was originally obtained from Dr. L.W. Cashdollar.

2.2.2 Production and purification

Vertrel® XF-CsCl density-gradient centrifugation (large scale purification)

Four 150cm² dishes with 100% confluent L929 were detached by Trypsin-EDTA (0.25%)(Gibco). Detached cells were mixed with 10ml JMEM medium (please see 2.1 Cell lines and culturing conditions) and added to a sterile 2L flat bottom flask with a metal stir bar containing 1L of JMEM medium. The flask was placed on a magnetic stirrer and stirred at low speed in the warm room without CO² regulation (37°C). Cell density was monitored every 24 hours until it reached 10⁶ cells/ml. Reovirus was inoculated into the flask at multiplicity of infection (MOI) of 0.01. Cell-death was monitored every 24 hours by performing Trypan Blue staining (Gibco, 15250061) using automatic cell-counter (Biorad). Cells were collected at 60-80% cell-death. Cells were pelleted at 1000g for 15 minutes. Cell pellet was resuspended in 15ml homogenization buffer (10mM Tris pH 7.4, 250mM NaCl, 10mM β-mercaptoethanol). Cell lysate was either frozen at -80°C or processed immediately.

For virus purification, cell lysate was transferred to a 50ml conical centrifuge tube and mixed with 10ml DuPont™ Vertrel® XF (Dymar Chemicals Limited, product number not available) and vortexed at maximum speed for 5 minutes, followed by probe sonication for 10 seconds to ensure complete lysis of cells. Phase separation was performed by centrifugation at 1500g for 10min at 4°C. The top aqueous layer (containing reovirus) was transferred to a new 50ml conical centrifuge tube and mixed with 10ml vertel XF. Phase separation was performed one more time following the above steps. The aqueous layer was layered on a CsCl gradient (9ml 1.4g/cc, 9ml 1.2g/cc) in SW28 ultra-clear tube. CsCl gradient ultracentrifugation was

performed at 100,000g at 4°C for 12-18 hours, resulting in a clear band that was extracted by a needle and syringe (Figure 4- 1). To remove CsCl, the extracted solution was loaded in dialysis tubing (10-20KDa) and dialyzed in dialysis buffer (10mM Tris pH 7.4, 150mM NaCl, 10mM MgCl). The dialysis buffer was changed every 6-12 hours for two more times. The dialyzed virus was transferred into 1.5ml eppendorf tube. Impurities or sediments were allowed to settle to the bottom of tube overnight at 4°C.

Capto Core 700 in-slurry (chapter 3, small or medium-scale purification)

Monolayer of L929 cells in 150mm plate were infected by reovirus. Infection was stopped when about 50% live cells remained, as confirmed by Trypan Blue staining (Gibco, 15250061). Infected cells were frozen and thawed at least three times. Cell lysate was transferred to a 50ml conical centrifuge tube and mixed with 10ml DuPont™ Vertrel® XF (Dymar Chemicals Limited, product number not available) and mixed thoroughly by inverting, followed by probe sonication for 10 seconds to ensure complete lysis of cells. The top aqueous layer (containing reovirus) was transferred to a new 50ml conical centrifuge tube and mixed with 10ml vertel XF. Phase separation was performed one more time following the above steps. The aqueous layer was transferred into the SW40Ti ultra-clear tube and centrifuged at 100,000g for at least 90 minutes. Supernatant was removed and the pellet was resuspended with 250µl of dialysis buffer. Reovirus in dialysis buffer was transferred to a 1.5ml eppendorf tube. Three hundred 300µl of Capto Core 700 beads in PBS (GE Healthcare Life Sciences, 17548102) was added to the sample and the mixture was allowed to incubate at 4°C for at least 10 hours with gentle agitation. To collect reovirus in the supernatant, the mixture was filtered

with 0.45 µm regenerated cellulose GD/X filter (GE Healthcare Life Sciences, 6869-2504) and collected into a 1.5ml eppendorf tube. Impurities or sediments were allowed to settle to the bottom of tube overnight at 4°C.

2.2.3 Viral infection and plaque assay

Ten-fold serial dilutions were performed by mixing reovirus with plain culture medium. The mixtures were added to 100% confluent monolayers of L929 cells (please see Table 2- 1 for volumes). L929 cells were allowed to incubate with reovirus for 1 hour at 37°C with gentle swishing every 5-10 minutes (this is the standard procedure for reovirus infections). Viral mixtures were aspirated. For a single well in 6-well plate, 2ml of culturing medium (containing 0.5ml of 2% percent agar in 1xPBS) was added on top of the cells. Formation of plaques (please see the paragraph below) was monitored every 24 hours. When plaques were seen, 4% formaldehyde solution was added on top of the agar and incubated for 2-4 hours. 4% formaldehyde solution was discarded and the agar was removed by scooping (may proceed to immunocytochemistry from here). Cells were fixed with methanol for 5-10 minutes at room temperature. After methanol was discarded, cells were incubated with 1% crystal violet solution for at least 5 minutes, followed by rinsing with warm tap water.

Growth rates of reovirus depended on cell lines. For the non-transformed NIH3T3 cells, plaque assays were stopped 7 days post-infection, and 3-4 days for all transformed cells (H1299, T47D, B16, L929).

2.3 Infectivity assays

2.3.1 Cell-based enzyme-linked immunosorbent assay (ELISA)

- Please refer to Table 2- 1 for volumes, Table 2- 2 for antibody information and Table 2- 3. List of common buffers.
- Infection was performed as described in section 2.2.1 Viral infection and plaque assay.

Cells were seeded into clear 96-well plates (Corning) and infection was performed as described except that one-third dilutions of reovirus were usually used. At 18 hour-post-infection (hpi), medium was discarded. Cells were rinsed with 1xPBS and fixed with methanol for at least 5 minutes (at room temperature if processed immediately or at 4°C overnight). Methanol was discarded and cells were rinsed with 1xPBS. For each well, 200µl of blocking solution was added and incubated for 1 hour at room temperature or at 4°C overnight. After the blocking buffer was discarded, 50µl of Rabbit anti-reovirus was added to each well and incubated for at least 2 hours at room temperature with gentle rocking. Cells were rinsed with PBST and incubated with goat anti-rabbit AP for one hour at room temperature with gentle rocking. Cells were rinsed with PBST with incubating with 200ul para-Nitrophenylphosphate (pNPP)(VWR, CA95054-268 [discontinued]) mixture diluted in Diethanolamine Buffer (97 ml diethanolamine with 100 mg MgCl₂ in 1 L of H₂O, adjusted pH to 9.8) at 1 mg/ml, followed by incubation in the dark at room temperature and scanned at the desired time points on the Perkin Elmer plate reader with Wallace Envision Manager software at 405 nm.

2.3.2 Immunocytochemistry

- Please refer to Table 2- 1 for volumes, Table 2- 2 for antibody information and Table 2- 3. List of common buffers.
- Infection, cell fixing and agar overlaying were performed as described in section 2.2.1 Viral infection and plaque assay.

Following the removal of agar, cells were rinsed with 1xPBS and incubated with blocking buffer for one hour at room temperature. After the blocking buffer was discarded, cells were incubated with rabbit reovirus antiserum for at least 2 hours at room temperature with gentle rocking or at 4°C overnight. Cells were rinsed 3 times with PBST, followed by secondary antibody (goat anti-rabbit AP) incubation for at least 2 hours at room temperature with gentle rocking. Cells were rinsed 2 times with PBST and incubated with 5-bromo-4-chloro-3-indolyl phosphate (BCIP)(Sigma, D4551) nitro blue tetrazolium (NBT)(Sigma, N6639) substrates diluted in AP buffer (1:100). The plate was stored in a dark place at room temperature and visually confirmed for dark-purple staining of infected cells every 10 minutes. The reaction was stopped by discarding BCIP/NBT mixture and addition of 1xPBS with TE buffer.

2.3.3 Immunofluorescence

- Please refer to Table 2- 1 for volumes, Table 2- 2 for antibody information and Table 2- 3. List of common buffers.
- Infection was performed as described in section 2.2.1 Viral infection and plaque assay.

Cells were seeded on circle coverslips (0.13mm thickness or 0.17mm thickness, Thermo Fisher) in 24-well or 12-well plates. Cells were infected as described above. Infected cells were fixed at the desired time points and fixed with 4% (paraformaldehyde) PFA for 30 minutes at room temperature. After two washes with 1xPBS, cells were permeabilized with 1xPBS with 0.2% Triton X-100 for 20 minutes at room temperature. Cells were washed 3 times with 1xPBS and incubated with a chosen primary antibody for at least 2 hours at room temperature or overnight at 4°C. After 3 washes with 1xPBS, cells were incubated with the mixture containing a secondary antibody conjugated to a fluorochrome and 0.3µg/ml Hoechst 33342 (Thermo Fisher) for at least 2 hours in a dark place at room temperature. Cells were washed 2 times with 1xPBS and the coverslips were lifted by forceps and mounted on glass slides using 15ul of VECTASHIELD® Antifade Mounting Media (Vector Laboratories). The coverslips were sealed by nail polish and the glass slides were visualized by Olympus IX-81 spinning disk confocal microscope (Quorum Technologies) or stored in the dark at 4°C.

2.4 Flow cytometry

- Please refer to Table 2- 1 for volumes, Table 2- 2 for antibody information and Table 2- 3. List of common buffers.
- Infection was performed as described in section 2.2.1 Viral infection and plaque assay.
- Before each wash, cells were pelleted by centrifugation at 600g for 5 minutes unless specified otherwise.

Monolayers of reovirus-infected cells was rinsed 3 times with 1xPBS and detached by Trypsin-EDTA (0.25%)(Gibco). Trypsinized cells were quenched with cell culture medium and cell pellet was collected by centrifugation at 600g for 5 minutes at room temperature. The supernatant was discarded and cells were resuspended in 4% PFA and incubated on ice for 20-30 minutes. After 3 washes with 1xPBS, cells were permeabilized with 1% Triton X-100 and 3% BSA in 1xPBS for one hour at room temperature with gentle mixing. Primary antibody in blocking buffer was added to the sample and incubated for at least 3 hours at room temperature or overnight at 4°C. Cells were washed 3 times with 1xPBS and incubated with secondary antibody conjugated to a fluorochrome for at least 2 hours in a dark place at room temperature. Cells were rinsed 2 times with 1xPBS and resuspended in flow buffer (1xPBS with 1mM EDTA and 2% fetal bovine serum). Samples were processed by the FACSCanto (BD Biosciences) and a minimum of 10,000 cells were detected. Data was analyzed by FSC Express 6 (De Novo Software).

2.4.1 Annexin V staining assay

L929 cells in 35mm dishes were exposed to T3wt (at MOI of 2.8) or T3v10^{M1} to express the equivalent amount of viral proteins. Cells were detached using 0.5ml CellStripper (Corning, 25-056-CI) by gentle agitation at 12, 15 and 18 hpi. Half of cell lysates were subjected to Western blot analysis (please refer to section 2.11) and at least 2x10⁶ cells were labelled with PE Annexin V and 7AAD (BD Biosciences, 556422) according to the manufacturer's instructions. Samples were processed by the FACSCanto (BD Biosciences) and a minimum of 10,000 cells

were detected. Setting up of controls and gating of cells were aided by Dr. Aja Rieger from the Faculty of Medicine and Dentistry Flow Cytometry Facility. Data was analyzed by FSC Express 6 (De Novo Software).

2.5 Virus release assay

- Please refer to Table 2- 1 for volumes and Table 2- 3. List of common buffers.
- Infection and plaque assay were performed as described in section 2.2.1 Viral infection and plaque assay.

To determine the percentage of progeny released by infected cells, 35mm dish was removed from the incubator at the desired time points. The dish was swirled gently to make sure the medium was evenly mixed. The medium (containing the released progeny) was transferred to a 15ml conical tube (Corning) and flash-frozen immediately. 1ml of 1xPBS was added to the 35mm plate and the plate was stored at -80°C. Before titering, the 35mm plate would be frozen and thawed at least 3 times to ensure the cells were fully lysed. After the last thawing, cells were detached by 0.5ml CellStripper (Corning, 25-056-CI) by gentle agitation and cell lysate was transferred to 15ml conical tube. The medium (containing the released progeny) and cell lysate (intracellular virus) were plaqued on monolayers of L929 cells independently. Percentage of release was calculated by dividing titers from the released progeny by (titers from the released progeny and titers from cell lysate).

2.6 Binding assays

To compare cell binding of reovirus, L929 cells at 100% confluency were prechilled at 4°C and exposed to equal amount of T3wt (at MOI of 4) or another reovirus variant (standardized by Coomassie Blue staining, please refer to Figure 4- 4) for one hour at 4°C with agitation every 5 minutes (all subsequent steps were performed at 4°C). Unbound virus was removed by three independent washes with ice-cold 1xPBS. Cells were detached by treating with Trypsin-EDTA (0.25%)(Gibco), and collected into 1.5ml eppendorf tube. Cells were pelleted by centrifugation at 1000g for 5 minutes, followed by two washes with 1xPBS. Cell pellets were either subjected to Western blot analysis or flash-frozen and stored at -80 °C.

2.7 Coomassie Blue staining

CsCl-purified reovirus was subjected to SDS-PAGE (10-12% gels, made in-house). All SDS-PAGE or native gels were made using Mini-PROTEAN® Casting Frame (BioRad, product number 1653304). The gel was run at 100V for 140 minutes at room temperature. Upon completion of the electrophoresis, the gel was rinsed with distilled water, followed by incubation with Imperial™ coomassie staining for at least 3 hours at room temperature with gentle rocking. The gel was destained using distilled water. Distilled water was changed as needed until viral protein bands were clearly visible. Protein bands were visualized by ImageQuant LAS4010 imager (GE Healthcare Life Sciences).

2.8 Agarose gel analysis of whole reovirus

To determine the volume of virus to be loaded on agarose gel, CsCl-purified reovirus was subjected to SDS-PAGE and quantified by Coomassie Blue staining. Equivalent viral particles were diluted with 5% Ficoll and 0.05% bromophenol blue and subjected to electrophoresis on a 1.0% agarose gel in TEA buffer (40mM Tris-HCl, 5 mM sodium acetate, 1mM EDTA [pH 7.3]) (140) at 10mA for 16 hours at room temperature. All agarose gels were made using the Original UV-Transparent Mini-Gel Tray (BioRad, product number 1704330). Reovirus-loaded agarose gel was rinsed with distilled water and stained with Imperial™ Protein Stain (Thermo Fisher, 24615) overnight. Reovirus species were visualized by UV transillumination on the ImageQuant LAS4010 imager (GE Healthcare Life Sciences).

2.9 Viral core generation and rNTP hydrolysis assays

Full virions of T3wt and T3v10^{M1} (previously subjected to SDS-PAGE and stained by Coomassie Blue staining, standardized and qualified. A minimum 5x10¹¹ viral particles were used) were incubated with 16ug/ml chymotrypsin (CHT) for 3 hours in a water bath set to 37°C. Conversion of full virions to cores of was confirmed by SDS-PAGE and Coomassie Blue staining (Figure 5- 2). The rNTP hydrolysis reactions were performed using 1.5ml eppendorf tube for the ease of manipulation and incubation. Reaction mixtures were transferred to 96-well plate (CELLSTAR) before detection. For each reaction, 0.1mM of rATP/rCTP/rGTP/rUTP was used and incubated with viral core for the desired length of incubation at pH of 7.0. The reaction mixtures were prepared using the Phosphate Assay Kit (Abcam, product number: ab65622)

according to the manufacturer's instructions.

2.10 *In vitro* reovirus core transcription assay and in cell transcription assay

The optimal amount of viral cores used for *in vitro* transcription assay was determined by preliminary experiments by incubating various volumes of T3wt full virions with CHT (section 2.9), and the cores were subjected to *in vitro* reovirus core transcription assay described below. Once the optimal amount of cores was determined (minimum of 10^{10} viral particles), it was used as a standard in Coomassie Blue staining for sequential experiments. To assess transcription activity of T3v10^{M1} core, equivalent amount of T3wt and T3v10^{M1} viral cores were resuspended in a mixture containing 2mM of ATP, CTP, GTP and UTP, 100mM Tris-HCl (pH8.0), 10 mM MgCl₂, 100 µg/ml pyruvate kinase, 3.3 mM phosphoenolpyruvate and 600 U/ml RNase inhibitor. For negative controls, ATP was omitted. The reaction mixtures were incubated at 40°C for the indicated durations. At the end of incubation, 400 µl TRIzol LS Reagent (Invitrogen, Cat: 10296010) containing 15 ng/ml green fluorescence protein (GFP) RNA generated by using T7 RiboMAZ *in vitro* transcription reactions (Promega) (according to the manufacturer's instructions) was added to each sample for normalization. The samples were frozen at -80°C or proceed with RNA extraction.

2.10.1 RNA extraction and detection

To extract RNA, 100µl of chloroform (Sigma, 319988) was added to each sample. Samples were mixed by vortex for 30 seconds, followed by centrifugation at 12,000g for 15

minutes at room temperature. Three-hundred μl of the aqueous layer was transferred to a new 1.5ml eppendorf tube and 0.5 μl of RNA-grade glycogen (Sigma, R0551) was added to each tube. To precipitate RNA, 250 μl of isopropyl alcohol was added to each tube and mixed by inverting for 30 seconds. Samples were centrifuged at 12,000g for 10 minutes at room temperature. Supernatant was carefully poured off and 250 μl of 75% ethanol was added to resuspend pellet and mixed by brief vortexing. Samples were centrifuged at 12,000g for 10 minutes at room temperature and ethanol was carefully poured off. To remove the residual ethanol, tubes were centrifuged at 12,000g for 3 minutes at room temperature and the remaining ethanol was removed by a 200 μl pipette tip. The tubes were left uncapped to air-dry the pellet for 10 minutes at room temperature. The pellet was resuspended with UltraPure™ DNase/RNase-Free water (Invitrogen, 10977015). Reovirus and GFP RNA levels were quantified by iScript One-Step RT-PCR Kit with SYBR Green (BioRad, SKU:1708892) according to manufacturer's instructions and RT-qPCR reactions were executed using a CFX96 system (BioRad).

2.10.2 In cell transcription assay

For the in-cell transcription assay, infections were performed with the presence of cycloheximide (CHX) or without CHX. Six-well plates were used and 2ml of medium was used per well for both conditions. For the CHX condition, cells were pre-exposed to CHX (Calbiochem, 239763) at a concentration of 50 $\mu\text{g}/\text{ml}$ 30 minutes before reovirus exposure. Cell medium was replaced by medium containing 50 $\mu\text{g}/\text{ml}$ of CHX every 6 hours to ensure CHX was working properly treatment efficiency (Figure 5- 5).

For the in-cell transcription assay, L929 cells were exposed with equal cell-bound T3wt or T3v10^{M1} (MOI = 4), unbound viruses were washed by 1xPBS and RNA were collected at the indicated time-points (Figure 5- 5 and Figure 5- 8). To collect RNA, cells were rinsed with PBS once and 1ml of TRIzol (Thermo Fisher, Cat: 15596026) was added to each well. Cell lysate was mixed by pipetting until it was homogeneous and has relatively low-viscosity. Two hundred μ l of chloroform (Sigma, 319988) was added to each sample. Samples were mixed by vortex for 30 seconds, followed by centrifugation at 12,000g for 15 minutes at room temperature. Four-hundred μ l of the aqueous layer was transferred to a new 1.5ml eppendorf tube. Three hundred μ l of 100% ethanol to aqueous phase and vortex briefly to mix. Viral RNAs were purified by GenElute Total RNA Purification Kit (Sigma, SKU: RNB100-100RXN) according to manufacturer's instructions and reovirus RNA levels were quantified as described above.

2.11 Cell lysate collection and Western blot analysis

- Please refer to Table 2- 1 for volumes, Table 2- 2 for antibody information and Table 2- 3. List of common buffers.

Cells from 35mm dish were rinsed with 1xPBS and detached by Trypsin-EDTA (0.25%)(Gibco). Detached cells were transferred to 1.5ml eppendorf tube. Cells were pelleted at 1500g for 5 minutes at room temperature. The cell pellet was resuspended and lysed with 200ul RIPA buffer (50mM Tris pH 7.4, 150mM NaCl, 1% IGEPAL CA-630 (NP-40), 0.5% sodium deoxycholate, 1x inhibitor cocktail [11873580001, Roche]) by vortexing. A 1:5 volume of 5x protein sample buffer (0.5M Tris-HCl pH6.8, 40% glycerol, 5% SDS, 12.5% β -mercaptoethanol, 0.05% bromophenol blue) was added to the cell lysate. The sample was heated to 100°C by

heat block for 10 minutes. After a brief centrifugation, the sample was flash-frozen and stored at -20°C or immediately subjected to SDS-PAGE (10-12% gels, made in-house). The gel was run at 100V for 140 minutes at room temperature. Proteins in the gel were transferred onto nitrocellulose membrane using the Trans-Blot® Turbo™ Transfer System (Bio-Rad). The membrane was rinsed with PBST and incubated in blocking buffer for at least one hour at room temperature with gentle rocking (for all the later steps, the membrane was placed on a rocker with gentle rocking unless specified otherwise). After blocking, the membrane was incubated with primary antibody for at least 2 hours at room temperature or overnight at 4°C. The membrane was washed 5 times with PBST and each wash lasted at least 5 minutes, and then the membrane was incubated with secondary antibody for at least 2 hours at room temperature. After 5 washes with PBST as described earlier, the membrane was visualized by ImageQuant LAS4010 imager (GE Healthcare Life Sciences) if fluorochrome-conjugated secondary antibody was used. For membrane with HRP-conjugated secondary antibody, it was incubated with 1ml ECL Plus Western Blotting Substrate (32132, ThermoFisher Scientific) in 4ml of distilled water (volume was used for 6cm x 8.5cm membrane) for 5 minutes at room temperature. After detection, the membrane was kept moist by incubated with 10ml PBST and stored at 4°C.

2.11.1 Analysis of σ 1 multimers by Western blot (Chapter 3)

A few procedures were modified from western blot analysis and specified below. Equal volumes of cell lysates and 2x Laemmli Sample Buffer with 0.05% β -mercaptoethanol (BioRad,

cat: 1610737) were mixed in PCR tubes and the samples were heated in T100™ Thermal Cycler (BioRad) at the indicated temperatures for 10 minutes. Samples were loaded into 10% gels and the rest of procedures were identical to standard Western blot described above.

2.12 Far-Western blot analysis

A few procedures from Far-Western blot analysis were modified from western blot analysis and specified below. For cells transfected with either μ 2 or μ NS, cells were harvested and detached by Cellstripper as detailed in section 2.5. Cells from three 35mm plates were pulled together into a single 1.5ml eppendorf tube and pelleted by centrifugation at 2000g for 5 minutes at room temperature. Cells were resuspended with 250 μ l CoIP lysis buffer (50mM Tris 7.4, 150mM NaCl, 0.5% NP40 with 1x protease inhibitor cocktail [Sigma]) and 500 μ l of native sample buffer (Biorad, Cat: 1610738) to sample and mixed with pipetting. The sample was analyzed immediately (30 μ l of sample per well) or store at -20°C. For the incubation lysate, cells with transfected μ 2 or μ NS were harvested and detached by Cellstripper as detailed in section 2.5. Cells from four 35mm plates were pulled together into a 15ml conical tube (Corning). Cells were pelleted by centrifugation at 2000g for 5 minutes at room temperature and resuspended with 10ml PBS. The sample was frozen and thawed three times. To ensure complete lysis of cells, the sample was put on ice and subjected to 5 seconds of sonication just before incubation with PDVF membrane.

For the gel electrophoresis, eight % native page was prepared similarly to Western blot analysis (section 2.10), except that sodium dodecyl sulfate (SDS) was completely omitted. 1x

running buffer and 1x transfer buffer were prepared by diluting 10x Tris/Glycine buffer (BioRad, cat: 1610734) with double-distilled water. For transfer buffer, methanol was omitted and 0.5% SDS (wt/vol) was added to the buffer. Transfer buffer was stored at 4°C and pH was adjusted to pH7.5 just prior to use. PVDF membranes were used for protein transfer. Following blocking with 3% BSA, PDVF member was incubated with 10ml PBS containing 1µg of purified µNS or cell lysate (please refer to the above paragraph for the incubation lysate) with transfected µNS or µ2. PVDF membrane was washed briefly with distilled water and incubated with 0.5% PFA for 30 minutes at room temperature. Sequential steps were performed as western blot analysis. Rabbit anti-reovirus antibodies were used to probe for different reovirus proteins as previously described.

2.13 Transfections and immunoprecipitations

2.13.1 Transfection of truncated or mutated σ1 plasmids (Chapter 3)

Transfections:

NIH3T3-Ras cells in 24-well plate at 70-80% confluency were used for truncated or mutated σ1 transfection. Cell medium was replaced by serum-free medium prior to the transfection (please refer to section 2.1). Transfection was performed using Lipofectamine™ 2000 Transfection Reagent (Invitrogen, 52887). For a single transfection reaction per well, 1.5 µg was mixed with 2.4µl of P2000™ reagent in a 1.5ml eppendorf tube with 50µl OptiMEM (Invitrogen, p31985070). The mixture was mixed by gently pipetting. In another 1.5ml eppendorf tube, 1.8 µl of Lipofectamine™ 3000 Reagent was mixed with 50µl of OptiMEM by

pipetting (Invitrogen, p31985070). The mixtures were incubated at room temperature for 5 minutes. The two mixtures were then combined into a single 1.5ml eppendorf tube and mixed by pipetting. The mixture was incubated at room temperature for 20 minutes and added to a well of cells in a dropwise manner. The medium was replaced with full medium at 6 hour-post-transfection (hpt). For some experiments, cells were exposed to FLAG-tagged T3wt at 30hpt (please see section 2.2.3 for viral infection).

Immunoprecipitations:

For cell harvesting, transfected and infected NIH3T3-Ras cells were rinsed with PBS. Cells were incubated with 600 μ l RIPA buffer (50mM Tris pH 7.4, 150mM NaCl, 1% IGEPAL CA-630 (NP-40), 0.5% sodium deoxycholate, 1x inhibitor cocktail [11873580001, Roche]) on ice for at least 30 minutes. Cells were pelleted at 4000g at 4°C for 10 minutes. The supernatant (cell lysate) was transferred to a new 1.5ml eppendorf tube and the pellet (debris) was discarded. For immunoprecipitation, 100 μ l of protein G magnetic beads (Millipore, LSKMAGG10) were washed twice with 1ml RIPA buffer and incubated with 1ml PBS with 1% BSA for one hour at room temperature. After incubation, the beads were washed three times with 1ml PBS and resuspended with 100 μ l RIPA buffer. Four-hundred-and-twenty μ l of the cell lysate was transferred to a 1.5ml eppendorf tube, and the remaining cell lysate was flash-frozen and store at -20°C. The cell lysate was cleared twice with 40 μ l beads in RIPA buffer using a benchtop rotary tumbler. Each clearing procedure took one hour at room temperature and the beads were discarded after transferring the cell lysate to a new 1.5ml eppendorf tube. The post-cleared cell lysate was equally split into two tubes. One tube was flash-frozen and the other tube was added with 4 μ l of anti-FLAG serum, followed by 1.5-hour mixing using a benchtop

rotary tumbler at room temperature. Twenty μl of beads in RIPA buffer was added to the cell lysate with anti-FLAG serum, followed by 1.5-hour mixing using a benchtop rotary tumbler at room temperature. The beads were rinsed with 1ml RIPA buffer and washed three more times with 1ml RIPA buffer, each wash took 15 minutes using a benchtop rotary tumbler at room temperature. After the last wash, fifty μl of 1x protein sample buffer (please refer to the recipe for 5x protein sample buffer in section 2.10) was added to resuspend the beads. The beads were boiled at 100°C for 10 minutes. After boiling, the sample was either subjected to Western blot analysis (section 2.10) or stored at -20°C.

2.13.2 Transfection of μ2 or μNS (Chapter 5)

Transfections:

H1299 cells in 12-well plate at 80-90% confluency were used for FLAG-tagged μ2 or μNS transfection. Prior to the transfection, full medium was replaced by plain medium (please refer to section 2.1). Transfection was performed using Lipofectamine™ 3000 Transfection Reagent (Invitrogen, L3000015). For a single transfection reaction per well, one μg of plasmid was mixed with 1 μl of P3000™ reagent in a 1.5ml eppendorf tube with 50 μl OptiMEM (Invitrogen, p31985070). The mixture was mixed by gently pipetting. In another 1.5ml eppendorf tube, 1.5 μl of Lipofectamine™ 3000 Reagent was mixed with 50 μl of OptiMEM by pipetting (Invitrogen, p31985070). The mixtures were incubated at room temperature for 5 minutes. The two mixtures were then combined into a single 1.5ml eppendorf tube and mixed by pipetting. The mixture was incubated at room temperature for 15 minutes and added to a well of cells in a

dropwise manner. The medium was replaced with full medium at 6 hpt. For some experiments, the cells were exposed to T3wt infection at 24 hpt (please see section 2.2.3 for viral infection).

Immunoprecipitations:

To Harvest H1299 cells, the cells were rinsed with PBS and detached by Cellstripper (Corning, Product number: 25-056-CI) at 24 hpt according to manufacturer's instructions. Cells from each well were pelleted by centrifugation at 2000g for 5 minutes. Cell pellet was lysed and resuspended in 200µl filtered CoIP lysis buffer (50mM Tris 7.4, 150mM NaCl, 0.5% NP40 with 1x protease inhibitor cocktail [Sigma]). For immunoprecipitations, 25µl of protein G magnetic beads (Millipore, LSKMAGG10) was added to each sample. The beads were washed twice with 1ml CoIP lysis buffer and incubated with 5ul of anti-tubulin (DSHB, 12G10), anti-µNS or anti-FLAG (Sigma, F1804) for 2 hours with agitation at room temperature. Excess antibody was washed three times with CoIP lysis buffer. Equivalent volume of beads-antibody mixture was added to cell lysate and incubated for 2 hours with agitation at room temperature or overnight at 4°C. Beads were pelleted by centrifugation at 2000g for 5 minutes and resuspended with 50µl CoIP lysis buffer with 1x inhibitor cocktail [11873580001, Roche]. The samples were heated at 100°C for 10 minutes and subjected to Western blot analysis immediately or froze at -20°C.

2.14 Plasmid and mutant constructions

2.14.1 Constructions of truncated or mutated σ 1 plasmids and mutants

- The plasmids containing truncate σ 1 and point mutations, as well as mutants containing truncated σ 1 were generated by Dr Heather E. Eaton.
- The mutants containing a single point mutation were generated by Francisca Cristi.

Transfection:

The truncated σ 1 plasmids were generated by PCR amplification of the S1 gene segment from T3wt (please see section 2.2.1) using the primers indicated in Table 2- 5. PCR amplicons were digested with Kpn I (FastDigest, Thermo Fisher) and EcoR I (FastDigest, Thermo Fisher) at 5' and 3' respectively, and ligated with pcDNA3.1 (Invitrogen) digested with Kpn I and EcoR I. Clones used for experiments were confirmed to have the correct sequence (McLab Sequencing Facility). Site-directed mutagenesis was then used to introduce the S66I, S66L, S66A, S66T, S66V, L28P and L28A mutations. The QuikChange II site-directed mutagenesis kit (Agilent) was used according to manufacturer instructions, with primers indicated in Table 2- 6.

To generate σ 1 mutants with truncations or single mutations, a plasmid-based reverse genetics system was used. Briefly, one well of a 24-well plate containing 85% confluent BHK-T7 cells was transfected with 10 plasmids each carrying a gene segment from T3wt reovirus (Addgene, Cambridge, MA) along with one plasmid expressing variations of T7RNAP, the capping enzyme NP868R, or both. For σ 1 mutants with truncations, two sequential stop codons were introduced at the truncated site by a pair of forward and reverse primers using the QuikChange II site-directed mutagenesis kit (Agilent). Primers are indicated in Table 2- 7. For

each transfection reaction, three μl of TransIT-LT1 transfection reagent was used per microgram of plasmid DNA, with a total of 2.25 μg of DNA added per well. At 24 hpt, the medium was placed with medium that included antibiotics. To determine virus titers, cells were scraped into PBS 1 to 5 days posttransfection and freeze-thawed three times. Viral titers were determined by plaque assay using L929 cells (please refer to section 2.2.3. The 2% agar overlay was maintained on the cells for 4 to 7 days.

2.14.2 Constructions of FLAG-tagged μ2 and μNS plasmids

To generate plasmid-based vectors expressing reovirus expressing M1 (T3wt or T3v10^{M1} with 5' or 3' FLAG tag) and M3 genes. L929 cells in 6-well plate (CELLSTAR) were infected with T3wt or T3v10^{M1} at MOI of 10 or T3v10^{M1} at MOI of 30. Infection was stopped when 50% cells displayed cytopathogenic effects such as rounding, swelling and clumping. Cells were washed with PBS twice and incubated with 1ml of TRIzol (Thermo Fisher, Cat: 15596026). Cell lysate was mixed thoroughly with TRIzol and transferred to 1.5ml eppendorf tube. 200 μl of chloroform was added to the mixture and mixed thoroughly, followed by 10 minutes of incubation at room temperature. Mixture was then centrifuged for 15 minutes at 12000g at 4°C and the top aqueous phase containing viral RNA was transferred to a new 1.5ml eppendorf tube. To pellet viral RNA, 0.5ml 100% isopropanol was added to the tube, mixed thoroughly and allowed to sit at room temperature for 10 minutes. The tube was centrifuged for 10 minutes at 12000g at 4°C and supernatant was discarded. The pellet was washed with 1ml 75% ethanol and vortex briefly, followed by centrifugation at 8000g for 10 minutes at 4°C.

Supernatant was discarded and pellet was air-dried for 5 minutes. Pellet was re-suspended using 30µl of UltraPure DNase/RNase-Free Distilled Water (Thermo Fisher, Cat: 10977015). The M1 or M3 reovirus genes were cloned in pcDNA3.0. To generate the plasmid expressing M3 gene, viral M3 transcript was reverse transcribed to cDNA using M-MLV Reverse Transcriptase Kit (Thermo Fisher, Cat: 28025013) according to manufacturer's instructions, with forward primer containing a *KpnI* site (5'-AAAGGTACCCACCATGGCTTCATTCAAGGGATT-3') and reverse primer with a *XhoI* site (5'-GGGCTCGAGTTACAACATCATCAGTTGGAAC-3'). The final PCR product and pcDNA3.0 vector were digested with *KpnI* and *XhoI*, gel purified, and ligated to obtain the final plasmid. To generate plasmids expressing T3wt or T3v10^{M1} M1 gene with 5' or 3' FLAG tag, M1 mRNA was reverse transcribed to generate M1 cDNA using the method described above with reverse primer gene containing the *XbaI* site (5'-GGGTCTAGATCACGCCAAGTCAGATCG-3'). M1 cDNA was joined a FLAG-tag on either the 5' or 3' end using iProof High-Fidelity PCR Kit (BioRad, Cat: 1725331). The 5' FLAG-tag was created using forward primer with a *HindIII* site (5'-AAAAAGCTTCCACCATGGATTACAAGGATGACGACGATAAGGATTACAAGGATGACGACGATAAGGGTGGCGGCATGGCTTACATCGCAGTTC-3) and reverse primer with reverse primer gene containing the *XbaI* site (5'-GGGTCTAGATCACGCCAAGTCAGATCG-3'). The 3' FLAG-tag was generated using a forward primer with a *HindIII* site (5'-AAAAAGCTTCCACCATG GCTTACATCGCAGTTCC-3') and reverse primer with a *XbaI* site (5'-GGGTCTAGATCACTTATCGTCGTCATCCTTGTAATCCTTATCGTCGTCATCCTTGTAATCGCCGCCACCCGCCAAGTCAGATCGGAAAG-3'). Each PCR product and a pcDNA3.0 vector were digested with

HindIII and *XbaI*, gel purified, and ligated to obtain the final plasmid. All plasmids were sanger-sequenced to verify the presence of desired inserts.

2.15 Comparing dsRNA segments by SDS-PAGE

To compare dsRNA segments of reovirus, a minimum of 4×10^6 pfu was loaded in the 8% SDS- polyacrylamide gel. The virus in PBS was first mixed with 2x Laemmli Sample Buffer with 0.05% β -mercaptoethanol (BioRad, cat: 1610737), followed by heating at 65°C for 5 minutes. The gel was run at 100V until all samples enter the stacking layer of gel. The gel was transferred to cold room (4°C) and run at 5mA per gel for 22 hours. Upon finishing electrophoresis, the gel was incubated with ethidium bromide (Invitrogen, 15585011) in SDS running buffer (and 25 mM Tris, 192 mM Glycine, 0.1% SDS, pH 8.3) for one hour at room temperature. The gel was rinsed once with distilled water and soaked into SDS running buffer (and 25 mM Tris, 192 mM Glycine, 0.1% SDS, pH 8.3) for at least one hour at room temperature. The gel was visualized by ImageQuant LAS4010 imager (GE Healthcare Life Sciences).

2.16 Collect cytoplasmic- and viral factory-associated protein

Transfected or infected cells were collected from 6-well plates at the indicated time points (see results sections from Chapters 3 and 5). Cells were washed 3 times with 1xPBS, and then the cells were incubated with 400 μ l of ice-cold buffer A (10mM Pipes (pH 6.8), 3mM MgCl₂, 100mM KCl, 30mM Sucrose, 1% Triton X-100 with 1x inhibitor cocktail [11873580001,

Roche]). The plate was placed on ice and rocked gently by hands for approximately 5 minutes. Dissolving of the cell membrane was visually confirmed by light microscope. The soluble fractions (cytoplasmic) were transferred to 1.5ml eppendorf tubes. The insoluble fractions (still attached to the plate) were lysed by 400ul of RIPA buffer (50mM Tris pH 7.4, 150mM NaCl, 1% IGEPAL CA-630 (NP-40), 0.5% sodium deoxycholate, 1x inhibitor cocktail [11873580001, Roche]) and transferred to 1.5ml eppendorf tubes. To remove cell debris, both the soluble and insoluble fractions were centrifuged at 4000g for 10 minutes at room temperature. Supernatants were transferred to new tubes and the pellets were discarded. A 1:5 volume of 5x protein sample buffer (0.5M Tris-HCl pH6.8, 40% glycerol, 5% SDS, 12.5% β -mercaptoethanol, 0.05% bromophenol blue) was added to each sample. The samples were heated to 100°C for 10 minutes on the heat block. After heating, the samples were briefly centrifuged and subjected to Western blot analysis or flash-frozen and stored at -20°C.

2.17 Growth curve

Monolayers of L929 cells in 12-well plates were used for single- and multi-step growth curves. For single step growth curve, cells were exposed to T3wt at MOI of 3.2 or T3v10^{M1} at MOI of 22.6. Flow cytometry analyses were performed to ensure about 70% of cells were infected by either virus. To determine viral titer, two milliliters of whole cell lysates were collected by frozen and thawed at least three times every 3-hour within 24 hours and at 30 hpi. A hundred of total cell lysates were used for plaque assay (please refer to section 2.2.3). For

multi-step growth curve, L929 cells were exposed to either T3wt or T3v10^{M1} at MOI of 0.01 and whole cell lysates were collected every 24-hour within 72 hours.

Plate/dish	Culture medium	Virus in medium (plain)	2% Agar overlay	4% PFA (paraformaldehyde)	1% Crystal violet	Methanol
6-well	2 ml	200 μ l	3 ml	2 ml	2 ml	2 ml
12-well	1 ml	100 μ l	1.5 ml	1 ml	1 ml	1 ml
24-well	0.5 ml	50 μ l	0.75 ml	0.5 ml	0.5 ml	0.5 ml
48-well	250 μ l	25 μ l	0.4 ml	250 μ l	250 μ l	250 μ l
96-well	125 μ l	12.5 μ l		125 μ l		100 μ l

Table 2- 1. Volume of reagents.

Antibody	Dilution and application	Catalog number	Source or company
Rabbit anti-reovirus pAb	1:2000 WB, ICC, FC, IF		Dr. Patrick Lee (Dalhousie University)
Rabbit anti- μ 2 pAb	1:1500 WB, ICC, IF	In-house	ProSci Inc
Rabbit anti- μ NS pAb			
Rabbit anti- σ 2 pAb			
Mouse anti- μ 1 mAb		10F6	DHSB
Rabbit anti-IRF3 pAb	1:1500 WB	sc-9082	SCBT
Rabbit anti p-IRF3 pAb		4947	CST
Rabbit anti-Cleaved Caspase-3 (Asp175) pAb	1:1000 WB	9661	CST
Mouse anti- β -actin mAb	1:2000 WB	47778	SCBT
Goat anti-rabbit HRP	1:10,000 WB	111-035-144	JIR
Goat anti-mouse HRP	1:10,000 WB	115-035-146	JIR
Goat anti-rabbit AP	1:10,000 ICC	111-055-144	JIR
Goat anti-rabbit Alexa Fluor 647	1:5000 WB, FC, IF	111-605-144	JIR
Goat anti-rabbit Alexa Fluor 488	1:5000 ICC, FC, IF	111-545-144	JIR
Goat anti-mouse Alexa Fluor 647	1:5000 WB, FC, IF	115-605-146	JIR

Table 2- 2. List of antibodies.

All antibodies were prepared in blocking buffer (1xPBS with 0.1% Triton X-100 and 3% BSA) unless specified otherwise.

Abbreviation:

WB: Western blot, ICC: Immunocytochemistry, FC: Flow cytometry, IF: Immunofluorescence, DHSB: Developmental Hybridoma Studies Bank, SCBT: Santa Cruz Biotechnology, JIR: Jackson ImmunoResearch, HRP: horseradish peroxidase, AP: alkaline phosphatase, pAb: polyclonal antibody, mAb: monoclonal antibody.

Name of solution	Application	Ingredients
Blocking buffer	WB, ICC, FC, IF	1xPBS with 0.1% Triton X-100 and 3% bovine serum albumin (BSA)
PBST	WB, ICC, FC, IF	1xPBS with 0.1% Tween 20
AP Buffer	ICC	100 mM Tris-HCl pH 9.5, 100 mM NaCl, 5 mM MgCl in ddH ₂ O
TE buffer	ICC	10mM Tris-HCl, 1mM EDTA at pH8.0
1xPBS	WB, ICC, FC, IF and generally used in washing steps	8g NaCl, 0.2g KCl, 1.44g Na ₂ HPO ₄ , 0.24g KH ₂ PO ₄ in 1 litre of ddH ₂ O (adjusted pH to 7.4 with HCl)

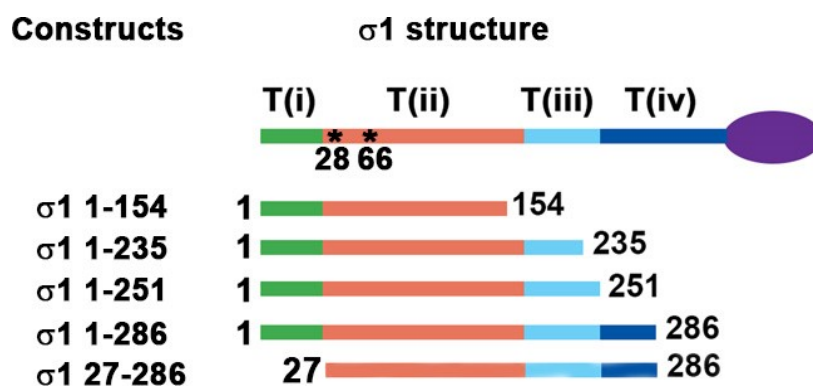
Table 2- 3. List of common buffers.

Abbreviation:

WB: Western blot, ICC: immunocytochemistry, FC: Flow cytometry, IF: Immunofluorescence, ddH₂O: double-distilled water

Name of medium	Catalog number	Manufacturer
MEM	M8028	Sigma
10% fetal bovine serum	F1051	Sigma
10% fetal bovine serum	10500056	Gibco
MEM non-essential amino acids	11140050	Gibco
Antibiotic-Antimycotic (100X)	15240062	Thermo Fisher
Sodium Pyruvate (100 mM)	11360070	Thermo Fisher
PBS	21-040-CVS	Focus Biosciences
PBS	10010023	Gibco
Trypsin-EDTA (0.25%)	25200072	Gibco
JMEM	M0518-10L	Sigma

Table 2- 4. List of common cell culturing media.



Construct	Forward Primer	Reverse Primer
σ1 1-154	GGTACCGGATCCTACTCCACCATG GACCCTCGCCTACGTGAAGAAG	TACTGAATTCGCGGCCGCTTA TATGGATGTTACTCGTAACGTC
σ1 1-235	GGTACCGGATCCTACTCCACCATG GACCCTCGCCTACGTGAAGAAG	TACT GAATTCGCGGCCGCTTA CTTGAGAGTCAAGTTATTATTAAC
σ1 1-251	GGTACCGGATCCTACTCCACCATG GACCCTCGCCTACGTGAAGAAG	TACTGAATTCGCGGCCGCTTA TTTGCTCAGTTGCGCCTATCC
σ1 1-286	GGTACCGGATCCTACTCCACCATG GACCCTCGCCTACGTGAAGAAG	TACTGAATTCGCGGCCGCTTA AACAGTTAGCTGTCCACTAGAA
σ1 27-286	GGTACCGGATCCTACTCCACCATG GGGCTTGAATCAAGGGTCTC	TACTGAATTCGCGGCCGCTTA AACAGTTAGCTGTCCACTAGAA

Table 2- 5. Primer sequences for σ1 plasmids with truncations.

A schematic diagram showing the relative positions of σ1 truncations on the top figure. Forward and reverse primers used for the generation of each plasmid are shown in the table below.

Mutation	Forward Primer	Reverse Primer
L28A	GCCGAGACCCTTGATTCAGCCCCTTTTGAC AGTGATGC	GCATCACTGTCAAAGGGGCTGAATCAAG GGTCTCGGC
L28P	CCGAGACCCTTGATTCAGGCCCTTTTGACA GTGAT	ATCACTGTCAAAGGGCCTGAATCAAGGGT CTCGG
S66I	AAGTCATCCCGAATTTGCTCAAGAGCGATG ATTCGT	ACGAATCATCGCTCTTGAGCAAATTCGGGA TGACTT
S66L	AACCAAGTCATCCCGTAGTTGCTCAAGAGC GATGATTCGTTTGTGTTG	CAAACAAACGAATCATCGCTCTTGAGCAAC TACGGGATGACTTGTT
S66A	CAAGTCATCCCGAGCTTGCTCAAGAGCGAT GATTCGTTTG	CAAACGAATCATCGCTCTTGAGCAAGCTCG GGATGACTTG
S66T	ACGAATCATCGCTCTTGAGCAAACCTCGGG ATGACTT	AAGTCATCCCGAGTTTGCTCAAGAGCGATG ATTCGT
S66V	CAAGTCATCCCGAACTTGCTCAAGAGCGAT GATTCGTTTG	CAAACGAATCATCGCTCTTGAGCAAGTTTCG GGATGACTTG

Table 2- 6. Primer sequences for $\sigma 1$ plasmids and mutants with single mutation.

The residue 28 or 66 mutation is introduced by the forward and reverse primers shown in the above table. The location of residues 66 and 28 are shown in the schematic diagram in Table 2-5.

Stop codon insertion site	Forward Primer	Reverse Primer
154	GGATATCCTAGATTCGAAATC CTATTATATGGATGTTACTCG TAACGTCAGAGTT	AACTCTGACGTTACGAGTAAC ATCCATATAATAGGATTTCGA ATCTAGGATATCC
235	CGCCTATCCTTGAGTTGATA GAATCAAACACTTACTACTT GAGAGTCAAGTTATTATTAA CTATCTGG	CCAGATAGTTAATAATAACTTG ACTCTCAAGTAGTAAGTGTT TGATTCTATCAACTCAAGGAT AGGCG
251	GCCGACGCCACCTATCATTG CTCAGTTGCGCCTATCC	GGATAGGCGCAACTGAGCAAT GATAGGTGGCGTCGGC
286	TACCTCAAATTCGGGGATGT CGATCTAACTCATTACTGTCC ACTAGAATTAATTTCAAGTGT TG	CAACACTTGAAATTAATTCTA GTGGACAGTAATGAGTTAGAT CGACATCCCCGAATTTGAGGTA

Table 2- 7. Primer sequences introducing stop codons into truncated $\sigma 1$ mutants.

Stop codons were introduced to $\sigma 1$ mutants with truncation by the above forward and reverse primers.

CHAPTER 3: INVESTIGATION OF σ 1 TAIL REGIONS AND THEIR EFFECTS ON VIRION ASSOCIATION

3.1. Introduction and chapter objective

Our previously published variants T3v1 and T3v2 formed bigger plaques on various types of cancer cells relative to T3wt, and they significantly prolonged survival of mice with subcutaneously grafted B16 melanoma (231). Both T3v1 and T3v2 shared the phenotype of σ 1 reduction. Our follow-up study used RNA interference and showed that reovirus oncolytic potency was directly enhanced by σ 1 reduction (180). Briefly, we propose that reovirus does not need full amount of σ 1 proteins to bind cells. Variants with reduced levels of σ 1 have the advantage to release all σ 1 proteins and uncoat faster than the wild-type virus in the tumor microenvironment (TME). The gastrointestinal tract has more proteases compared to the TME and σ 1 proteins on reovirus can be cleaved by proteases, leading to the loss of infectivity. The optimal infectivity of reovirus toward tumorigenic versus intestinal cells depends on the level of σ 1. However, how σ 1 is assembled onto virion has yet to be determined.

In this chapter, we used variants with mutations in σ 1 that reduced virion-association, as well as truncated or mutated σ 1 constructs, and genetically modified mutants to explore the contribution of σ 1 domains to σ 1 intracellular localization and virion encapsidation.

3.2 Results

3.2.1 Reovirus variants generated by directed evolution form larger plaques than wild-type virus on tumorigenic cells

One major goal of our lab is to isolate and characterize mutations in reovirus that promote replication in cancer cells and tumor environments, with the long-term hope that such mutations may promote reovirus oncotherapy. We sought to generate variants that were capable of forming big-plaques by exposing L929 cells with T3wt or T3v2 in the presence of either proflavine or 5-fluorouracil (5FU) (Figure 3- 1), and then 6 variants (named T3v4, T3v5, T3v8, T3v11, T3v14 and T3v16) were chosen to test for plaque formation on mouse and human tumorigenic cells (Figure 3- 2, T3v1 and T3v2 were included as controls). All 6 variants formed significantly bigger plaques than T3wt, except that T3v8 formed plaques with similar sizes as T3wt on B16 mouse melanoma. Importantly, all variants formed only small foci of reovirus-antigen-positive cells on non-transformed NIH3T3 fibroblasts even at 7 day-post-infection. Our data showed that these variants possessed greater oncolytic potency than T3wt towards cancer cells while their enhanced infectivity remained specific towards transformed cells.

3.2.2 Reovirus variants with enhanced replication in transformed cells have different gene mutations that ultimately lead to the reduction of $\sigma 1$

Since reduction of $\sigma 1$ is a mechanism that promotes reovirus plaque sizes on transformed cells, we proceeded to assess $\sigma 1$ levels on the 6 variants. The variants were first purified using cesium chloride (CsCl) gradient centrifugation, and then they were subjected to

Western blot analyses (Figure 3- 3A). Levels of $\sigma 1$ were quantified and standardized to capsid proteins $\mu 1$ and $\sigma 3$. Results from 3 independent experiments showed that all variants had significantly less $\sigma 1$ protein than T3wt (Figure 3- 3A, dot plot). To confirm findings from Western blot analyses, agarose gel electrophoresis was performed (Figure 3- 3B). The experimental principle was based on a study by Larson *et al.* (140). When intact reovirus virions were loaded onto an agarose gel, they produced up to 12 bands. The lowest band represents reovirus completely devoid of any $\sigma 1$, while virus with relatively full amounts of $\sigma 1$ often produces a few bands near the top of the gel. On an example gel, T3wt had multiple bands at the top of the gel. T3v4 produced multiple bands near the middle and the lower parts of the gel; T3v5 had a few fast migrating bands near the bottom of gel. These observations agree with Western blot analyses that T3wt particles have more $\sigma 1$ proteins than the two variants and T3v5 has the fewest $\sigma 1$ molecules. In conclusion, our data demonstrated that all the variants possess fewer $\sigma 1$ proteins than T3wt, and based on our previous published findings (180), this phenotype can augment their oncolytic potency towards the tested tumorigenic cells (Figure 3- 2).

Next, we determined which gene mutation(s) are responsible for the reduction of $\sigma 1$ in the 6 variants. Sanger-sequencing analyses revealed that only 2 out of 6 variants had a single mutation in the $\sigma 1$ protein (Table 3- 1. Mutations in reovirus variants., T3v1 and T3v2 are also included as references). T3v8 had a S66I mutation and T3v16 had a L28P alteration in $\sigma 1$. Interestingly, these 2 mutations were located near the N-terminus of the $\sigma 1$ tail and both sites were not reported to reduce $\sigma 1$ levels previously. The T3v2 had a single S18I mutation in the $\sigma 1$ anchoring domain that was predicted to interact with $\lambda 2$ protein (35,82,146,165); this could

directly impair virion association. Previous studies showed that the midpoint region of the $\sigma 1$ tail is important for virion association (30,78), and our data provided evidence that two previously uncharacterized residues are also important for the incorporation of $\sigma 1$ on virion. Our findings made us speculate that other uncharacterized regions in the $\sigma 1$ tail play a role in virion association and this will be further discussed later.

Our sequencing data also showed that reovirus can achieve the phenotype of $\sigma 1$ reduction through mutations in non- $\sigma 1$ -encoding genes (Table 1). The T3v5 and T3v14 had a single amino acid mutation in $\lambda 2$ protein (I1273T and M1148S, respectively). The T3v4 had 3 different mutations, and each mutation resided in a separate viral protein: the outer capsid protein $\sigma 3$ had an H230Q alteration; the $\lambda 3$ polymerases carried the M892I mutation and the last I1274M mutation occurred in the $\lambda 2$ protein. The T3v11 had a single A962P alteration in the core protein $\lambda 1$. Taken together, our data showed that 4 out of 6 variants have mutations in non- $\sigma 1$ encoding genes, and this suggests that reovirus can be adapted to infect transformed cells more effectively (Figure 3- 2) by accumulating mutations in different genes to reduce overall $\sigma 1$ levels (Figure 3- 3).

We just showed that reduction of $\sigma 1$ is an adaptation allowing reovirus to infect transformed cells more effectively, and wild-type reovirus might be benefited by having more $\sigma 1$ in its natural environments (180). We hypothesized that reovirus field isolates would have similar levels of $\sigma 1$ comparably to the lab strain T3wt. To test this, we obtained field isolates from effluent and sewage in Edmonton, Canada (generously provided by Dr. Xiaoli Lilly Pang from the University of Alberta). Agarose gel electrophoresis analysis showed that all tested

field isolates possessed similar amounts of $\sigma 1$ relative to T3wt. The T3v1 was known to have fewer $\sigma 1$ than T3wt and was loaded as a control (Figure 3- 4A). Furthermore, we analyzed their genome segments alongside prototype serotypes T1L, T2J and T3D by polyacrylamide gel electrophoresis. Our data revealed that the four reovirus field isolates we assessed were reassortants between all three serotypes because the migration pattern of their genome segments did not match a specific serotype (Figure 3- 4B).

In conclusion, our data showed that regardless of the reovirus serotype and genetic background, the natural environment favors reovirus possessing more $\sigma 1$ proteins. Reduction of $\sigma 1$ levels is likely a shared mechanism by various reovirus variants in promoting oncolytic potency, and importantly, many variants obtained this phenotype by having mutations in non- $\sigma 1$ encoding genes. This suggests that parallel evolution occurred and reovirus variants were able to generate mutations in different genes to reduce $\sigma 1$.

3.2.3 Mutations in $\sigma 1$ variants do not affect trimerization of $\sigma 1$

Having discovered that 6 variants have reduced $\sigma 1$ (Figure 3- 3), we proceeded to investigate the mechanism leading to this phenotype. Previous studies showed that the functional form of virion-associated $\sigma 1$ exists as a homotrimer (144,243). It is possible that the $\sigma 1$ trimerization is impaired by the mutations (Table 3- 1) of the variants and this could directly reduce total $\sigma 1$ or impact $\sigma 1$ -virion association.

To test $\sigma 1$ trimerization, we first collected mock-infected L929 cells or cells infected with the indicated variants at 17 hour-post-infection (hpi), and then we incubated cell lysates and

purified T3wt as control with SDS-containing protein sample buffer at 22 °C, 36°C, 50°C, 65 °C or 100°C for 10 minutes before subjecting the samples to SDS-PAGE analysis. Expression of $\sigma 1$ was detected by both anti- $\sigma 1$ tail (N-terminal) and head (C-terminal) sera (Figure 3- 5). Previous studies showed that the trimeric form of $\sigma 1$ could be preserved if it was incubated with SDS-containing sample buffer at 37°C or lower temperatures (15,243). In agreement with previous studies, our results demonstrated that $\sigma 1$ from cell lysates and purified virions existed as trimers at 22 and 36°C (Figure 3- 5). In both conditions, a ~220 kDa band and a ~180 kDa band were observed. A third dominant ~130kDa band was also detected. All three bands were observed in blots independently probed with specific $\sigma 1$ tail and $\sigma 1$ head antisera (Figure 2A). These three bands suggest that trimeric $\sigma 1$ has three or more major folding conformations. When the incubation temperature increased to 50-65 °C, sigma 1 from cell lysates and purified virion produced three distinct bands again and the molecular sizes of these bands were identical to the previously observed $\sigma 1$ bands at lower incubation temperatures, but the intensity of each band was changed. Specifically, the intensity of the ~130kDa band decreased, while the ~220 and ~180kDa bands increased in intensities. This suggests that conformations of $\sigma 1$ trimer are temperature-dependent. Conformations of $\sigma 1$ trimer at different temperatures will be further discussed later (section 6.1.3). Taken together, our data showed that $\sigma 1$ exists as a trimer on Western blots when incubation temperatures with protein sample buffer are at 65°C or lower.

We also observed that the T3wt infected cell lysates produced a ~60kDa band on the blot probed with anti- $\sigma 1$ tail serum (Figure 3- 5, lanes showing L929 cells exposed to T3wt with incubation temperatures that are equal or below 65 °C) while the same band is not detected in

the purified virus. We hypothesize that this band represents the cleaved $\sigma 1$ product, as L929 cells are known to produce proteases Cathepsin B and L that cleave $\sigma 1$ (85). At the 100°C condition, a single band of ~40kDa was detected, suggesting that the band was the monomeric form of $\sigma 1$. In summary, we showed that trimeric $\sigma 1$ may be susceptible to proteolytic cleavage, and secondly, multimerization of $\sigma 1$ can be reliably detected by altering incubation temperatures with protein sample buffer. Accordingly, we chose to use this approach to test whether the mutations (Table 3- 1) associated with our variants affect $\sigma 1$ trimerization.

Next, we examined whether the reduction of $\sigma 1$ from variants (Figure 3- 3) was due to impaired $\sigma 1$ trimerization. At 17 hpi, we incubated variants-infected L929 cells with SDS-containing protein sample buffer at 36, 50 and 100°C (Figure 3- 6). The $\sigma 1$ bands were independently probed with anti- $\sigma 1$ tail (top blots) or anti- $\sigma 1$ head (lower blots) serums. Our data consistently showed that T3wt and all variants produced $\sigma 1$ bands with high molecular sizes at 36 and 50°C (the patterns were similar to Figure 3- 5), suggesting that they were capable of trimerization. At the 100°C, a single monomeric $\sigma 1$ band is detected for T3wt and each variant. The results therefore suggest that none of the mutations described in Table 3- 1 affect trimerization of $\sigma 1$.

During our Western blot analyses with the variants (Figure 3- 6), we noticed that all variants produced trimeric or monomeric $\sigma 1$ with similar sizes to T3wt, except for T3v16. First, the T3v16 produced a trimeric $\sigma 1$ that appeared to migrate faster than T3wt and other variants at both 36 and 50°C conditions. To confirm our findings, we analyzed cell lysates infected with T3wt or T3v16 from two independent experiments (labeled as n=1 and n=2 on the top of blots) on the same blot and the results were reproducible. Second, the T3v16 did not have a

detectable cleaved $\sigma 1$ band at the ~ 60 kDa position at 36 and 50°C. We repeated the same experiment using the 36 and 100°C conditions to validate the above observations regarding T3v16 (Figure 3- 7), and again, trimeric $\sigma 1$ of T3v16 migrated faster than T3wt and other variants; the proposed cleaved $\sigma 1$ is not detected from the T3v16 trimers (Figure 3- 7, the 36°C condition). In conclusion, the sole L28P $\sigma 1$ mutation may alter the migration of $\sigma 1$ trimer in SDS-PAGE and the mutation is associated with a lack of detectable cleaved $\sigma 1$ product. As will be discussed in section 6.1.2, this finding is interesting because L28P is very distant from the $\sigma 1$ hypercleavage domain (residues 245-261), and therefore suggests that conformation may link these domains functionally.

3.2.4 Sigma 1 proteins with different lengths do not aggregate or form heterotrimer

All of the previously described mutations reduce $\sigma 1$ levels but do not affect trimerization of $\sigma 1$. The T3v2, T3v8 and T3v16 were the only variants carrying a mutation in $\sigma 1$, and interestingly, while S18I is within the domain known to anchor $\sigma 1$ to virions, the other mutations were outside of the anchorage domain but still within the tail N-terminal half of $\sigma 1$. This suggests that different domains in the $\sigma 1$ tail may play roles in mediating reovirus $\sigma 1$ levels, and therefore, we chose to focus on the tail region of $\sigma 1$ by generating $\sigma 1$ constructs with truncations. The T3v8 has an altered residue 66 (S66I) and T3v16 has a mutated residue 28 (L28P). Each mutation reduces $\sigma 1$ levels by 50% compared to T3wt. We sought to examine

the importance of residue 28 and 66 in $\sigma 1$ assembly onto virions by generating multiple constructs with a single mutation at either residue site, but in the context of truncated $\sigma 1$.

To assess $\sigma 1$ -virion association, we developed a pull-down assay and the procedures are depicted in Figure 3- 8. First, we exposed NIH3T3-Ras cells (NIH3T3 transformed by Harvey ras oncogene) to T3wt expressing full-length $\sigma 1$ with a FLAG tag (Reo^{FLAG}). At 24 hpi, cells were transfected with the desired truncated or mutated $\sigma 1$ construct. At 24 hour-post-transfection (hpt), cell lysates were collected to determine the total protein expression of FLAG-tagged $\sigma 1$ and transfected $\sigma 1$. The lysates were also used to compare the levels of plasmid-derived truncated/mutated $\sigma 1$, by pulling down whole virions with anti-FLAG antibodies and then assessing the levels of truncated/mutated $\sigma 1$ that co-precipitated with the whole virions. This method is possible because a single virion has up to 12 $\sigma 1$ trimers, and therefore could be composed of a mixture of virus-derived and plasmid-derived $\sigma 1$ at distinct vertices. Post-pull-down samples were then subjected to Western blot analysis with anti-FLAG to detect virus-derived $\sigma 1$ and anti- $\sigma 1$ -N to detect plasmid-derived and virus-derived $\sigma 1$ which could then be distinguished based on molecular weight. The rationale of using this approach is that reovirus indiscriminately assembles different species of $\sigma 1$ s ($\sigma 1$ -FLAG or transfected $\sigma 1$) onto the mature virion, allowing us to compare $\sigma 1$ -virion association among different constructs. One possible caveat of this approach is that different $\sigma 1$ species may form trimers or aggregate, thereby making our results uninterpretable. Previous studies suggested that $\sigma 1$ forms trimer as the protein is being synthesized (102), and therefore it was unlikely that plasmid-derived and virus-derived $\sigma 1$ would form heterotrimers. Nevertheless, it was imperative that we confirmed the absence of heterotrimerization.

To test whether σ 1-FLAG and truncated σ 1 form aggregates or multimers (Figure 3- 9), we compared molecular sizes of σ 1 bands from NIH3T3-Ras cells transfected with either σ 1-FLAG or a truncated σ 1 that possessed the first 251 amino acids (σ 1¹⁻²⁵¹) to cells co-transfected with both constructs. Transfection (Tf) of σ 1 construct is indicated by “+” on the top of Western blot. At the 23 °C incubation condition, σ 1-FLAG transfected (Tf) cells produced a dominant band with ~220kDa and a faint ~180kDa band, while cells expressing σ 1¹⁻²⁵¹ produced a ~100kDa band. Both constructs independently produced the proposed cleaved σ 1 product around 60kDa. When both σ 1-FLAG and σ 1¹⁻²⁵¹ were co-transfected, four bands were observed: the ~220kDa and ~180kDa bands matched the sizes of σ 1-FLAG-derived products, and the ~100kDa band matched the size σ 1¹⁻²⁵¹-derived protein. Lastly, the ~60kDa cleaved σ 1 could be produced by both σ 1-FLAG and σ 1¹⁻²⁵¹ constructs. We concluded that σ 1 expressed by different vectors do not form heterotrimers or aggregates because no σ 1 products with intermediate sizes were observed (Figure 3- 9, schematic diagram at the bottom).

When incubation temperature increased to 100°C, cells transfected with σ 1-FLAG had a detectable band at 50kDa while cells expressing the transfected σ 1¹⁻²⁵¹ produced a 25kDa band. These bands matched the predicted size of monomeric σ 1-FLAG and σ 1¹⁻²⁵¹ respectively. When cells were co-transfected with both plasmids, a σ 1-FLAG-derived 50kDa band and a σ 1¹⁻²⁵¹-derived 25kDa band were detected. We did not observe any σ 1 band with higher molecular weight and this suggests that σ 1 monomers of σ 1-FLAG and σ 1¹⁻²⁵¹ do not form aggregate at this temperature. Note that, a 20kDa band was observed in cells transfected with either the σ 1-FLAG and σ 1¹⁻²⁵¹ construct. The band is likely a cleaved product of σ 1, as this band is associated with transfected σ 1-FLAG and σ 1¹⁻²⁵¹, but not detected in untransfected cells. In

addition, this proposed cleaved $\sigma 1$ is observed in other figures (Figure 3- 13, 100°C blot and Figure 3- 14, Lysate (total protein)). In conclusion, our results revealed that $\sigma 1$ expressed by different constructs do not aggregate or form heterotrimers. Our data also agree with previous observations that $\sigma 1$ is assembled by coupling trimerization and translation of its mRNA (102).

3.2.5 $\sigma 1$ residues 155-235 are important for viral factory localization

We have evidence that different $\sigma 1$ molecules do not form heterotrimers or aggregates (Figure 3- 9), so we can use the approach described in Figure 3- 8 to investigate whether virion association is impaired by progressive truncation of residues from the C-terminus in the $\sigma 1$ tail. We also created a construct that encodes for $\sigma 1^{27-286}$. This construct has the anchoring domain removed, and previous studies suggested the anchoring domain plays a key role in associating $\sigma 1$ to the virion (14,27,29) (Figure 3- 10, truncated $\sigma 1$ constructs are depicted in a diagram above the Western blots). First, we infected NIH3T3-Ras cells as described in Figure 3- 8, and then the infected cells were transfected with one of the truncated $\sigma 1$ constructs as indicated on the Western blots. Total cell lysates (Lysate (total protein)) were analyzed to determine the absolute expression levels of full-length $\sigma 1$ -FLAG and each of the truncated $\sigma 1$ construct. Relative expression levels of truncated $\sigma 1$ constructs were standardized to $\sigma 1$ -FLAG. To assess virion-truncated $\sigma 1$ association, we first pulled down $\sigma 1$ -FLAG-protein complex with anti-FLAG serum, and then the co-immunoprecipitated truncated $\sigma 1$ (IP: α -FLAG blot) was standardized to its own relative expression level (Lysate (total protein)) to calculate the relative virion association. Our data demonstrated that $\sigma 1^{1-104}$ was the only construct that was not detected

in the pull-down assay (IP: α -FLAG blot) despite the fact that the protein was expressed (Lysate (total protein)). The second shortest construct σ 1-154 was barely detected in the pull-down condition, whereas constructs containing the first 235 or more residues were effectively pulled-down. These results suggest that (1) virion association requires an N-terminal segment in the region between residues 154 and 235, and (2) constructs that are not detected in the pull-down condition may either fail to get recruited to the site of virion assembly (viral factory) or they are not able to get incorporated into virions.

To distinguish these two possibilities, we infected and transfected NIH3T3 cells as described in Figure 3- 8. At 24 hpt, we independently collected viral proteins that were either in the cellular cytoplasm (NF) or associated with the viral factories (F). To separate these fractions, we used a previously-published method of selectively solubilizing non-factory components with 0.1% Triton X 100 (170). Western blot analysis was performed and the percent of viral factory-associated σ 1 was calculated for each construct and represented in a dot plot (Figure 3- 11). About 80% of σ 1¹⁻²³⁵, σ 1¹⁻²⁵¹, and σ 1¹⁻²⁸⁶ were able to associate with viral factories. Extending amino acids beyond residue 235 did not seem to provide additional advantage for σ 1 to accumulate into viral factories. However, truncation of residues 155-235 significantly decreased viral factory accumulation: with only 7% of σ 1¹⁻¹⁵⁴ associating with viral factories ($n=3$, mean \pm SD, one-way ANOVA - Dunnett's multiple comparisons test, $p=0.0038$). The shortest construct σ 1¹⁻¹⁰⁴ was not detected in viral factories. Our data suggest that the first 26 residues may also play role in viral factory accumulation. Compared to σ 1¹⁻²⁸⁶, factory accumulation of σ 1²⁷⁻²⁸⁶ was reduced to 55% from 81%, but the differences were not significant (paired T-test, $n=4$, $p=0.096$). Taken together, our data provided evidence that σ 1 residues 155-

235 play an essential role in viral factory localization. Sigma 1 construct possessing only the first 104 residues is not detected in the viral factory by Western blot analysis (Figure 3- 19A). Viral factories are sites for reovirus progeny assembly. Sigma 1¹⁻¹⁰⁴ is not able to accumulate in the viral factories and it is unlikely to get incorporated into the mature virion.

3.2.6 Sigma 1 constructs with mutated amino acids 28 or 66 were able to form trimers

We showed that our truncated $\sigma 1$ constructs possessing at least 235 amino acids from the N-terminal effectively accumulate in viral factories (Figure 3- 11). With this knowledge, we were able to test how single residue mutations in $\sigma 1$ ¹⁻²⁵¹ affect $\sigma 1$ trimerization and virion association. We previously showed that T3v16 has the $\sigma 1$ L28P mutation and T3v8 has the $\sigma 1$ S66I mutation (Table 3- 1). Both variants had a 2-fold reduction in $\sigma 1$ levels relative to T3wt (Figure 3- 3). We used this opportunity to examine how amino acids with different physico-chemical properties at these two residue sites affect virion association by swapping multiple residues at site 28 or 66 in $\sigma 1$ ¹⁻²⁵¹ (Figure 3- 12).

Before testing our constructs with altered 28 or 66 in trimer formation and virion association, we will briefly describe the choices of the replaced residue at the two sites. For residue 28, we decide to swap the wild-type leucine with proline or alanine, generating construct L28P and L28A respectively (Figure 3- 12). The L28P corresponds to the residue observed in T3v16. Like leucine, proline is non-polar and non-charged but its 3-carbon side-chain is covalently linked to the main-chain nitrogen. This distinctive cyclic structure makes

proline conformationally rigid and the modified main-chain nitrogen disrupts normal hydrogen bonding in α -helices and β -sheets (161,202). The alanine in the L28A mutant lacks the leucine side-chain atoms beyond C_{β} (gamma-hydroxyl) without affecting the main-chain properties and thus tests the role of the leucine side chain.

For amino acid 66, we replaced wild-type serine with isoleucine, leucine, alanine, threonine and valine. This generated constructs S66I, S66L, S66A, S66T and S66V respectively (Figure 3- 12). The wild-type serine has a hydroxyl group attached to C_{β} . Alanine is a very similar residue that just lacks the hydroxyl, so S66A tests the role of the hydroxyl. Threonine in the S66T mutant has a gamma-hydroxyl but differs in having an extra methyl group attached to C_{β} (gamma-methyl). That makes it a beta-branched side-chain just like isoleucine. Valine in the S66V mutant is also a beta-branched residue it is more similar to isoleucine because both atoms attached to C_{β} are methyl groups (54). S66I represents our T3v8 variant and its side chain has just one extra methyl group compared to valine. Finally, leucine in the S66L mutant has the same number of methyl groups, and thus very similar hydrophobicity, as isoleucine but it is not beta-branched. In summary, replacing residue 28 and 66 with amino acids that differ in polarity and hydrophobicity allows us to test how these two sites affect $\sigma 1$ trimerization and virion association.

Exchanging residues at site 28 or 66 may disrupt multimer formation as $\sigma 1$ residues 26-170 are proposed to be important for trimerization (15,144,243). To examine whether the swapped amino acids at residue 28 or 66 affect $\sigma 1$ trimerization, we subjected $\sigma 1$ -transfected NIH3T3-Ras cells to Western blot analysis (Figure 3- 13). At the 23°C and 50°C conditions, the full-length $\sigma 1$ control ($\sigma 1$, second left lane) and all $\sigma 1^{1-251}$ constructs produced trimeric $\sigma 1$ at

~140kDa and ~110 kDa respectively. At the 100°C condition, full-length $\sigma 1$ control ($\sigma 1$, second left lane) produced the monomeric $\sigma 1$ at ~45kDa and all $\sigma 1^{1-251}$ constructs had a detectable monomeric $\sigma 1$ band at ~25kDa. Our data demonstrated that none of the swapped residues 28 or 66 affect trimerization of $\sigma 1$.

We previously observed that the $\sigma 1$ with L28P alteration from variant T3v16 migrated faster than other variants, and the cleaved $\sigma 1$ product was not detected on Western blots (Figure 3- 6 and Figure 3- 7). Our data showed that $\sigma 1$ trimers of constructs L28P and L28A migrated faster than $\sigma 1$ proteins with altered residue 66 (Figure 3- 13, 23°C and 50°C blots). Additionally, in all 3 temperature conditions, full-length $\sigma 1$ control ($\sigma 1$, second left lane) and $\sigma 1$ molecules with mutated residue 66 produced the cleaved $\sigma 1$ underneath the uncleaved proteins, except for the L28P- and L28A-derived $\sigma 1$. To verify the identity of cleaved $\sigma 1$ fragment, we subjected T3wt to chymotrypsin digestion (Reo + CHT) and analyzed the cleaved $\sigma 1$ on a separate blot (100°C condition). Our results confirmed that the ~23kDa bands were indeed the cleaved $\sigma 1$ fragment. Taken together, results from Western blot analyses showed that alterations of residue 28 affect migration of $\sigma 1$ trimer encoded by variant T3v16 (Figure 3- 6 and Figure 3- 7) and transfected plasmids (Figure 3- 13, 23°C and 50°C blots). Also, we were not able to detect any proposed cleaved $\sigma 1$ product from $\sigma 1$ proteins carrying an altered residue 28.

3.2.7 The length of $\sigma 1$ tail and residue 28 or 66 are important for virion association

We previously showed that $\sigma 1$ with different lengths did not form heterotrimers or aggregates (Figure 3- 9), and $\sigma 1$ constructs possessing at least 235 residues from the N-terminus were able to accumulate in viral factories effectively (Figure 3- 11). All our constructs with altered residue 28 or 66 were able to form trimers (Figure 3- 13). With all the above information, we proceeded to test how $\sigma 1$ truncations and $\sigma 1^{1-251}$ constructs with mutated residue 28 or 66 affected virion association (Figure 3- 14). NIH3T3-Ras cells were infected and transfected with the desired vectors as described in Figure 3- 8. Virion association of each construct was calculated by standardizing immunoprecipitated truncated or mutant $\sigma 1$ (IP: α -FLAG blot) to its own relative expression levels (Lysate (total protein)) as described in Figure 3- 10 (Figure 3- 11, dot plot). Note that, $\sigma 1^{1-104}$ was not tested, because it could not accumulate in the viral factory (Figure 3- 11). Results from 4 independent experiments were used to generate the dot plot in Figure 3- 14. The longest construct $\sigma 1^{1-286}$ has the best association with the virion. Sigma 1-virion association decreases as more residues from the C-terminus are removed. One-way ANOVA and Dunnett's multiple comparisons tests were performed to compare $\sigma 1$ levels between each construct. Compared to $\sigma 1^{1-286}$, the mean $\sigma 1$ level of $\sigma 1^{1-251}$ decreased to 0.77 ($n=4$, $SD=0.13$, $p=0.32$) and the mean $\sigma 1$ level of $\sigma 1^{1-235}$ reduced to 0.19 ($n=4$, $SD=0.073$, $p=0.0052$). Expression $\sigma 1^{1-154}$ is not detected in IP: α -FLAG blot. Surprisingly, $\sigma 1^{27-286}$ (a construct without the anchoring domain) is able to associate with virion, but its mean $\sigma 1$ level is reduced to 0.37 ($n=4$, $SD=0.086$, $p=0.00050$) compared to $\sigma 1^{1-286}$. This suggests that residues at the 3' of the anchoring domain play role in virion association. In

conclusion, our data show that the quantity of $\sigma 1$ proteins being pulled down increases as amino acids are extended toward residue 286 from the N-terminus of $\sigma 1$ tail (Figure 3- 19A).

Next, we compared to $\sigma 1^{1-251}$ with mutated residue 28 or 66 to the unaltered $\sigma 1^{1-251}$. Our data show that mutations of either site decrease virion association by about 2-fold (Figure 3- 14, dot plot: $n=4$, mean \pm SD, one-way ANOVA - Dunnett's multiple comparisons test, $p<0.0001$). The implications of how physical properties of different amino acids at site 28 or 66 affect virion association will be discussed in detail later.

3.2.8 Mutants generated by reverse genetics (RG) system with $\sigma 1$ truncated residues 155-251 and the L28P or S66I mutation have reduced $\sigma 1$ levels

Our data demonstrated that virion association with $\sigma 1$ was impaired by $\sigma 1$ truncations and mutation at residue 28 or 66 (Figure 3- 14). It is unclear whether such relationship would apply to viral particles and how reovirus replication is affected by $\sigma 1$ modifications. To test this, we used the reverse genetics (RG) system to generate T3wt (referred as RG-T3wt), and truncated or mutated $\sigma 1$ viruses (referred as mutant) that mirror the previously characterized constructs (Figure 3- 15).

To determine $\sigma 1$ levels of RG-viruses, freshly purified RG-T3wt and mutants were first subjected to Western blot analysis (Figure 3- 16), and then their $\sigma 1$ levels were verified by agarose gel electrophoresis (Figure 3- 17). Pearson correlation analysis (Figure 3- 18) showed that results from Western blots and agarose gel electrophoresis had a very strong linear positive relationship ($r=0.97$, $n=4$, $p<0.00001$), suggesting that the two experimental

approaches generated results that were highly consistent and similar. One-way ANOVA: Dunnett's multiple comparisons tests were performed to compare $\sigma 1$ level between RG-T3wt and truncated $\sigma 1$ mutants in both methods by taking the mean value of $\sigma 1$ levels in each independent experiment. Mutant 1-154 had the largest C-terminal region truncated and its mean $\sigma 1$ level reduced to 0.047 ($n=4$, $SD=0.071$, $p=0.0005$), reaching the detection limits of Western blot analysis. Mutant 1-235 had a mean $\sigma 1$ level of 0.26 ($n=4$, $SD=0.071$, $p=0.005$). Mutant 1-251 had the highest average level of $\sigma 1$ among all truncated $\sigma 1$ mutants. Its mean $\sigma 1$ level was 0.47 ($n=4$, $SD=0.17$, $p=0.029$) compared to RG-T3wt. Overall, findings from our mutants are similar to results obtained from the plasmid-derived $\sigma 1$. Sigma 1 proteins associated with mutant 1-154 are barely detectable. Extension of amino acids towards residue 251 increases $\sigma 1$ levels of truncated $\sigma 1$ mutants.

However, unlike the plasmid-derived $\sigma 1$ ¹⁻²⁸⁶, mutant 1-286 had fewer $\sigma 1$ proteins than mutant 1-251 on average (Figure 3- 16 and Figure 3- 17, $n=4$, $mean=0.31$, $SD=0.31$; one-way ANOVA - Dunnett's multiple comparisons test, $p=0.86$), but one should be cautious to interpret the findings as $\sigma 1$ levels of mutant 1-286 varied greatly among 4 independent experiments and some virions might be completely devoid of $\sigma 1$. The effect of $\sigma 1$ residues 252-286 on virion association will be further discussed later (Figure 3- 19A).

For mutants with single amino acid alteration, replacing amino acids at either residue 28 or 66 decreased $\sigma 1$ levels by two-fold (Figure 3- 14). One-way ANOVA: Dunnett's multiple comparisons tests were performed to compared $\sigma 1$ levels among RG-viruses. Compared to RG-T3wt, the average $\sigma 1$ level of full-length $\sigma 1$ mutant with L28P mutation (FL (L28P)) reduced to 0.44 ($n=4$, $SD=0.23$, $p=0.052$); the mean $\sigma 1$ level of mutant FL (S66I) reduced to 0.4 ($n=4$,

SD=0.17, p=0.027) relative to RG-T3wt. Compared to the truncated $\sigma 1$ mutant 1-286, the L28P or S66I mutation reduced average $\sigma 1$ level of both mutants 1-286 (L28P) and 1-286 (S66I) to 0.45 and 0.082 respectively, but the differences were not significant due to large variations between 4 independent experiments. In conclusion, the L28P or S66I mutation reduces $\sigma 1$ levels of RG-viruses, when either mutation is introduced into RG-T3wt or truncated $\sigma 1$ mutant 1-286 (Figure 3- 19A).

3.3 Summary

Our lab created 6 variants using directed evolution that formed plaques as large as the previously described T3v1 and T3v2 (Figure 3- 2). Similar to T3v1 and T3v2, all variants had reduced levels of $\sigma 1$ (Figure 3- 3). Strikingly, four variants did not have any mutation in $\sigma 1$ (Table 3- 1) and this suggests reovirus achieved the same phenotype through parallel evolution. We predicted that $\sigma 1$ reduction was an adaption that promotes reovirus specific-infectivity towards transformed cells. To test this, we compared $\sigma 1$ of field isolates with our lab strain T3wt and found that field isolates possessed similar levels of $\sigma 1$ relative to T3wt (Figure 3- 4). Overall, our data provides evidence that optimal reovirus infectivity towards natural versus transformed-cell niches depends on $\sigma 1$ level. We decided to investigate which $\sigma 1$ domain is important for virion association.

The T3v2 has a mutation in the anchoring domain that is known to impair virion assembly. Two variants we characterized in this chapter have mutations in a domain that is proposed to be important for $\sigma 1$ trimerization. However, we showed that all variants were able

to form trimeric $\sigma 1$ (Figure 3- 6). We proceed to test how other previously uncharacterized $\sigma 1$ regions affect assembly of $\sigma 1$ onto the virion at different stages of replication, by creating truncated and single-residue altered constructs (Figure 3- 10) and viruses (Figure 3- 15). Our results demonstrated that $\sigma 1$ residues 155-235 are required for viral factory localization.

For virion association, alteration of either residue 28 or 66 reduced $\sigma 1$ -virion association by 2-fold (Figure 3- 14, Figure 3- 16 and Figure 3- 17). Residues in the C-terminal region also enhanced virion association. Interestingly, residues 252-286 enhanced virion association for transfected $\sigma 1$ to virion (Figure 3- 14), but the same residues reduce overall $\sigma 1$ levels of the genetically engineered virus (Figure 3- 16 and Figure 3- 17) by mechanism(s) yet to be identified. A schematic diagram is created to summarize new knowledge generated by our study about the $\sigma 1$ protein (Figure 3- 19).

Reovirus variants	Reovirus gene	Reovirus protein	Nucleotide mutation	Amino acid change
T3v4	S4	σ 3	U722G	H230Q
	L1	λ 3	G2697A	M892I
	L2	λ 2	A3825G	I1274M
T3v5	L2	λ 2	U3824C	I1273T
T3v8	S1	σ 1	G209U	S66I
T3v11	L3	λ 1	G2887U	A962P
T3v14	L2	λ 2	A3446G	M1148S
T3v16	S1	σ 1	U95C	L28P
T3v1	L1	λ 3	C1216U	P400S
	L2	λ 2	G3316A	M1101I
	L3	λ 1	A425G	N138D
T3v2	S1	σ 1	G45U	S18I

Table 3- 1. Mutations in reovirus variants.

Nucleotide mutations in the indicated genes of each variant relative to T3wt and corresponding alterations in the deduced amino acid are shown respectively.

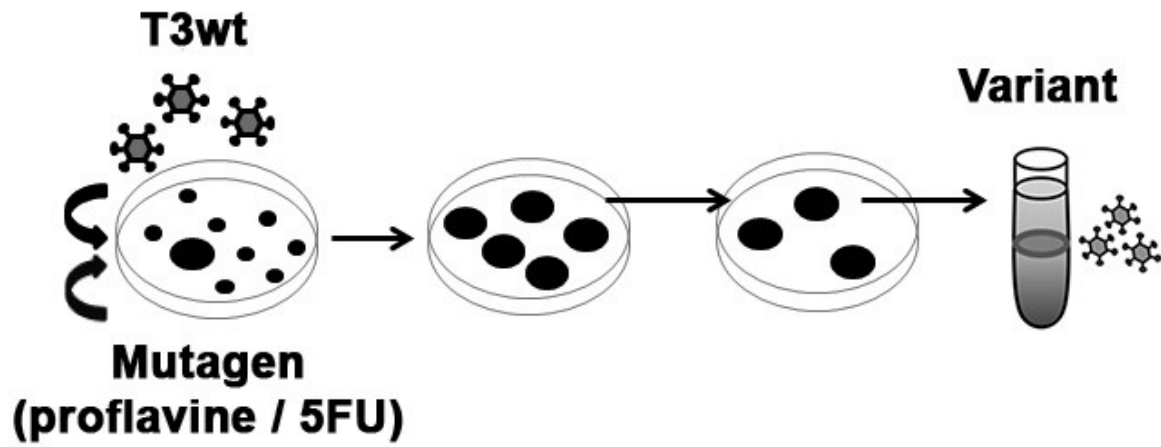


Figure 3- 1. Plaque picking of reovirus variant on L929 cells.

L929 cells were exposed to T3wt or T3v2 in the presence of either proflavine or 5-fluorouracil (5FU). Variants associated with big-plaque phenotype were hand-picked and purified by undergraduate Nashae Narayan. He was also responsible for Sanger-sequencing these variants.

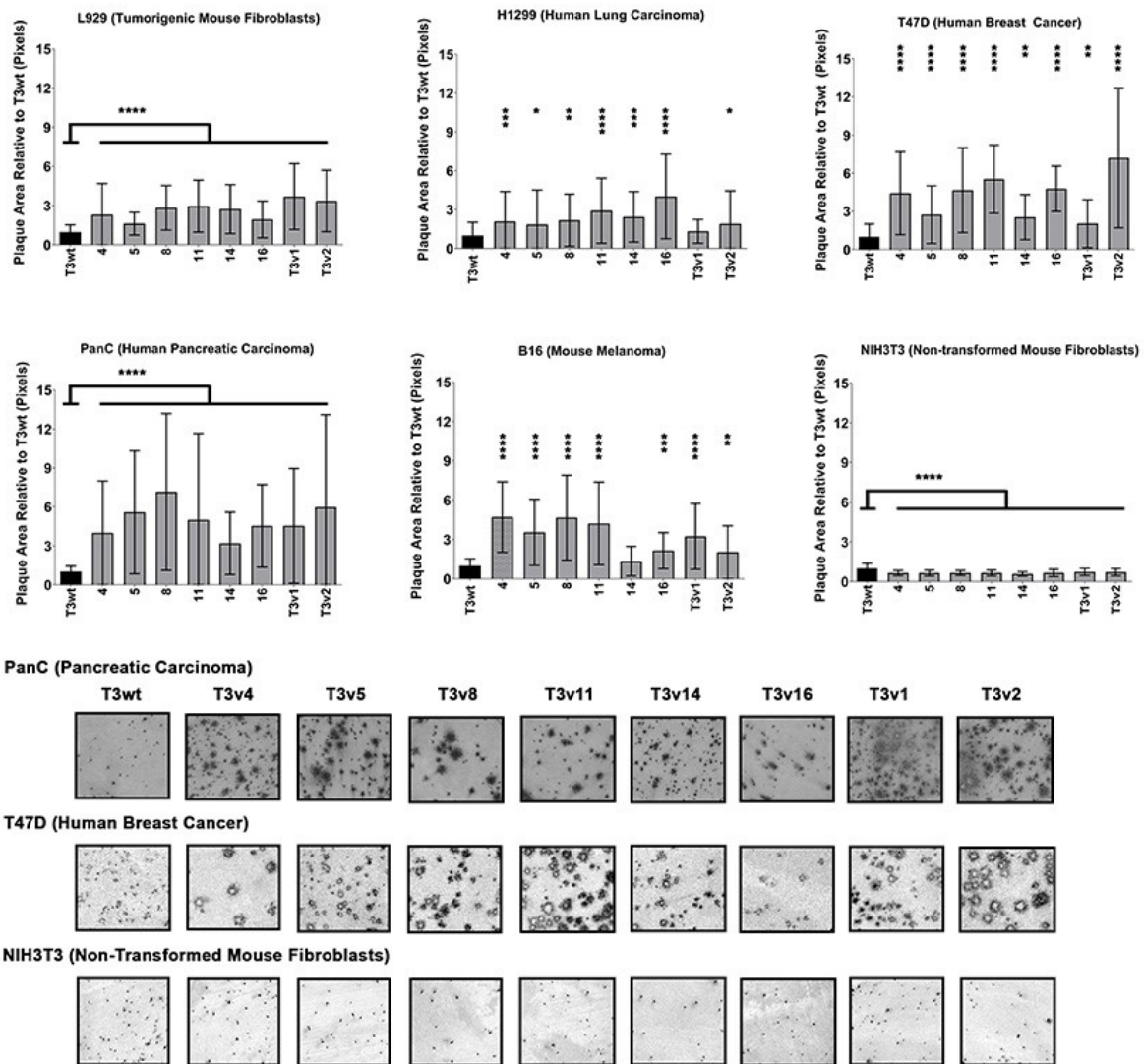


Figure 3- 2. Reovirus variants form large plaques on various mouse and human cancer cells

Plaque sizes of the reovirus variants were compared with previously characterized variants T3v1 and T3v2 on the indicated mouse and human cell cancer lines, the NIH3T3 (non-transformed mouse fibroblast) is also included. For statistics, one-way ANOVA analyses – Dunnett’s multiple comparisons test were performed and mean \pm SD are shown in bar graphs (for L929, $n=3$; for H1299, $n=1$; for T47D, $n=2$; for PanC, $n=6$ for T3wt, T3v4, T3v5, T3v8, T3v11, T3v14, T3v16, and $n=4$ for T3v1 and T3v2; $n=4$ for T3wt, T3v4, T3v5, T3v8, T3v11, T3v14, T3v16, and $n=2$ for T3v1 and T3v2). For significance levels, * = $P<0.05$, ** = $p<0.01$, *** = $p<0.001$ and **** = $p<0.0001$. These experiments were performed by undergraduate Georgi Trifonov.

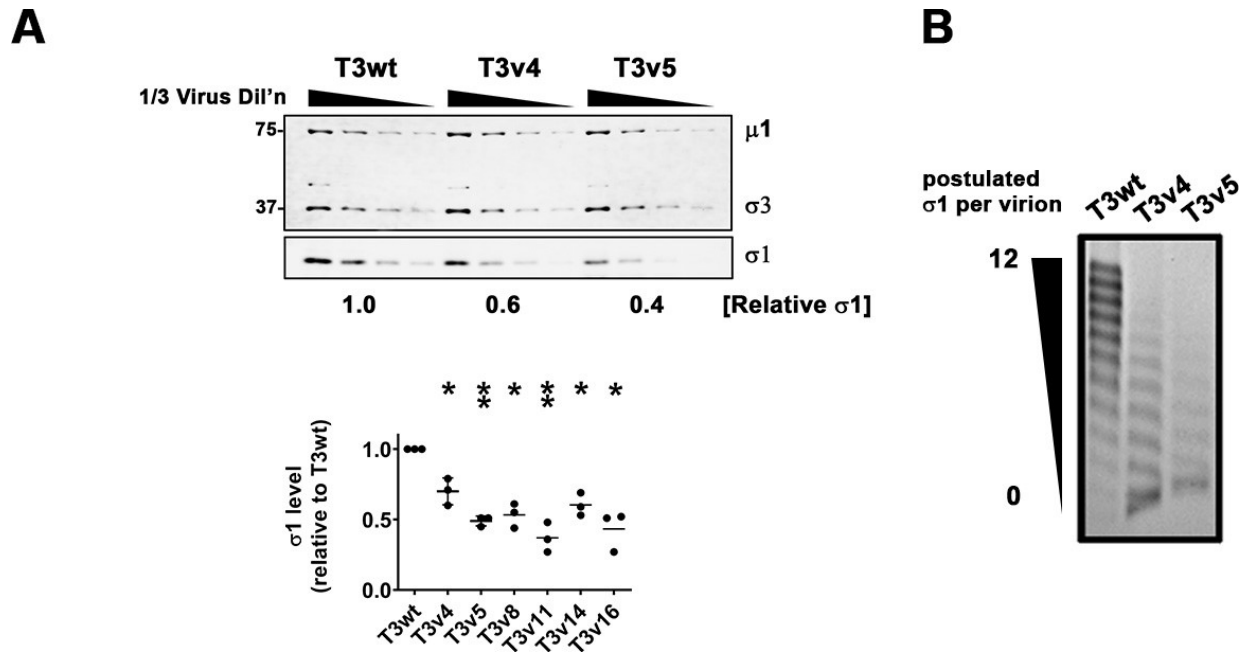


Figure 3- 3. All variants have reduced levels of $\sigma 1$.

Reovirus variants were freshly purified by cesium chloride (CsCl) gradient centrifugation. Their $\sigma 1$ levels were assessed by, **(A)** an example blot showing Western blot comparing $\sigma 1$ levels of T3wt to T3v4 and T3v5. The relative $\sigma 1$ levels were standardized to capsid proteins $\mu 1$ and $\sigma 3$ (one-way ANOVA - Dunnett's multiple comparisons test; $n=3$, mean \pm SD). Note that the two blots were detected and exposed independently. **(B)** Agarose gel electrophoresis was performed to confirm findings from Western blots. Reovirus has a maximum of 12 trimeric- $\sigma 1$. For statistics, * = $P < 0.05$, ** = $p < 0.01$ *** = $p < 0.001$ and **** = $p < 0.0001$.

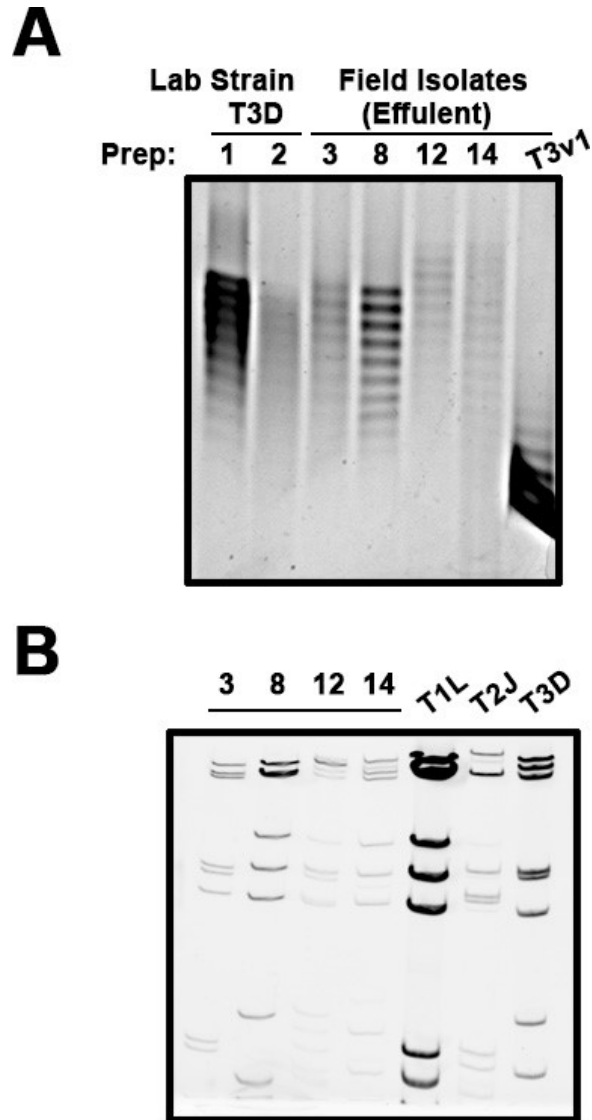


Figure 3- 4. Reovirus field isolates have similar levels of $\sigma 1$ relative to lab stain T3D, and they are reassortants between T1L, T2J and T3D.

(A) Levels of $\sigma 1$ from field isolates were compared to lab strain T3D by agarose gel electrophoresis. **(B)** The dsRNA segments of field isolates were compared to lab strains of reovirus T1L, T2J and T3D by SDS-PAGE. These experiments were performed by Dr. Shmulevitz.

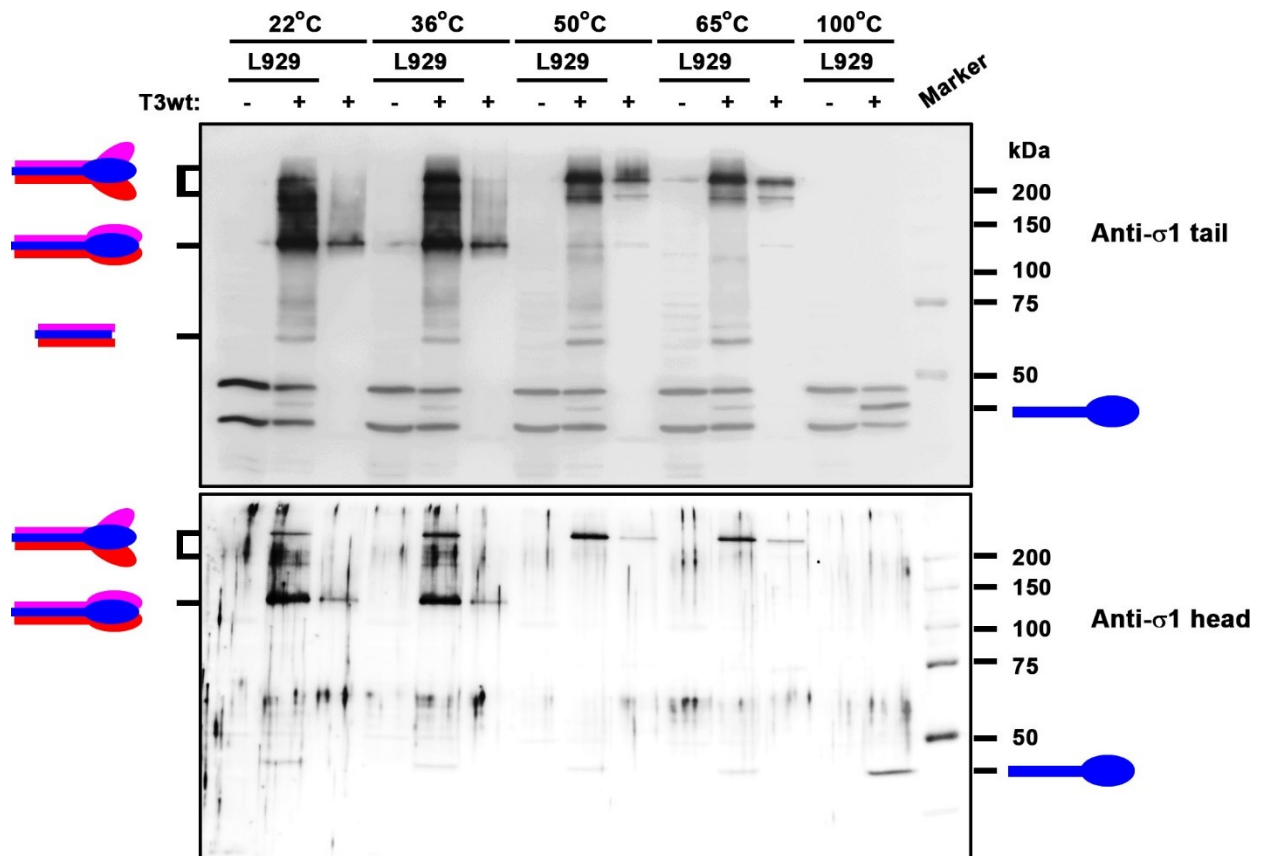


Figure 3- 5. Multimerization of $\sigma 1$ can be detected by altering incubation temperatures with protein sample buffer.

Mock-infected (“-”) or T3wt-infected (“+”) L929 cell lysates and pure T3wt virion (“+”) were incubated with SDS-containing protein sample buffer at the indicated temperatures for 10 minutes. Samples were analyzed by Western blots. The top blot was probed by anti- $\sigma 1$ serum and the bottom blot was detected with anti- $\sigma 1$ head serum.

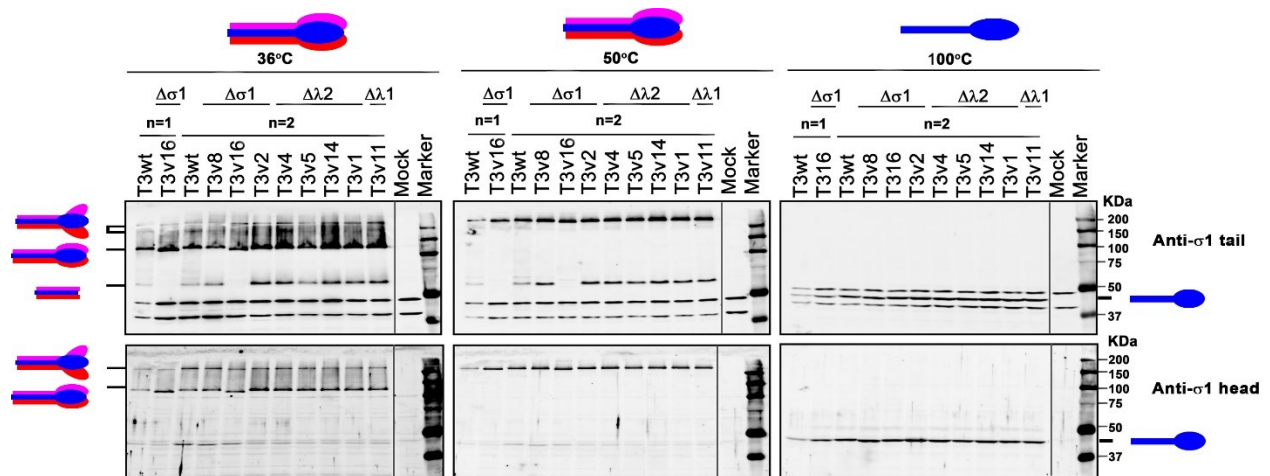


Figure 3- 6. All variants are capable of trimerization.

L929 cells infected with the indicated variants were incubated with SDS-containing sample buffer at 36, 50 and 100°C for 10 minutes, followed by SDS-PAGE analysis. T3wt and T3v16 were duplicates as indicated by n=1 and n=2. The top blot was probed by anti- σ 1 serum and the bottom blot was detected with anti- σ 1 head serum. Protein mutation of each variant is indicated by the Δ symbol on of the variants. Samples from two independent experiments (indicated by “n”) were analyzed on the same blots.

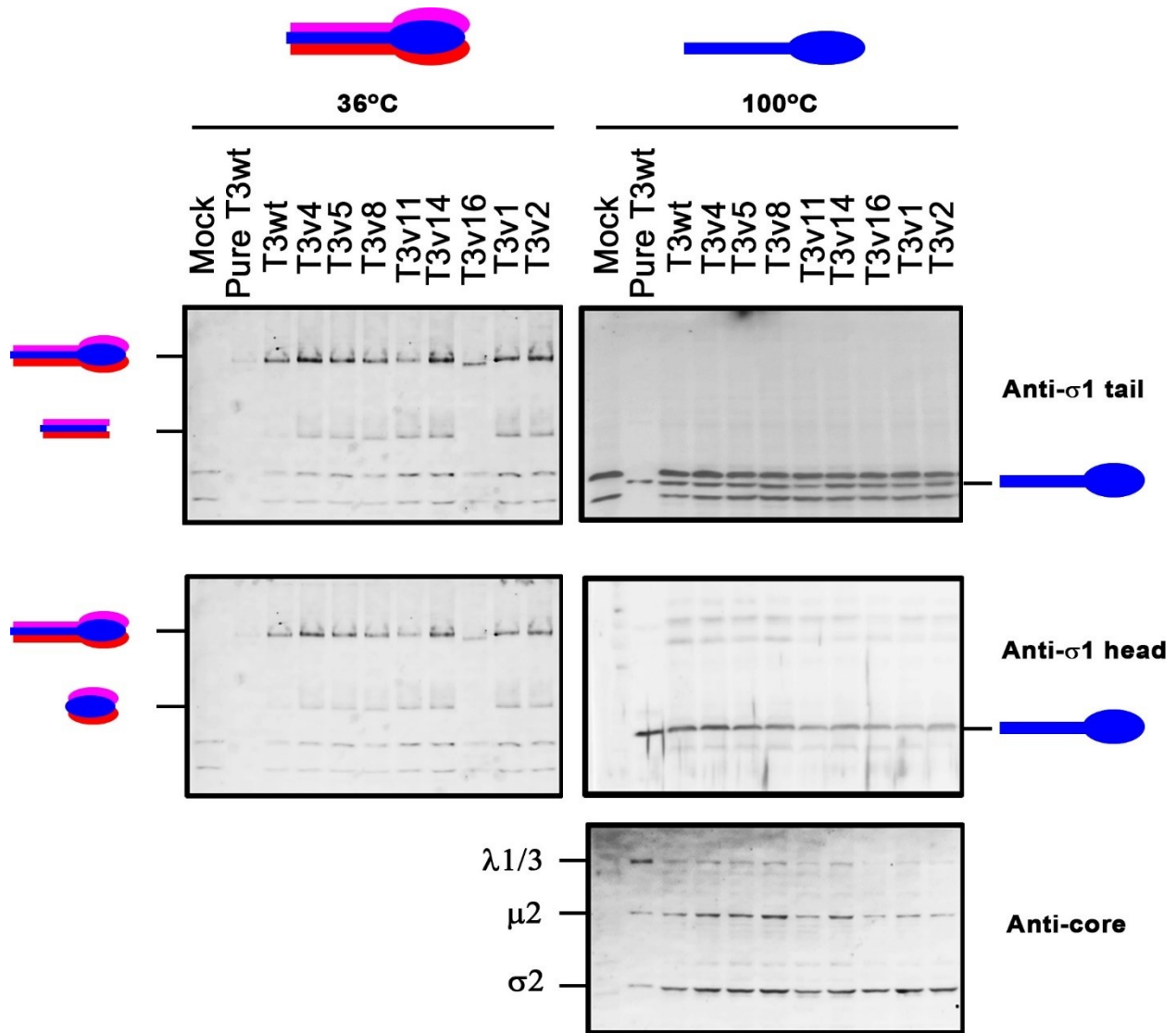


Figure 3- 7. T3v16 σ 1 migrates faster than other variants on SDS-PAGE and does not produce detectable cleaved σ 1 product.

Western blot analysis was performed as described in Figure 3- 6 to confirm migration of σ 1 encoded by T3v16. The blot at the lower right side was probed by anti-reovirus core serum to confirm the loading of viruses.

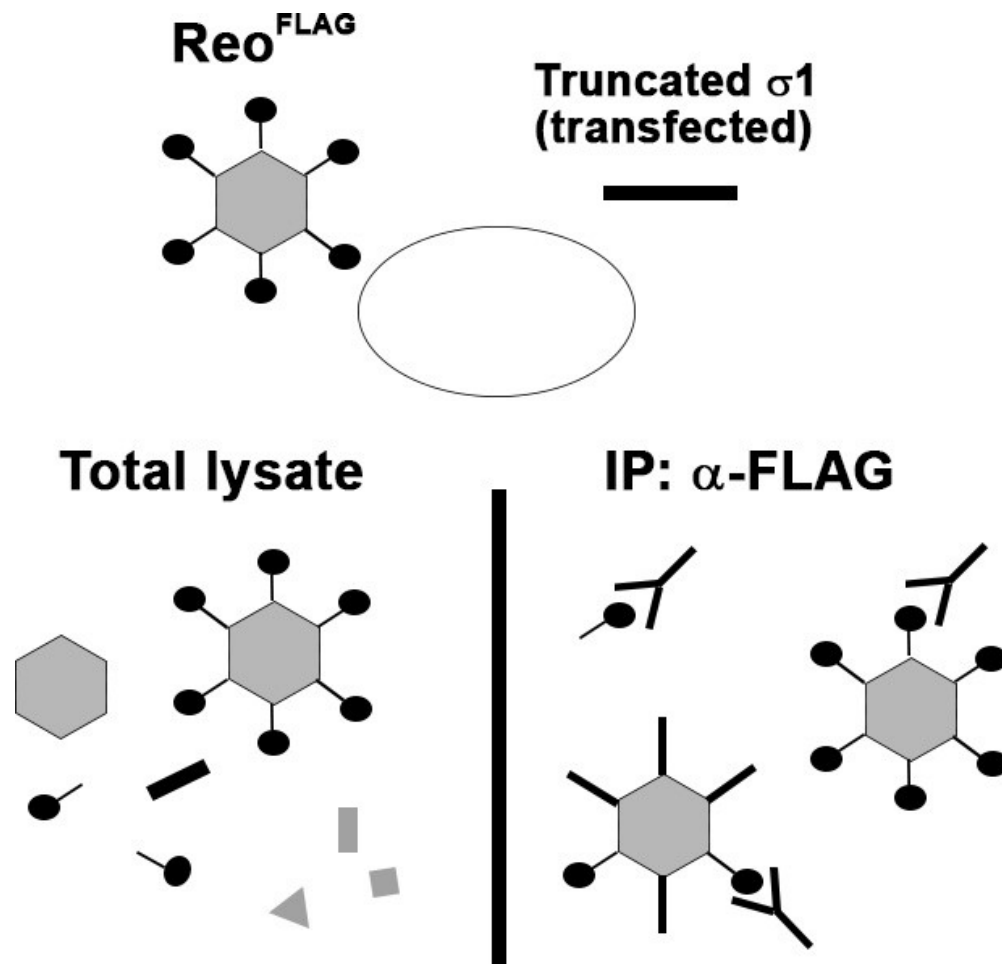


Figure 3- 8. Associations between transfected σ 1-virion is examined by immunoprecipitation.

To compare associations between different transfected σ 1 proteins, NIH3T3-Ras cells were exposed to T3wt with FLAG-tagged σ 1 (Reo^{FLAG}) for 24 hours, followed by transfection of a desired σ 1 construct. At 24 hpt, Western blot analysis was performed using total lysate to examine σ 1 expression levels or virion-associated σ 1s pulled down by anti-FLAG serum.

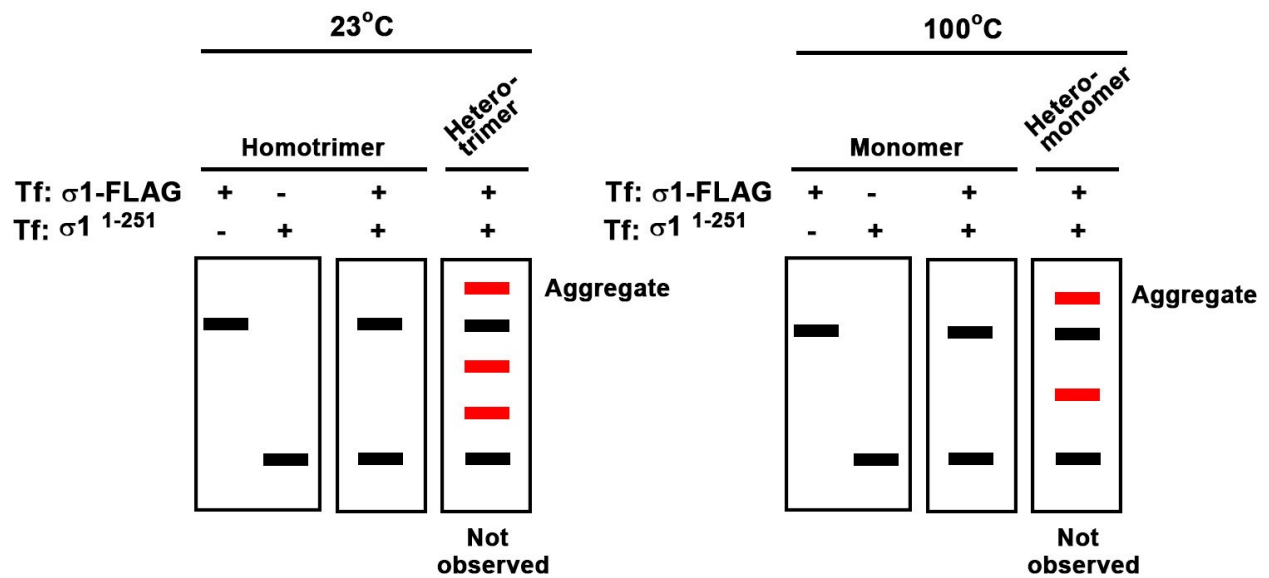
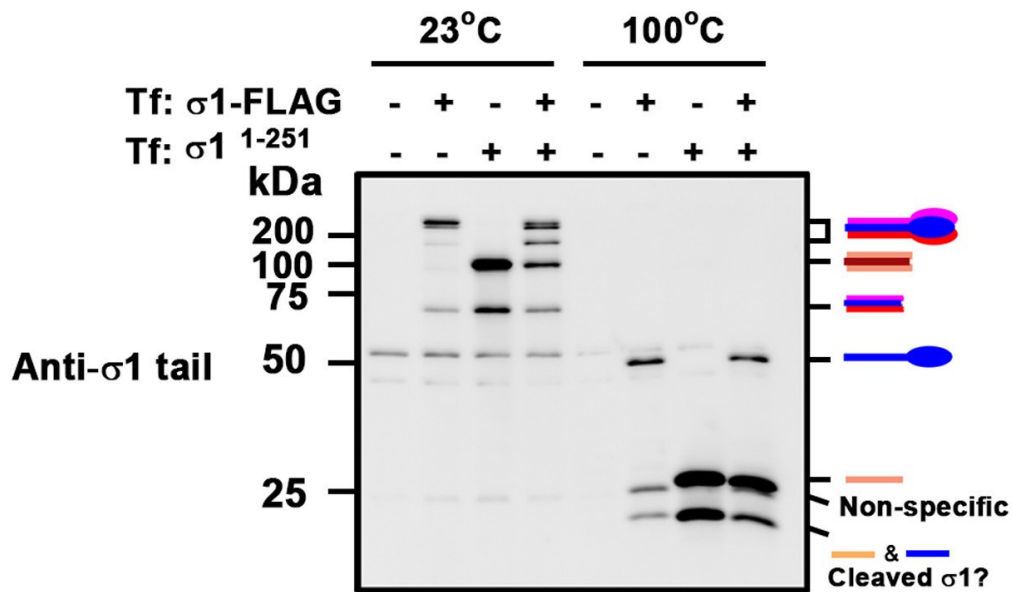


Figure 3- 9. Different σ 1 species do not form aggregate or heteromer.

To determine whether σ 1 with different lengths form aggregate or heteromer, NIH3T3-Ras cells were transfected (Tf) with σ 1 with FLAG-tag (σ 1-FLAG) or σ 1¹⁻²⁵¹, or co-transfected with both constructs. At 24 hpt, cells lysates were subjected to Western blot analyses as described in Figure 3- 5. A schematic diagram below shows the predicted (hypothetical) bands of σ 1 in trimeric or monomeric forms.

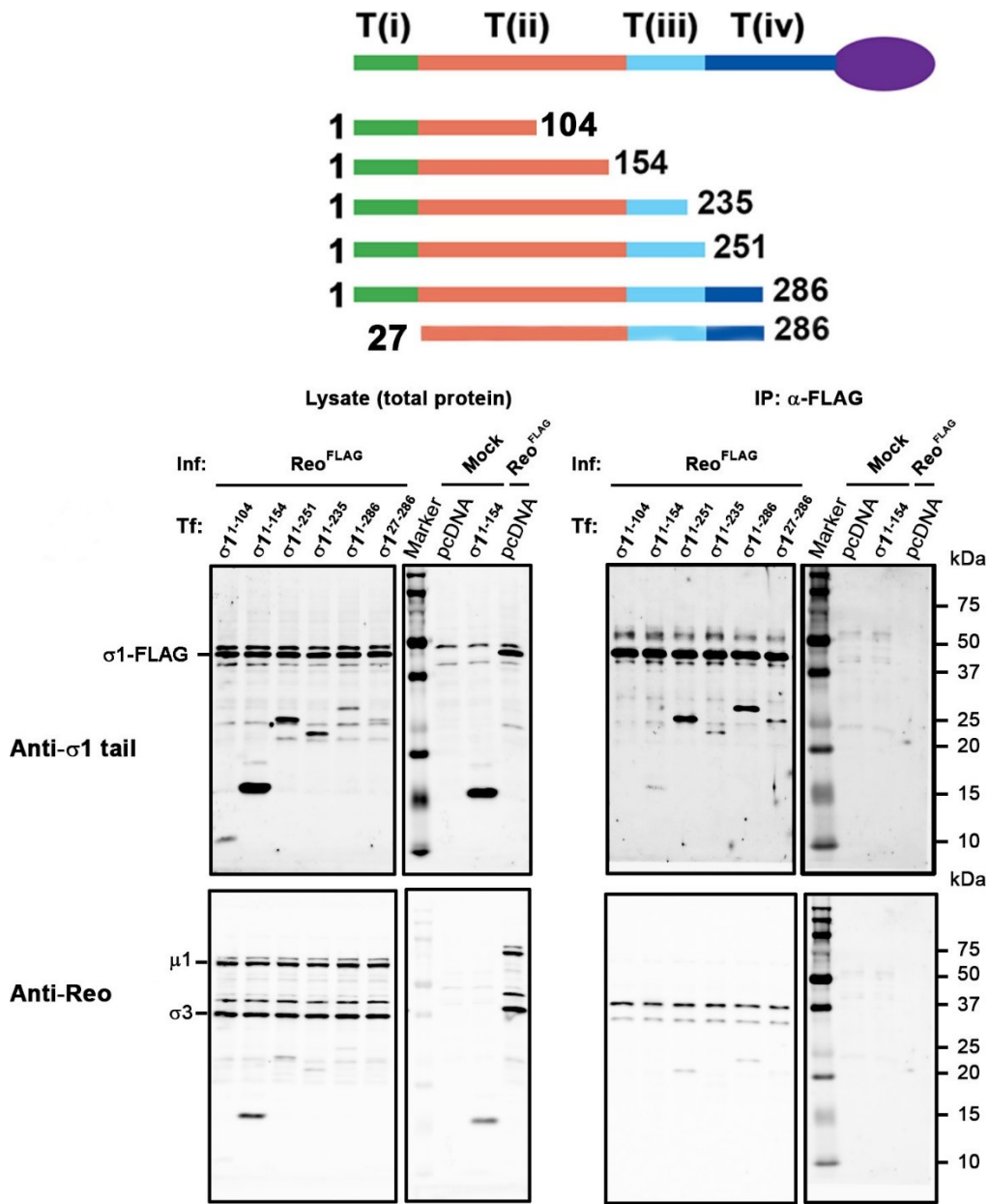


Figure 3- 10. The truncated $\sigma 1^{1-104}$ is not able to be co-immunoprecipitated with virion.

Sigma 1-virion association was examined by infecting (Inf) NIH3T3-Ras cells with T3wt expressing FLAG-tagged $\sigma 1$ (Reo^{FLAG}), followed by transfection (Tf) with the indicated constructs as depicted in the diagram on the right. At 24 hpt, half of cell lysates were directly subjected to Western blot analyses to determine protein expression levels for $\sigma 1$ -FLAG and transfect $\sigma 1$, and the other portion was incubated with anti-FLAG serum for pull-down assays, followed by Western blot analyses. Our controls suggested that co-immunoprecipitation of truncated $\sigma 1$ was through association with Reo^{FLAG} virion because $\sigma 1^{1-154}$ was not pull-downed in the absence of reovirus infection (IP:α-FLAG, the right blot: mock infection).

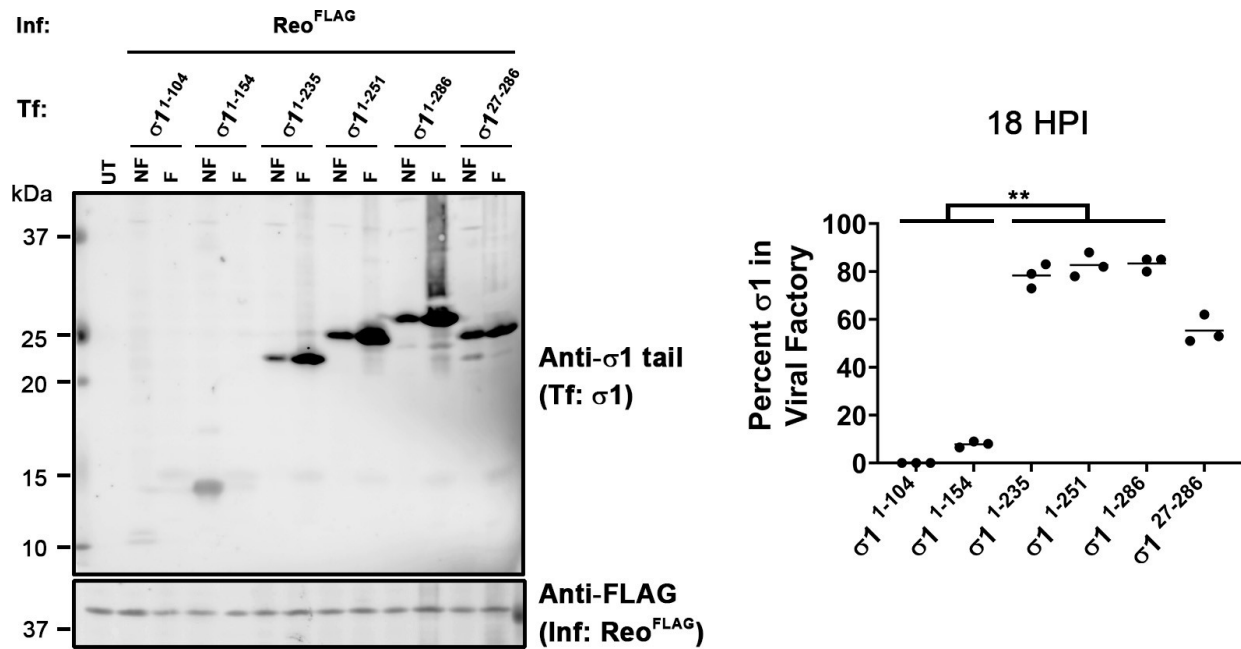


Figure 3- 11. Sigma 1 residues 155-235 play crucial role in viral factory accumulation.

Infection and transfection of NIH3T3-Ras cells performed as described Figure 3- 8. Reoviral factory associated proteins (F) and cytoplasmic proteins were collected (NF), and subjected to Western blot analyses (one-way ANOVA - Dunnett's multiple comparisons test; $n=3$, mean \pm SD). Percent $\sigma 1$ in viral factory was calculated by dividing densitometric intensity of protein band from the F fraction by protein bands from the NF and F fractions. Results were standardized to percent $\sigma 1$ -FLAG in viral factory (lower blot). For statistics, * = $P < 0.05$, ** = $p < 0.01$ *** = $p < 0.001$ and **** = $p < 0.0001$.

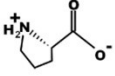
Hydro-phobicity		Construct (residue 28)	Hydro-phobicity		Construct (residue 66)
+-	Proline	 L28P	-	Serine	 wild-type
++	Alanine	 L28A	+-	Threonine	 S66T
+++	Leucine	 wild-type	++	Alanine	 S66A
			+++	Isoleucine	 S66I
			+++	Leucine	 S66L
			+++	Valine	 S66V

Figure 3- 12. Constructs with single amino acid changes at residue 28 or 66 of σ 1 protein.

The above chart summarizes the physical properties of constructs containing single residue replacement of σ 1 protein. Hydrophobicity of each amino acid is indicated by “-” and “+” signs. For example, serine is hydrophilic, as indicated by “-” and valine is very hydrophobic with “+++”. The side chain of the amino acid is shown. Serine and Threonine are polar because of the -OH side chain and all other amino acids are non-polar.

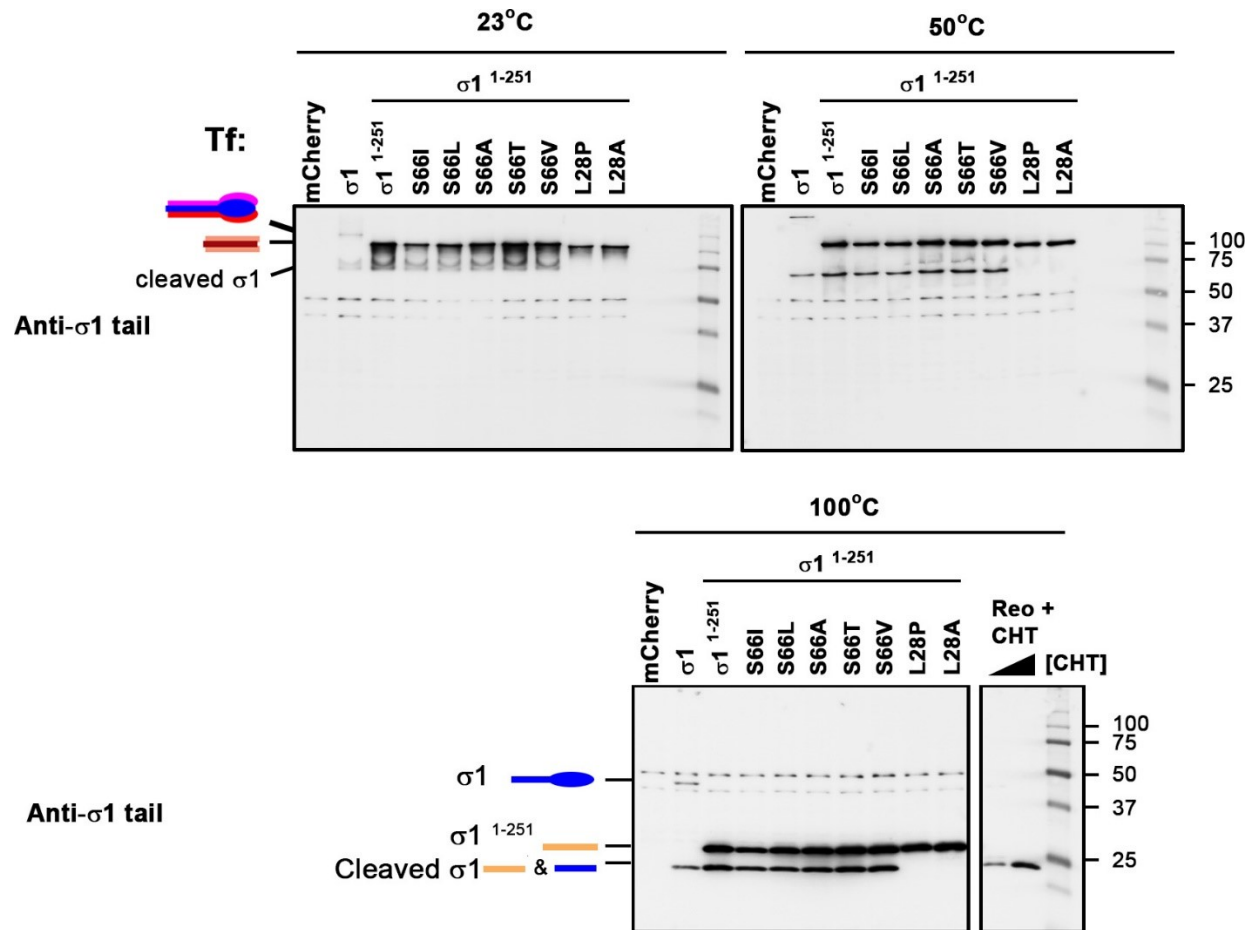


Figure 3- 13. Trimerization of $\sigma 1$ is not affected by the swapped amino acids at residue 28 or 66.

NIH3T3-Ras were transfected with $\sigma 1$ ¹⁻²⁵¹ possessing the indicated alterations at residue 28 or 66. Cell lysates were collected 24 hpt and analyzed by Western blot. Cells transfected with plasmid expressing the red fluorescent protein mCherry were included as negative control (first left lane of each blot). Trimerization of each construct was tested at 23, 50 or 100°C temperature conditions as described in Figure 3- 5.

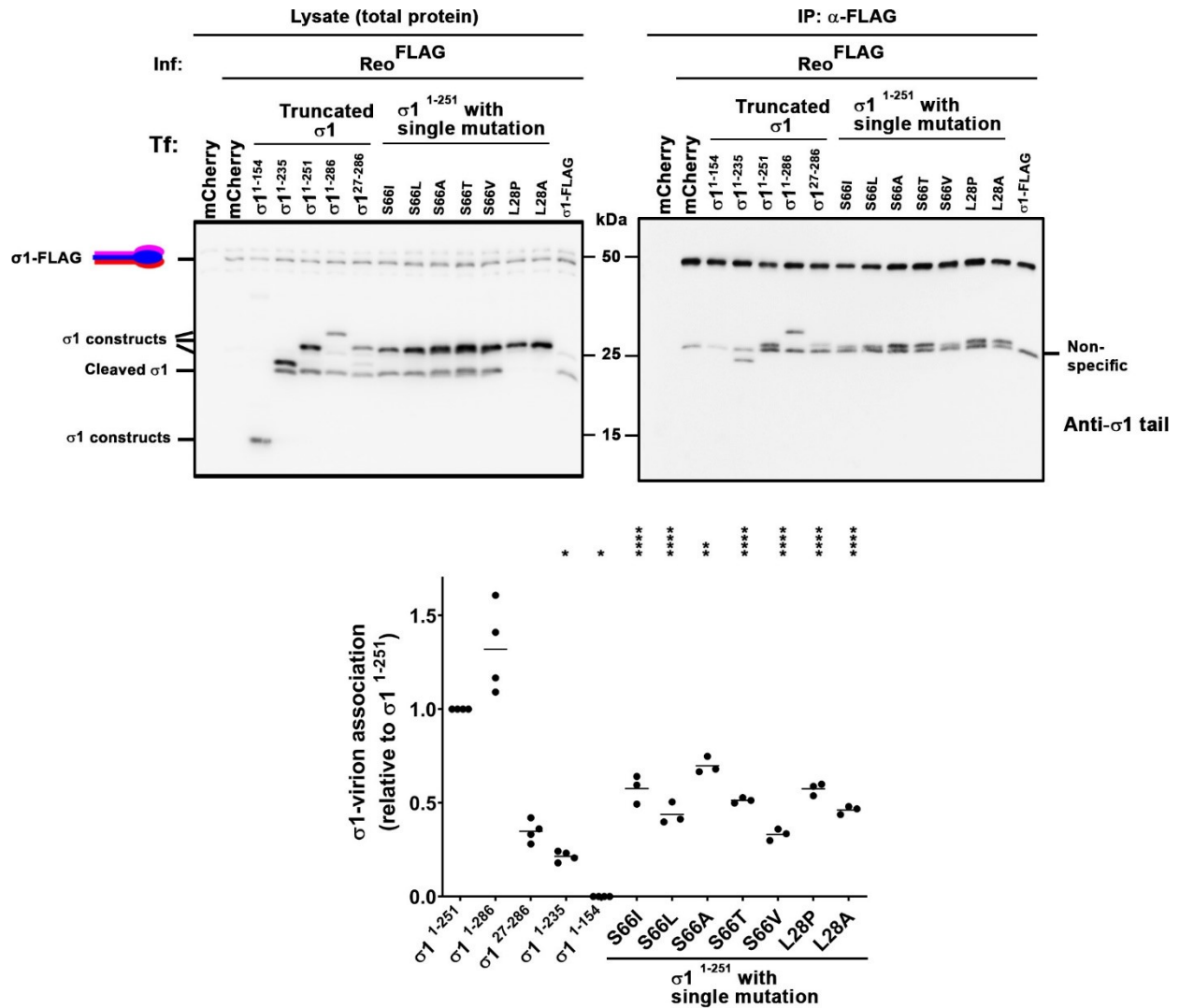


Figure 3- 14. The length of $\sigma 1$ tail and residue 28 or 66 are important for virion association.

Truncated $\sigma 1$ and $\sigma 1$ with single amino acid alterations were tested for virion association by infecting and transfecting NIH3T3-Ras with the indicated constructs as described in Figure 3- 8, followed by Western blots analysis (one-way ANOVA - Dunnett's multiple comparisons test; $n=4$, mean \pm SD). The mCherry is a negative control described in Figure 3- 13. For statistics, * = $P<0.05$, ** = $p<0.01$ *** = $p<0.001$ and **** = $p<0.0001$. Abbreviation: Inf: Infection, Tf: Transfection.

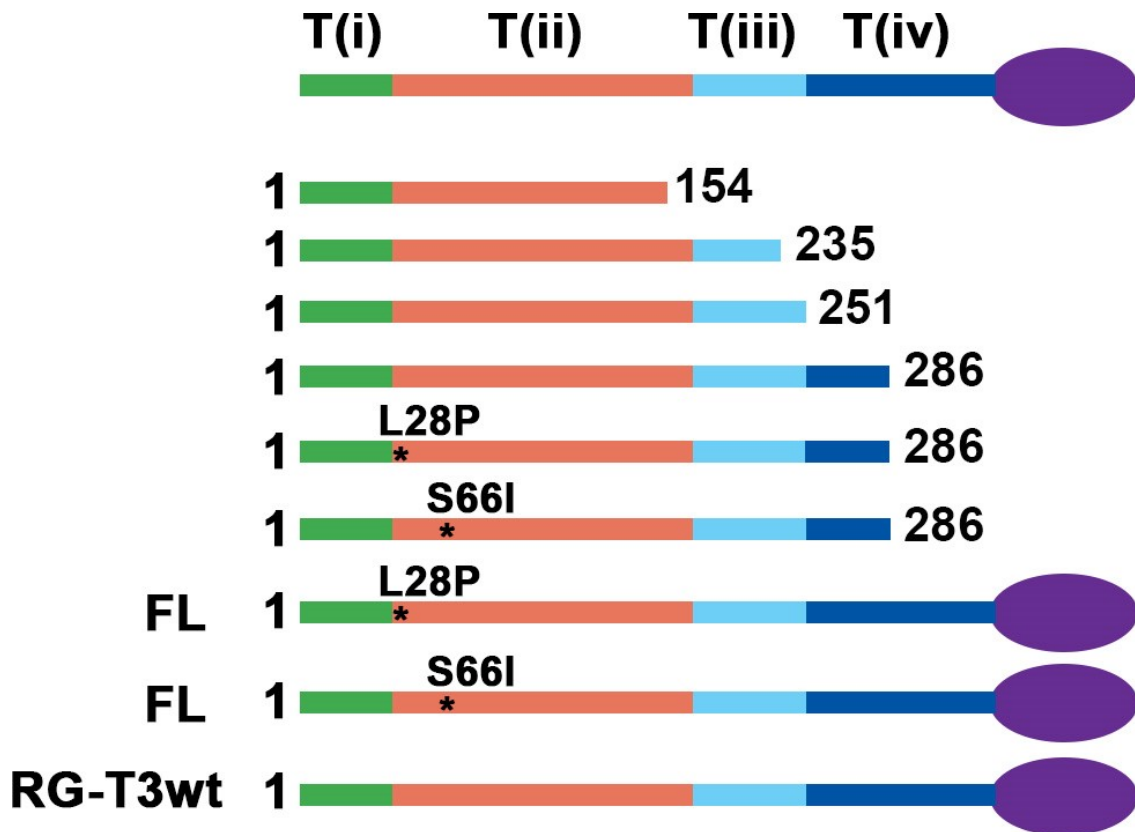


Figure 3- 15. Sigma 1 truncations and single-site mutations are introduced to mutants generated by the reverse genetics (RG) system.

Mutants with $\sigma 1$ truncations and single amino acid mutations were generated by the RG system. The truncated regions and single-site mutations mirror the constructs described in Figure 3- 14. FL indicates full-length $\sigma 1$.

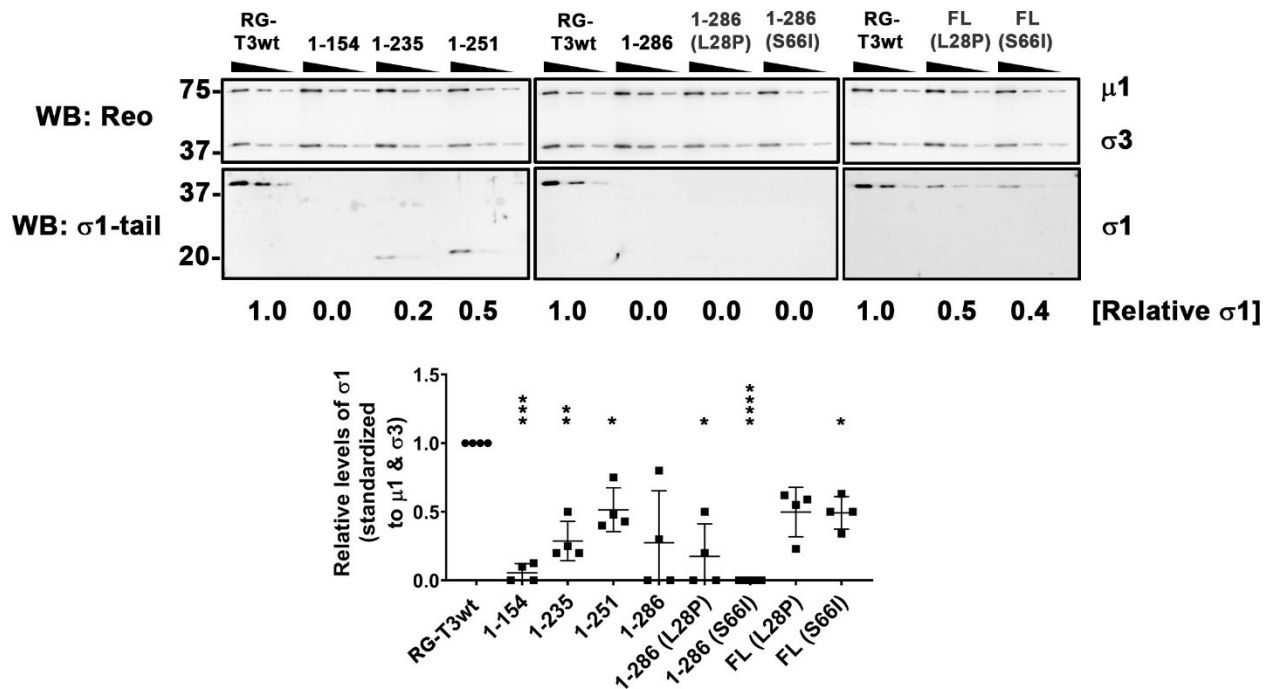


Figure 3- 16. Sigma 1 levels of mutants are analyzed by Western blots.

Mutants were collected and purified using a high-throughput approach (120). Pure virions were subjected to Western blot analyses. Relative levels of σ 1 were standardized to capsid proteins σ 3 and μ 1 (one-way ANOVA - Dunnett's multiple comparisons test; $n=4$, mean \pm SD). For statistics, * = $P < 0.05$, ** = $p < 0.01$, *** = $p < 0.001$ and **** = $p < 0.0001$.

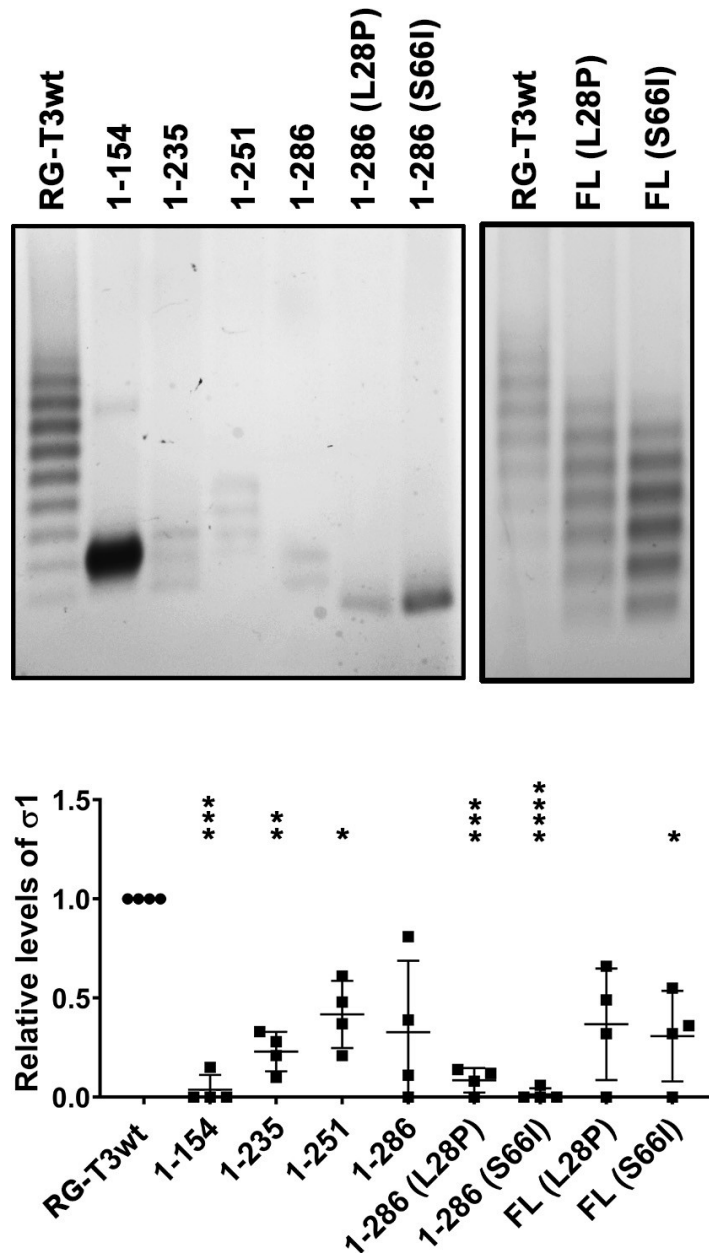


Figure 3- 17. Sigma 1 levels of mutants are analyzed by agarose gel electrophoresis

Agarose gel electrophoresis was performed with pure virions to confirm findings from Western blot analyses from Figure 3- 16 (one-way ANOVA - Dunnett's multiple comparisons test; $n=4$, mean \pm SD). For statistics, * = $P < 0.05$, ** = $p < 0.01$ *** = $p < 0.001$ and **** = $p < 0.0001$.

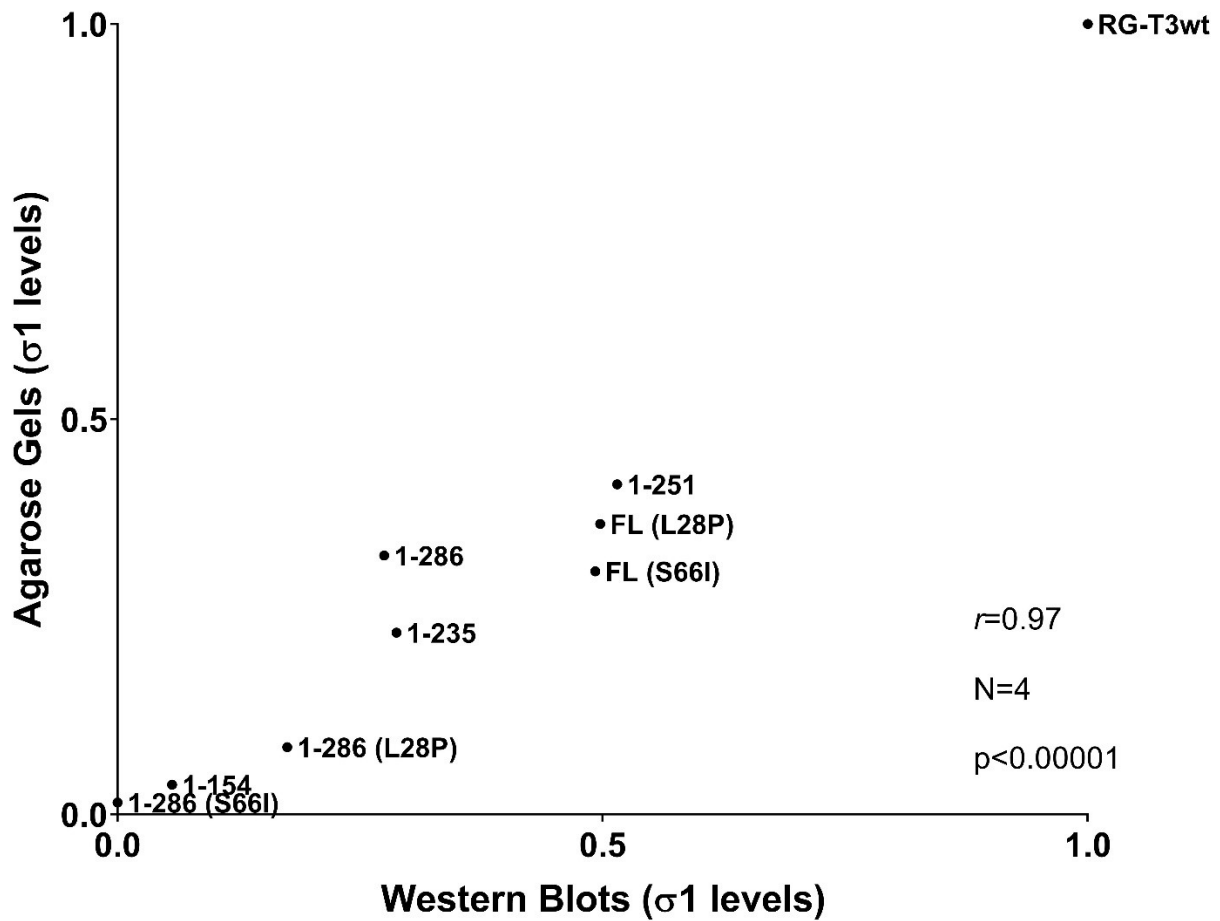
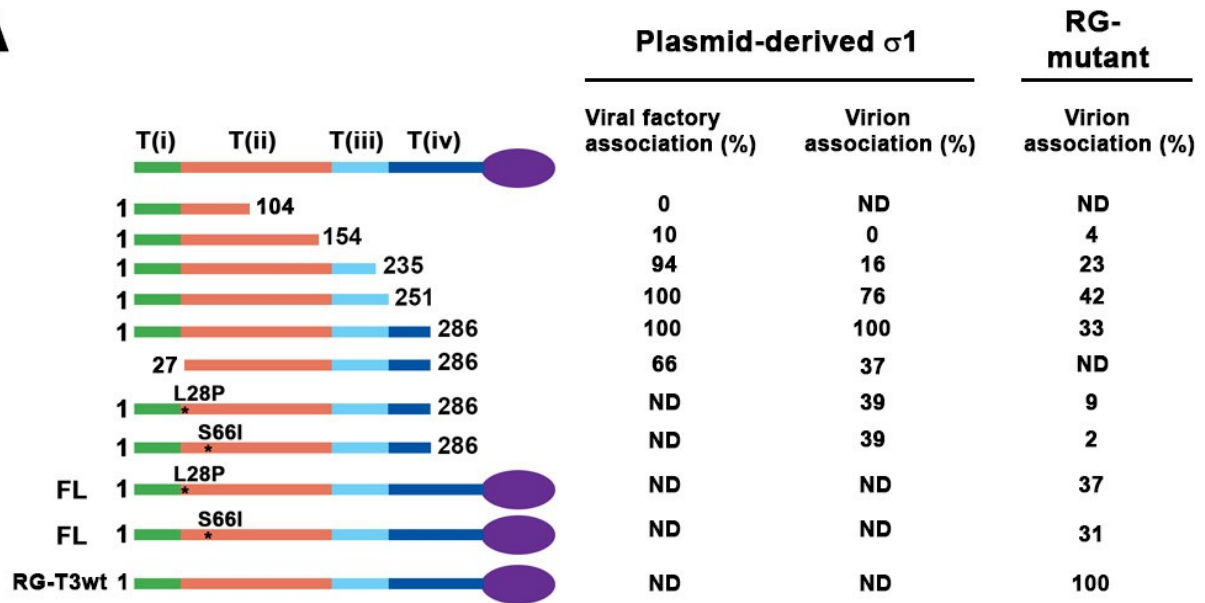


Figure 3- 18. Results from Western blot analysis and agarose gel electrophoresis have a very strong positive correlation.

Analyses of $\sigma 1$ levels from Western blots and agarose gel electrophoresis were used to generate a dot plot depicting the strength of correlation between the two data sets. Each dot represents the mean value.

A



B

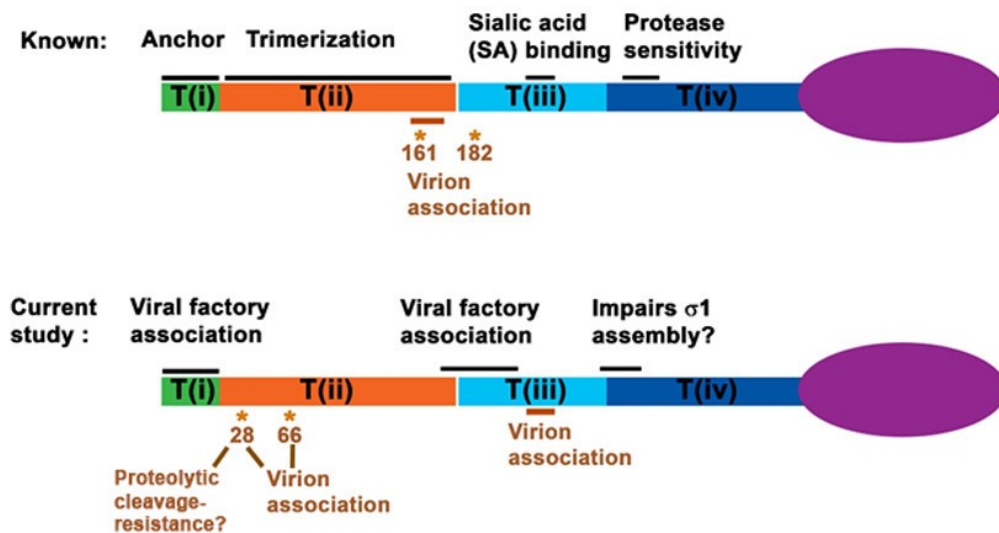


Figure 3- 19. Novel functions of $\sigma 1$ discovered by the current study.

(A) A schematic diagram showing the truncations and mutations of plasmid-derived $\sigma 1$ s and mutants generated by the RG system. Their viral factory and virion associations are represented as percentages. ND = not determined or construct not available. **(B)** Two linear $\sigma 1$ structures are shown above. Known functional domains are summarized in the top structure and findings from our study are depicted in the structure below.

CHAPTER 4: IDENTIFYING A NOVEL MECHANISM TO IMPROVE ONCOLYTIC REOVIRUS

4.1 Introduction

4.1.1 Chapter objective

Our findings in Chapter 3 suggested that reduction of $\sigma 1$ is a widely shared mechanism by many variants; a phenotype acquired by parallel evolution that allows reovirus variants with reduced $\sigma 1$ on particles to uncoat faster in transformed cells. All previously described variants had altered infectivity towards cancer cells in the entry step (cell attachment and uncoating). To our knowledge, reovirus mutations that increase infectivity at post-entry steps have yet to be described. If late stages of reovirus replication could be enhanced in tumor cells, then the mutations that promote these late stages could potentially further promote reovirus oncolysis. Accordingly, in this chapter, I sought to identify novel mutations and mechanism(s) that augment post-entry replication steps.

4.1.2 Introduction to five reovirus variants that were selected for characterization in this chapter.

I began my screening for a variant of interest by focusing on 5 variants that were generated by directed evolution (Figure 3- 1), but not previously characterized. These variants were selected from multiple rounds of plaque picking, where each time the largest plaques were chosen. Note that increased plaque size is used as a preliminary assessment for the overall-enhancement of virus infection, cell death, or cell-cell spread. The five variants

consistently caused larger plaques than wild-type reovirus, and therefore were likely to have a hereditary change. Sanger-sequencing was performed to identify the mutations in these variants. A summary of all 5 variants and their mutations is provided in Table 4- 1. I will briefly describe each mutation and how it potentially affects the functions of viral proteins.

Variant T3v6 has multiple mutations in 3 different genes. Note that in this section, the gene numbering starts at the transcription start site.

1. The S1 gene encodes for the cell-attachment $\sigma 1$ and it has one mutation. The G663U mutation causes a glutamine to histidine replacement of residue 217. Results from chapter 3 showed that $\sigma 1$ residues 155-235 were involved in virion association (please refer to section 3.2.5), but it is unclear whether a single amino acid replacement at residue 217 affects virion association. The mutation is close to the residues 198, 202-204 and these amino acids were implicated in SA binding on host cell (please refer to section 1.5.2). Overall the most-likely effect of this mutation, if it contributes to increased plaque size of T3v6, is the changes in $\sigma 1$ levels or cell binding.
2. The M1 gene encodes for the polymerase co-factor $\mu 2$ and it has two mutations. The C347U mutation causes a leucine to phenylalanine replacement of residue 114 and the U1850G mutation results in a serine to alanine replacement of residue 613. The altered residue 613 is not mapped to any known functional domain, but residues 115-138 have been identified as immunoreceptor tyrosine-based activation motifs (ITAMs) (27,71,90,241). Stebbing *et al.* examined the functions of T3D $\mu 2$ ITAMS by introducing null alleles into the ITAM-encoding sequence, which specifically inhibited the biological

functions of ITAM (241). Plaque assays suggested that reovirus bearing mutant $\mu 2$ -ITAM had impaired spreading and replication in L929 and AD (Adeno) 293 cells. AD 293 was derived from HEK293 and showed a more superior adherence to tissue culture dishes. Since altered residue 114 is very close to the ITAMs sequence, replication of T3v6 may be altered.

3. The L2 gene encodes for turret protein $\lambda 2$ and it has one mutation. The G1225A mutation causes the aspartic acid to asparagine replacement of residue 408. The altered residue is in the putative methyltransferase domain (residues 400-450) of $\lambda 2$ and it may affect mRNA synthesis (40,137,290).

Variant T3v10 has two mutations, one in the S1 gene and the other in the M1 gene.

1. The S1 gene has an A946G mutation which causes the asparagine to arginine replacement of residue 312 in $\sigma 1$. The replaced amino acid is located in the “neck” region where the $\sigma 1$ tail connects to the $\sigma 1$ head, and therefore, structural stability of $\sigma 1$ and JAM-A binding capability of the $\sigma 1$ head may be affected. Please refer to section 1.5.3 for a review of the $\sigma 1$ “neck” region.
2. The M1 gene has a C1848U mutation that changes residue 612 from alanine to valine. Functions associated with this region have not been identified to date, but I will discuss this mutation in detail in Chapter 5.

Variant T3v11 has a single mutation in the L3 gene.

1. The G2897U mutation in the L3 gene causes an alanine to serine change at residue 962 of the core protein $\lambda 1$. Comparisons between protein sequences of λA from two different strains of avian orthoreovirus (ARV) to the MRV ortholog $\lambda 1$ suggested that the mutated residue 962 is not mapped to any conserved or known functional domain (274). It is possible that this mutation affects mRNA capping and synthesis because $\lambda 1$ has the well-characterized RTPase activities and cooperates with the mRNA capping and export protein $\lambda 2$ (please see section 1.2.3 for a review of reovirus genome transcription). Furthermore, a study visualized the structure of viral core by X-ray crystallography and showed that residue 962 might belong to a subdomain that interacted with $\lambda 2$ (206). Taken together, this unique mutation may affect mRNA synthesis of T3v11. In addition, another earlier study used cryo-electron microscopy (cryo-EM) analysis to show that $\lambda 1$ interacts with $\sigma 2$ to form the main structure of core (82). In conclusion, the altered residue may have an impact on the stability of the viral core.

Variant T3v12 has 4 mutations and each mutation is located in a different gene.

1. The S1 gene inherited the G65U mutation from T3v2, a variant that has been described in the previous publication from our lab (231). This mutation is known to cause a serine to isoleucine alteration at residue 18, which is located in the anchoring domain of $\sigma 1$. Based on previous observations, this mutation is expected to reduce $\sigma 1$ levels by a factor of two.

2. The S4 gene encodes for outer capsid protein $\sigma 3$. The A222G gene mutation causes a glutamic acid to lysine change at residue site 64. Multiple publications suggested that residue 64 is one of the main sites that plays a crucial role in $\mu 1$ binding (150,160,192). This mutation can affect T3v12 in three different ways. First, $\sigma 3$ and $\mu 1$ form interlocking $\sigma 3$ - $\mu 1$ heterohexamers, and these heterohexamers are the backbone for the outer capsid. I predict that the S4 mutation may alter the stability of the outer capsid of reovirus. Second, mutant $\sigma 3$ may affect its strength in binding with $\mu 1$ and complete removal of $\sigma 3$ is required for the cleavage of $\mu 1$ during uncoating (please refer to section 1.2.2), and therefore, uncoating of the variant may be affected. Lastly, $\sigma 3$ has been shown to bind dsRNA and inhibit the PKR-mediated antiviral response. Two studies directly examined the role of $\sigma 3$ in binding dsRNA (please refer to section 1.3.4 for a review of reovirus replication and antiviral response). The first study showed that the dsRNA-binding domain of $\sigma 3$ is located in the C-terminal region (158), and the mutated residue 64 is not a part of the proposed dsRNA binding domain. The second study showed that free $\sigma 3$ was able to bind dsRNA and prevent the activation of PKR. However, when $\sigma 3$ was bound to $\mu 1$, the dsRNA binding capacity of $\sigma 3$ was lost (281). The crystal structure of $\sigma 3$ suggested that the N-terminal region of the protein was responsible for $\mu 1$ binding (192), and mutations of residue 16, 64, 66 and 67 greatly reduced or completely abolished $\mu 1$ binding (159). And thus, the altered residue 64 of $\sigma 3$ in variant T3v12 is likely to affect binding with $\mu 1$ and thereby alter $\sigma 3$ -modulated PKR-mediated antiviral responses and/or impact outer capsid stability and uncoating.

3. The L1 gene has an A2933G mutation that leads to a single amino acid change at site 972 in the $\lambda 3$ polymerase where a glutamine is being replaced by arginine. Although the $\lambda 3$ mutation is not in any domains or regions that were predicted to interact with $\lambda 2$ or mRNA directly, based on the published model from cryo-EM analysis (287), genome transcription may be affected by the mutation, as the stability of $\lambda 3$ may be altered.
4. The Last mutation is found in the L3 gene that encodes for the structural core protein $\lambda 1$. The U398C gene mutation results in a tyrosine to histidine change at residue 122. One study examined the importance N-terminal residues of $\lambda 1$ in the formation of reovirus core-like structures by infecting insect cells with baculoviruses that co-expressed reovirus core proteins $\lambda 2$, $\sigma 2$ and $\lambda 1$ constructs with a series of deletion mutations within the first 315 amino acids of $\lambda 1$ (133). The cell lysates were subjected to cesium chloride (CsCl) gradient centrifugation (viral core-like structure would form as distinct bands with different buoyant densities, depending on whether $\lambda 1$ was incorporated into the core-like structure). The resulting bands were collected and purified. SDS-PAGE, Coomassie staining and cryo-EM were performed to confirm the incorporation of $\lambda 1$ mutants. The authors concluded that deletion of the first 230 amino acids did not affect the formation of core-like structures. Although data from truncated mutants suggested the N-terminal region is dispensable for core formation, sequence comparison analyses revealed that residues 5-12, 100-103 form the motifs of the NTP binding domain (24). The mutated residue 122 may therefore affect NTPase activity of $\lambda 1$.

Variant T3v13 has two mutations in the S1 gene.

1. The A352C gene mutation causes a threonine to proline replacement at residue 114. As discussed in chapter 3, residue 114 is located in the T(ii) region that is proposed to be important for $\sigma 1$ trimerization, and therefore, $\sigma 1$ levels of T3v13 may be affected.
2. The G668A gene mutation changes the arginine at residue 219 to glutamine. Residue 219 is very close to the SA binding domain of $\sigma 1$ (please refer to section 1.5.2), and thus host cell binding may be altered.

4.2 Results

4.2.1 All 5 variants form bigger plaques on L929 and PanC cells relative to T3wt

Although the five variants were chosen based on their ability to form bigger plaques compared to T3wt during the positive selection process, it was necessary to quantify plaque size and demonstrate significant differences. I am also interested in comparing their efficiency at different stages of infection such as cell binding and progeny release. To obtain a large quantity of virus, I infected L929 cells in suspension culture with each variant and collected cell lysates when ~50% of cells were visually lysed. The cell lysates were subjected to CsCl density-gradient centrifugation and purified (Figure 4- 1). Three independent preparations of variants and T3wt control were plaque titrated on monolayers of L929 cells (Figure 4- 2). Variants T3v6, T3v10 and T3v11 formed plaques that were 3-fold bigger than T3wt. Average plaque sizes from T3v12 and T3v13 were 2-fold bigger than T3wt. These results suggested that replication and/or

dissemination of all variants was enhanced by their mutations ($n=3$, $p<0.0001$ for T3v12 and $p<0.01$ for T3v13).

While I was determining plaque sizes of the 5 variants in L929 cells, undergraduate Georgi Trifonov assessed plaque size for T3v6, T3v10, T3v11 and T3v13 on human pancreatic carcinoma (PanC) cells and non-transformed mouse fibroblast (NIH3T3) (Figure 4- 3). The 4 variants had significantly larger plaques than T3wt in PanC cells and plaque size of T3v10 was 8-fold bigger than T3wt. Importantly, T3wt and all 4 variants only produced small foci of reovirus-antigen-positive infected cells on NIH3T3 fibroblasts even at 7 days post-infection. These foci indicated that the viruses were able to produce proteins but they were restricted in cell-cell spread. Furthermore, one-way ANOVA - Dunnett's multiple comparisons test revealed that all variants actually produced significantly smaller foci than T3wt ($n=3$, $p<0.0001$) on non-transformed cells. Taken together, the above results demonstrated that the variants were adapted to replicate and/or spread more efficiently in transformed cells, but that the virulence of the variants towards non-transformed cells was attenuated.

4.2.2 Variants T3v11 and T3v12 had reduced levels of $\sigma 1$

The main goal of this chapter was to find novel mechanisms that augment reovirus replication in transformed cells at post-entry steps. It was important that these mutants therefore not exhibit the previously characterized reduction of $\sigma 1$ that augments reovirus entry. I therefore sought to determine $\sigma 1$ levels of the 5 variants. To determine $\sigma 1$, freshly-purified virions were subjected to SDS-PAGE and stained with Coomassie Brilliant dye to

determine the relative concentration of virus preparations (Figure 4- 4). Once the concentrations of T3wt and variants were determined, equivalent particle amounts of T3wt and variants were subjected to Western blot analysis for reovirus capsid proteins (Figure 4- 5). Compared to T3wt, T3v11 and T3v12 had 3-fold less $\sigma 1$ ($n=4$; mean \pm SD; one-way ANOVA and Dunnett's multiple comparisons test, $p<0.0001$). In conclusion, the phenotype of T3v11 and T3v12 can be explained by effects on $\sigma 1$ levels and are therefore not pursued as candidates for further characterization.

4.2.3 All variants had similar host-cell binding and uncoating relative to T3wt

With a focus to identify variants that have advantage at post-entry steps of replication, I then compared early stages of virus infection such as cell binding and virus uncoating among the variants. To assess cell binding, 12-well plates containing monolayers of L929 cells were pre-chilled at 4°C for 30 minutes to prevent virus internalization (233). Pre-chilled cells were then exposed to an equivalent particle dose of T3wt or variants and incubated for 1 hour at 4°C with gentle swishing. Unbound viral particles were washed away with PBS and cell lysates were collected for Western blot analysis to measure cell-associated virus proteins (Figure 4- 6). Despite that T3v11 and T3v12 had reduced levels of $\sigma 1$, their bindings to host-cell were relatively similar to T3wt; this was not surprising based on our previous data showing that $\geq 20\%$ sigma 1 is sufficient for binding (180). Important for my aim, none of the variants had a deficiency in binding and were assessed further for other entry steps.

We next determined if the early steps of uncoating were affected in our reovirus variants. Reovirus uncoating involves two major processes: (1) The degradation of $\sigma 3$ and cleavage of $\mu 1$ to δ , and (2) disassociation of all $\sigma 1$ from the virion (please refer to section 1.2.2 and Figure 1- 3 for the review of reovirus uncoating). Undergraduate Georgi Trifonov performed the reovirus uncoating assays, by exposing L929 cells to equal cell-bound T3wt or variant at 4°C to synchronize infection, followed by transfer to 37°C to permit internalization and uncoating. Cell lysates were collected every hour for up to 5 hours, followed by Western blot analysis to monitor cleavage of $\mu 1$ (Figure 4- 7). All variants exhibited similar rates of $\mu 1$ cleavage compared to T3wt. In summary, our results suggested that none of the variants had an advantage over T3wt in the binding and early steps of uncoating.

4.2.4 T3v10, T3v12 and T3v13 are less effective in establishing productive infection

So far, the test for sigma 1 levels eliminated T3v11 and T3v12 as best-candidates for post-entry mechanisms of enhanced reovirus infectivity, but binding and uncoating studies did not further eliminate variants as candidates. Next, I decided to test whether they could establish productive infection by examining protein expression. A quick way to determine viral protein expression in cells was to perform immunocytochemistry staining. This technique allowed me to visualize the localization of reovirus proteins in cells by using polyclonal reovirus antiserum which specifically recognized viral proteins. I exposed L929 cells to equal doses of cell-bound T3wt or variants. At 18hpi, cells were processed as indicated in section 2.3.3 and

visually examined by light microscope (Figure 4- 8). Surprisingly, T3v10, T3v11, T3v12 and T3v13 were less effective at establishing productive infection compared to T3wt. The experiment was repeated two more times and the results consistently showed that 8-fold more virions of T3v10 were required to infect the same amount of cells, relative to T3wt (Figure 4- 8). However, I should emphasize that although these 4 mutants produced fewer reovirus-antigen-positive cells at 18hpi, they produced bigger plaques on L929 (Figure 4- 2) and PanC cells (Figure 4- 3). This suggests that these variants most-likely have replicative advantages at a step of replication or spread that comes after establishing infection.

4.2.5 T3v10 and T3v13 release progeny earlier during infection than T3wt

Our data from immunocytochemistry (ICC) staining unexpectedly showed that variants T3v10, T3v11, T3v12 and T3v13 were less effective at establishing productive infection (Figure 4- 8), but consistently produced bigger plaques on two test cell lines (Figure 4- 2 and Figure 4- 3). The wild-type reovirus takes an average of 24 hours to complete one replication cycle. Production of viral proteins can be detected at 12hpi (Figure 5- 10) and total progeny synthesis gradually increased from 10hpi to 24hpi (Figure 5- 1A). One possible way to interpret the unexpected findings (Figure 4- 8) is that the variants have an advantage in releasing progeny prior to 18hpi (the time point I performed the ICC staining), but the released progenies have not synthesized enough detectable proteins at 18hpi.

To test my hypothesis that some variants might release progeny at earlier time points, plaque assays were used to assess progeny release between T3wt and the variants. Note that I

excluded T3v12 because it inherited the S1 mutation from T3v2, and this mutation was known to enhance infectivity of its parental virus T3v2 (180). L929 cells were exposed to equal doses of T3wt or variants (Figure 4- 9). At 12 and 24hpi, intracellular- and released-virus (from media) were collected independently and plaque titrated on monolayers of L929 cells. Percent release was calculated by dividing titer from released-virus) by total titers (titer from released-virus plus titer from intracellular virus). On average, T3v10, T3v11 and T3v13 released at least 2.5-fold more progeny than T3wt at 12hpi, while T3v6 released similar amount of progeny relative to T3wt. This suggested that these T3v10, T3v11 and T3v13 indeed had an advantage in releasing progeny at an earlier time point, and mutations in T3v6 appear to enhance its progeny release at 24hpi: about 2.5 fold higher than T3wt.

4.2.6 T3v10 is chosen for further characterization

Based on the above data, T3v10, T3v11 and T3v13 were less effective in establishing productive infection (Figure 4- 8), but they had an advantage in releasing progeny at an earlier time point (Figure 4- 9). T3v11 had reduced levels of $\sigma 1$ (Figure 4- 5) and was therefore excluded from further characterization. T3v6 and T3v10 were the desired candidates and both of these two variants had one mutation in outer capsid protein $\sigma 1$ and one mutation in the polymerase co-factor $\mu 2$. However, $\sigma 1$ levels of both variants were similar to T3wt and this suggested that plaque size on transformed cells was augmented by a potentially new mechanism that is not associated with $\sigma 1$ reduction. Based on the above information, T3v10 was chosen for further characterization, as its $\sigma 1$ levels (Figure 4- 5) and cell binding (Figure 4-

6) were similar to T3wt, but it was capable of releasing progeny earlier than the wild-type virus (Figure 4- 9). Thus, mutations from T3v10 are likely to augment plaque size by promoting a post-uncoating step. To verify that T3v10 indeed possessed enhanced oncolytic potency, Georgi Trifonov compared plaque size of T3v10 to T3v1 and T3v2 (the two variants that were found to promote survival of mice grafted with human melanoma, please refer to section 1.4.1) on various cancer cells (Figure 4- 10). Our data suggested that T3v10 formed plaques that were at least as big as T3v1 and T3v2, and therefore, we decided to focus on T3v10.

4.2.7 The A612V alteration in μ 2 is responsible for the large-plaque phenotype of T3v10

T3v10 had two mutations and we did not know whether one or both mutations contributed to the big plaque phenotype. We sought to isolate the two mutations by reassortment. Undergraduate Georgi Trifonov generated reassortants by co-infecting L929 cells with T3wt and T3v10 and successfully generated the variant T3v10^{M1} (Figure 4- 11). He also confirmed that T3v10^{M1} inherited the M1 gene mutation from T3v10, while other genes had sequences identical to the wild-type virus.

Finally, I repeated several key analyses to determine if T3v10^{M1} shared phenotypes with the parental T3v10; in other words, if the mutation in μ 2 was sufficient for these phenotypes. Plaque assay demonstrated that T3v10^{M1} formed plaques with similar size compared to T3v10 (Figure 4- 12). I also performed Western blot analysis (Figure 4- 13) and agarose gel electrophoresis (Figure 4- 14) to determine σ 1 levels. T3v10^{M1} had similar levels of σ 1 relative

to its parental virus T3wt and T3v10; all 3 viruses showed similar binding to L929 cells (Figure 4-15). Since previous data suggested that T3v10 uncoated at similar rates compared to T3wt, I did not perform uncoating assay to compare T3v10^{M1} with T3wt. In conclusion, the single mutation in $\mu 2$ was responsible for the phenotype of T3v10 and this mutation was chosen for further characterization in chapter 5.

4.3 Summary

In this chapter, five variants generated by directed evolution (Figure 3- 1) were showed to form big plaques on L929 (Figure 4- 2) and PanC cells, while sparing non-transformed NIH3T3 (Figure 4- 3). They were selected for characterization in an attempt to identify novel mechanisms that augment reovirus replication in post-uncoating step(s). T3v6, T3v10 and T3v13 possessed similar levels of $\sigma 1$ relative to T3wt (Figure 4- 5). Despite that T3v11 and T3v12 had 3-fold lower $\sigma 1$ levels compared to T3wt (Figure 4- 5), host cell binding (Figure 4- 6) and rates of uncoating (Figure 4- 7) were relatively similar between all the variants and T3wt. Surprisingly, T3v10, T3v12 and T3v13 less effectively established productive infection at 18hpi (Figure 4- 8), but had an advantage in releasing progeny at 12hpi (Figure 4- 9) which may explain why immunocytochemistry staining detected fewer reovirus-antigen-positive cells. Based on all the above results, I decided to exclude variants with reduced $\sigma 1$ (T3v11 and T3v12) and the variant possessing a single S1 gene mutation (T3v13) from further investigation. Both T3v10 and T3v6 had an M1 gene mutation that resulted in a single amino acid alteration in $\mu 2$. $\mu 2$ is a multifunctional viral protein and its mutation can potentially affect mRNA synthesis and

the later steps of the replication cycle. We chose to focus on T3v10 as our results suggested its replication was likely to be enhanced in later steps of replication (please refer to section 4.2.6) and T3v10 produced plaques as large as T3v1 and T3v2 (Figure 4- 10). Reassortment was performed by co-infecting L929 cells with T3wt and T3v10 (Figure 4- 11) to generate the variant T3v10^{M1}. Sequencing data confirmed that it possessed the M1 gene mutation from T3v10, while nucleotide sequences of other genes were identical to the wild-type virus. Furthermore, plaque assay confirmed that T3v10^{M1} formed plaques with similar sizes compared to parental virus T3v10 on L929 cells (Figure 4- 12). Western blot analysis (Figure 4- 13) and agarose gel electrophoresis (Figure 4- 14) showed T3v10^{M1} had similar levels of σ 1 compared to its parental viruses T3v10 and T3wt, and as expected, all 3 viruses attached to L929 cells in similar manner (Figure 4- 15). In conclusion, it appeared that T3v10^{M1} was augmented by mechanism(s) that was not previously identified and the next chapter will focus on this variant.

Reovirus variants	Reovirus gene	Reovirus protein	Nucleotide mutation	Amino acid change
T3v6	S1	σ 1	G663U	Q217H
	M1	μ 2	C347U	L114F
	L2	λ 2	U1850G G1225A	S613A D408N
T3v10	S1	σ 1	A946G	N312R
	M1	μ 2	C1848U	A612V
T3v11	L3	λ 1	G2897U	Q962R
T3v12	S1	σ 1	G45U	S18I
	S4	σ 3	A222G	K64E
	L1	λ 3	A2933G	Q972R
	L3	λ 1	U398C	Y122H
T3v13	S1	σ 1	A352C	T114P
			G668A	R219S

Table 4- 1. Mutations in reovirus variants.

Gene mutations and their associated amino acid changes are shown above.



Figure 4- 1. Viral bands generated by Vertrel® XF-CsCl density-gradient centrifugation.

Reovirus particles can be extracted from cell lysate subjected to Vertrel® XF-CsCl density-gradient centrifugation (174). The above picture shows two distinct bands with different buoyant densities. In this example, the top white band contains virions without dsRNA and the full virions are in the bottom band.

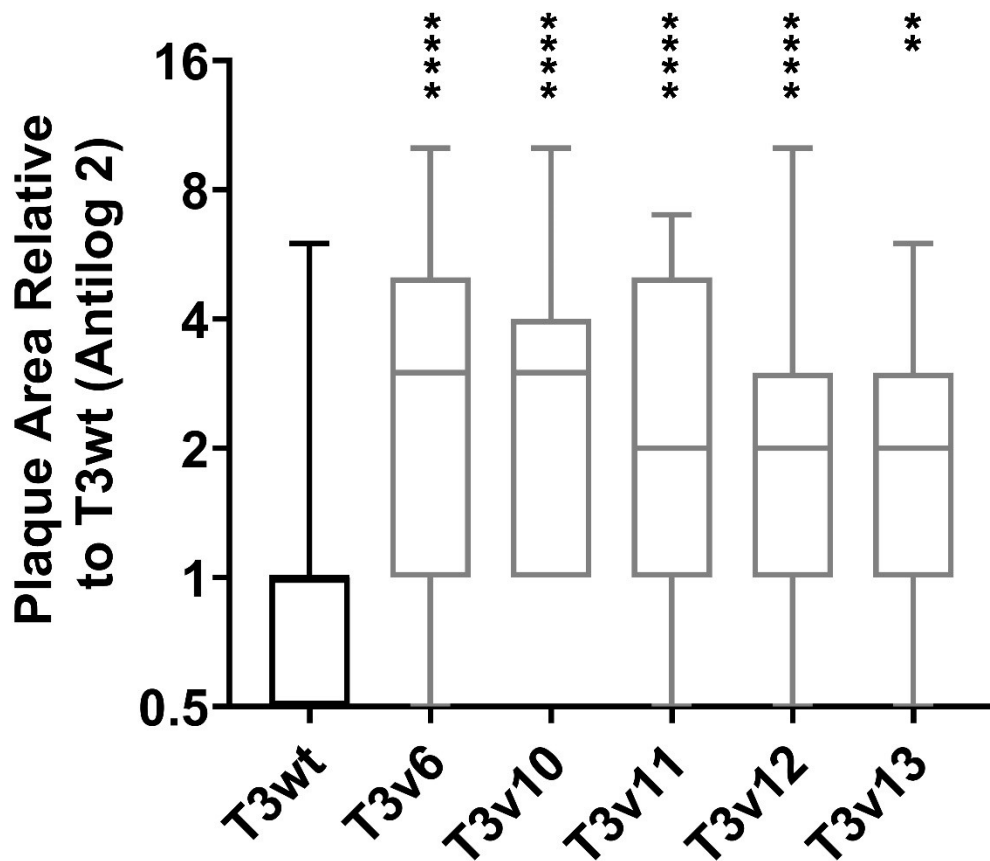
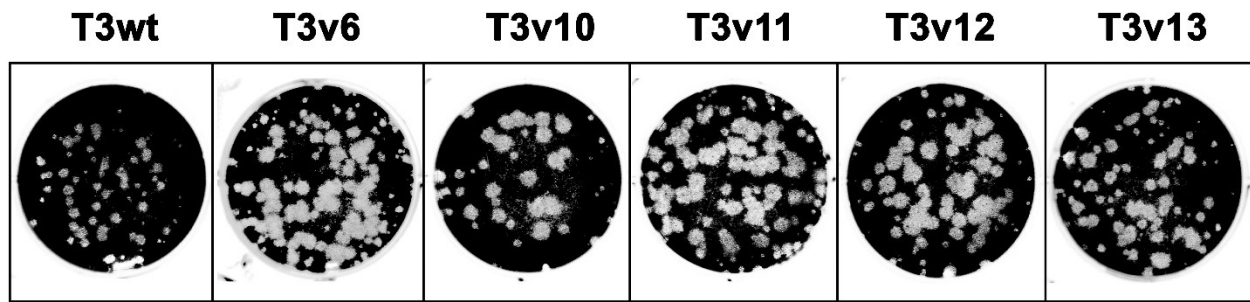


Figure 4- 2. Plaque assay comparing variants with T3wt on L929 cells.

Monolayers of L929 cells were exposed to the indicated variants under plaque assay conditions described in Materials and Methods. Cells were stained with crystal violet 4 days post-infection. Sizes of plaques were quantified by ImageQuant TL and are presented in a box-and-whisker plot showing four quartiles ($n=3$; mean \pm SD; one-way ANOVA - Dunnett's multiple comparisons test). For statistics, * = $P < 0.05$, ** = $p < 0.01$, *** = $p < 0.001$ and **** = $p < 0.0001$.

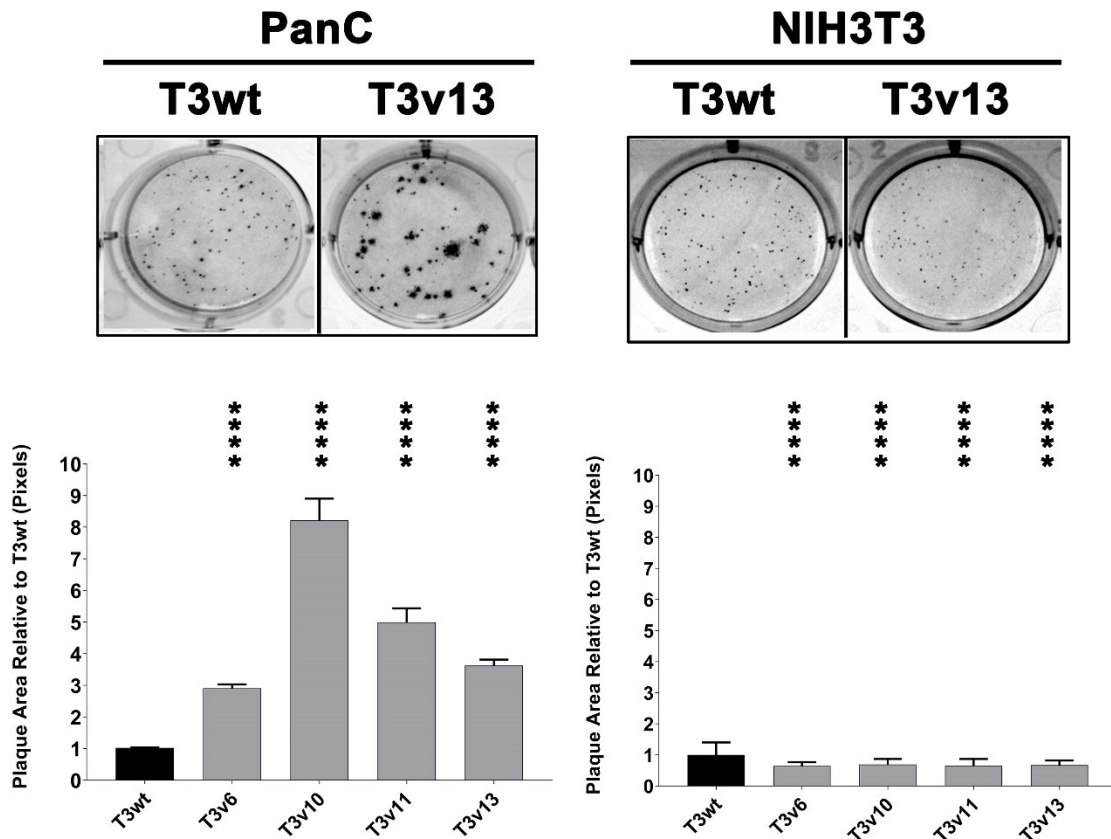


Figure 4- 3. Plaque assay comparing variants with T3wt on PanC and NIH3T3 cells.

Monolayers of PanC or NIH3T3 cells were exposed to T3wt or variants indicated in the bar graphs. Comparisons between T3wt and T3v13 were shown for human pancreatic carcinoma (PanC) and non-transformed mouse fibroblast (NIH3T3) as examples. Sizes of plaques were quantified by ImageQuant TL ($n=3$; mean \pm SD; one-way ANOVA - Dunnett's multiple comparisons test). For statistics, * = $P<0.05$, ** = $p<0.01$ *** = $p<0.001$ and **** = $p<0.0001$. The above experiment was performed by undergraduate Georgi Trifonov and I did the statistical analysis.

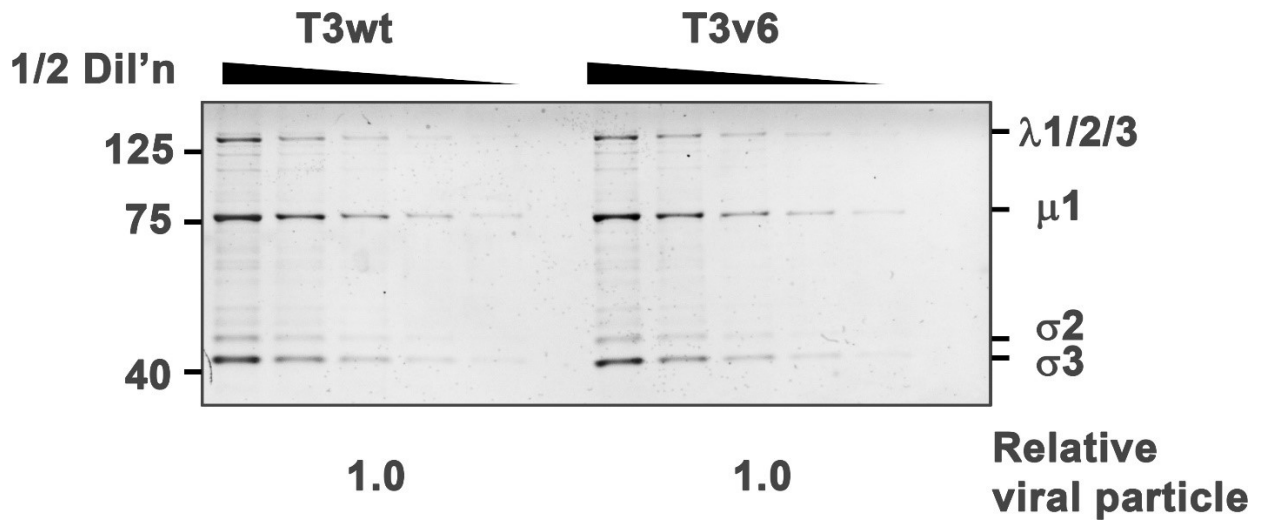


Figure 4- 4. Coomassie Blue staining of reovirus proteins.

Above is an example of Coomassie Blue staining. This is a standard procedure used in our lab to quantify viral particles for sequential experiments such as cell-binding assay. Note that serial dilutions of the virions were performed so the linearity range of T3wt and T3v6 could be compared. The quality of the virus could be inferred from the appearances of the indicated viral protein bands.

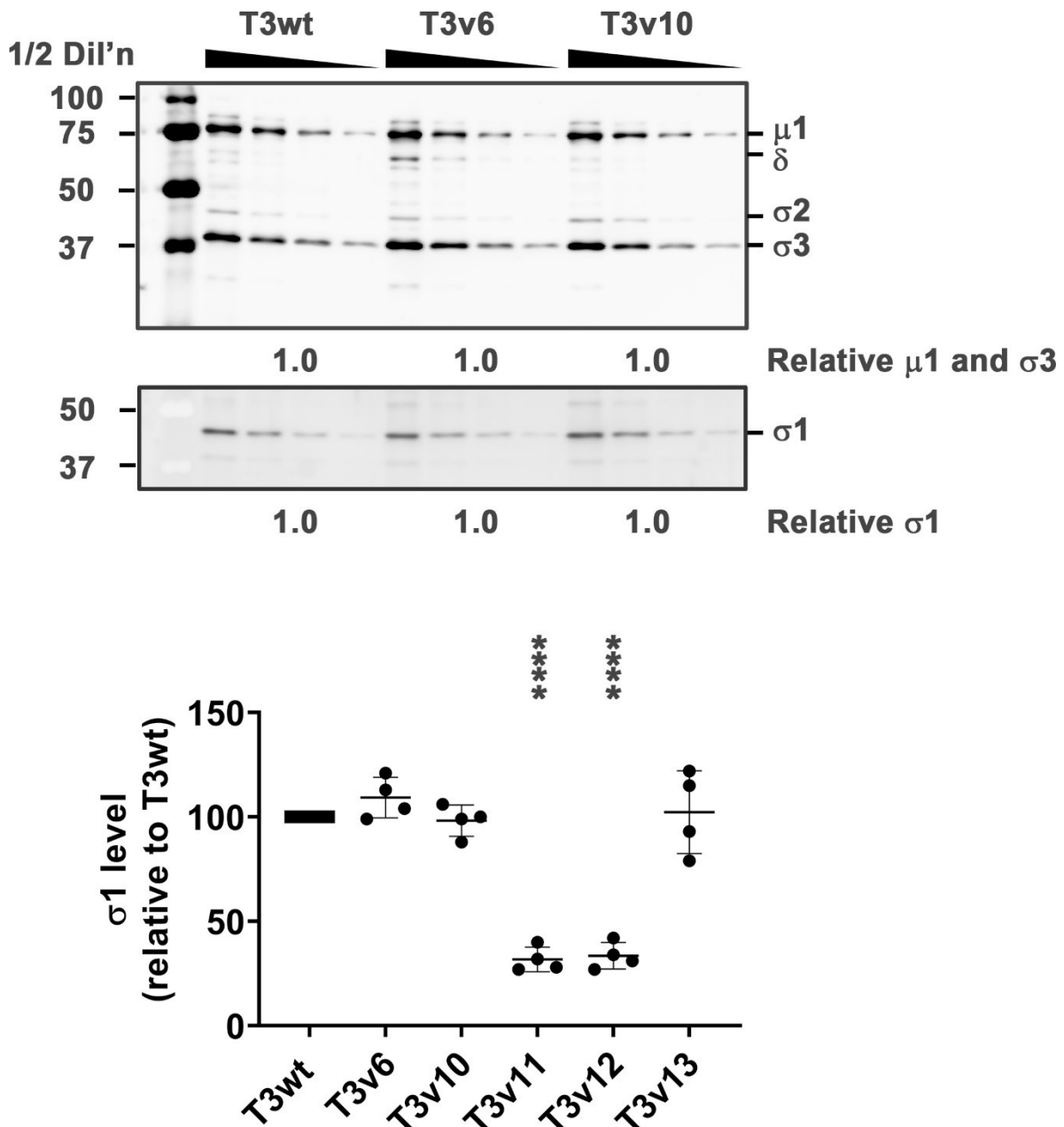


Figure 4- 5. Western blot analysis comparing reovirus $\sigma 1$ levels.

Equivalent amount of T3wt and variants were subjected to Western blot analysis. An example blot is shown above. Polyclonal reovirus antiserum was used to detect the indicated viral proteins. Note that the antibody might not detect core protein $\sigma 2$ reliably, as its specific sensitivity was lower compared to outer capsid protein capsid proteins $\mu 1$ and $\sigma 3$. Protein bands were quantified by ImageQuant LAS4010 imager. Relative levels of $\sigma 1$ were standardized to capsid proteins $\mu 1$ and $\sigma 3$ ($n=4$; mean \pm SD; one-way ANOVA - Dunnett's multiple comparisons test). For statistics, * = $P < 0.05$, ** = $p < 0.01$, *** = $p < 0.001$ and **** = $p < 0.0001$.

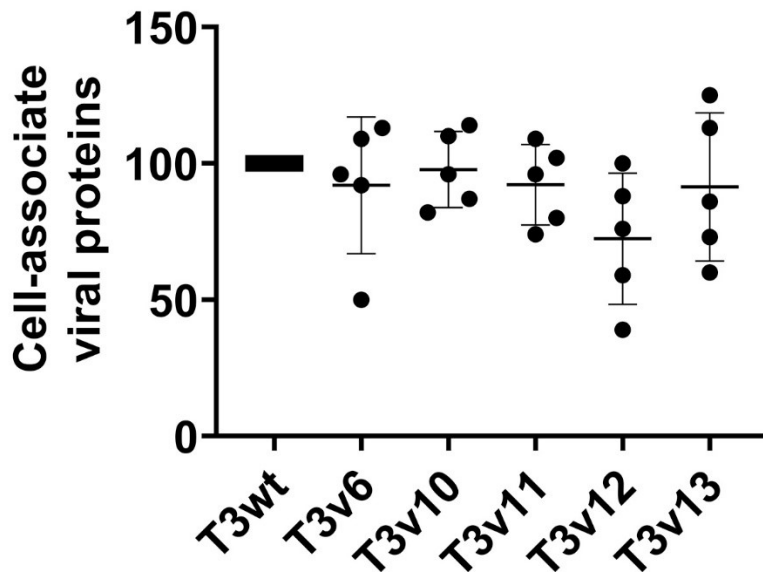
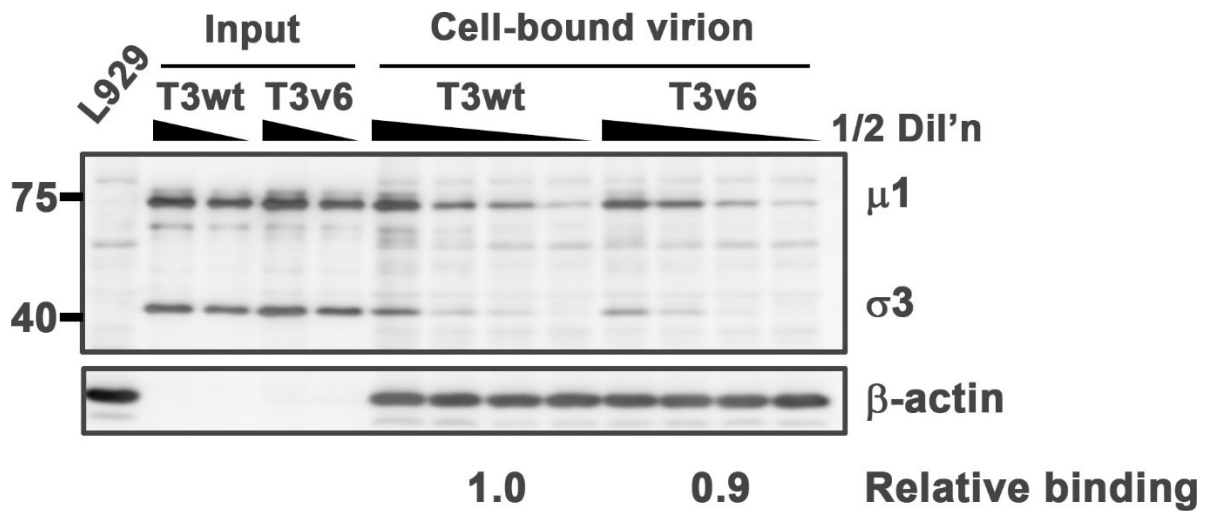


Figure 4- 6. Reovirus binding assay.

Pre-chilled L929 cells were exposed to equal doses of T3wt or T3v6 at 4°C for 1 hour. Unbound viruses were washed by PBS and cell lysates were subjected to Western blot analysis. Input virions of each virus were loaded as controls and no significant differences were detected ($n=5$; mean \pm SD; one-way ANOVA - Dunnett's multiple comparisons test).

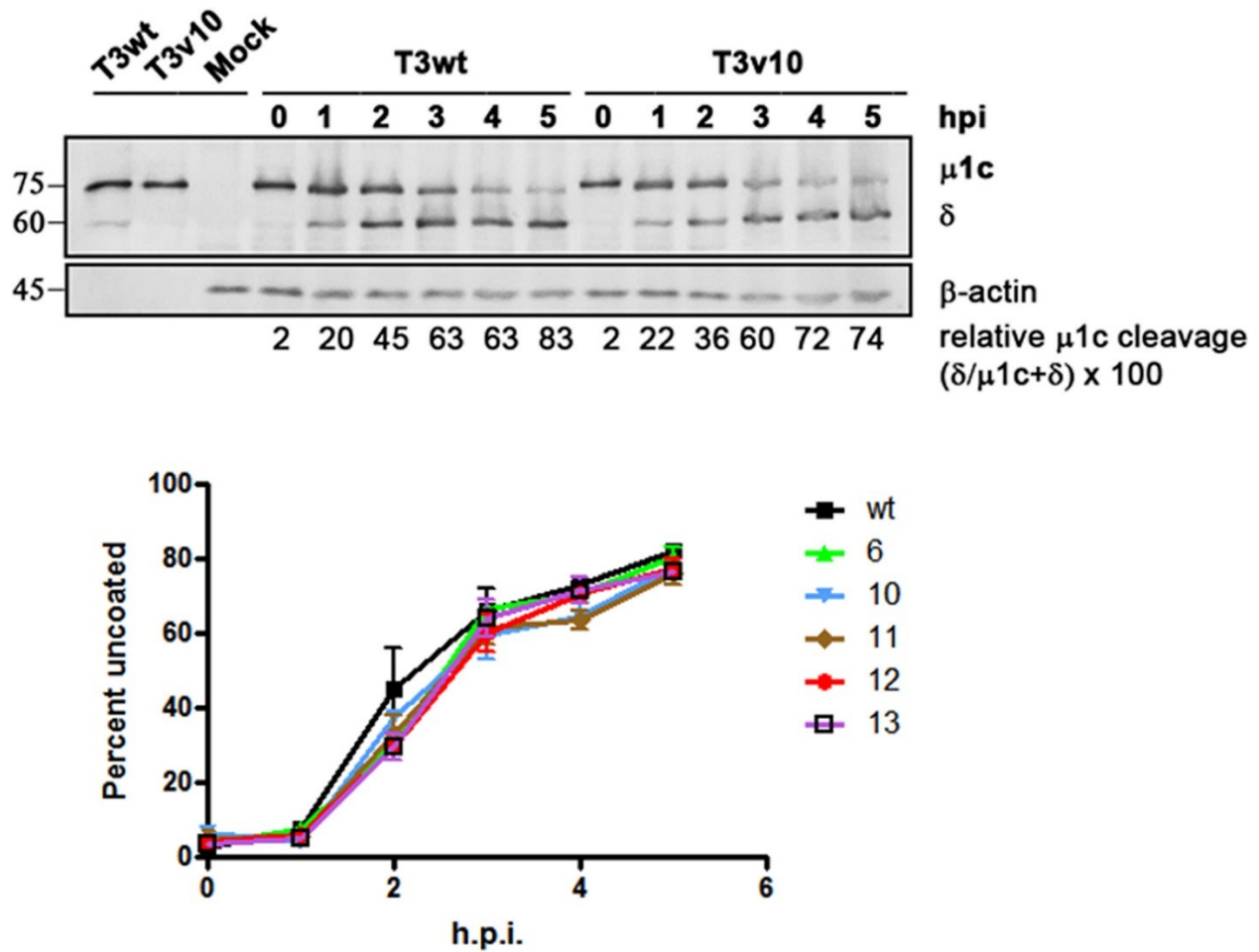


Figure 4- 7. Uncoating of reovirus is monitored by Western blot analysis.

Reovirus uncoating is associated with the hallmark conformational change of the virion. These include the full degradation of outer capsid $\sigma 3$, and cleavage of $\mu 1c$ to generate δ fragment. These structural shifts allow the virus to exit endosome upon completion of uncoating. Cleavage of $\mu 1c$ to δ was monitored by Western blotting. Line graphs were used to represent percent uncoating at each indicated time point and the differences were not significant ($n=3$; mean \pm SD, one-way ANOVA - Dunnett's multiple comparisons test were conducted for all time points). The above experiment was performed by Georgi Trifonov. He generously provided me the Western blots and line graphs for my thesis.

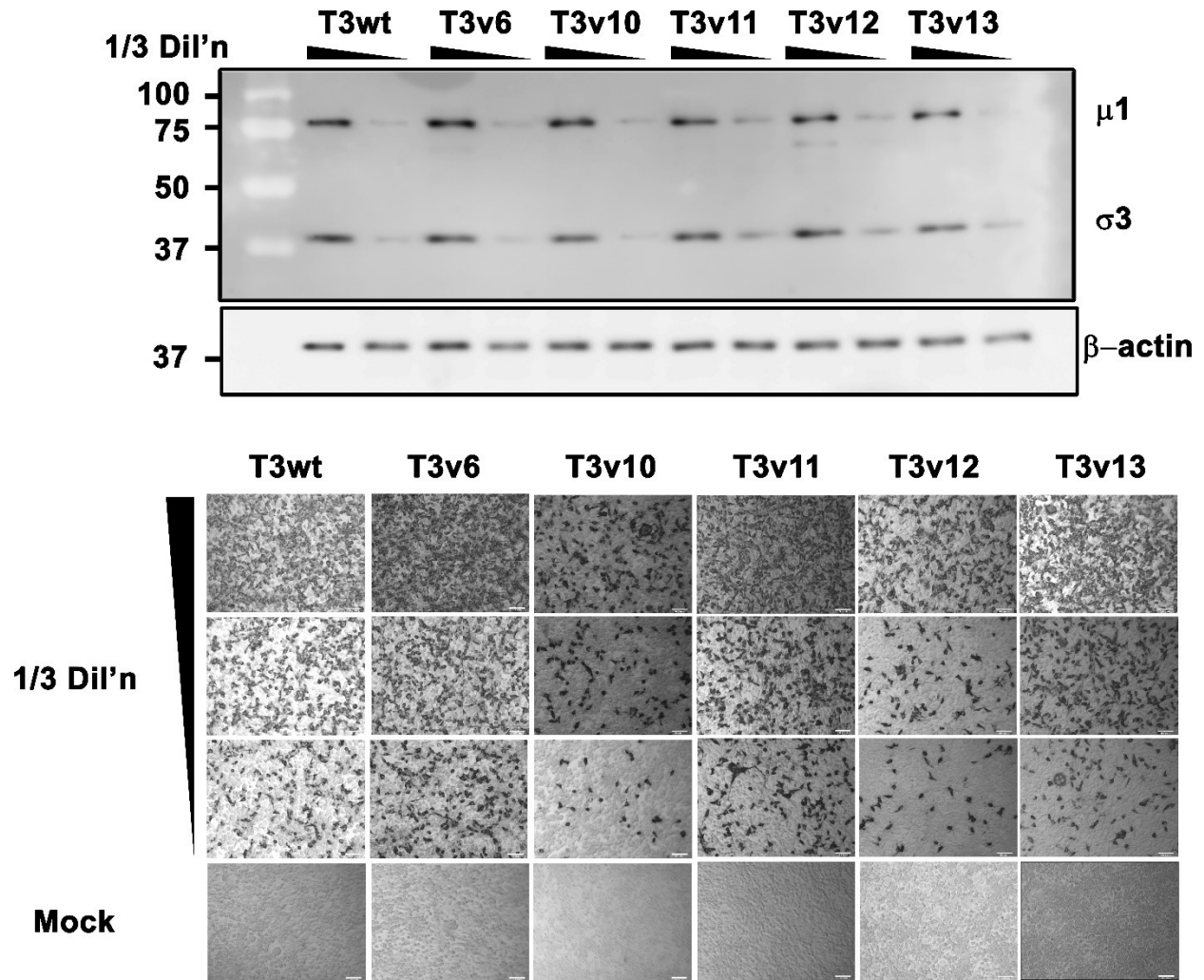


Figure 4- 8. Immunocytochemistry staining of reovirus-infected L929 cells.

L929 cells were exposed with equal doses of cell-bound T3wt or variants as confirmed by Western blot at the bottom (please refer to section 2.5 for binding assay). At 18hpi, the cells were fixed by 4% PFA and visualized by light microscope. Reovirus antigen-positive cells visually produced dark-purple staining.

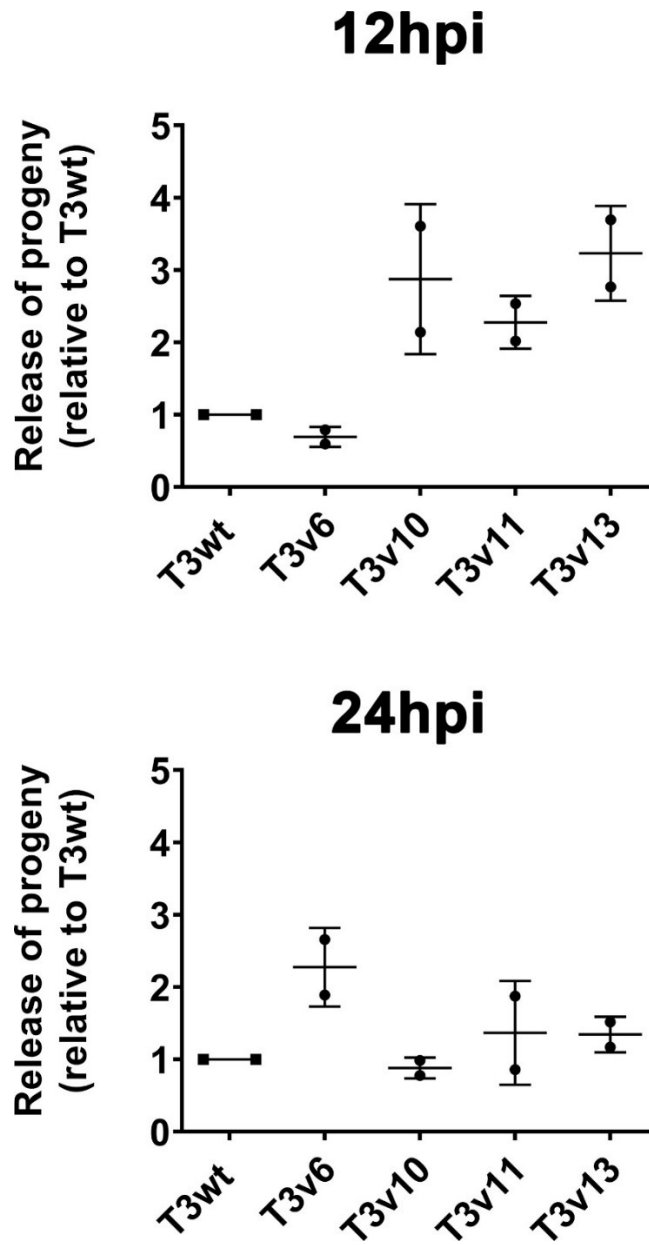
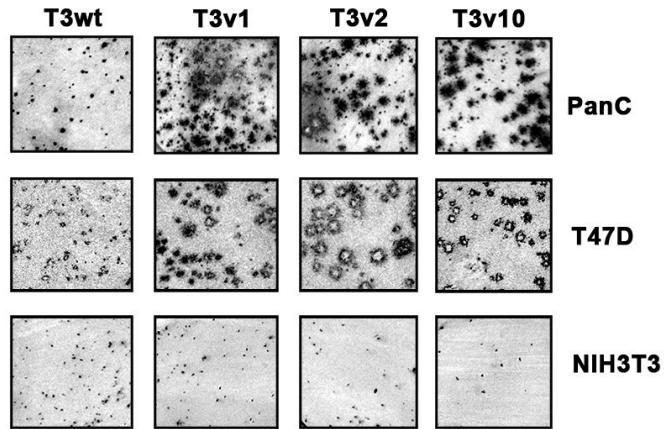


Figure 4- 9. Release of viral progeny is compared by plaque assay.

L929 cells were exposed to equal cell-bound T3wt or the indicated variants. Intracellular- and released-virus (from media) was collected independently. Percent release was calculated by dividing released viral titer (from media) by total titer (in cell and media), and the data was standardized to T3wt for easy interpretation. Significance could not be determined ($n=2$), but the trend was sufficiently informative to suggest further characterization of these mutants.

A



B

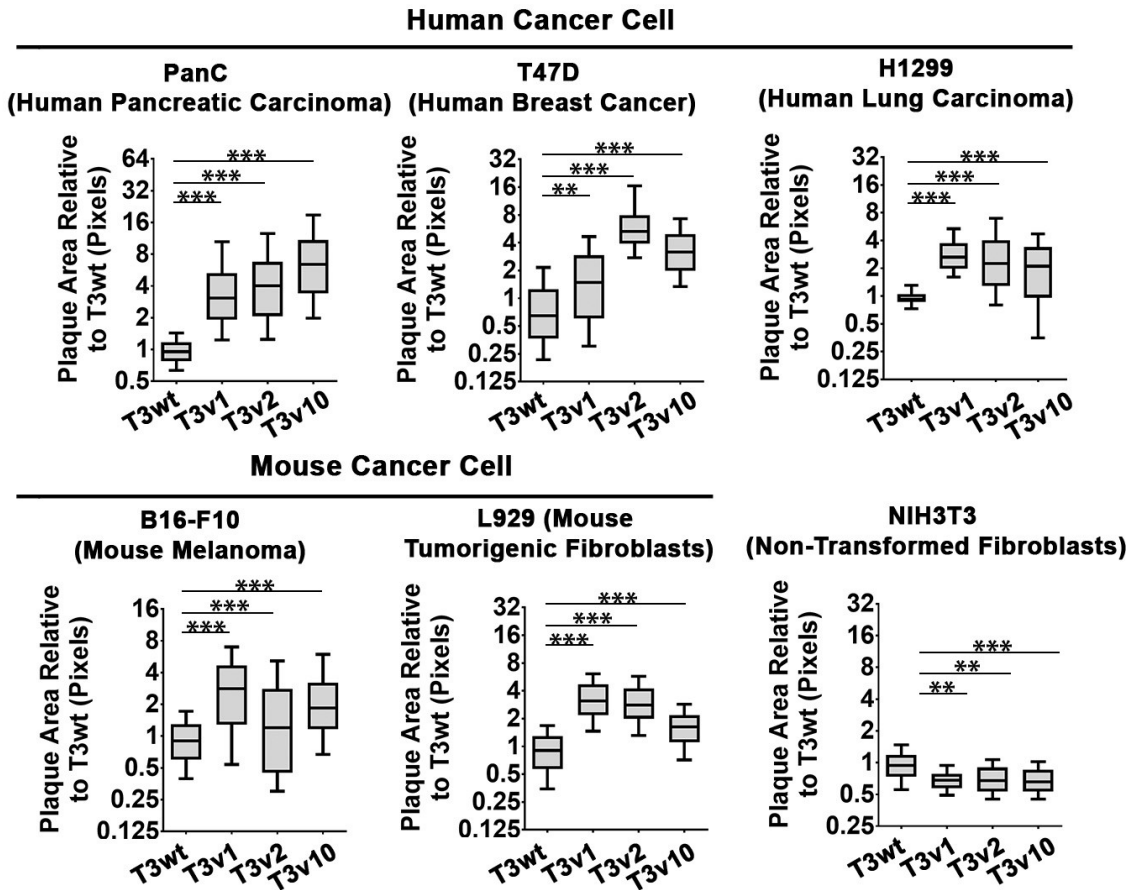


Figure 4- 10. T3v10 forms large plaques on various cancer cells.

(A) Plaque sizes of T3v10 were compared with previously characterized variants T3v1 and T3v2. All three variants selectively replicated in T47D (human breast cancer cell) and PanC (human pancreatic cancer cell), but had restricted replication in NIH3T3 (non-transformed mouse fibroblast). **(B)** Plaque sizes associated with each variant was compared in different cell-lines and represented by whisker plots ($n=3$, mean \pm SD; one-way ANOVA – Dunnett’s multiple comparison tests). The experiments were performed by undergraduate Georgi Trifonov. For statistics, * = $P<0.05$, ** = $p<0.01$ *** = $p<0.001$ and **** = $p<0.0001$.

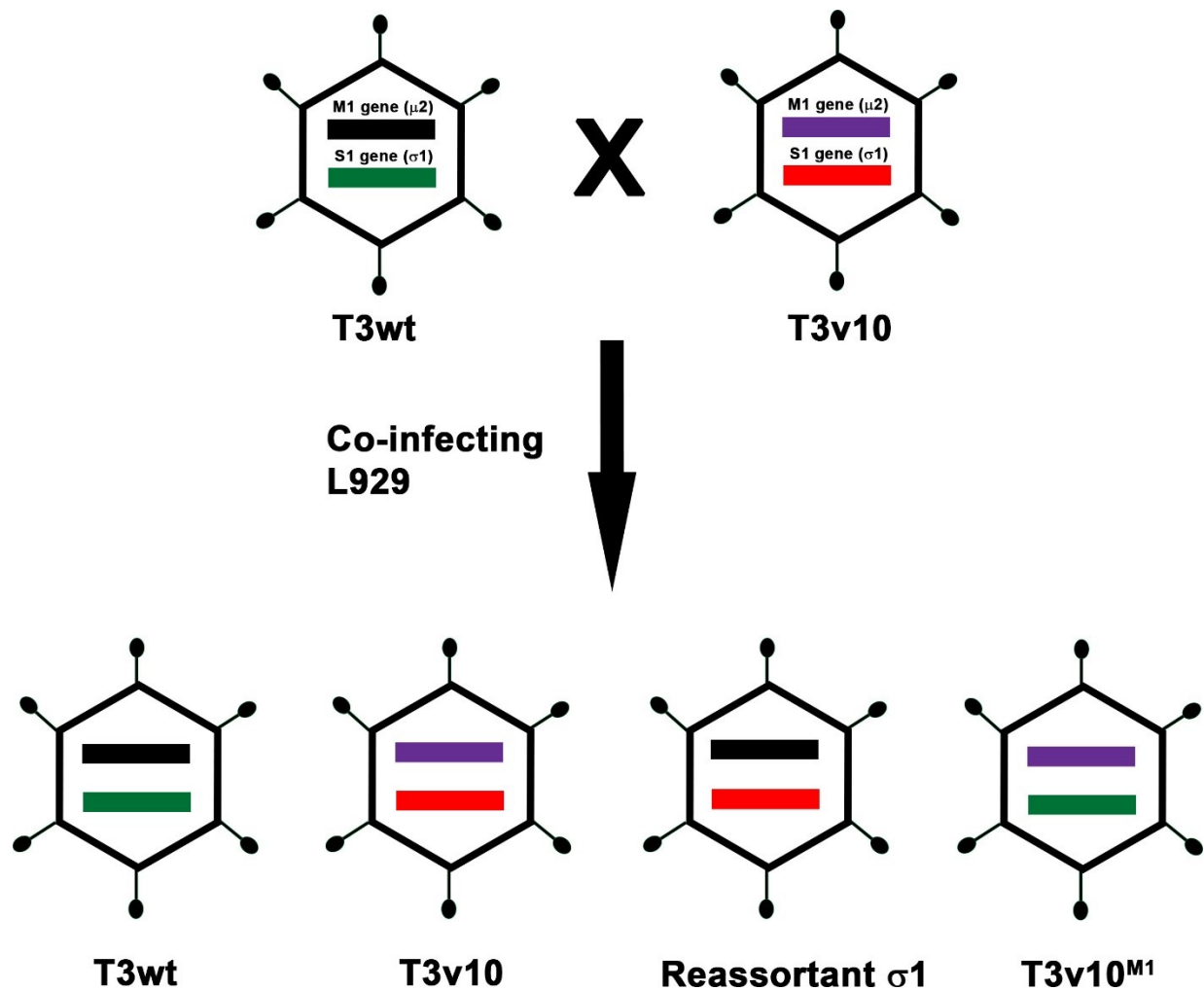


Figure 4- 11. T3v10^{M1} is generated by co-infecting L929 with T3wt and T3v10.

T3v10 had two mutations, one in the M1 gene and the other one in S1 gene. To isolate the desired M1 gene mutation, undergraduate Georgi Trifonov co-infected L929 cells with T3wt and T3v10. Reovirus has segmented dsRNA and this allows the two viruses to exchange gene segments in the same cell, generating 4 possible reassortants. Georgi purified viruses that formed plaques with sizes similar to T3v10. Sequence analysis showed that reassortant T3v10^{M1} had the only M1 gene mutation, while other genes were identical to the T3wt. For the purpose of simplicity, only M1 and S1 genes are shown.

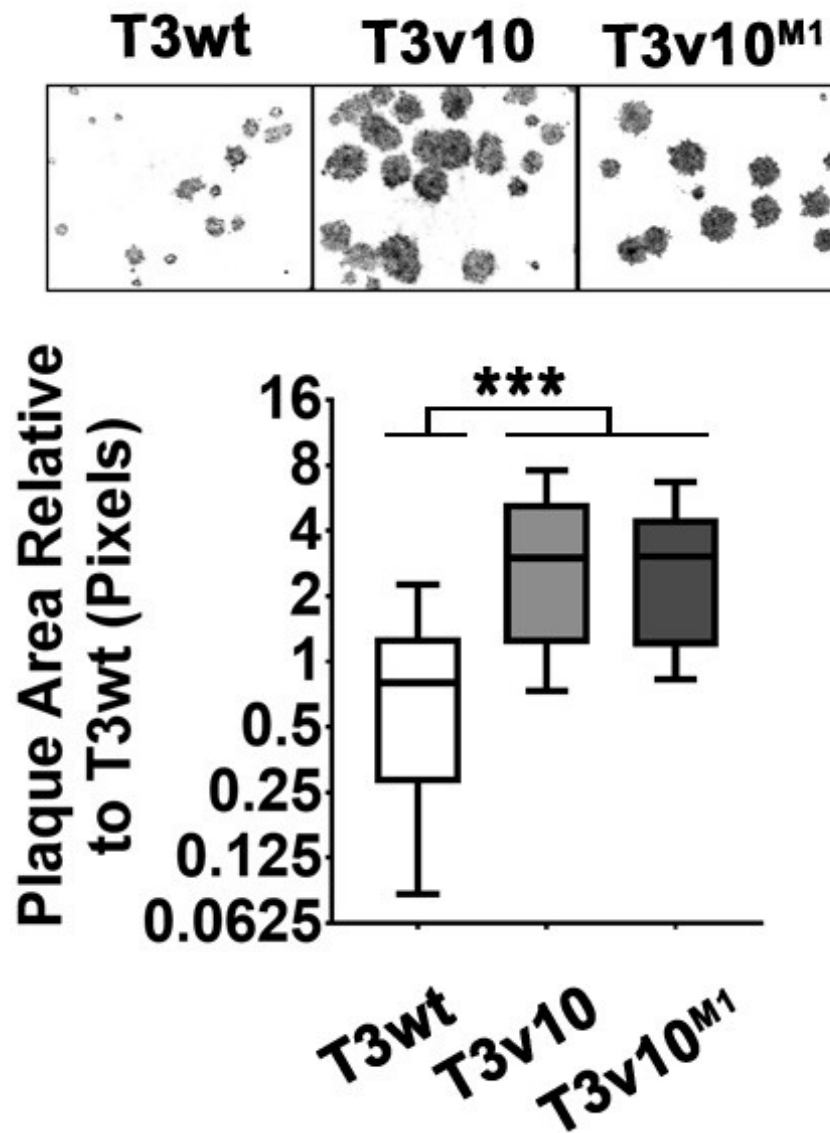


Figure 4- 12. T3v10^{M1} has the same phenotype as its parental viruses T3v10 and T3wt.

Plaque sizes of T3v10^{M1} were compared to its parental viruses T3v10 and T3wt in L929 cells ($n=4$, mean \pm SD; one-way ANOVA – Dunnett’s multiple comparison tests). For statistics, * = $P < 0.05$, ** = $p < 0.01$ *** = $p < 0.001$ and **** = $p < 0.0001$.

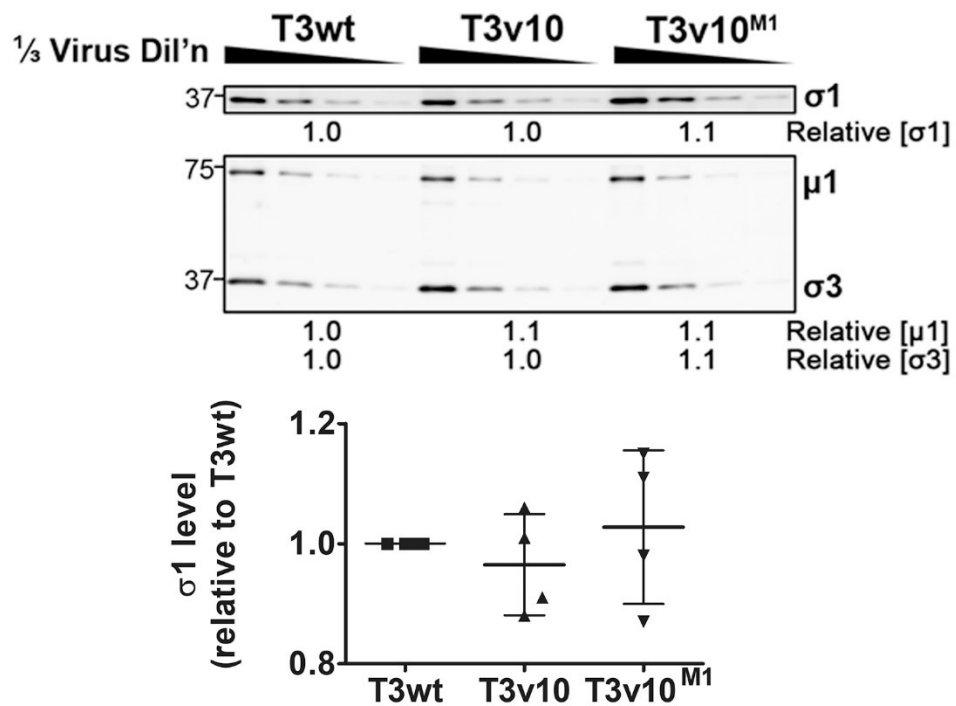


Figure 4- 13. Western blot analysis comparing $\sigma 1$ levels of T3wt, T3v10 and T3v10^{M1}.

Equal amount of cesium chloride (CsCl) gradient-purified T3wt, T3v10 and T3v10^{M1} virions were analyzed by Western blotting. Relative levels of $\sigma 1$ were normalized to capsid proteins $\mu 1$ and $\sigma 3$. Results from 4 fresh viral preparations were represented by dot plot and no significant differences were detected ($n=4$; mean \pm SD; one-way ANOVA - Dunnett's multiple comparisons test).

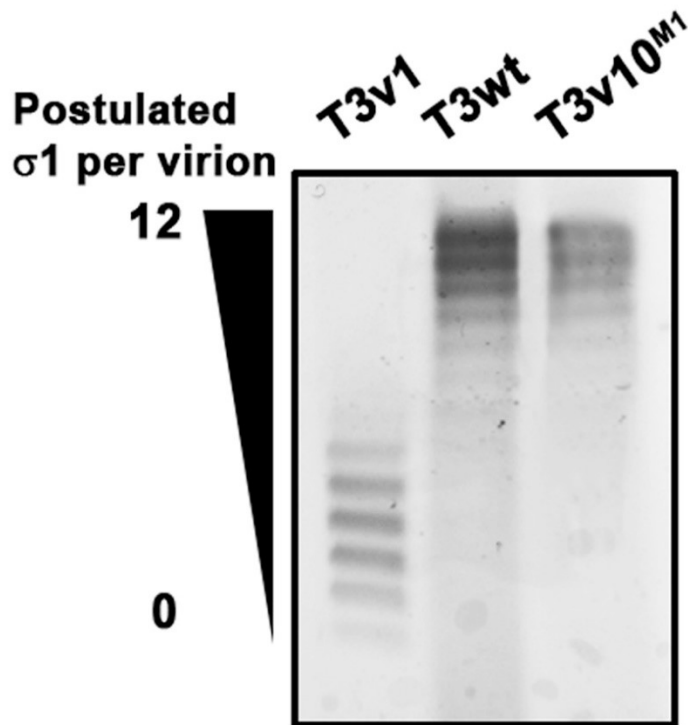


Figure 4- 14. Agarose gel electrophoresis comparing σ_1 levels of T3wt, T3v10 and T3v10^{M1}.

According to a study by Larson *et al.* (140), reovirus can produce up to 12 bands that migrate at different speed on agarose gel, depending on the quantity of virion-associated σ_1 . T3v1 produced species with faster migrating speed as the virus possesses three-fold less σ_1 compared to T3wt, while T3wt and T3v10^{M1} species migrated at similar speeds and this supported data from Western blot analysis that both viruses had similar amount of σ_1 .

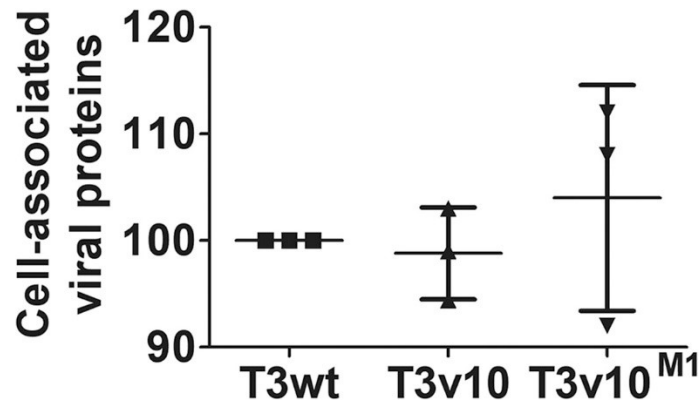
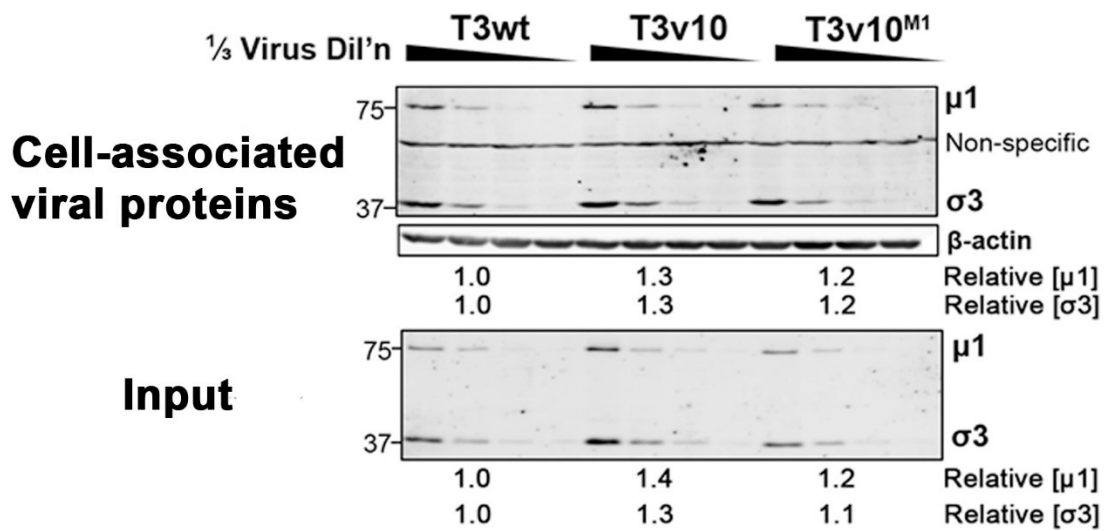


Figure 4- 15. Western blot analysis comparing cell-binding of T3wt, T3v10 and T3v10^{M1}.

L929 cells were exposed to equivalent viral particles of T3wt, T3v10 and T3v10^{M1} for 1 hour at 4°C. Unbound viruses were washed away with PBS. Cell lysates were subjected to Western blotting analysis. Cell-associated viral proteins were normalized to input viral proteins to calculate percent of binding and no significant differences were detected ($n=3$; mean \pm SD; one-way ANOVA - Dunnett's multiple comparisons test).

CHAPTER 5: A REOVIRUS μ 2 C-TERMINAL LOOP INVERSELY REGULATES NTPASE AND TRANSCRIPTION FUNCTIONS VERSUS BINDING TO FACTORY-FORMING μ NS AND PROMOTES REPLICATION IN TUMORIGENIC CELLS

5.1. Introduction and chapter objective

In the previous chapter, we chose variant T3v10 as a candidate for further characterization. T3v10 had one mutation in the S1 gene and one mutation in the M1 gene. By performing reassortment (Figure 4- 11), we successfully separated the two mutations. T3v10^{M1} inherited the M1 gene mutation which caused an alanine-to-valine replacement of residue 612 in the μ 2 protein. T3v10^{M1} was confirmed to exhibit the same phenotype of its parental virus T3v10. Both viruses formed plaques with similar sizes on L929 cells (Figure 4- 12), possessed similar amount of σ 1 (Figure 4- 13 and Figure 4- 14) and attached to host cells in a similar manner (Figure 4- 15).

However, it remained unknown whether the A612V mutation in μ 2 directly promoted post-entry steps of reovirus replication in tumor cells. In this chapter, I focus on characterizing this mutation in post-uncoating steps.

5.2 Results

5.2.1 The A612V mutation in $\mu 2$ promotes reovirus replication

We previously showed that T3v10^{M1} produced plaques that were 3-fold bigger than T3wt (Figure 4- 12), but plaque size assesses viral replication, spreading and dissemination over multiple rounds of replication. I wanted to determine if T3v10^{M1} had advantages in a single round of replication by monitoring single-cycle growth kinetics at high multiplicity of infection (Figure 5- 1A) (please refer to section 2.17 for the method). One round of reovirus replication in L929 cells is completed at approximately 24 hour-post-infection (hpi). T3v10^{M1} produced 2.5-fold higher titers than T3wt per infected cell at 24hpi (paired t-test, $n=5$, $P<0.0001$). In other words, per infected cell (reovirus antigen-positive cell enumerated by flow cytometric analysis), T3wt produced ~1000 plaque-forming units (pfu), which is typical for this virus. T3v10^{M1} however produced ~2500 pfu per infected cell, indicating a ~2.5-fold increase in progeny production. During a multi-step growth curve analysis at an MOI of 0.01, T3v10^{M1} accumulated 10-fold higher titers than T3wt by 48hpi (paired t-test, $n=3$, $P=0.008$) (Figure 5- 1B). The A612V mutation in $\mu 2$ therefore provides an advantage in a single infectious cycle that is augmented over successive rounds of virus replication.

5.2.2 T3v10^{M1} is impaired at hydrolyzing ribonucleoside tri-phosphates (rNTPs) and RNA synthesis *in vitro*

The $\mu 2$ protein is a structural protein of the inner core and proposed to be the polymerase co-factor. One study showed that in presence of purified $\mu 2$, reovirus polymerase

$\lambda 3$ could be pulled-down by $\mu 2$ -specific polyclonal antibodies, supporting the $\mu 2$ and $\lambda 3$ interacts within core of reovirus and electron cryomicroscopy analysis observed that the two proteins juxtaposed in the core interior (267). It was also revealed that the purified $\mu 2$ protein alone possesses both RNA 5'-triphosphatase (RTPase) and nucleoside-triphosphatase (NTPase) activities, and the addition of $\lambda 3$ could mildly enhance RTPase activities of $\mu 2$ (132). We sought to determine if the A612V mutation in $\mu 2$ of T3v10^{M1} impacts $\mu 2$ triphosphatase activities, by performing rNTP hydrolysis assays using $\mu 2$ -bearing viral cores.

To obtain viral cores, equivalent amounts of T3wt or T3v10^{M1} full virions were incubated with the proteolytic enzyme chymotrypsin (CHT) until the outer capsid proteins were completely digested; a procedure well established for reovirus (162). Successful conversion of full virion to core was confirmed by SDS-PAGE, followed by Coomassie Blue staining. Compared to the full virion, outer capsid protein $\sigma 3$ and $\sigma 1$ were completely degraded from the core while core proteins ($\lambda 1/2/3$ and $\sigma 2$) were preserved (Figure 5- 2). High-speed ultracentrifugation was performed to isolate pure viral cores from CHT reaction mixture. NTPase activities of $\mu 2$ were measured by incubating viral cores with rATP, rGTP, rCTP or rUTP in separate reactions, and release of phosphate ions was measured by Phosphate Assay Kit (Colorimetric) (ab65622). Surprisingly, nonlinear regression analyses revealed that T3v10^{M1} was about 2-fold slower at hydrolyzing rATP, rGTP and rCTP compared to T3wt ($p=0.03$ for rGTP and $p=0.005$ for rCTP) (Figure 5- 3, 37°C). Furthermore, hydrolysis of rATP and rGTP by viral cores of T3v10^{M1} plateaued at the 120-180-minute time point while T3wt continued to hydrolyze all 4 rNTPs up to the final 240-minute time point. Previous studies showed that enzymatic activities of $\mu 2$ are affected by pH and temperature *in vitro* (188). However, we obtained similar results at pH 7.0

and temperatures of 37°C or 40°C (Figure 5- 3). Therefore, although we initially set out to identify an advantage of the A612V μ 2 mutation that conferred larger plaques, rNTP hydrolysis analysis suggested that this mutation may contrarily confer a *disadvantage* to T3v10 with respect to nucleotide processing.

5.2.3 T3v10^{M1} is impaired at RNA synthesis *in vitro*

The reduced rNTPase activities of T3v10^{M1} provided an opportunity to test the relationship of μ 2 rNTPase activities with core transcription in an *in vitro* transcription assay (Figure 5- 4) and during infection of cells (Figure 5- 5). To measure RNA synthesis *in vitro*, viral cores were obtained using the method described above, cores were incubated with substrates for RNA synthesis, and accumulation of reovirus RNAs was monitored by quantitative reverse transcription PCR (RT-qPCR). Reovirus has 10 genes that fall into three size classes: small (S), medium (M) and large (L). Primers for qRT-PCR that provided linear relationships between RNA quantity and SYBR green signal were established for representative genes of each size class (S4, M1, L2, and L3). Nonlinear regression analyses indicated that T3v10^{M1} produced viral RNAs at a slower rate than T3wt (Figure 5- 4). Moreover, RNA synthesis plateaued for T3v10^{M1} by 120-180 minutes while RNA synthesis continued up to the last 240-minute time point for T3wt. Results from the *in vitro* transcription assay (Figure 5- 4) and rNTP hydrolysis assay (Figure 5- 3) were strikingly similar; the current study therefore provides evidence to support that μ 2 plays a direct role in the process of RNA synthesis.

T3v10^{M1} synthesized RNAs at comparatively slower rates than T3wt *in vitro*, but whether T3v10^{M1} exhibited the same behavior in cells remained to be elucidated. To assess reovirus core transcription during cell infection, it became essential to inhibit post-transcription steps of virus replication and prevent potential confounding effects of virus amplification. Specifically, reovirus transcribes its genome in two overlapping but different phases in a single replicative cycle. During the primary phase of transcription, incoming virions uncoat, become transcriptionally active, and transcribe and release positive-sense viral RNAs into the cytoplasm. The (+) RNAs then serve two functions; as mRNAs they template viral protein synthesis, and also they can be re-encapsidated by newly synthesized viral proteins into progeny cores. Within the progeny cores, the (+) RNAs serve as templates for generating negative-sense RNAs and thereby the full dsRNA viral genome. The progeny cores undergo the secondary phase of transcription, releasing more (+) RNAs to amplify virus replication. Accordingly, to study reovirus core RNA synthesis directly, it was imperative to stop subsequent steps of protein synthesis and progeny core assembly, as these steps could have indirect effects on viral RNA accumulation. We therefore treated L929 cells with cycloheximide (CHX) to inhibit protein expression and used RT-qPCR to monitor viral RNA synthesis of only incoming T3wt and T3v10^{M1} virions. Western blot analysis was performed to verify that CHX treatment completely inhibited the synthesis of viral proteins (Figure 5- 5). Reovirus-infected cells were collected at 3hr intervals over a 24-hour period, subjected to RNA purification and RT-qPCR analysis for viral RNAs relative to cellular GAPDH. To distinguish (+) versus (-) RNAs, sense-specific primers were used during the reverse transcription reaction. Both T3wt and T3v10^{M1} were able to synthesize (+) RNAs (Figure 5- 5), with the normalized fold changes of RNA synthesis recapitulating the *in*

in vitro transcription assay (Figure 5- 4). Importantly, nonlinear regression analysis indicated that T3wt produced (+) RNAs at about 2-fold faster rates than T3v10^{M1} for all tested genes and the differences were statistically significant. Negative-sense RNAs were not detected during infection, which was anticipated given that CHX prevents protein expression and therefore progeny cores. Altogether, the data consistently showed that T3v10^{M1} was less effective at RNA synthesis *in vitro* and in cells.

5.2.4 Incoming T3v10^{M1} virion is less effective at establishing productive infection

Given the deficiencies in RNA synthesis exhibited by T3v10^{M1}, we next compared the ability of T3v10^{M1} to establish productive infection relative to T3wt. First, we equalized T3wt and T3v10^{M1} doses to generate the same number of cell-bound virus particles by Western blot analysis (Figure 5- 6). This equalization ensured that any differences observed between the viruses are related to post-binding steps of virus infection. L929 cells exposed to equivalent cell-bound T3wt or T3v10^{M1} particles were then subjected to immunocytochemical staining at 18hpi with polyclonal anti-reovirus antibodies (Figure 5- 6). T3wt produced notably higher numbers of reovirus protein-expressing cells relative to T3v10^{M1}. Second, to obtain a quantitative comparison, flow cytometric analysis was used to count the number of reovirus antigen-positive cells following exposure to matched PFU/cell of T3wt or T3v10^{M1} (Figure 5- 7). Approximately 8-fold higher titers of T3v10^{M1} were required to establish the same number of productively infected cells as T3wt (this data demonstrated that T3v10^{M1} and T3v10 have the

same phenotype, please see section 4.2.5). These results suggest that the $\mu 2$ mutation reduces reovirus core RNA synthesis and decreases the probability of effectively establishing an infection. At the same time, given that the same titer of T3v10^{M1} produced fewer initially infected cells (Figure 5- 6 and Figure 5- 7), that T3v10^{M1} generated larger plaques (Figure 4- 12), and that higher titers were achieved by T3v10^{M1} in a one-step growth curve (Figure 5- 1A), the results indirectly suggested that the disadvantages in RNA synthesis and productive infectivity were overcome by a separate advantage in post-transcription stages of reovirus replication.

5.2.5 Cells productively infected by T3v10^{M1} accumulate higher levels of viral RNAs and proteins over the course of infection relative to T3wt

To determine if T3v10^{M1} acquired advantages at post-transcription stages of virus replication, as was indirectly suggested by the single-step growth kinetics, we directly assessed viral RNA and protein synthesis over the course of infection. In these experiments, it was essential to omit CHX and permit normal virus amplification. To monitor RNA accumulation, L929 cells were exposed to equivalent amounts of cell-bound T3v10^{M1} and T3wt virions. RNA from total cell lysates were collected every 3 hours in a 24-hour period. The RT-qPCR analysis was performed to monitor positive- and negative-sense RNA synthesis, as described above. For the first 9 hours of infection, T3wt produced more detectable positive-sense RNA than T3v10^{M1} in 3 out of 4 tested genes (Figure 5- 8A). Although the superior RNA synthesis of T3wt over T3v10^{M1} in the absence of CHX was less striking and significant than in CHX experiments (Figure 5- 5), this was to be expected given the overlap of primary and secondary phases of

transcription when CHX is omitted. Importantly, starting at approximately 9hpi, which corresponds to the secondary phase of transcription, rates of RNA synthesis became faster for T3v10^{M1} (Figure 5- 8A). Specifically, by 24hpi, T3v10^{M1} achieved at least 2-fold higher levels of viral RNAs than T3wt. Nonlinear regression analyses suggested the differences were significant for all tested genes. When negative-sense RNA syntheses were compared between the two viruses (Figure 5B), the results resembled (+) RNA synthesis. As to be expected, (-) RNAs were not detected prior to 9hpi owing to the need for robust secondary phase of transcription to achieve detectable levels; however, T3v10^{M1} achieved significantly higher levels of (-) RNAs than T3wt starting at 9hpi and progressing to 24hpi.

In congruence with higher accumulation of viral RNAs, experiments that follow indicated that accumulation of viral proteins is also enhanced in cells productively infected by T3v10^{M1} relative to T3wt. To examine viral protein expression level on a per-infected cell basis, L929 cells were exposed to T3v10^{M1} or T3wt at doses that produced equivalent numbers of reovirus antigen-positive cells. This equalization permitted us to overcome differences in establishing infection, and ask whether reovirus-positive infected cells produced less-or-more viral proteins. Cells were then subjected to flow cytometric analysis at 15hpi (Figure 5- 9A). The uninfected cell population (left peak) was similar for both T3v10^{M1} or T3wt, but the reovirus antigen-positive cell population (right peak) was consistently shifted towards higher mean fluorescence intensity (MFI). The same analysis was then performed over a spectrum of virus doses to modulate the percent of reovirus-antigen-positive cells (Figure 5- 9B). Under all conditions, MFI was higher for cells infected by T3v10^{M1} than T3wt, suggesting higher viral protein production per productively infected cell. Since MFI does not provide a direct indication of fold-differences

in protein abundance, cells were also subjected to Western blot analysis at 12hpi and 15hpi. Representative capsid protein $\sigma 3$ and core protein $\mu 2$ are shown in Figure 5- 10. Densitometric comparisons indicated that at 15hpi, T3v10^{M1} accumulated 1.7-fold more $\sigma 3$ and 3.5-fold more $\mu 2$ relatively to T3wt (Figure 5- 10). In conclusion, the data suggested that although T3v10^{M1} initially struggles to establish infection due to hampered RNA synthesis, the fate of infection by T3v10^{M1} is reversed during the secondary phase of transcription where T3v10^{M1} achieves higher accumulation of viral RNAs and proteins.

5.2.6 T3v10^{M1}- $\mu 2$ and μNS exhibit increased association during infection and transfection relative to T3wt- $\mu 2$

In addition to its role as polymerase co-factor within cores, soluble $\mu 2$ produced during infection plays a secondary function; it supports the formation of localized sites for virus amplification and assembly called viral factories, defined as intracellular compartments (inclusions) enriched for viral RNAs and proteins, as well as newly assembled progeny. Our T3wt belongs to serotype 3 Dearing (T3D). However, there are two known lab strains of T3D and they have distinct viral factory morphology. The T3D^C lab strain is the same T3wt we use in the lab and it forms filamentous viral factories. We have unpublished evidence suggesting that T3D^C possesses superior oncolytic potency relative to another lab strain T3D^N, which forms globular viral factories (195).

Studies showed that microtubules (MT) were being embedded into reoviral factories (11,70), but it is unclear how MTs are recruited to the factory sites. One study transfected CV-1

cells with $\mu 2$ and confocal microscopic analysis showed that $\mu 2$ was capable of stabilizing and colocalizing with MTs, labeled with anti-tubulin serum (195). Another study performed immunofluorescence (IF) microscopic analysis and discovered that CV-1 and Mv1Lu cells transfected with reovirus non-structural protein μ NS formed globular viral factory like structures which closely resembled viral factories observed in T3D^N infected cells (39). Transfected μ NS did not colocalize with or reorganize MTs. However, the same study employed (IF) microscopic analysis and demonstrated that CV-1 cells expressing co-transfected μ NS and $\mu 2$ were able to colocalize with each other. The authors concluded that $\mu 2$ played an essential role in mediating the redistribution of μ NS to MTs, allowing viral factories to maintain a proper morphology and structure. More recently, a study showed that viral growth can be sustainably inhibited when $\mu 2$ or μ NS protein expression was repressed by stable expression of siRNAs. Compared to normal HEK293T cells infected with T3D, viral titer was inhibited more than 3000-fold when $\mu 2$ was targeted by siRNA, and 2000-fold in μ NS knock-down cells (45).

Given that viral factory formation directly affects reovirus replication and $\mu 2$ - μ NS cooperation is needed to assemble the viral factory properly, we wondered if the A612V mutation in $\mu 2$ might affect association with μ NS, and therefore developed assays to monitor $\mu 2$ - μ NS interactions. First, co-immunoprecipitation (Co-IP) was performed on lysates of L929 cells infected with T3v10^{M1} or T3wt. To account for differences in establishing infection and *de novo* protein expression, cell infections were standardized to produce equivalent virus protein levels between the two viruses, as was confirmed by Western blot analysis (Figure 5- 11, pre-IP samples). Second, anti- $\mu 2$ antibodies were then used to pull down proteins that associated with

$\mu 2$. Western blot analysis revealed that up to 9-fold more μ NS was co-precipitated with T3v10^{M1} $\mu 2$ relative to T3wt $\mu 2$ (Figure 5- 11, post-IP samples).

Co-association between $\mu 2$ and μ NS during virus infection does not infer direct interactions, since these proteins could interact through an intermediate complex. To focus on $\mu 2$ - μ NS associations independently of other viral factors, we generated eukaryotic expression plasmids containing wild-type μ NS, as well as $\mu 2$ from T3wt and T3v10^{M1}, and assessed interactions between these proteins in transfected cells (Figure 5- 12). A FLAG tag was added to $\mu 2$ at either 5'-terminal ($\mu 2$ -5F) or 3'-terminal ($\mu 2$ -3F) ends, to account for possible interference between the FLAG tag and $\mu 2$ interaction domains. Also, since L929 cells are poorly transfectable, the reovirus-permissive and easily transfected H1299 human lung carcinoma cell line was used. H1299 cells were either left untransfected (UT), or transfected with wild-type μ NS alongside either wild-type $\mu 2$ -5F (wt 5F), wild-type $\mu 2$ -3F (wt 3F), T3v10^{M1}-derived $\mu 2$ -5F (10^{M1} 5F), or T3v10^{M1}-derived $\mu 2$ -3F (10^{M1} 3F). When samples were immunoprecipitated with μ NS-specific antibodies, despite equivalent levels of μ NS between samples, there was on average 1.5-fold more 10M- $\mu 2$ than wt- $\mu 2$ protein that co-associated with μ NS (Figure 5- 12).

To verify our findings that 10M- $\mu 2$ had a stronger association with μ NS, we performed the reciprocal pull-downs, where antibodies for $\mu 2$ were used during immunoprecipitation and Western blot analysis was conducted for μ NS, there was also on average 1.5-fold more μ NS co-precipitated with 10M- $\mu 2$ than wt- $\mu 2$. The results were consistent for $\mu 2$ with either a 5' or 3' FLAG tag, and were highly consistent over several independent experiments and statistically significant. Finally, a similar co-IP experiment was performed, except that at 24 hours post-

transfection, cells were infected with T3wt (Figure 5- 13). In this context, it was important that transfected $\mu 2$ was FLAG-tagged and thereby could be distinguished from wild-type $\mu 2$ provided by the infection. Lysates were collected at 12hpi and 20hpi, immunoprecipitated with either FLAG (FL)- or μ NS- specific antibodies, and then subjected to Western blot analysis with FLAG (FL)- and μ NS- specific antibodies to monitor co-association. In each experiment, a fraction of cells co-transfected with $\mu 2$ and μ NS, but not yet exposed to T3wt were analyzed by Western blotting to ensure equivalent expression of both transfected proteins. Co-IP analysis consistently showed 1.5-2.5-fold higher association between μ NS and T3v10^{M1}- $\mu 2$ versus wild-type- $\mu 2$ (Figure 5- 13).

The co-immunoprecipitation experiments suggested that the A612V mutation in $\mu 2$ may improve association of $\mu 2$ with μ NS, but while the 9-fold increase in association during infection was striking, the 1.5-2.5-fold increased association in transfected cells required further validation. We therefore developed Far-Western as an alternative assay to investigate direct $\mu 2$ and μ NS interactions *in vitro* (Figure 5- 14 A and B). H1299 cells were transfected with μ NS alone, wild-type $\mu 2$ -5F (wt $\mu 2$) alone, T3v10^{M1}-derived $\mu 2$ -5F (10^{M1} 5F) alone, or FLAG-tagged dengue virus capsid protein (NS1) as a negative control. In addition, we had HIS-tagged wild-type μ NS (Purified μ NS) and $\mu 2$ (Purified $\mu 2$) that were previously purified from bacterial expression systems, which we included during electrophoresis as additional controls. Three serial dilutions of each lysate, alongside the two purified proteins were subjected to non-denaturing gel electrophoresis to preserve native protein structure, and then transferred to PVDF membranes. Direct Western blot analysis with FLAG-specific antibodies showed that wild-

type- $\mu 2$ and T3v10^{M1}- $\mu 2$ were present at similar levels (Figure 5- 14 A and B, bottom anti-FLAG blot). Far-Western blot analysis was then performed with either purified μ NS (Figure 5- 14A, $n=5$, $SD=1.029$, $p=0.04$) or with lysates of H1299 cells transfected with μ NS (Figure 5- 14B, $n=4$, $SD=1.045$, $p=0.05$), followed by detection of associated μ NS using rabbit μ NS-specific antibodies.

Under both conditions and over 4 independent experiments, an average of 2-fold more μ NS associated with T3v10^{M1}- $\mu 2$ than with wild-type- $\mu 2$. The $\mu 2$ - μ NS interaction was specific, because FLAG-tagged NS1 (Dengue virus capsid protein) did not interact with μ NS, and FLAG-tagged $\mu 2$ did not interact with FLAG-tagged NS1, suggesting that the FLAG-tag did not promote protein-protein interaction. Furthermore, $\mu 2$ did not self-associate after the PVDF membrane was incubated with purified HIS- $\mu 2$ (Figure 5- 21). Results from pull-down assays and Far-Western blotting concordantly demonstrated that T3v10^{M1} $\mu 2$ had stronger association with μ NS and such interaction is specific.

5.2.7 When co-transfected with μ NS, T3v10^{M1} $\mu 2$ has increased association with reovirus capsid proteins relative to T3wt $\mu 2$

Although it was previously suggested that $\mu 2$ and μ NS interact, and that such interactions are involved in factory formation, it has yet to be determined whether a stronger interaction between these proteins would promote subsequent steps of virus protein accumulation at factories and thus virus amplification. Compared to its wild-type protein,

T3v10^{M1} μ 2 exhibited stronger interaction with μ NS, and this provided us an opportunity to examine the implications of increased μ 2- μ NS associations. Therefore, we determined if the A612V mutation in μ 2 affects recruitment of other viral proteins to the μ 2- μ NS complex (proposed viral factory). First, during L929 infections with T3wt versus T3v10^{M1} described in Figure 5- 11, we assessed the levels of reovirus capsid proteins μ 1 and σ 3, and core protein σ 2 that co-immunoprecipitated with anti- μ 2 antibody and found that about 3-fold more capsid proteins μ 1 and σ 3 were pulled down (Figure 5- 15). Second, H1299 cells were co-transfected with wild-type μ NS and one of the FLAG-tagged μ 2 derived from either T3wt or T3v10^{M1}, followed by T3wt exposure (described in Figure 5- 13 above). Lysates were then subjected to immunoprecipitation with antibodies specific for FLAG (FL) tag or μ NS. Western blot analysis was conducted for reovirus capsid proteins μ 1, σ 3 and σ 1. T-test analyses revealed that all three tested capsid proteins had 1.5-2 fold stronger associations with T3v10^{M1}- μ 2 (5F and 3F)-embedding protein complex ($P < 0.05$) (Figure 5- 16), similar results were observed regardless of the antibody that was used for the immunoprecipitation. In conclusion, stronger μ 2- μ NS interaction enhances subsequent accumulation of viral proteins to the proposed factory sites.

5.2.8 Co-transfection of μ NS and T3v10^{M1} μ 2 promotes progeny production

The pull-down assays described previously (Figure 5- 16) showed that more viral capsid proteins were associated with T3v10^{M1} μ 2- constituted protein complex. It is unclear whether T3v10^{M1} μ 2 enhances viral protein accumulation in the proposed viral factory, or it will ultimately promote progeny production. To answer this question, a small portion of whole-cell

lysates collected for the pull-down assays (Figure 5- 16) were subjected to plaque assay analysis (Figure 6H). At 9hpi, viral plaques were barely detectable. At 12 and 20hpi, co-transfected T3v10^{M1} μ 2 and μ NS increased viral titers about 2-fold compared to cells co-transfected with T3wt μ 2 and μ NS ($p < 0.05$), positions of FLAG tags in the μ 2 constructs did not affect the differences (Figure 5- 17). When the same experiment was repeated without transfection of μ NS, T3v10^{M1} μ 2 increased viral titers about 1.3 fold compared to wild-type μ 2 at 24hpi. This suggests that cooperation of T3v10^{M1} μ 2 and μ NS is required to promote progeny synthesis. Data from the current study support findings from previous studies - μ 2 and μ NS interacts with each other in forming the viral factory, and such cooperation is enhanced by the altered T3v10^{M1} μ 2, which promotes viral replication in tumorigenic cells.

5.2.9 T3v10^{M1} induces more cell-death

Reovirus has been shown to induce multiple cell-death pathways to enhance progeny release (please refer to section 1.2.5), and many apoptotic pathways converge to activate caspase-3, the main executioner caspase in apoptosis (153,237). Activation of caspase-3 involves two sequential cleavage events to generate the cleaved (active form) caspase-3 with ~20 and ~10kDa fragments (151). To determine whether T3v10^{M1} is associated with increased induction of caspase-3 dependent apoptosis, L929 cells were infected with either T3wt or T3v10^{M1} to express the equivalent amount of viral proteins and harvested at 12, 15 and 18hpi. A portion of the cell lysates was subjected to Western blot analysis for cleaved caspase-3 expression (Figure 5- 18), and the rest of cell lysates was used for Annexin V staining assay

(Figure 5- 19). Variant T3v10^{M1} induced about 2-fold more cleaved caspase-3 compared to T3wt and the results were significant at 15hpi. Our data demonstrated that T3v10^{M1} may induce cell-death via the caspase-3 dependent pathway.

To directly assess cell-death, the Annexin V staining assay was performed using flow cytometry. This method has the advantage of detecting both apoptosis and necrosis quantitatively, the principles and procedures of Annexin V staining assay are detailed by Crowley and colleagues (69). Collection and processing of cell samples were described in section 2.6. Infection with variant T3v10^{M1} was associated with more apoptotic and necrotic cells (Annexin V positive cells and Annexin V + 7AAD positive cells) relative to T3wt, and the differences were statistically significant at 15 and 18hpi (Figure 5- 19). In conclusion, replication of T3v10^{M1} in L929 cells is associated with increased cell-death, and activation of caspase-3 is involved in reovirus mediated cell-death.

5.2.10 T3v10^{M1} has reduced induction of p-IRF3

In section 1.2.4, I described that reovirus infection induces IFN response and the IRF3-mediated antiviral response is one of the major pathways activated by T3D infection. Previous studies used reassortant viruses and showed that the $\mu 2$ protein is associated with sensitivity to the IFN response, but $\mu 2$ is also implicated in repressing IFN induction (please refer to section 1.6.3). With this knowledge, we decided to compare IRF3 induction between T3wt and T3v10^{M1}.

To determine activation of IRF3, we exposed L929 cells to T3wt or T3v10^{M1}, flow cytometry was performed to verify that about 70% of cells were infected by each virus. Cell lysates were collected at 6 and 9hpi. The samples were analyzed by Western blotting. Transcriptional activity of IRF3 is regulated by phosphorylation (280). Total levels of IRF3 and phosphorylated (active form) IRF3 were independently probed by different antisera on two different blots (Figure 5- 20). Our data consistently showed that T3v10^{M1} had a reduced induction of p-IRF3 relative to T3wt at both time points, despite that more viral proteins were synthesized from the T3v10^{M1}-infected cells.

5.3 Summary

Using directed evolution, we successfully identified T3v10^{M1} as the first reovirus variant with enhanced infectivity in cancer cells relative to T3wt due to advantages at post-entry steps of replication. Subsequent experiments revealed that the A612V mutation in μ 2 of T3v10^{M1} comes with both benefits and costs to virus fitness (model depicted in Figure 6- 11). The data is consistent with a role for the previously uncharacterized C-terminal region in transcription by incoming reovirus cores; specifically, T3v10^{M1} had 2-3-fold reduced NTPase and transcription processivity relative to T3wt *in vitro* (Figure 5- 3), and produced significantly less RNA per input virion in L929 cells when cycloheximide was added to preclude secondary rounds of replication (Figure 5- 5). Despite reduced probability of establishing infection, T3v10^{M1} particles that did successfully establish infection then produced more viral proteins (Figure 5- 8, Figure 5- 9 and Figure 5- 10) and progeny (Figure 5- 1) relative to T3wt, which in turn exponentially amplified

genome replication (secondary phase of transcription – Figure 5- 8). The A612V mutation in $\mu 2$ led to enhanced interaction between $\mu 2$ with both μNS and tubulin (Figure 5- 11 and Figure 5- 12). Moreover, plasmid-derived $\mu 2$ containing the A612V mutation associated better with μNS and was sufficient to increase progeny production by T3wt (Figure 5- 17). Together, the data implicates the C-terminal domain of $\mu 2$ in both the transcription of incoming cores, and μNS association of de-novo virus proteins. Infection of T3v10^{M1} is also associated with increased cell-death and activation of caspase-3 is implicated (Figure 5- 18 and Figure 5- 19). In addition, despite that T3v10^{M1} accumulates more viral proteins in infection cells (Figure 5- 9, Figure 5- 10 and Figure 5- 20), activation of IRF3 is reduced relative to T3wt (Figure 5- 20). In conclusion, the net costs and benefits of the A612V mutation produced an overall 2-fold enhancement of replication relative to T3wt in growth curves, and overall larger plaque size.

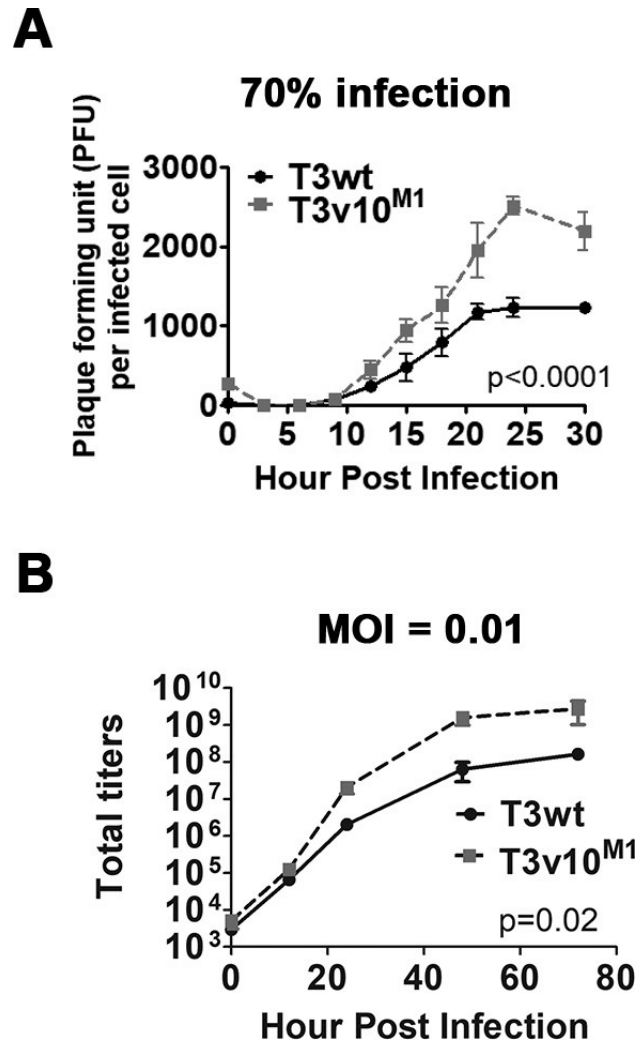


Figure 5- 1. A612V mutation in $\mu 2$ enhances reovirus growth in L929 cells.

(A) Single-step growth curve: reovirus takes about 24 hours to complete one replication cycle. Progeny production per infected cell was compared between T3wt and T3v10^{M1} by plaque assay using L929 cells, about 70% cells were infected (MOI=3.2 for T3wt and MOI = 22.6 for T3v10^{M1}) to prevent re-infection. Flow cytometry analyses were performed to verify percent of infected cells ($n=5$; mean \pm SD; nonlinear regression analysis). **(B)** Multi-step growth curve: L929 cells were infected at MOI of 0.01 and progeny synthesis was monitored for 72 hours between T3wt and T3v10^{M1} ($n=3$; mean \pm SD; nonlinear regression analysis).

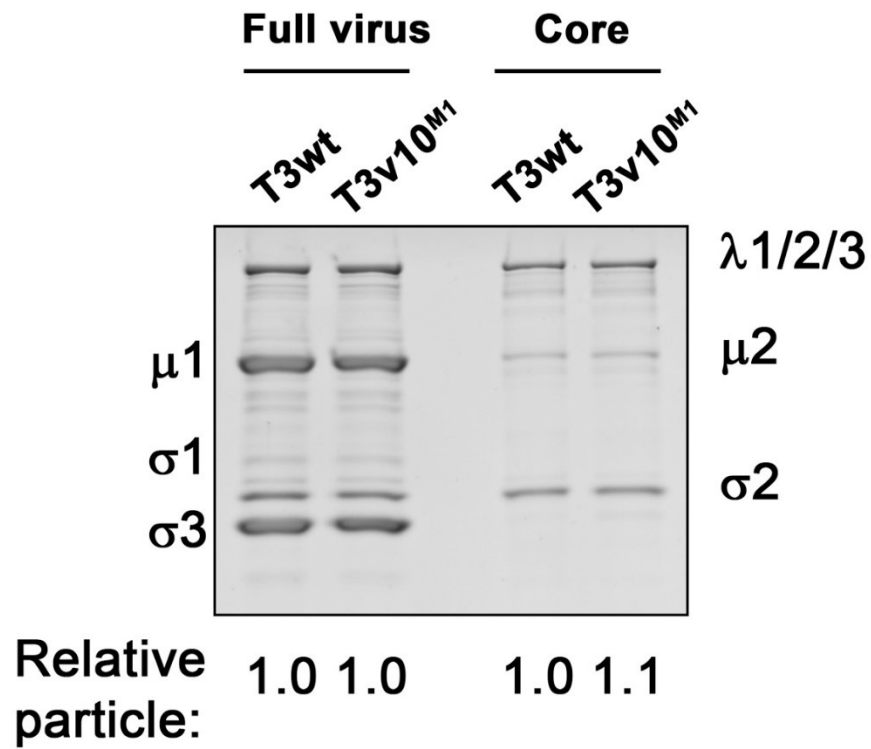
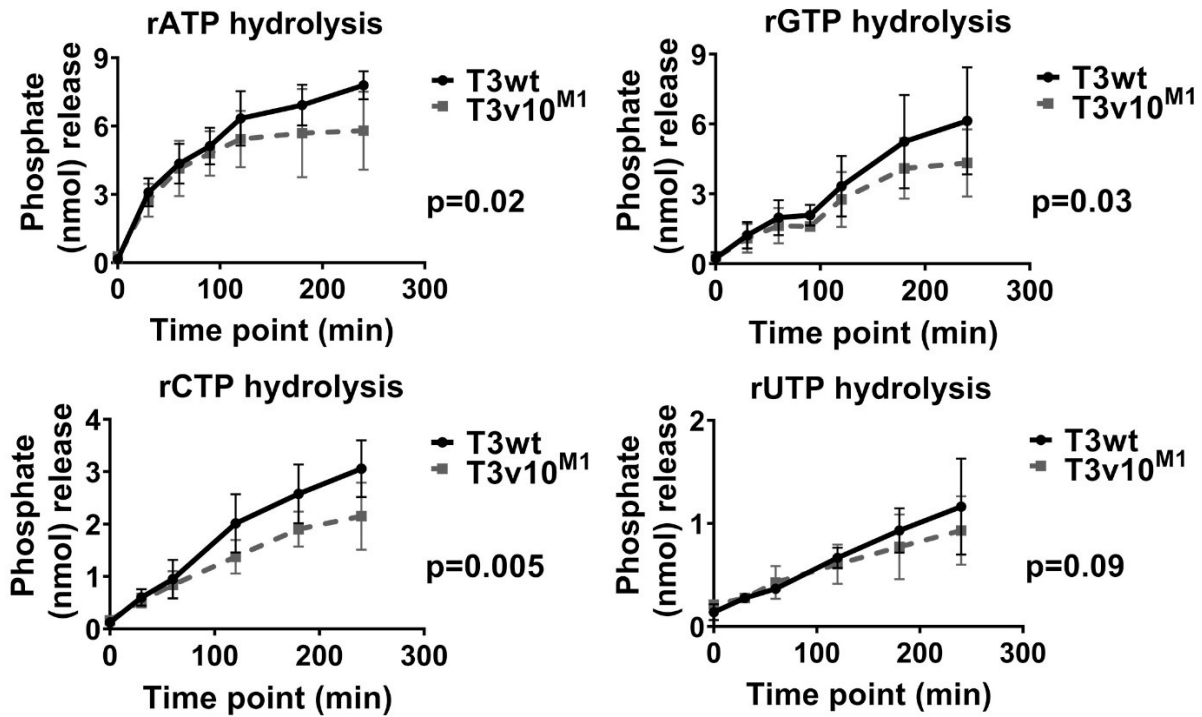


Figure 5- 2. Generating reovirus core by chymotrypsin (CHT) digestion.

Equivalent amount of T3wt and T3v10^{M1} full virions were digested by chymotrypsin (CHT) to obtain μ 2-bearing viral cores. Coomassie Blue staining showed that the outer capsid proteins of both viruses were fully degraded.

37°C



40°C

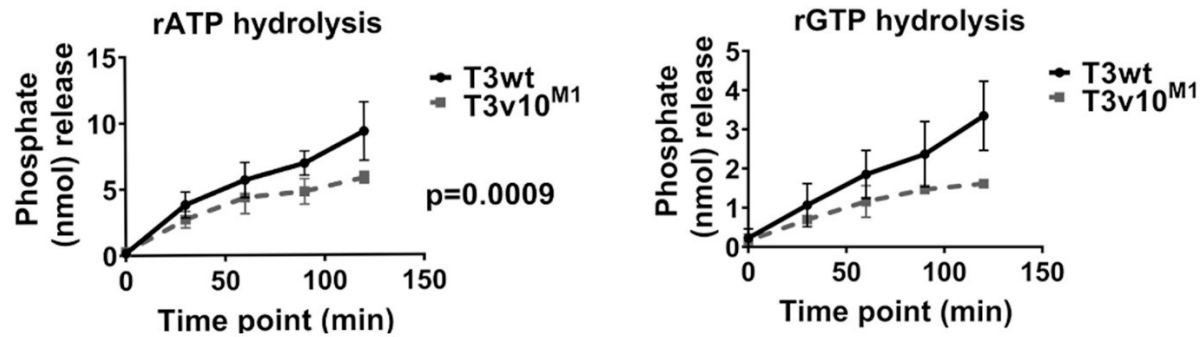


Figure 5- 3. T3v10^{M1} is less effective in hydrolyzing rNTPs *in vitro*.

T3wt and T3v10^{M1} viral cores were incubated with rNTPs at 37°C or 40 °C. Hydrolysis of rNTPs by T3wt or T3v10^{M1} μ 2 was determined by the formation of chromogenic complex when phosphate ions reacted with colorimetric reagents (for 37°C, $n=4$; mean \pm SD; nonlinear regression; for 40°C, $n=3$ for rATP hydrolysis and , $n=2$ for rGTP hydrolysis; mean \pm SD; nonlinear regression)

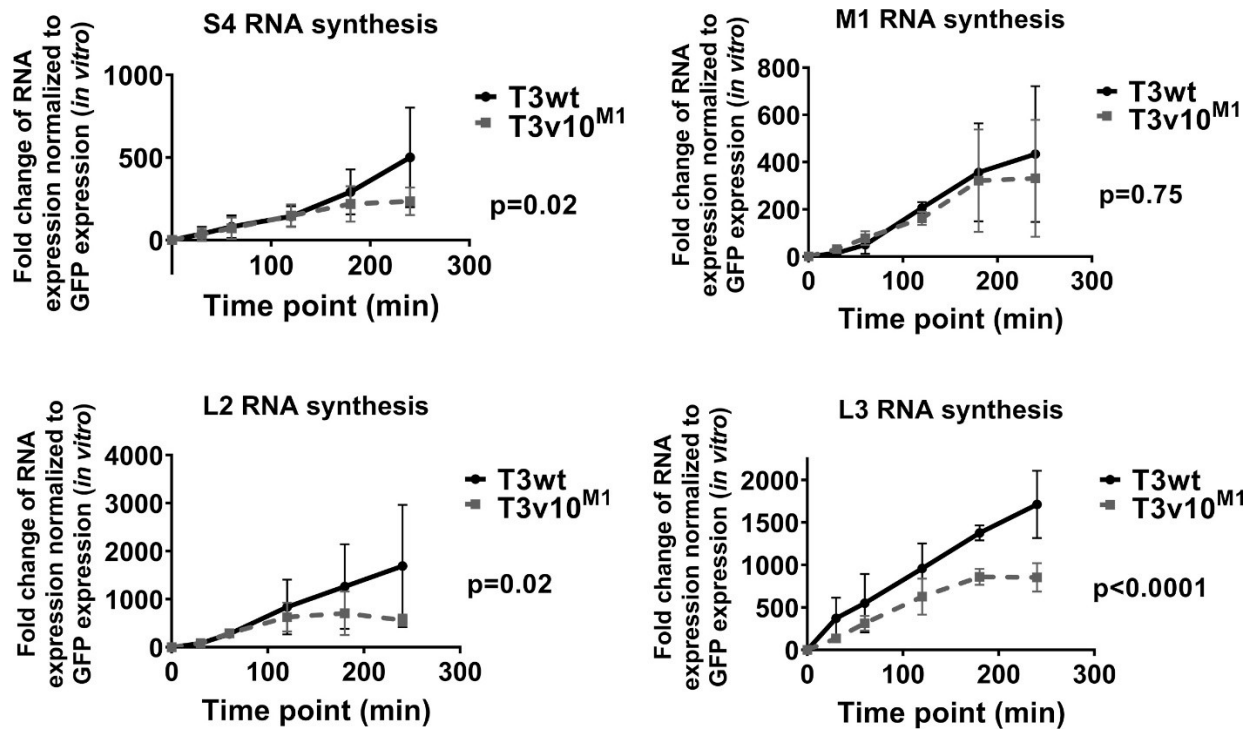


Figure 5- 4. T3v10^{M1} is less effective in synthesizing RNAs *in vitro*.

In vitro synthesis of viral RNAs was measured by RT-qPCR ($n=3$ for S1, M1 and L2 RNA synthesis; $n=4$ for L3 RNA synthesis; mean \pm SD; nonlinear regression).

+ Cycloheximide (L929)

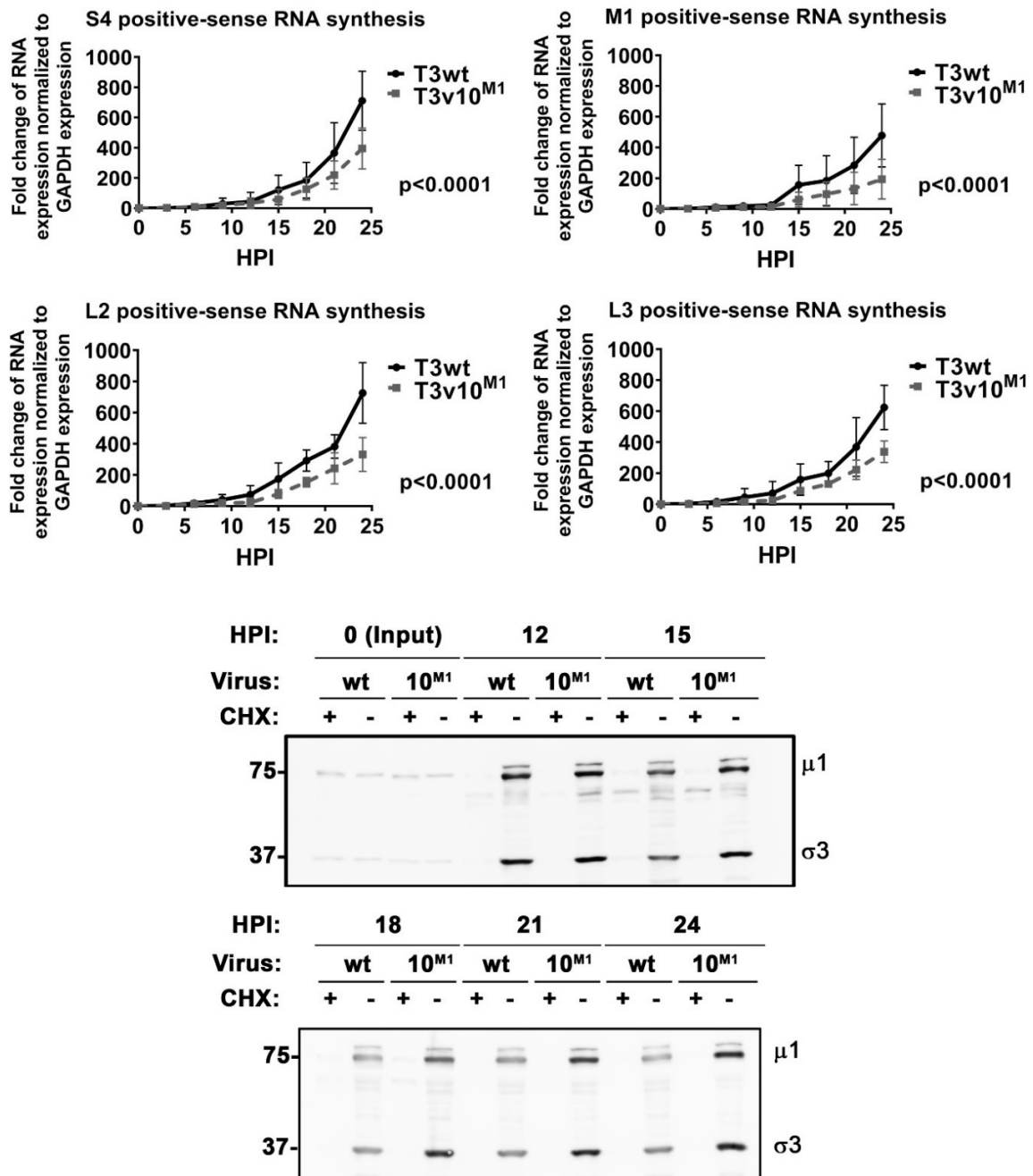


Figure 5- 5. Incoming T3v10^{M1} virion produces less RNAs in L929 cells.

Top panel: L929 cells were exposed to equivalent amount of T3wt or T3v10^{M1} cell-bound virions in the presence of CHX. Synthesis of 4 representative positive-sense RNAs were compared between the two viruses ($n=4$; mean \pm SD; nonlinear regression). Bottom panel: Equivalent amounts of T3wt- or T3v10^{M1}-exposed L929 cells from the top panel were subjected to Western blot analysis to confirm inhibition of protein synthesis by CHX. Note that more viral proteins were detected from T3v10^{M1}-exposed L929 cells at 12hpi or later time points.

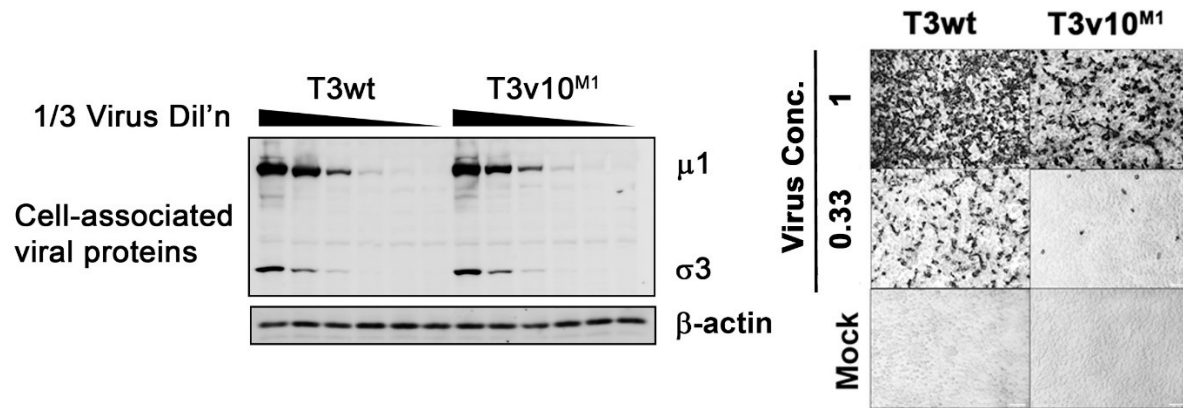


Figure 5- 6. Incoming T3v10^{M1} virion is less effective at establishing productive infection.

L929 cells were exposed to equal cell-bound T3wt and T3v10^{M1}, as confirmed by Western blotting. Immunofluorescence showing reovirus-infected cells (stained with dark purple color) at 18 hpi.

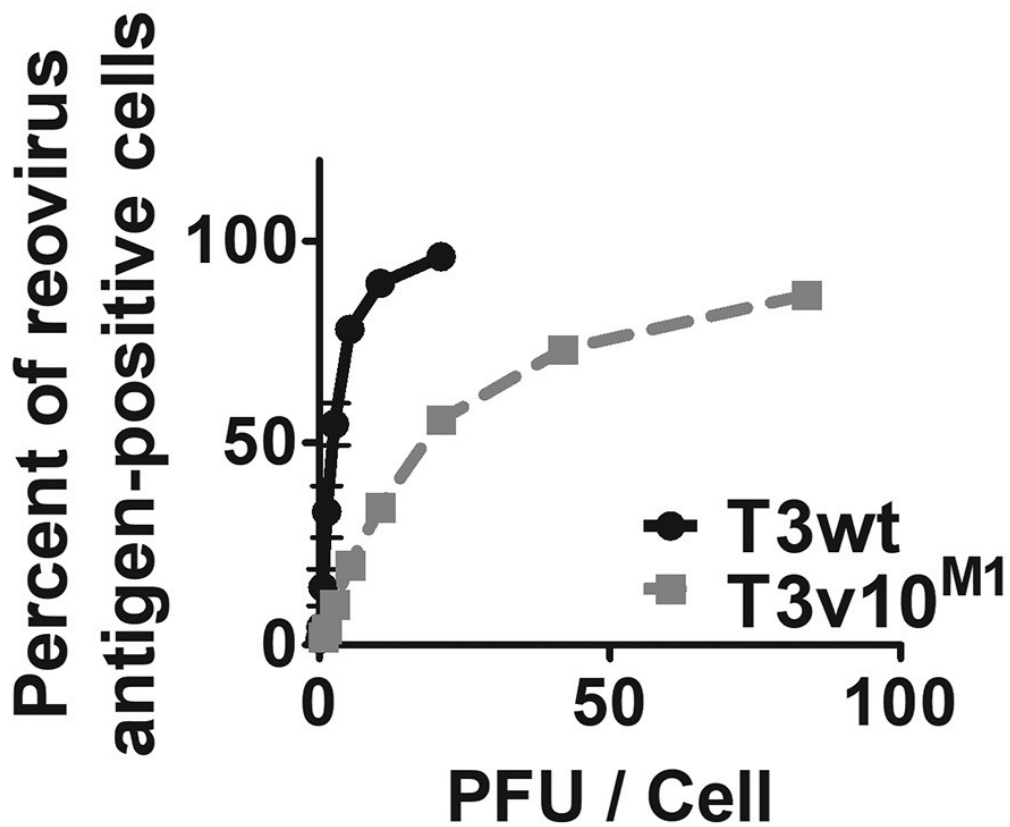
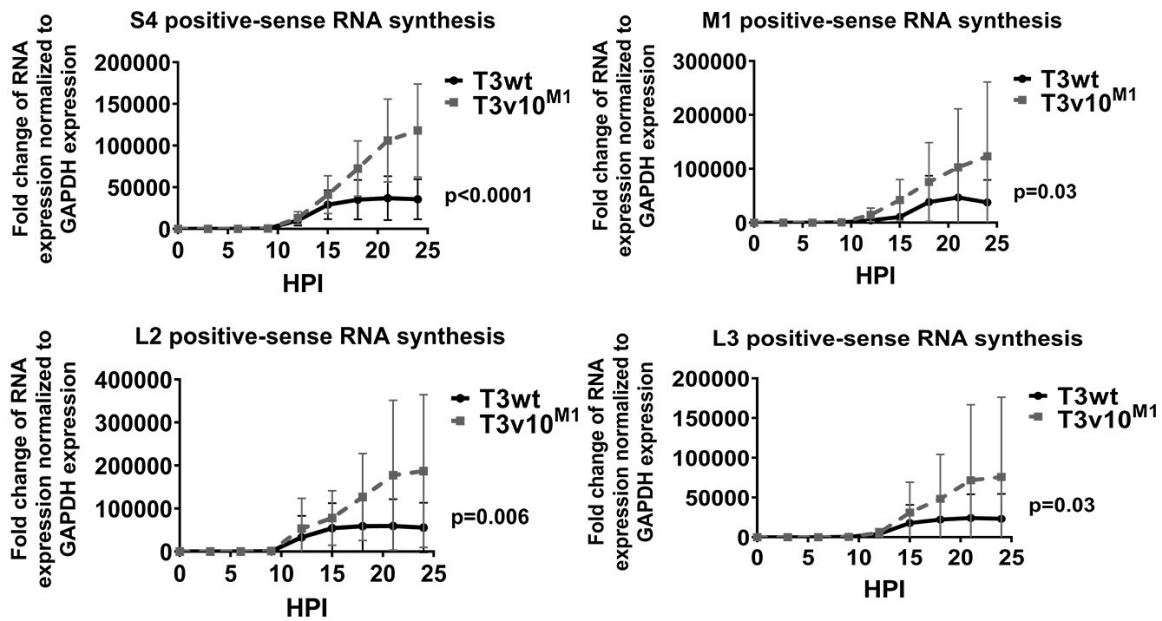


Figure 5- 7. T3v10^{M1} produces fewer reovirus antigen-positive cells relative to T3wt at the same multiplicity of infection (MOI).

Flow cytometry analysis showed relationship between the indicated plaque-forming units (PFU) per infected cell and its associated percent of reovirus antigen-positive L929 cells ($n=3$; mean \pm SD).

A

No cycloheximide (L929)

**B**

No cycloheximide (L929)

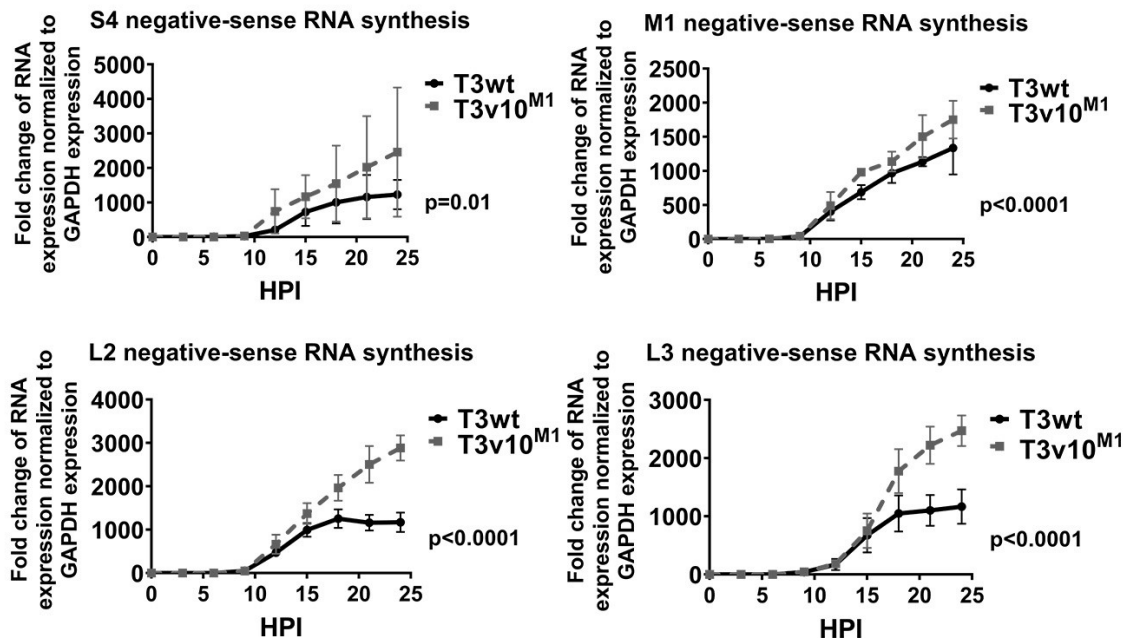


Figure 5- 8. T3v10^{M1} produces 2-fold more RNAs than T3wt in L929 cells per infected cell.

(A) Positive-sense RNA and, **(B)** negative-sense RNA syntheses were compared between T3wt and T3v10^{M1} in L929 cells by RT-qPCR ($n=4$; mean \pm SD; nonlinear regression).

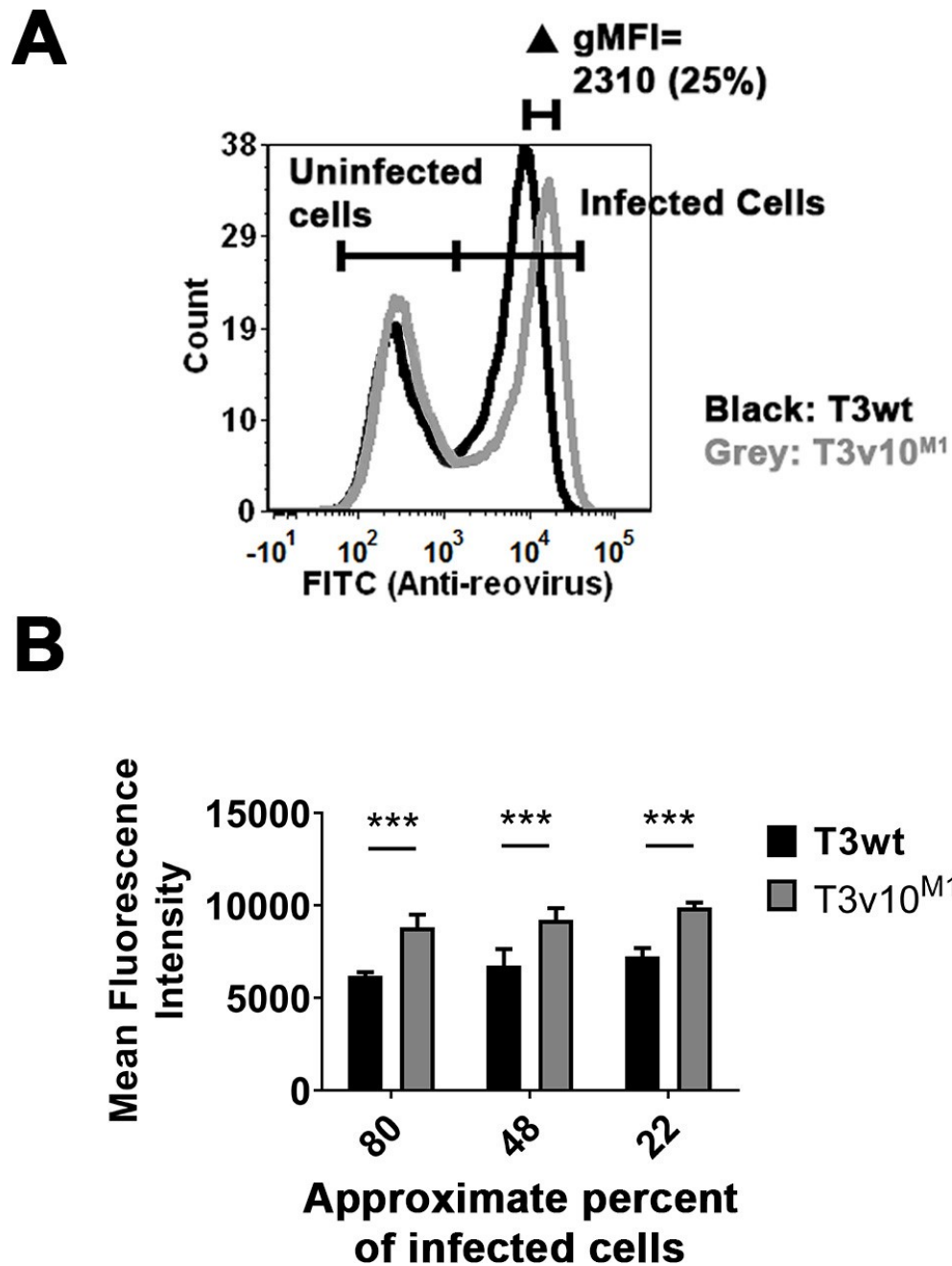


Figure 5- 9. T3v10^{M1} accumulates more viral proteins in infected L929 cells.

(A) Histogram from flow cytometry analysis compared mean fluorescence intensity (MFI) of T3wt- and T3v10^{M1}-infected L929 cells at 15hpi. Reovirus antigen-positive cell population (right peak) represented viral infected cells. **(B)** L929 cells were infected with different doses of T3wt or T3v10^{M1} for 15 hours and MFIs are compared by bar graphs ($n=3$; mean \pm SD; two-way ANOVA - Dunnett's multiple comparisons test). Please refer to Figure 5- 7 for the approximate MOIs for the approximate percent of infected cells. For statistics, * = $P<0.05$, ** = $p<0.01$ *** = $p<0.001$ and **** = $p<0.0001$.

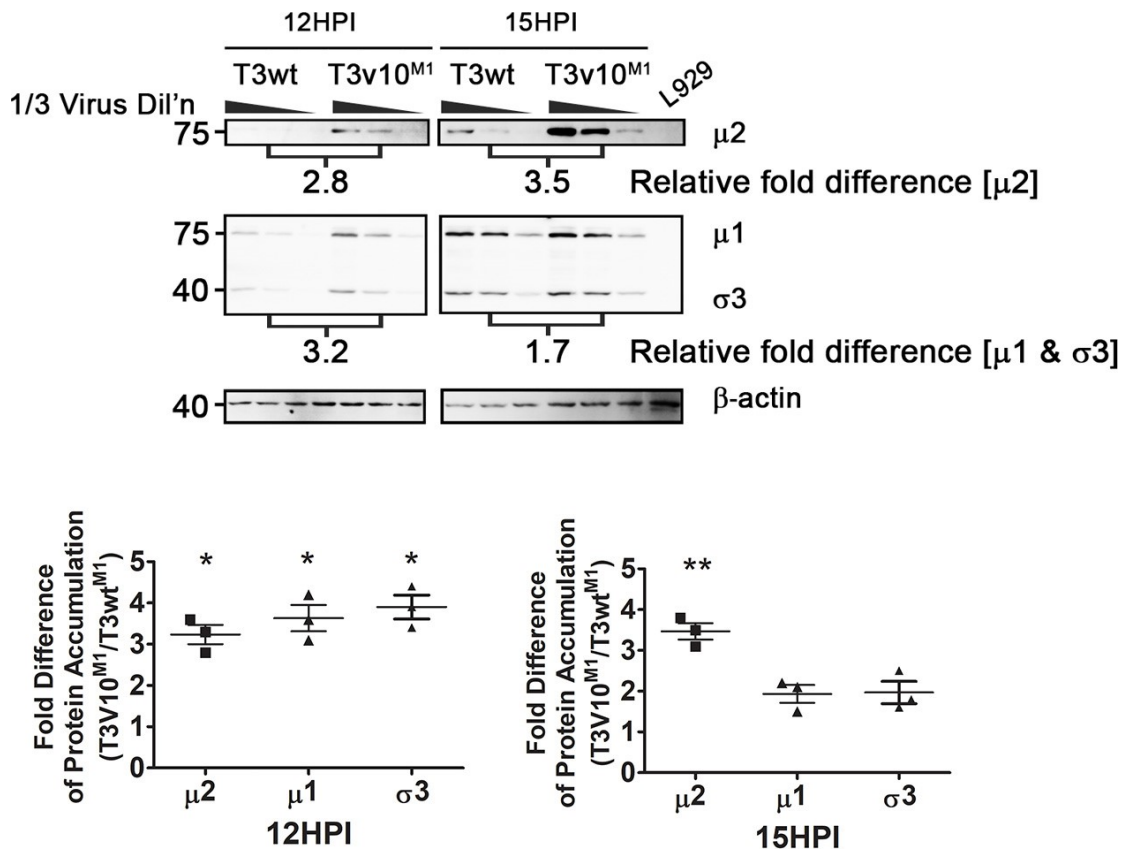


Figure 5- 10. T3v10^{M1} accumulates up to 3.5-fold more viral proteins in infected L929 cells at 15hpi.

Equivalent amount of L929 cells were infected by T3wt or T3v10^{M1}. Total cell lysates were subjected to Western blotting analysis and intensities of protein bands were quantified by ImageQant. Fold difference of protein accumulation (T3v10^{M1}/ T3wt) was showed by dot plot ($n=3$; mean \pm SD; One sample t-test – comparing fold difference to theoretical mean of 1). For statistics, * = $P<0.05$, ** = $p<0.01$ *** = $p<0.001$ and **** = $p<0.0001$.

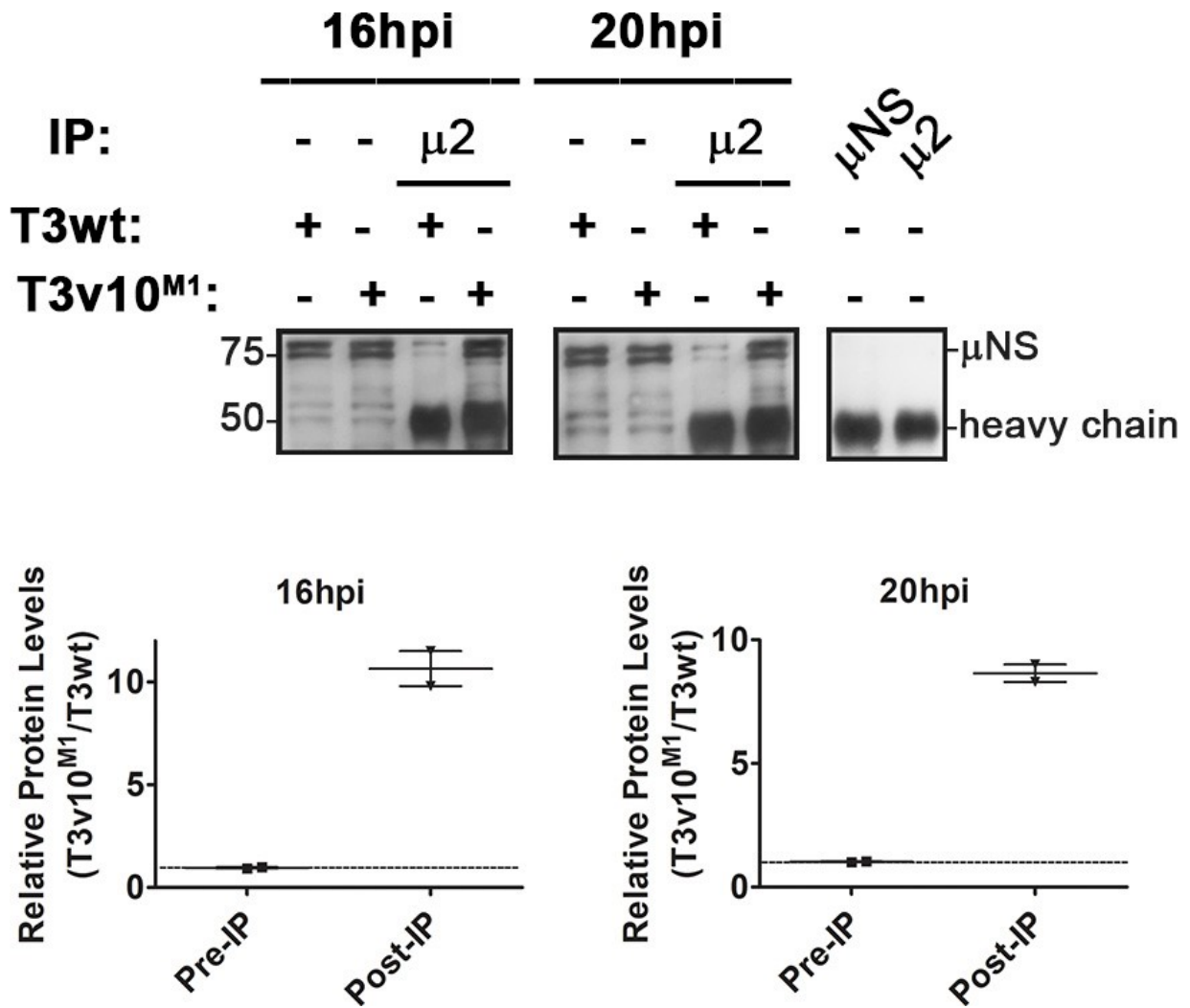


Figure 5- 11. $\mu 2$ and μNS has increased association in T3v10^{M1}-infected L929 cells.

L929 cells were infected with T3wt or T3v10^{M1}. Whole cell lysates were collected at the indicated time points and $\mu 2$ was immunoprecipitated by specific antigen. μNS that was co-immunoprecipitated was analyzed by Western blotting analyses ($n=2$; mean \pm SD).

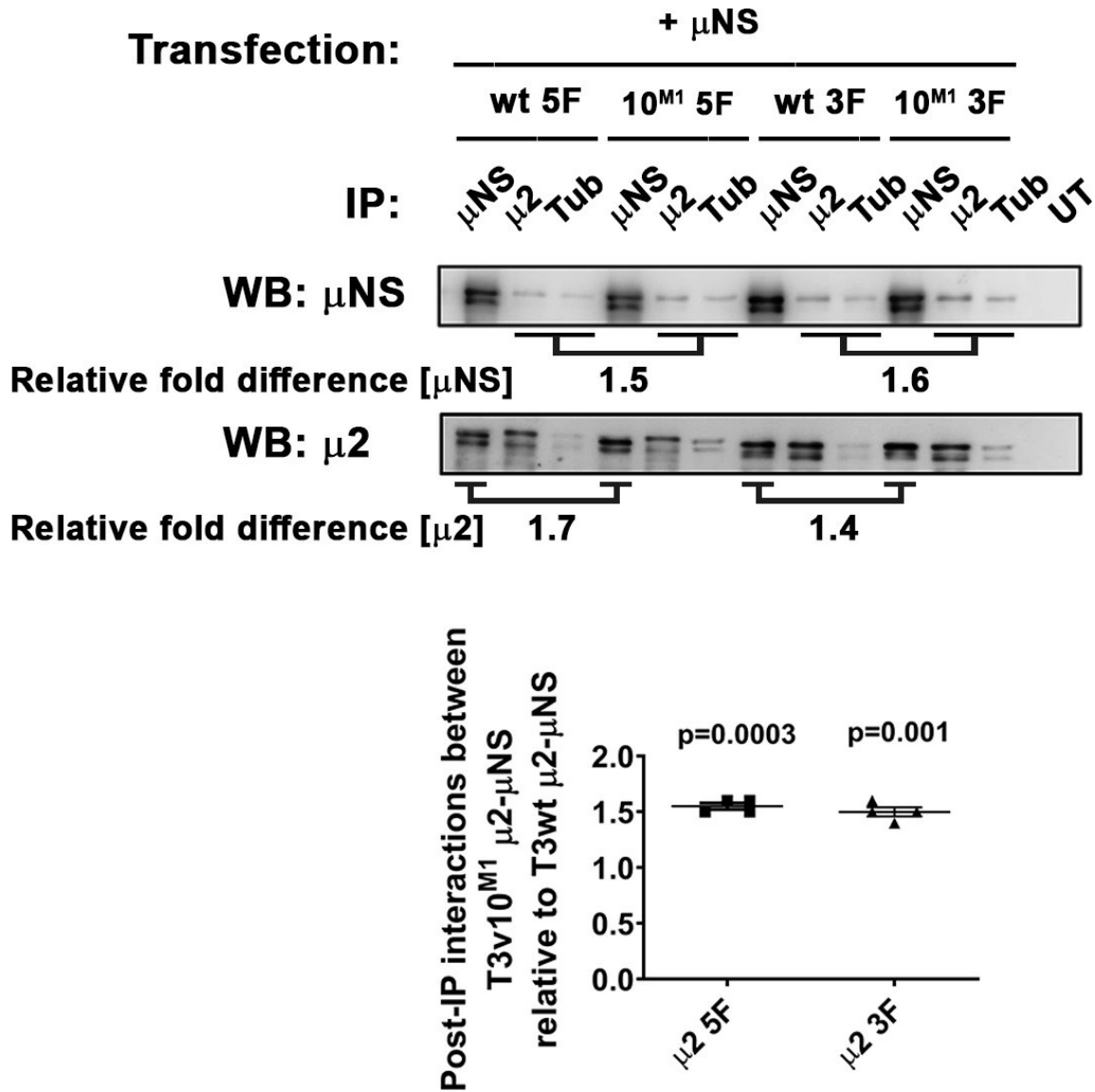


Figure 5- 12. Transfected T3v10^{M1}-derived μ 2 (10^{M1} μ 2) shows increased association with μ NS in H1299 cells.

H1299 cells were co-transfected with μ NS and wild-type (wt) μ 2 or μ 2 derived from T3v10^{M1} (10^{M1}). All μ 2 proteins had either a 5' terminal FLAG-tag (5F) or 3' terminal FLAG-tag (3F). Whole cell lysates were harvested 24 hours post transfection (hpt) and subjected to Western blotting analyses to examine interaction between μ 2 and μ NS ($n=4$; mean \pm SD; One sample-t test – comparing sample mean to theoretical mean of 1).

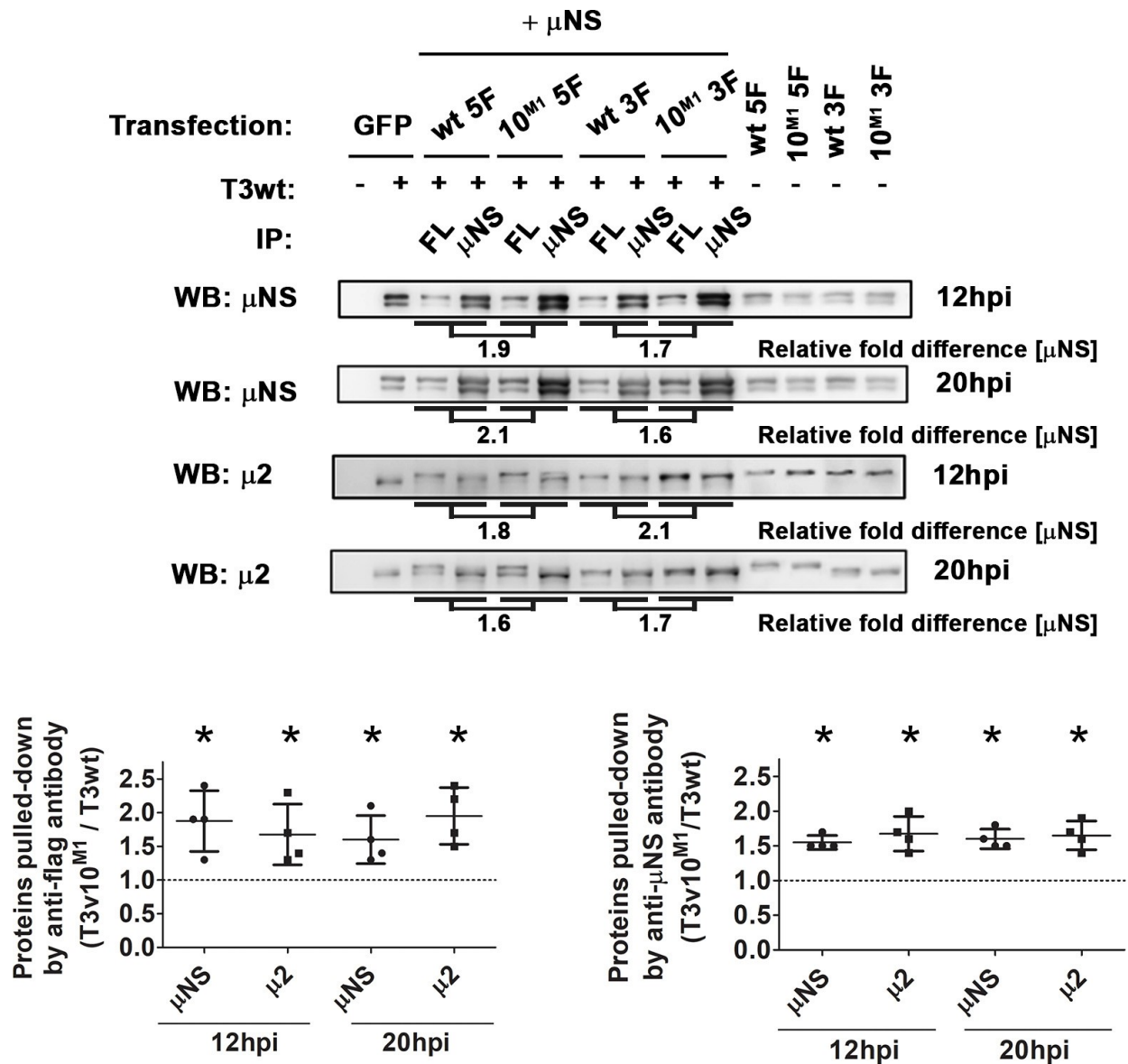


Figure 5- 13. Pre-transfection of T3v10^{M1}-derived μ 2 (10^{M1} μ 2) and wild-type μ NS enhances association of 10^{M1} μ 2 and virus-expressed mNS.

H1299 cells were co-transfected with μ NS and one of the four μ 2 constructs as described in Figure 5- 12 ($n=4$; mean \pm SD; One sample t test – comparing sample mean to theoretical mean of 1). At 24hpt, cells were exposed to T3wt. Whole cell lysates were collected at 24hpi and subjected to Western blotting analyses. μ 2 and μ NS association was plotted in dot plots. For statistics, * = $P<0.05$, ** = $p<0.01$ *** = $p<0.001$ and **** = $p<0.0001$.

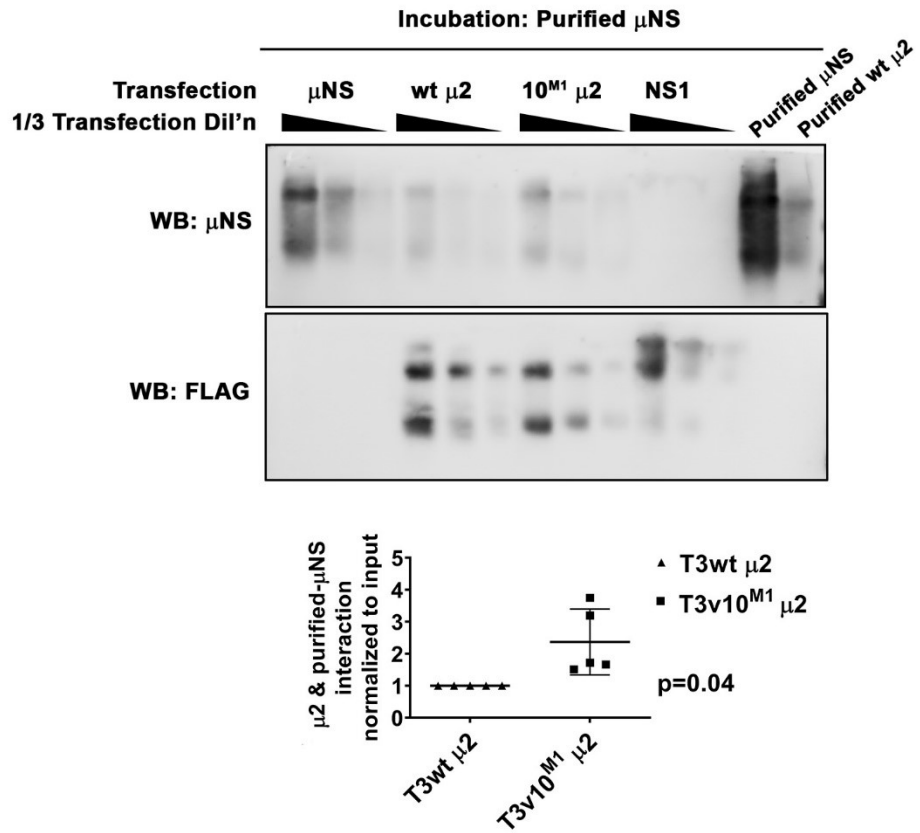
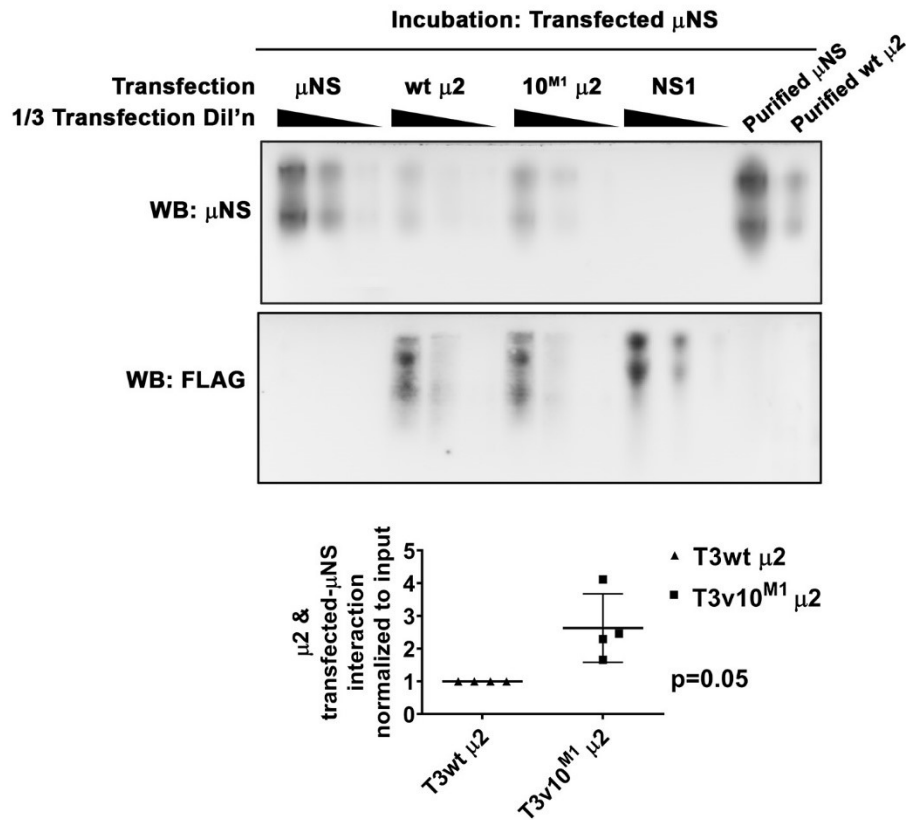
A**B**

Figure 5- 14. Far-Western blot analysis shows T3v10^{M1}-derived μ 2 has stronger physical interaction with μ NS.

(A and B). H1299 cells were transfected with serial diluted plasmids that expressed the indicated proteins. Only plasmids expressing 5F μ 2 were used in this experiment. NS1 was a FLAG-tagged Dengue virus capsid protein and included as a negative control. μ NS and μ 2 proteins purified from bacterial expression system (right 2 lanes) were used as positive controls. Transfected cells were lysed in non-denaturing lysis buffer and proteins were separated by polyacrylamide gel electrophoresis in non-denaturing conditions. PVDF membranes were then used for protein transfer and incubated with purified μ NS **(A)** ($n=5$; mean \pm SD; paired t-test) or H1299 whole cell lysate with transfected μ NS **(B)** ($n=4$; mean \pm SD; paired t-test). Interaction of μ 2- μ NS was examined by Western blotting analysis (top), and transfection of the FLAG-tagged proteins was confirmed in the blot below. Densitometric analyses were performed using cells transfected with undiluted plasmids and showed as dot plots ($n=4$; mean \pm SD, t-test).

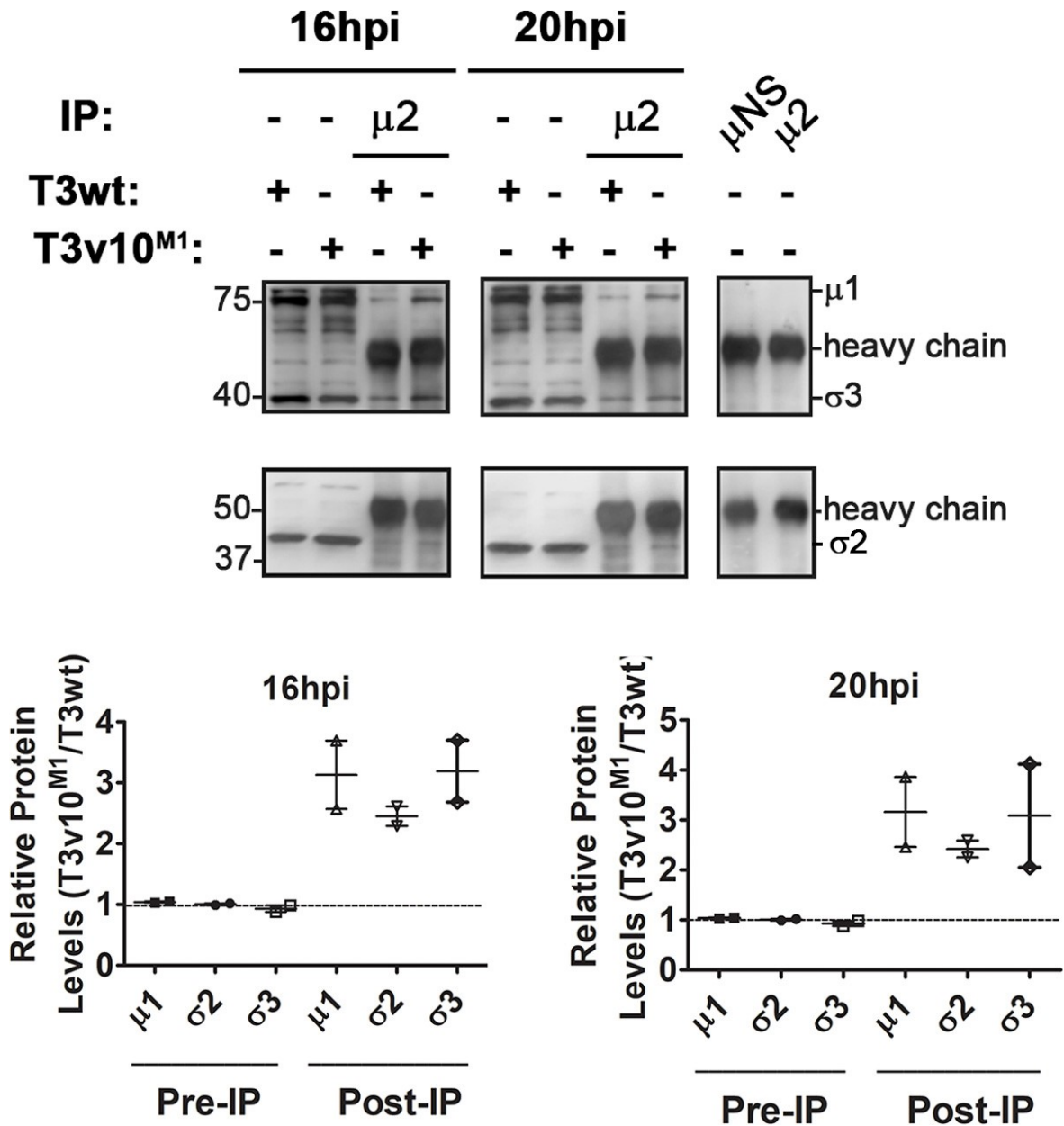


Figure 5- 15. Increased $\mu 2$ - μNS association in T3v10^{M1}-infected L929 cells enhances core and outer capsid proteins recruitment.

L929 cells infected with T3wt or T3v10^{M1} were processed as described in Figure 5- 11 ($n=2$; mean \pm SD). Associations between viral capsid proteins $\mu 1$ and $\sigma 3$, and core protein $\sigma 2$ with T3wt- or T3v10^{M1}- $\mu 2$ protein complex were compared on Western blots.

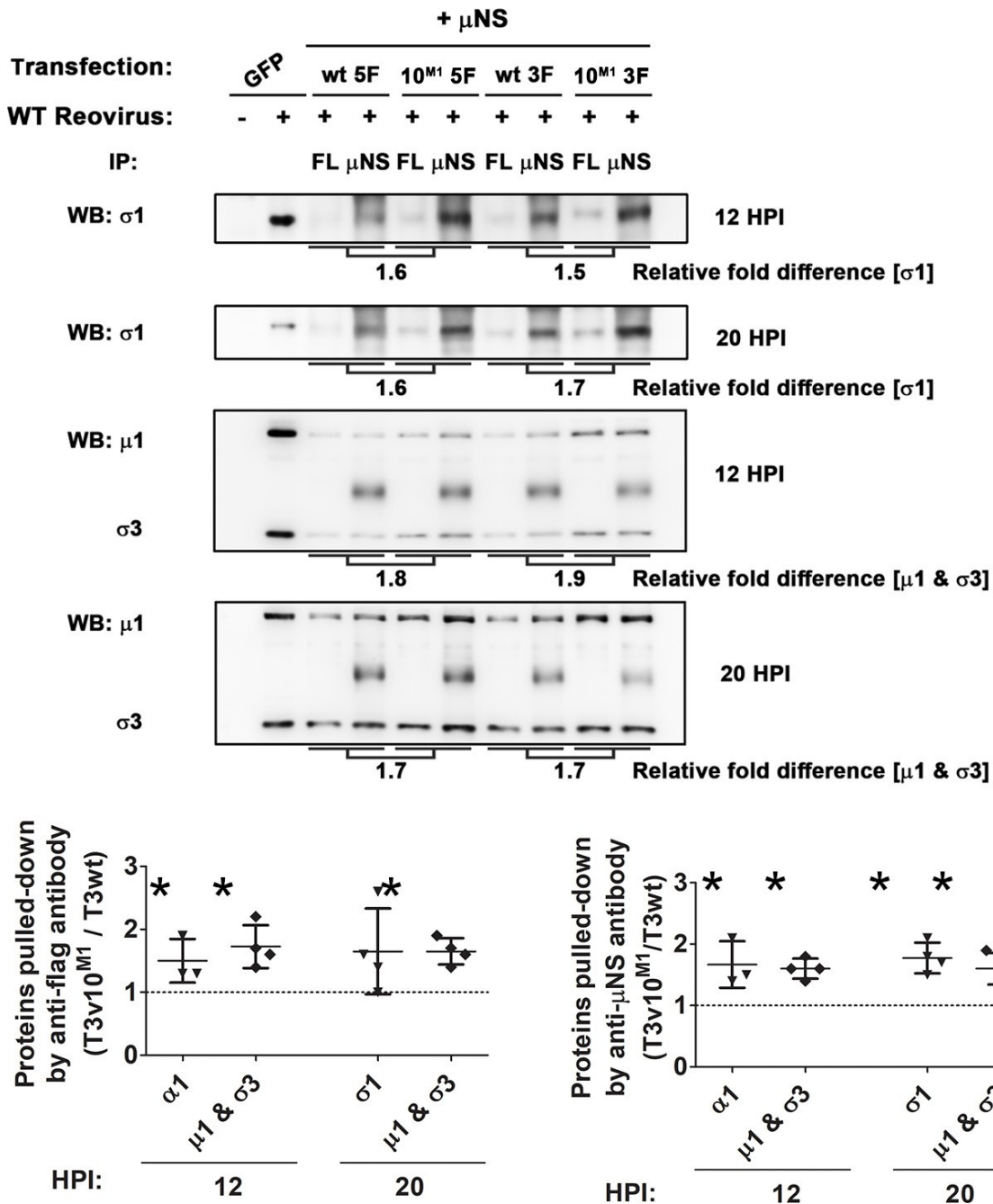


Figure 5- 16. Pre-transfection of T3v10^{M1}-derived μ 2 and wild-type μ NS enhances core and outer capsid proteins recruitment.

Transfected H1299 cells were processed as described in Figure 5- 12. Interactions between reovirus capsid proteins (μ 1, σ 3 and σ 1) and protein complex pulled down by anti-FLAG (FL) or anti- μ NS (μ NS) antigen were examined on Western blots ($n=3$ for σ 1 and $n=4$ for μ 1 & σ 3); mean \pm SD; One sample t-test – comparing sample mean to theoretical mean of 1). For statistics, * = $P<0.05$, ** = $p<0.01$ *** = $p<0.001$ and **** = $p<0.0001$.

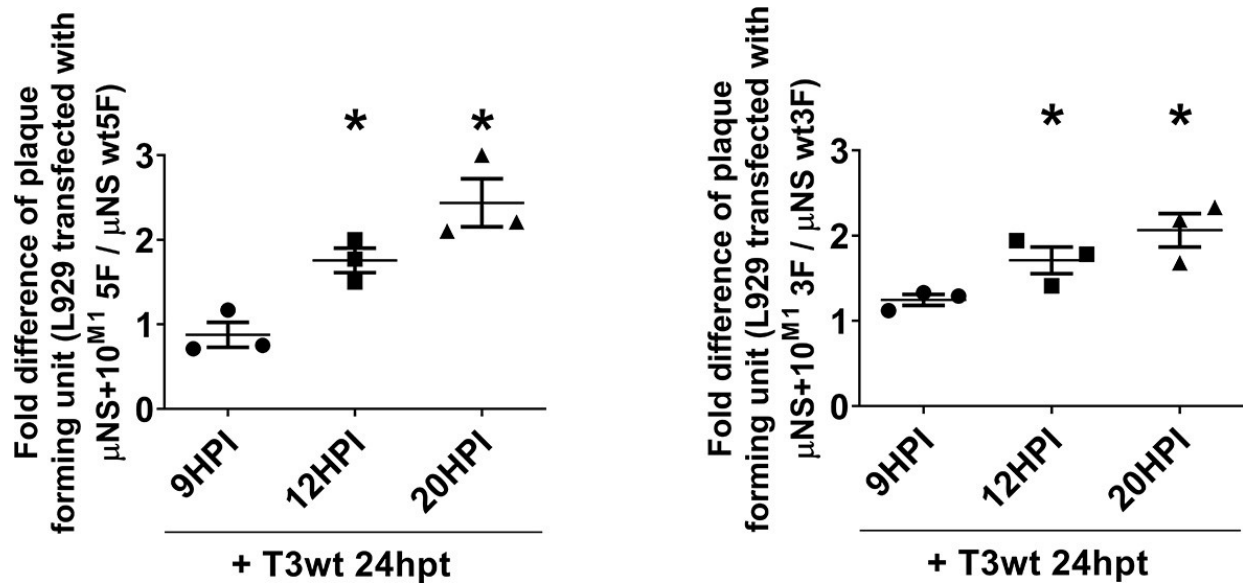


Figure 5- 17. Pre-transfection of T3v10^{M1}-derived $\mu 2$ (10^{M1} $\mu 2$) and wild-type μ NS promotes progeny production.

H1299 cells were transfected and infected as described in Figure 5- 13. Whole cell lysates were frozen and thawed at least three times to allow full release of reovirus progeny. Plaque assays were performed and fold difference of plaque forming unit was showed by dot plots ($n=4$; mean \pm SD; One sample t-test – comparing sample mean to theoretical mean of 1). Protein band intensities were quantified by ImageQuant. To compare fold difference between protein bands of T3v10^{M1} and T3wt, T3wt samples were theoretically referenced as 1. For statistics, * = $P < 0.05$, ** = $p < 0.01$ *** = $p < 0.001$ and **** = $p < 0.0001$.

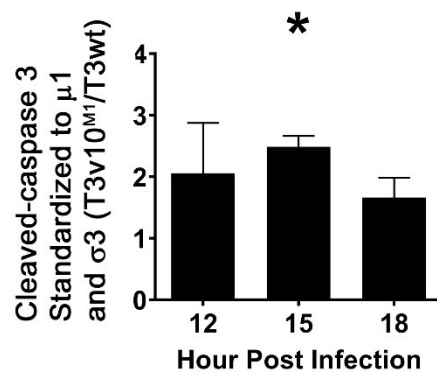
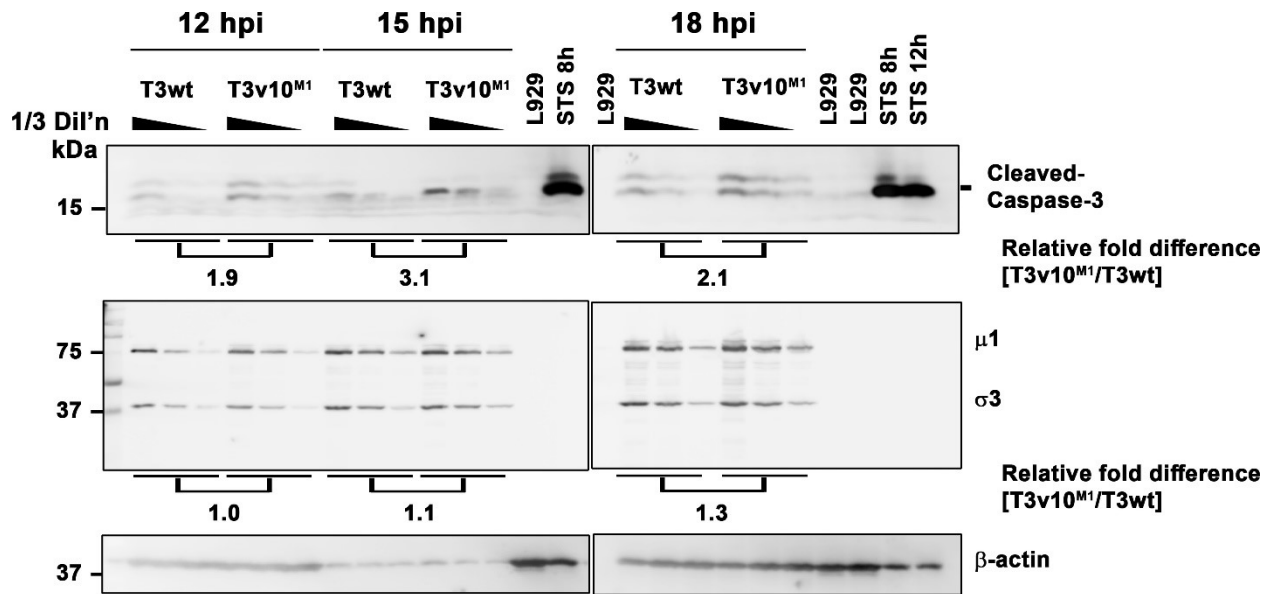
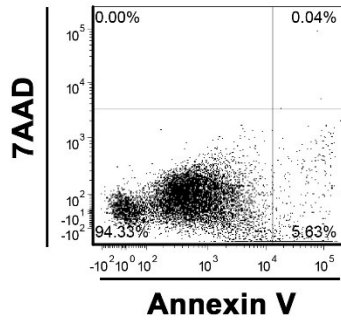


Figure 5- 18. T3v10^{M1} infection induces more cleaved caspase-3.

L929 cells were exposed to T3wt or T3v10^{M1} to express equivalent amount of capsid proteins μ1 and σ3. Expression of cleaved caspase-3 was detected at 12, 15 and 18 hpi by caspase-3 antiserum (Cell Signaling, 9661). Fold difference of caspase-3 expression was standardized to fold difference of μ1 and σ3 (T3v10^{M1}/ T3wt). Results from 3 independent experiment were plotted as bar graph (mean ± SD; One sample t-test – comparing fold difference to theoretical mean of 1). For statistics, * = P<0.05, ** = p<0.01 *** = p<0.001 and **** = p<0.0001.

Uninfected L929



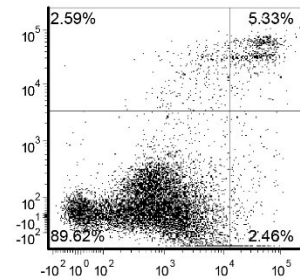
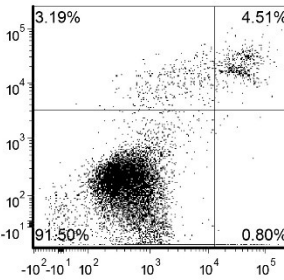
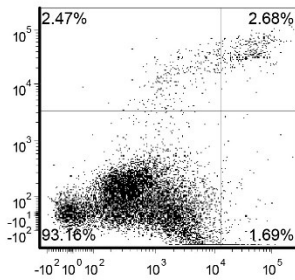
T3wt

HPI

12

15

18



T3v10^{M1}

HPI

12

15

18

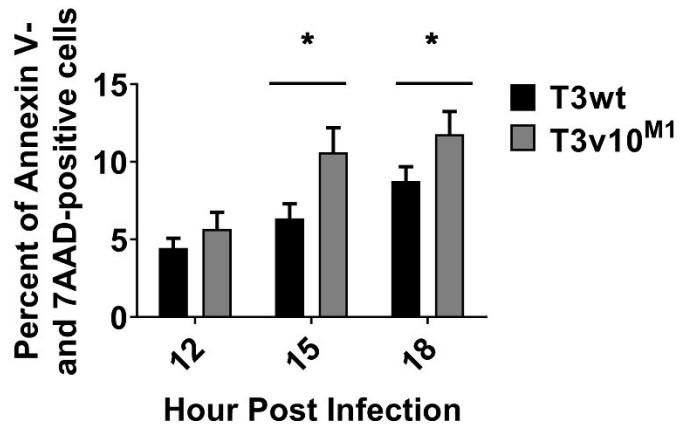
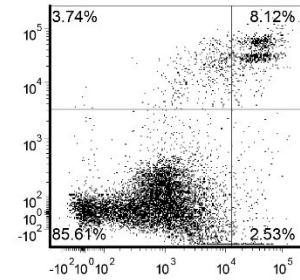
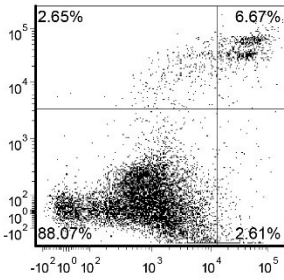
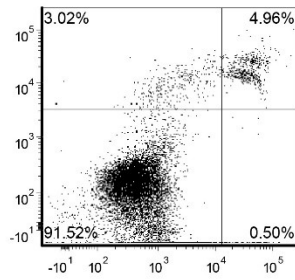


Figure 5- 19. T3v10^{M1} infection induces more cell-death.

L929 cells were mock-infected or infected with T3wt or T3v10^{M1} as described in Figure 5- 18. Cells were collected and analyzed using the method detailed in section 2.4.1. The percentage of cells localized in each quadrant is indicated (lower left, -Annexin V, -7AAD; lower right, +Annexin V, -7AAD; upper left, -Annexin V, +7AAD; upper right, +Annexin V, +7AAD). Results from 3 independent experiment were plotted as bar graph (mean \pm SD; two-way ANOVA – Dunnett’s multiple comparison tests). For statistics, * = P<0.05, ** = p<0.01 *** = p<0.001 and **** = p<0.0001.

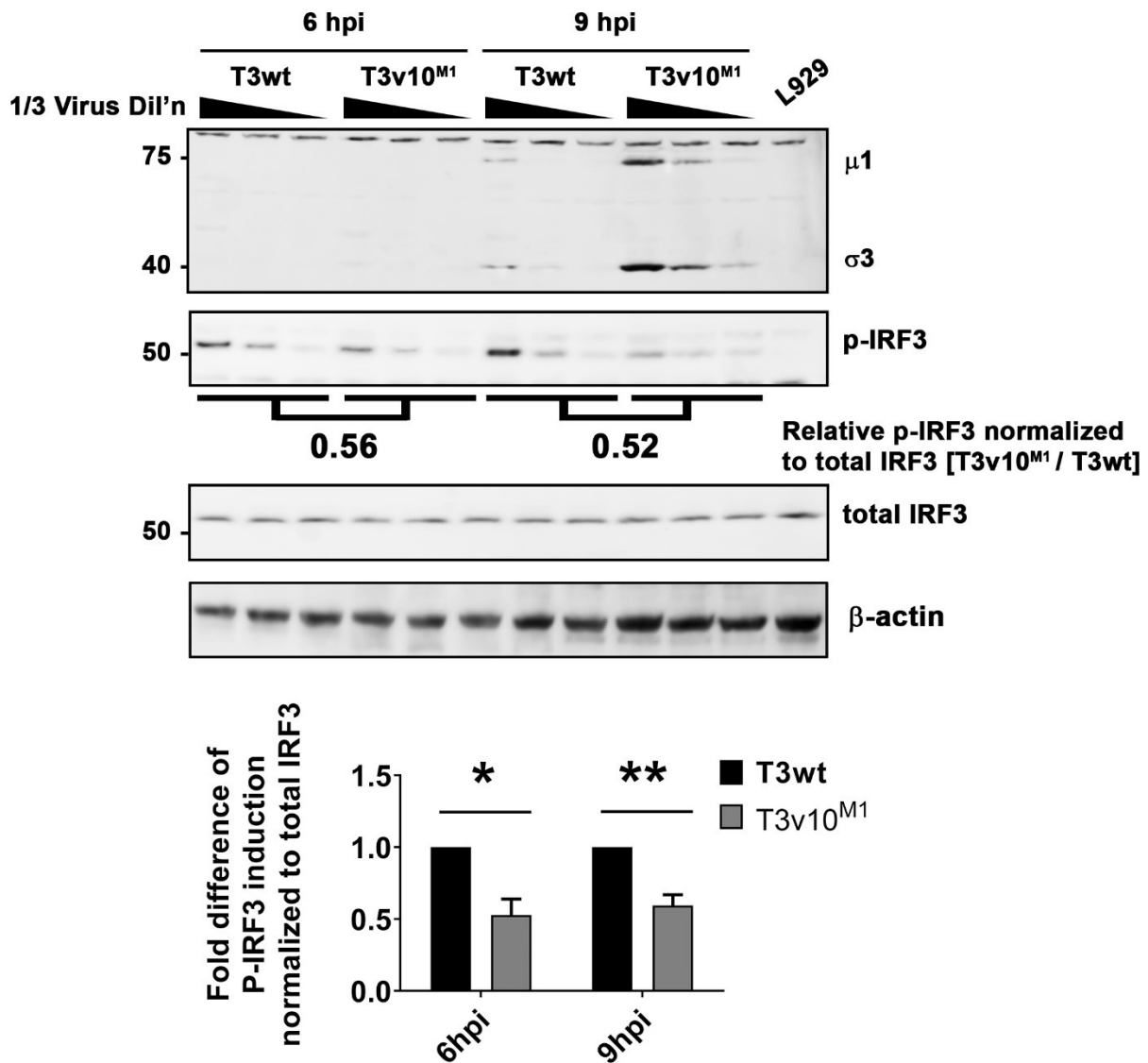


Figure 5- 20. T3v10^{M1} has reduced of p-IRF3.

Equivalent of L929 cells were infected with T3wt or T3v10^{M1}. Cell lysates were collected at 6 and 9hpi and analyzed by Western blots. Expressions of p-IRF3 were normalized to total IRF3. Three independent experiments were performed and the results were represented using bar graphs (mean \pm SD; two-way ANOVA – Dunnett’s multiple comparison tests). For statistics, * = $P < 0.05$, ** = $p < 0.01$ *** = $p < 0.001$ and **** = $p < 0.0001$.

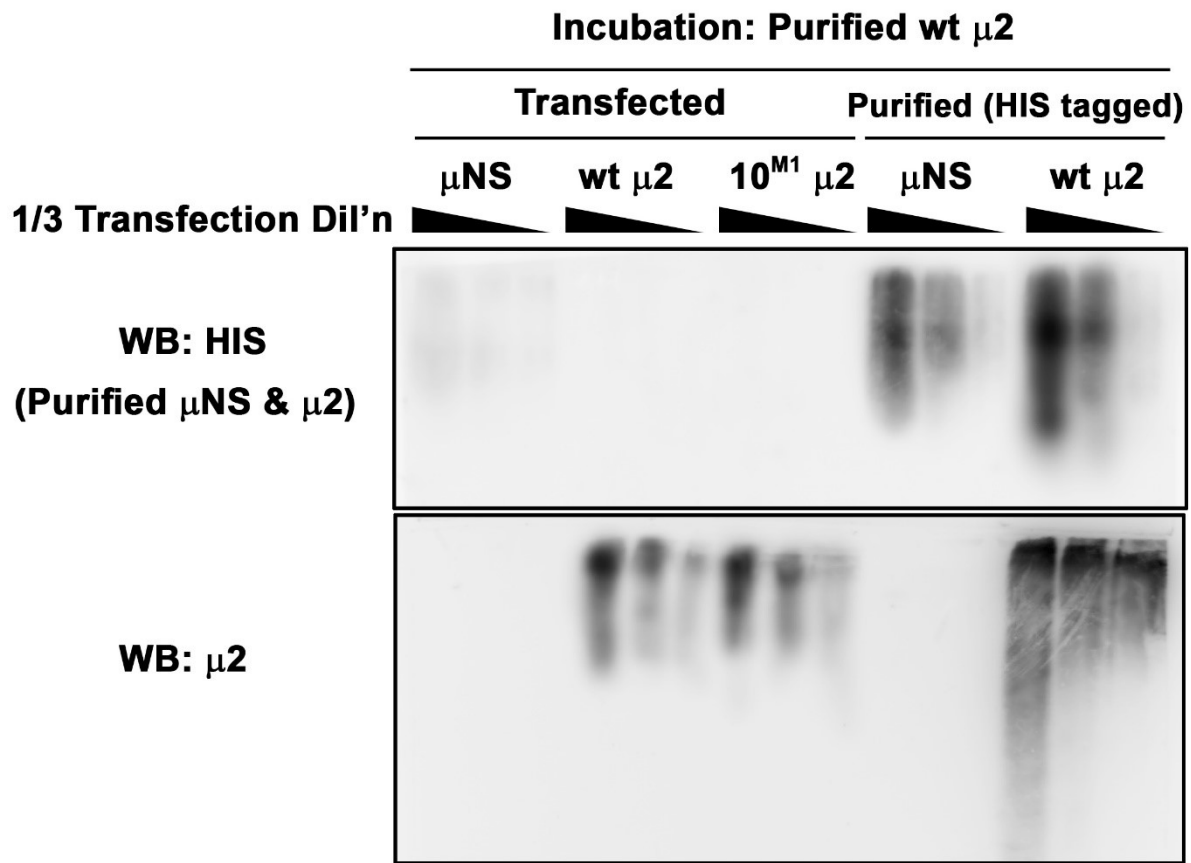


Figure 5- 21. Mu2 does not self-associate on Far-Western blot.

Far-Western blot analysis was performed as described previously (Figure 5- 14) to investigate μ 2 self-association. Transfected T3wt (wt) μ 2 or T3v 10^{M1} (10M) μ 2, and along with other controls were loading into native gels and proteins were transferred to PVDF membrane, followed by incubation with PBS containing HIS-tagged μ 2. Membranes were probed with anti-HIS serum (top) and anti- μ 2 serum (bottom) to confirmed the presence of transfected μ 2.

CHAPTER 6: DISCUSSION AND FUTURE DIRECTIONS

6.1 Chapter 3: investigation of $\sigma 1$ tail regions and their effects on virion association

6.1.1 Residues 28 and 66 of $\sigma 1$ are unique compared to neighboring amino acids

Although reduction of $\sigma 1$ is a main mechanism shared by our variants with enhanced replication in transformed cells, little is known how $\sigma 1$ levels are regulated and mediated by different regions in the $\sigma 1$ tail. Variants T3v16 and T3v8, have the L28P and S66I single amino acid replacements in the $\sigma 1$ tail respectively. We sought to understand how a single residue change affects $\sigma 1$ levels. Despite both mutations are found in the region proposed to be important for $\sigma 1$ multimerization, we showed that both alterations did not affect trimerization of $\sigma 1$ (Figure 3- 6 and Figure 3- 7), suggesting that a single replaced residue could have a dramatic impact on the $\sigma 1$ -virion association (Figure 3- 3).

We wondered if the 2 residues are located in any known domain that is potentially involved in protein-protein interactions because both mutations are close to the anchoring domain (residues 1-25) and may participate in the interaction with $\lambda 2$. Sequence comparisons between serotypes reveal that neither residue 28 nor 66 is conserved among T1L, T2J and T3D (Figure 6- 1). Residues 28 and 66 reside in the region that is predicted to form a long α -helical coiled-coil that is proposed to be important for $\sigma 1$ trimerization and stability (please refer to section 1.5.1), and therefore, we wondered if the two altered residues are close to any conserved or well-defined functional domains. We performed PHI-BLAST using 40-50 residues near the altered site in an attempt to find known domain with similar structure, but our search

did not generate any meaningful results. Lastly, we submitted a recently published $\sigma 1$ crystal structure (PDB ID: 6GAJ) (78) to PDBePISA for protein interfaces analysis (Figure 6- 2). The analysis suggests that residues 28 and 29 directly participate in protein-protein interaction. The residue 66 does not directly engage in interactions with other proteins, but its neighboring residues are predicted to interact with other molecules. In summary, alteration of either residue 28 or 66 may impact interactions between $\sigma 1$ and other proteins, including cell-binding, virion association and multimerization (Figure 3- 13 shows that trimerization is not affected).

We speculated that the physical properties and structure of the residue at site 28 or 66 play key roles in $\sigma 1$ -virion association. To test this, we generated multiple $\sigma 1^{1-251}$ constructs by swapping the residue at site 28 or 66. Residue 28 has a wild-type leucine, and we changed it to either proline or alanine in two separate constructs. Each mutant construct reduces $\sigma 1$ level by about 2-fold relative to the wild-type construct. The wild-type leucine is more hydrophobic than alanine and proline. Given that different $\sigma 1$ region is characterized by physical properties of amino acids, we performed hydrophobicity analysis with the Jalview software, and it was revealed that residue 28 is sandwiched between two rather hydrophilic (underlined) groups of residues (S-K-G-L-E-S-R), this suggests that the highly hydrophobic leucine may play some important structural role and replacing this residue could dramatically impact $\sigma 1$ -virion association.

For residue 66, a schematic model has been created (Figure 6- 3) to explain our findings. Below the structure of $\sigma 1$, residues 60-75 are shown and the wild-type serine at site 66 is very unique compared to the neighboring residues. First, serine is slightly hydrophilic and surrounded by a group of charged and very hydrophilic residues (Figure 6- 3A). Second, the

hydrophilic residues are sandwiched between two highly hydrophobic groups (Figure 6- 3A). This region may be important in maintaining the structural stability of $\sigma 1$ and play role in protein-protein interaction, potentially affecting virion $\sigma 1$ -association. Figure 6- 3B summarizes results of virion association with $\sigma 1^{1-251}$ that possess the indicated residue-66 replacement. All replaced residues are very hydrophobic (except that threonine has a neutral hydrophobicity). Changing the hydrophobicity of residue-66 could impair virion association. Secondly, serine is a small amino acid with a simple hydroxyl group as side chain, while threonine, leucine and valine have very bulky and Y shape side chains. These three amino acids are very hydrophobic and structurally different from serine, and this may explain why $\sigma 1$ -association was impaired the most.

6.1.2 The L28P mutation may prevent proteolytic cleavage of $\sigma 1$

As discussed earlier, the L28P mutation from T3v16 reduced $\sigma 1$ level by 2-fold, but the same mutation may also alter the conformation of $\sigma 1$ trimer and prevent proteolytic cleavage of $\sigma 1$. During our assessment of $\sigma 1$ trimers and monomers of the variants, T3v16-encoded $\sigma 1$ migrated faster than all other $\sigma 1$ proteins; T3v16 was the only variant that did not produce a cleaved $\sigma 1$ at ~ 60 kDa in Figure 3- 6 (36 and 50°C), Figure 3- 7 (36°C). Similarly, transfected $\sigma 1$ carrying residues 1-251 with the L28P or L28A mutation had a faster migration and the mutated $\sigma 1$ trimer and monomer did not produce any detectable cleaved product (Figure 3- 13). Our data suggest that the altered residue 28 changed the conformation of trimeric $\sigma 1$, and therefore, affect its migration on SDS-PAGE.

There are two possibilities to explain the lack of cleaved $\sigma 1$ (Figure 6- 4). First, the altered residue 28 does not prevent proteolytic cleavage of $\sigma 1$, but the mutation renders the cleaved product undetectable by anti- $\sigma 1$ serums. Second, the mutation may reduce the sensitivity of $\sigma 1$ to proteases. To distinguish the two possibilities, future studies can subject wild-type control and T3v16 or transfected $\sigma 1$ with altered residue 28 to different concentrations of trypsin or chymotrypsin treatments. I expect that the uncleaved $\sigma 1$ band will remain unchanged if the mutation prevents the cleavage, while the control band will completely disappear when high concentrations of protease are used.

6.1.3 Sigma 1 trimers may have different conformations on SDS-PAGE in an incubation temperature-dependent manner

During our characterization of $\sigma 1$ multimerization, we observed that the apparent molecular sizes of T3wt $\sigma 1$ trimers shifted between 22°C to 65°C (Figure 3- 5), similar observations were made from reovirus variants (Figure 3- 6). Specifically, when reovirus virions were incubated with SDS-containing sample buffer at 22 or 36°C prior to SDS-PAGE, two faint bands at ~220kDa and ~180kDa and a dominant ~130kDa band were observed on Western blots. The same three bands were observed again when incubation temperatures are increased to 50 or 65°C (Figure 3- 5), but the intensities of ~220kDa and ~180kDa bands increased while the ~130kDa band was barely detectable. These observations suggest that $\sigma 1$ trimers can adopt to different conformations in a temperature-dependent manner.

In fact, similar observations were made in a previous study (243). Strong and colleagues observed that $\sigma 1$ trimers produced a protein band with $>200\text{kDa}$ at 37°C , but the band shifted to $\sim 150\text{kDa}$ at lower incubation temperatures. They further concluded that the band with lower molecular weight was the expected size of $\sigma 1$ trimer and represented the natural and native conformation of the protein; the conformation change at higher temperature was due to the disruptions of the C-terminal head dissociated and disrupted, creating the “hydra” conformation (probably due to the combined effects of higher incubation temperature and the presence of denaturants in protein sample buffer). We also predict that the $\sim 130\text{kDa}$ trimeric $\sigma 1$ bands we observe in Figure 3- 5 and Figure 3- 6 are the native form, and the molecular size of monomeric $\sigma 1$ is $\sim 45\text{kDa}$, which is about 3 times smaller than $\sim 130\text{kDa}$ band. A diagram summarizes all our findings regarding $\sigma 1$ multimerization and all the potential incubation temperature-dependent conformations of trimeric $\sigma 1$ (Figure 6- 5). However, we would also emphasize that our data does not suggest $\sigma 1$ exists as “hydra” under physiological temperatures because we performed the experiments in denaturing conditions that would disrupt the natural conformation of $\sigma 1$.

6.1.4 Assembly of $\sigma 1$ onto virion involves multiple steps

Our study focuses on how different regions of the $\sigma 1$ tail affect its assembly onto virion. Our data provides evidence that the assembly of $\sigma 1$ involves multiple steps (Figure 6- 6). In our pull-down experiments (Figure 3- 10), we showed that transfected $\sigma 1$ with residues 1-104 ($\sigma 1^{1-104}$) was expressed in cells, but it was not pulled down with the virion. Furthermore, $\sigma 1^{1-104}$ was

detected in the cytoplasm, but not in the viral factory of transfected cells (Figure 3- 11). Our data also suggests that residues 155-235 significantly promoted accumulation of $\sigma 1$ in the viral factory. However, we need to interpret the data carefully. First, the band intensity of $\sigma 1^{1-104}$ was much weaker compared to other bands, and therefore, $\sigma 1^{1-104}$ might associate with the viral factory but its expression was below detection. Secondly, our data does not exclude the possibility that $\sigma 1^{1-104}$ was less stable than other constructs and the protein is degraded before we harvest the cells. Nevertheless, residues on the C-terminal of $\sigma 1$ tail may be required for effective accumulation in the viral factory.

Our model proposes that following recruitment and accumulation in the viral factory, $\sigma 1$ needs to associate with the virion before it is assembled (Figure 6- 6). To support this model, Figure 3- 14 shows that 37% of $\sigma 1^{27-286}$ was pulled-down with the virion compared to $\sigma 1^{1-251}$. The $\sigma 1^{27-286}$ has the anchoring domain truncation and is predicted not able to assemble on the virion. However, our data cannot determine if $\sigma 1^{27-286}$ is properly assembled into the virion. It is also unclear whether $\sigma 1^{27-286}$ is functional and capable of host-cell binding. Future studies can generate virus expressing $\sigma 1^{27-286}$ and compare its cell-binding with viruses possessing similar amount of $\sigma 1$.

Results from our pull-down assays suggest that residues in the midpoint region and C-terminus of $\sigma 1$ are involved with virion association. The $\sigma 1^{1-154}$ was not being pulled down or its expression was below detection limit (Figure 3- 14). The longer construct, $\sigma 1^{1-235}$ was detected in our co-immunoprecipitation assay and this suggests that residues 155-235 contribute to virion association. This is not surprising, because previous studies showed that

residues 155-182 are crucial for $\sigma 1$ encapsidation (please see sections 1.5.1 and 1.5.2). As discussed previously, residues 155-235 are crucial for viral factory accumulation; during our mutational sensitivity analysis of the entire T3D $\sigma 1$ using the Phyre2 web portal for protein modeling, the region composed of residues 190-232 was very conserved relative to other parts of $\sigma 1$ protein, suggesting that these residues are important for $\sigma 1$ functions (Figure 6- 7). Extension of residues towards the C-terminus further enhanced virion association. Compared to $\sigma 1^{1-235}$, the $\sigma 1^{1-251}$ promoted virion association by 4-fold (Figure 3- 14). This is the first study showing that $\sigma 1$ residues 235-251 are implicated in virion association. Data from the mutants generated by the RG system also agree with our findings from vector-expressed $\sigma 1$ (Figure 3- 16 and Figure 3- 17): sigma 1 carrying only residues 1-154 could barely associate with the virion and extending residues towards residue site 251 improved virion association.

Our pull-down assays showed that the transfected $\sigma 1^{1-286}$ has the best virion association (Figure 3- 14), but the average $\sigma 1$ levels of mutant 1-286 were lower than mutant 1-251 (Figure 3- 16 and Figure 3- 17), and we also noticed that results from 4 independent experiments were less consistent compared to other mutants. Our model may be able to explain the contradictory findings (Figure 6- 8). Sigma 1 residues 252-286 promote virion association, but the $\sigma 1$ may not assemble onto the virion properly. For the vector-expressed construct, a large amount of virion-associated $\sigma 1^{1-286}$ may get co-immunoprecipitated by anti-FLAG serum (Figure 3- 14) because the pull-down assays are performed in conditions to preserve $\sigma 1$ -virion interactions. However, the procedures we use to purify mutants generated by RG system are rather harsh. First, reovirus-infected L929 cell lysate is incubated with Capto Core 700 resin that bind small proteins and impurities from cell lysates while excluding large particles such as

the whole particle of reovirus. After removing the beads by filtering, reovirus containing medium is subjected to ultra-high-speed centrifugation to pellet the virions. These processes can remove a large amount of $\sigma 1$ proteins that are associated, but do not assemble onto the virion. Variations in the purification procedures can also have large effects on $\sigma 1$ -virion association for mutant 1-286.

6.1.5 Major contributions and limitations of the current study

In conclusion, our data support the model that assembly of $\sigma 1$ involves various stages of the replication cycle such as $\sigma 1$ localization and accumulation in the viral factory, and the encapsidation of $\sigma 1$ may require separate steps of $\sigma 1$ -virion association and the actual assembly as the final step. Contributions of our study regarding the function of $\sigma 1$ tail are summarized in Figure 3- 19. Our data also suggests the $\sigma 1$ head increases virion-associated $\sigma 1$ because $\sigma 1$ levels of RG-T3wt are 2-fold higher than mutant 1-251 (Figure 3- 16 and Figure 3- 17).

There are two major limitations of our study that could be addressed by future studies. First, we did not assess the stability of truncated $\sigma 1$. The C-terminal region and the head of $\sigma 1$ may promote protein stability. Future studies may perform CHX-chase assay to determine the stability of full-length and truncated $\sigma 1$. Secondly, our model proposes that virion association and assembly of $\sigma 1$ are two separate steps, but we did not test whether the truncated or mutated $\sigma 1$ proteins were properly assembled onto virion. Future studies can assess the binding function of truncated mutants using cell-binding assay or hemagglutination assay.

Results from these assays can infer whether $\sigma 1$ is properly assembled and functional.

Furthermore, sigma 1 truncations may affect viral growth (please see section 1.5). Infectivity assays such as IF staining for reovirus-antigen positive cells and plaque assay can be performed to determine how different domains in the $\sigma 1$ tail affect viral replication.

6.2 Chapter 4: identifying novel mechanisms to improve oncolytic reovirus

6.2.1 Oncolytic potency of T3v6 and T3v13 may be enhanced by novel mechanism(s)

In chapter 4, we show that T3v6 and T3v13 have similar levels of $\sigma 1$ relative to T3wt (Figure 4- 5). Further characterization of these two variants can possibly lead to the discovery of novel mechanisms that augment reovirus replication in transformed cells. The T3v13 has two mutations in $\sigma 1$ protein and T3v6 has a total of 4 mutations. The T3v6 has a single mutation in $\sigma 1$ and $\lambda 2$ respectively, and two mutations in the $\mu 2$ protein (Table 4- 1). In this chapter, I will briefly outline some key experiments and directions to pinpoint the effects of these mutations.

For T3v13, the $\sigma 1$ mutations may affect uncoating (please refer to section 1.2.2). In chapter 4, we show that the rates of $\mu 1c$ cleavage (early step of uncoating) do not differ between T3wt and T3v10 (Figure 4- 7. Uncoating of reovirus is monitored by Western blot analysis. Figure 4- 7), but the cleavage and release of $\sigma 1$ (late step of uncoating) may be affected by the mutations. To test this, *in vitro* digestion (please refer to section 2.9) can be performed and equivalent amounts of T3wt or T3v13 ISVPs can be pull-downed by $\sigma 1$ -head antiserum,

followed by SDS-PAGE analysis of ISVP-associated $\sigma 1$ (normalized to core proteins such as $\mu 1$ and $\sigma 2$). By comparing the quantity of ISVP-associated $\sigma 1$ from T3v13 to T3wt, we can infer whether $\sigma 1$ mutations from T3v13 affect cleavage and release of $\sigma 1$ from ISVP.

The $\sigma 1$ protein is also implicated in the induction of cell-death (29,254), cell-death assays such as Annexin V staining can be performed. However, increased cell-death can be the consequence of enhanced replication. A more direct way to test whether the role of mutant $\sigma 1$ in cell-death induction is to transfect equivalent amounts of T3wt or T3v6 $\sigma 1$ into cells, followed by exposing transfected cells to cell-death inducer. Transfected cells will be collected at different time points and subjected to Annexin V staining (flow cytometry). I expect that cell-death induction is dependent on $\sigma 1$ transfection.

The T3v6 has 4 mutations in 3 different proteins. It is important to isolate each mutation and assess their effects independently. The 4 mutations can be separated by reassortment (Figure 4- 11) or introduced into wild-type virus by the RG system. The $\sigma 1$ mutation may affect uncoating and cell-death (please see the descriptions above for variant T3v13). The $\lambda 2$ protein directly interacts with $\sigma 1$ (please see section 1.5.1) and the mutation may affect release of $\sigma 1$ which consequently affects rate of uncoating. The $\lambda 2$ and $\mu 2$ proteins both play roles in genome transcription, and therefore, RNA synthesis should be assessed for T3v6 (please refer to section 1.2.3). The S613A $\mu 2$ for T3v6 is just one residue away from the altered residue 612 from T3v10^{M1}. This T3v10^{M1} has enhanced protein synthesis. Viral protein synthesis can be compared between mutant carrying the $\mu 2$ S613 mutation and T3wt. The L114F mutation is very close to the ITAM motif. The $\mu 2$ ITAM has been shown to activate NF- κ B signaling pathway that aids reovirus replication and may enhance reovirus induced cell-death.

In conclusion, the experiments discussed in this section can be performed first as they are predicted to measure the processes that are likely to be affected by the mutations in T3v6 and T3v11.

6.3 Chapter 5: A reovirus μ 2 C-terminal loop inversely regulates NTPase and transcription functions versus binding to factory-forming μ NS and promotes replication in tumorigenic cells.

6.3.1 Mu2 is the most conserved reovirus protein among different serotypes and field isolates

The A612V alteration in μ 2 is not mapped to any known domain. Also, the lack of x-ray crystal structure of MRV μ 2 makes it difficult to predict how the T3v10^{M1} μ 2 mutation affects its biological functions. We performed PHI-BLAST with short residues (40-50 amino-acid long) near the altered valine as an attempt to identify functional homologs, but no significant result has been found. A previous study also failed to find homologs for both M1 gene and μ 2 amino acid sequences in Genbank using computer-based comparisons (279). Nevertheless, the same study concluded that μ 2 is the most conserved reovirus protein, as different lab strains and field isolates were compared and the amino acid sequence approach 99% identity. This implies that μ 2 plays crucial role in reovirus replication.

6.3.2 Effects of the $\mu 2$ C-terminal domain on NTP hydrolysis

In the absence of crystal structures for mammalian orthoreovirus (MRV) $\mu 2$, we turned to a recently published structural model of VP5 (the Aquareovirus ortholog of $\mu 2$) to deduce how the A612V alteration could affect NTPase activities (267). Previous studies identified two putative NTP-binding motifs (KxxxK and SDxxG) that are widely conserved in different genera and subspecies of *Reoviridae*, despite that the length of $\mu 2$ sequences vary remarkably (187,279). Among all species of *Reoviridae*, Aquareovirus VP5 is the closest relative of MRV $\mu 2$ and VP5 is only 8 residues shorter than MRV $\mu 2$. The NTP-binding motifs are found between residues 400-450 in both VP5 and $\mu 2$ (187). Based on the linear amino acid sequence of $\mu 2$ (279), and the structural model recently published by Wang et al (267), residue 612 is not close to the NTP-binding motifs (Figure 6- 9). Moreover, residue 612 is not mapped to any known functional domain. It is possible that the altered residue (or its nearby region) affect nucleotides binding in several ways: First, the amino acid replacement may affect nucleotide binding kinetics of $\mu 2$. For example, it has been found that purified T1L $\mu 2$ would hydrolyze ATP most effectively around pH 6.5-7.0, at 35°C (we used similar experimental conditions to perform the *in vitro* rNTP hydrolysis assay in Figure 5- 3) (132), but these may not be the optimal conditions for the altered T3v10^{M1} $\mu 2$. Nevertheless, the T3v10^{M1} $\mu 2$ is most effective in hydrolyzing ATP and GTP (Figure 5- 3), and this agrees with previous findings (132). Second, our data may suggest that T3v10^{M1} $\mu 2$ has different affinity for NTP binding from T3wt. For example, high concentration of NTPs may be needed for the mutant $\mu 2$ to achieve the same degree of substrate binding. This explanation seems to be supported by our data that NTP hydrolysis of T3v10^{M1} $\mu 2$ was greatly impacted at 100-minute and later time points as the pool

of available NTP depleted beyond a threshold level for its NTPase (Figure 5- 3). An alternative explanation is that the altered $\mu 2$ is more susceptible to product inhibition (264), the released phosphate or NDP may bind $\mu 2$ and inhibits its enzymatic activities. Lastly, the mutant $\mu 2$ may be less stable and lose its enzymatic activities at later time points. In conclusion, our findings shed lights on the relationship between the $\mu 2$ residue 612 and NTPase activities.

6.3.3 Effects of the $\mu 2$ C-terminal domain on RNA transcription

Previous studies performed *in vitro* transcription assay (the same approach we employed for Figure 3C) using viral core and demonstrated that $\mu 2$ plays a key role in RNA synthesis and genome transcription (74,234,282). We sought to gain insights of how the A612V amino acid replacement impairs transcriptional activities from the Aquareovirus VP5 structural model. Up to now, no architectural model of the Mammalian Orthoreovirus $\lambda 3$ - $\mu 2$ transcriptional complex has been published. However, the near-atomic resolution structure of Aquareovirus VP2 (MRV $\lambda 3$ ortholog) and its cofactor VP5 (ortholog of MRV $\mu 2$) complex has been discovered by Wang and colleagues as discussed above (267). Pairwise alignment of the T3v10^{M1} $\mu 2$ amino acid sequence with the Aquareovirus VP5 (UNIPROT: Q8JU68) revealed that alanine 612 of T3wt $\mu 2$ corresponds to isoleucine or leucine in two close homologs of Aquareovirus VP5. Interestingly, the valine 612 in T3v10^{M1} is a closer match to the VP5 sequences in terms of bulkiness and hydrophobicity (267,279). The VP5 residue 612 and remaining C-terminal residues are believed to interact with dsRNA approaching the transcriptional complex, since this C-terminus domain abuts the entrance where RNA template

enters the channel of VP2(λ 3) (Figure 6- 10) (267). Furthermore, Wang and colleagues argued that VP5 may couple NTP hydrolysis to drive conformational change of the C-terminal domain, which may affect interactions between RNA templates and VP2 in the process of genome transcription (Figure 6- 10) (267). In summary, based on the published structural model of the μ 2 homolog VP5, we speculate that transcriptional activities of T3v10^{M1} μ 2 can be impaired in two ways. First, residue 612 may directly interact with the template entry site of λ 3 and impacts its transcriptional processes. Second, following predictions by Wang and colleagues, the impaired NTP hydrolysis (Figure 5- 3) of T3v10^{M1} μ 2 may consequently affect conformational change of its C-terminal domain, reducing the effectiveness of transcriptional complex.

6.3.4 Effects of the μ 2 C-terminal domain on association with μ NS and tubulin

The A612V mutation also enhanced the association of μ 2 with μ NS and tubulin. Since the enhancement was modest, \sim 2-fold, we confirmed this finding using several diverse approaches such as co-immunoprecipitation and Far-Westerns, as well as during transfection or infection conditions. It is not surprising to see μ 2 complexed with μ NS, since μ 2 was already demonstrated to bridge μ NS and tubulin and proposed to facilitate virus assembly through interactions between μ NS and other structural proteins (45,89,193,195,222). It was also recently proposed that μ 2 multimerizes (90), but we did not detect μ 2- μ 2 associations by Far-Western blot analyses (Figure 5- 21). The most straightforward explanation for enhanced progeny production by T3v10^{M1} relative to T3wt is therefore that the A612V mutation in μ 2

promotes recruitment of μ NS to microtubules, enhancing virus protein accumulation and assembly. Increased core assembly would amplify viral RNA (Figure 5- 8), protein (Figure 5- 9 and Figure 5- 10), and progeny production (Figure 5- 1). A model was created to depict how the μ 2 A612V mutation promoted T3v10^{M1} replication in transformed cells (Figure 6- 11).

It is interesting that the A612V mutation in μ 2 did not just increase the rate of these virus replication steps, but increased the overall RNA/protein maximum levels and virus burst size. In other words, wild type reovirus RNA synthesis normally plateaus at ~12hpi (Figure 5- 8), and progeny production at ~20hpi. This saturation point was exceeded by T3v10^{M1}, suggesting that μ 2 activities are limiting during T3wt infection.

6.3.5 Potential implications of the μ 2 C-terminal domain

We originally isolated T3v10^{M1} in an attempt to discover viruses that replicate better than T3wt in tumor cells and therefore could be tested for cancer therapy. Our mechanistic studies on T3v10^{M1} both support and refute testing this specific virus *in vivo*. On the positive side, T3v10^{M1} presents a strategy to enhance late stages of reovirus replication in many cancer cells (Figure 4- 12, Figure 5- 1 and Figure 5- 8) while actually reducing infectivity in non-transformed cells (Figure 4- 10). Moreover, it may be possible to combine the A612V mutation in μ 2 with previously characterized mutations that enhance entry steps of reovirus replication, to further compound reovirus replication in tumor cells. However, since an oncolytic virus is likely to require high initial infectivity before immune clearance, our discovery that the A612V mutation in μ 2 also drastically reduces establishment of infection (Figure 5- 3 and Figure 5- 4)

suggests T3v10^{M1} is not yet ready for *in vivo* oncolysis testing. Instead, we propose that a better fundamental understanding of $\mu 2$ could yield a strategy to uncouple the early- versus late-functions of this protein and enhance $\mu 2$ - μ NS/tubulin association in absence of reduced NTP hydrolysis and transcription. If this is possible, it will explain why MRV did not evolve such an advantage in nature. Conversely, it is possible that the two functions of $\mu 2$ cannot be uncoupled and that MRV evolved a balance of the two functions at the expense of having enhanced replication in transformed cells.

6.3.6 Limitations of the current study and future directions

Although we showed that transfection of the mutant $\mu 2$ was sufficient to promote progeny production (Figure 5- 17) and we proposed that the enhanced interaction with μ NS was crucial for the observed phenotype, we were not able to show enhanced $\mu 2$ - μ NS using immunofluorescent (IF) staining. We attempted to examine co-localizations of $\mu 2$ - μ NS and $\mu 2$ -microtubules in H1299 cells co-transfected with $\mu 2$ and μ NS. One possible reason was that interaction between the transfected mutant $\mu 2$ and μ NS was enhanced by 1.5-2 fold (Figure 5- 12), and this difference was not very noticeable in IF staining. Secondly, most published works showing $\mu 2$ - μ NS co-localization use CV-1 cells and we used H1299 cells. Future studies may use CV-1 cells or other cell-lines to perform similar experiments.

Our data also showed that T3v10^{M1} was associated with increased cell-death and reduced induction of the p-IRF3. However, it is not clear whether the mutant $\mu 2$ directly participates in mediating both cellular responses. The most straightforward explanation is that

T3v10^{M1} accumulates more viral proteins and progeny in infected cells, which may induce cell-death. We also showed that T3v10^{M1} was impaired in the primary phase of RNA synthesis (Figure 5- 4 and Figure 5- 5, ~6-9 hpi) and reduced production of viral RNAs may induce less p-IRF3 relative to T3wt.

Reduced activation of IRF3 may confer T3v10^{M1} replicative advantages in different stages. The IRF3 is a main factor inducing IFN- β response that inhibits viral growth within a single replication cycle and the sequential spreading of virus to neighboring cells. The IFN response upregulates many downstream targets and I will discuss a few pathways that are known to associate with reovirus infection. The IFN response activates the double-stranded RNA-activated protein kinase (PKR) which inhibits both cellular and viral proteins translation (99). Activation of PKR is a rapid response to repress viral growth and PKR protein expression can be detected as early as 9hpi when cells are exposed to virus (101). IRF3 induction also activates the 2',5'-oligoadenylate synthetase (OAS)/RNase L pathway (16). Activated RNase L inhibits viral replication by cleaving viral RNAs (48). In addition to antiviral effects exerted at the single-cell level, reovirus infection also induces major histocompatibility complex (MHC) proteins (9,42). The MHC proteins present viral peptides on the infected cells. This allows activated T cells to kill the infected cells and prevent virus from spreading (122). In conclusion, reduced induction of IRF3 may allow T3v10^{M1} to replicate more effectively because infected cells have a weakened antiviral response. Future studies may explore whether T3v10^{M1} preferably targets a particular antiviral pathway by assessing the gene and protein expression of PKR, OAS, RNase L and MHC.

Previous studies showed that viral factories can sequester IRF3 to inhibit IFN activation (please see section 1.2.4), and my data show that T3v10^{M1} infection is associated with increased cell-death. Future studies may investigate whether mutant μ 2 alone is directly involved in mediating both cellular processes. Cells can be transfected with mutant or wild-type μ 2, followed by exposing transfected cells to apoptosis inducers or poly:IC to stimulate the IFN response. Pull-down assay can be performed to examine whether mutant μ 2 has increased association with IRF3 and other interferon regulatory factors such as IRF7 and IRF9.

The N-terminal and midpoint of μ 2 have been characterized by previous studies (Figure 1- 6), but the functions of the C-terminus is poorly understood. According to the VP5 model (Figure 6- 10), the A612V mutation resides in the C-loop of μ 2. It would be interesting to test whether truncated μ 2 containing a small region with the A612V is sufficient to enhance μ NS and MT associations.

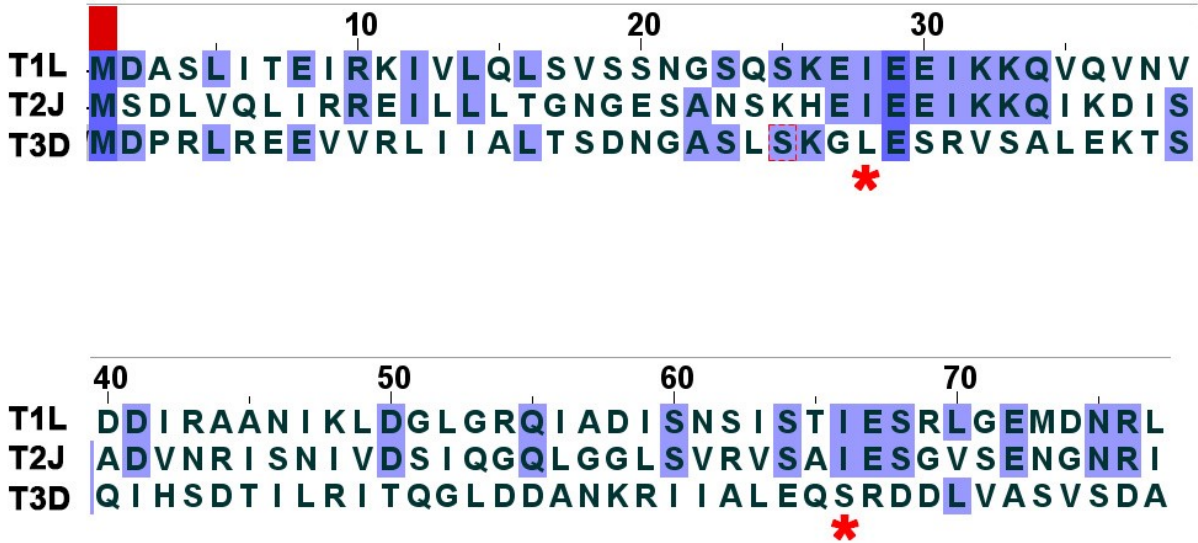


Figure 6- 1. Sigma 1 protein sequence comparisons of residues near the N-terminus between T1L, T2J and T3D.

Sigma 1 residues are compared among serotypes T1L,T2J and T3D in the software Jalview. The altered residues 28 and 66 are indicated with asterisks. Conserved residues between two serotypes are highlighted by light blue and amino acids that are conserved among all 3 serotypes are highlighted in dark blue.

Interfacing residues (not a contact table) Display level:

 Inaccessible residues  HSDC Residues making Hydrogen/Disulphide bond, Salt bridge or Covalent link

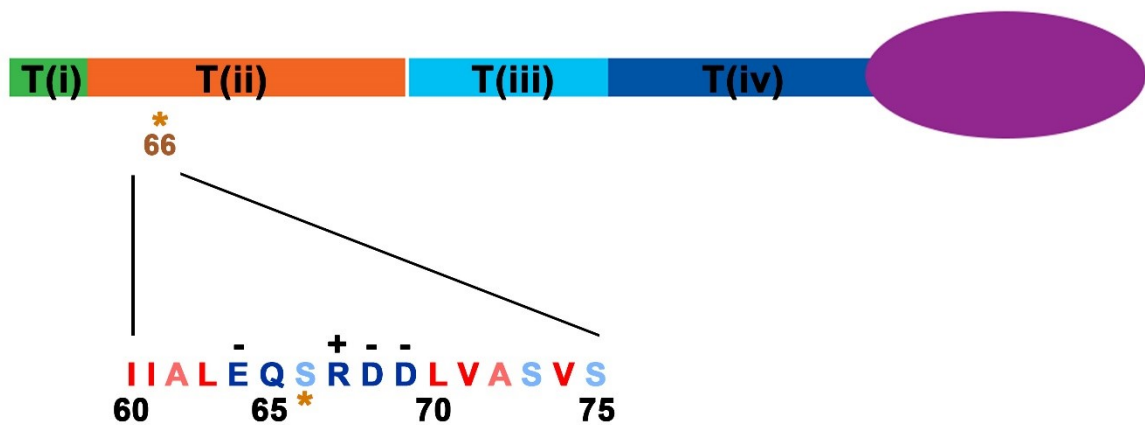
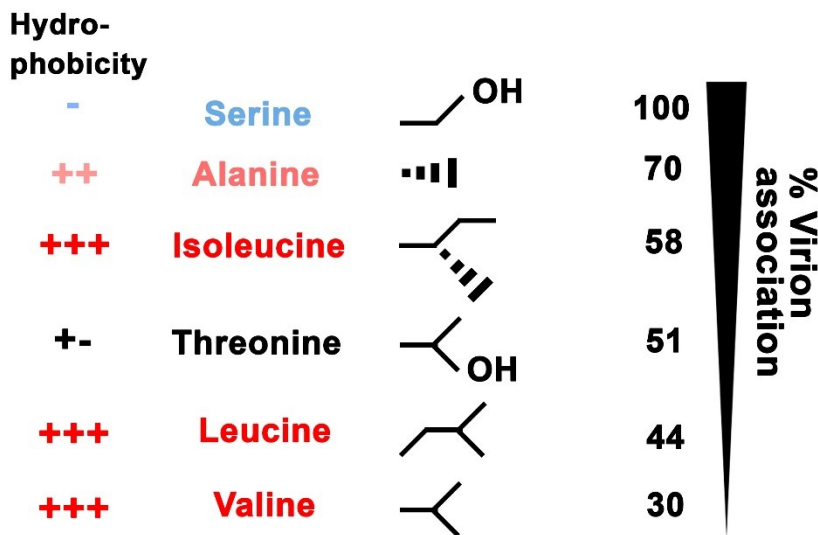
 Solvent-accessible residues  Interfacing residues

ASA Accessible Surface Area, Å² BSA Buried Surface Area, Å² ΔG Solvation energy effect, kcal/mol |||| Buried area percentage, one bar per 10%

	Structure 1	HSDC	ASA	BSA	ΔG
	C: GLY 27		87.41	0.00	0.00
*	C: LEU 28		123.65	23.42	0.37
	C: GLU 29	HS	140.91	40.08	0.16
	C: SER 30		65.20	0.00	0.00
	C: ARG 31		164.38	0.00	0.00
	C: ILE 60		89.95	73.02	1.17
	C: ILE 61		95.52	14.24	0.23
	C: ALA 62		57.90	0.00	0.00
	C: LEU 63		121.20	20.42	0.31
	C: GLU 64	HS	79.31	44.03	-0.29
	C: GLN 65		106.54	0.00	0.00
*	C: SER 66		56.59	0.00	0.00
	C: ARG 67	H	127.96	72.53	-0.16
	C: ASP 68		78.08	0.00	0.00
	C: ASP 69		99.36	0.00	0.00
	C: LEU 70		113.12	21.75	0.35
	C: VAL 71		87.96	18.39	0.29

Figure 6- 2. PDBePISA analysis of σ 1 residues 28 and 66.

The mutated residues 28 and 66 are indicated by asterisks. The column HSDC indicates residues that contain the across-interface hydrogen bond (H) or salt bridge (S). The BSA column indicates the solvent-accessible surface area of the corresponding residue that is buried upon interface formation; the vertical bars on the right from the value give a mnemonic representation of the buried area fraction: one bar corresponds to 10% of the total solvent-accessible surface area buried. The Column ΔG indicates the solvation energy of the corresponding residue, in kcal/M. The solvation energy gain of the interface is calculated as difference in solvation energies of all residues between dissociated and associated (interfacing) structures. A positive or negative value indicates the residue is engaged in protein-protein interaction.

A**B**

$\sigma 1$ with altered residue 66

Figure 6- 3. Residue 66 of $\sigma 1$ has unique physical properties.

(A) Residues near the amino-acid 66 are shown. Hydrophobicity is shown using different colors: very hydrophobic residues are represented by dark red and hydrophobic residues are represented by pink color. The very hydrophilic residues are represented by dark red, while hydrophilic residues are represented in light blue color. **(B)** Serine is the wild-type residue in T3D $\sigma 1$ protein. We generated 5 constructs with the indicated residue to investigate the importance of residue 66 on virion association. Hydrophobicity of each residue is indicated by “+” or “-” sign. Residues with -OH side chain are polar and percentage of virion association for each construct is depicted on the right.

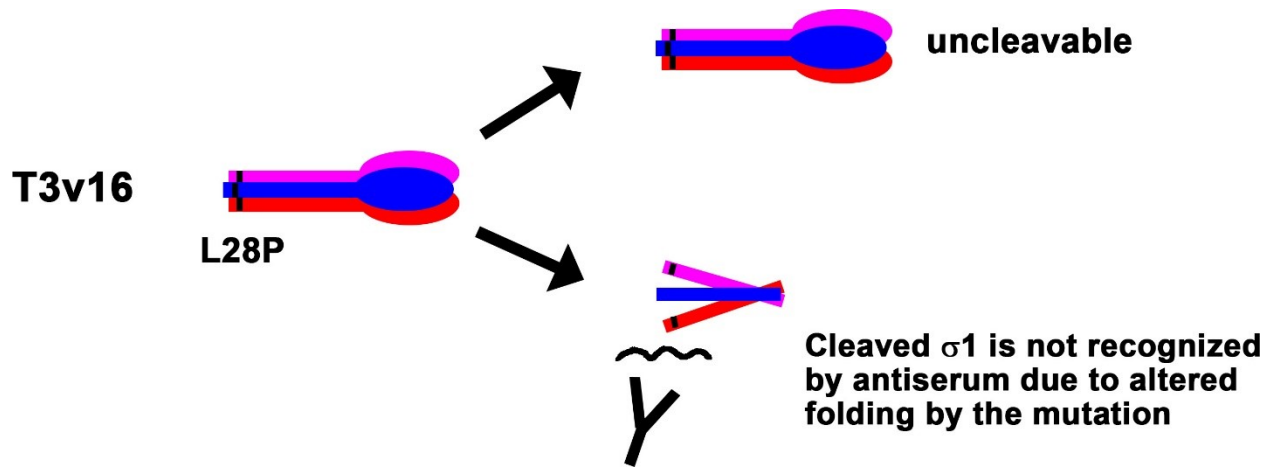


Figure 6- 4. A model showing the effect of altered residue 66 on $\sigma 1$ cleavage.

The $\sigma 1$ L28P mutation in variant T3v16 may render the $\sigma 1$ protein uncleavable by proteases. Alternatively, $\sigma 1$ cleavage may not be affected, but the mutation changes the folding or conformation of cleaved $\sigma 1$ and makes it unrecognizable by antiserum. The same model also applies to transfected $\sigma 1$ with altered residue 66.

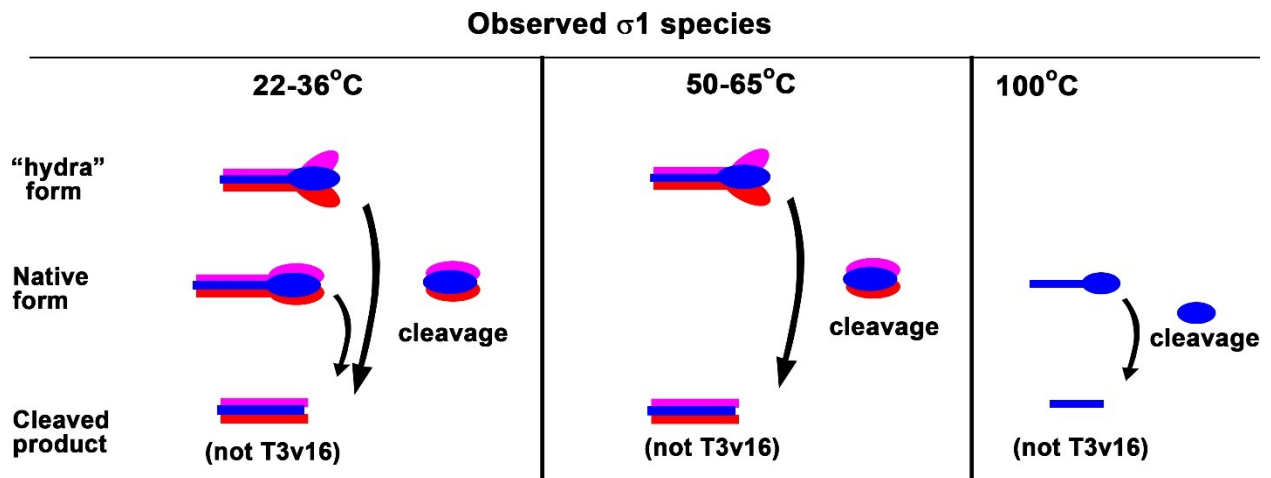
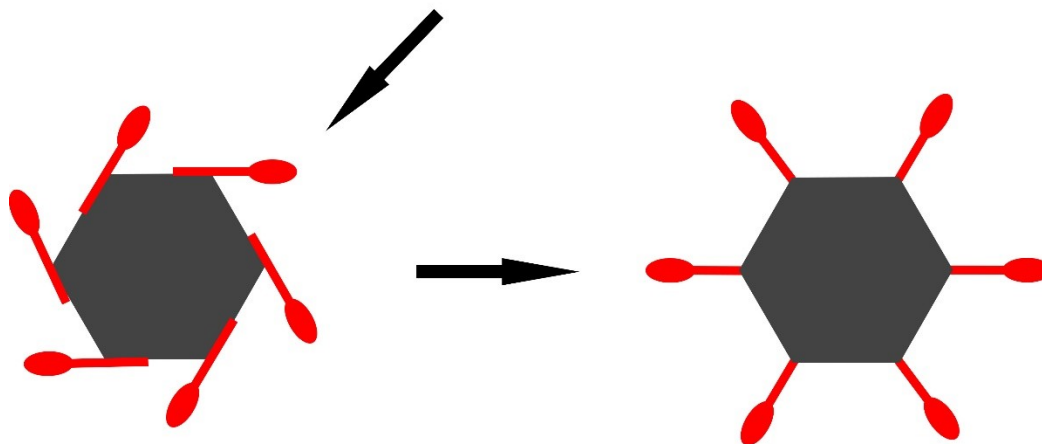
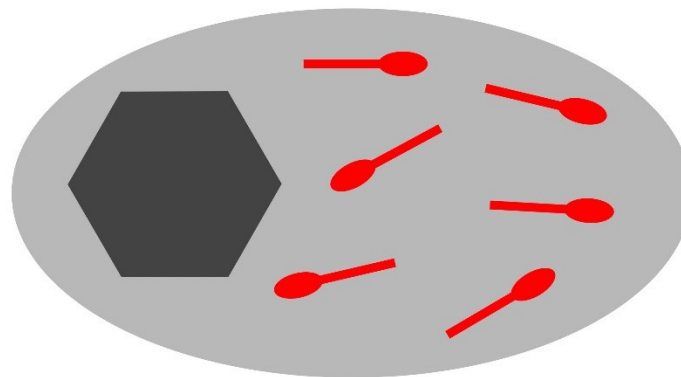


Figure 6- 5. Observed $\sigma 1$ species and conformations from different incubation temperatures.

The above diagram shows all the observed $\sigma 1$ proteins from different incubation temperatures with SDS-containing protein sample buffer.

1. Accumulation of $\sigma 1$ in the viral factory



2. Association of $\sigma 1$ and virion

3. Assembly of $\sigma 1$ onto virion

Figure 6- 6. Model of $\sigma 1$ assembly onto virion.

Our data suggest that assembly of $\sigma 1$ is a multi-step process. Sigma 1 proteins are first recruited and accumulated in the viral factory. Residues 155-235 are important for viral factory accumulation. Before the actual assembly of $\sigma 1$, sigma 1 proteins may need to physically associate with the virion. Residues 252-286 may promote $\sigma 1$ and virion association. Lastly, the $\sigma 1$ proteins are properly assembled onto virion and this step may require the anchoring domain.

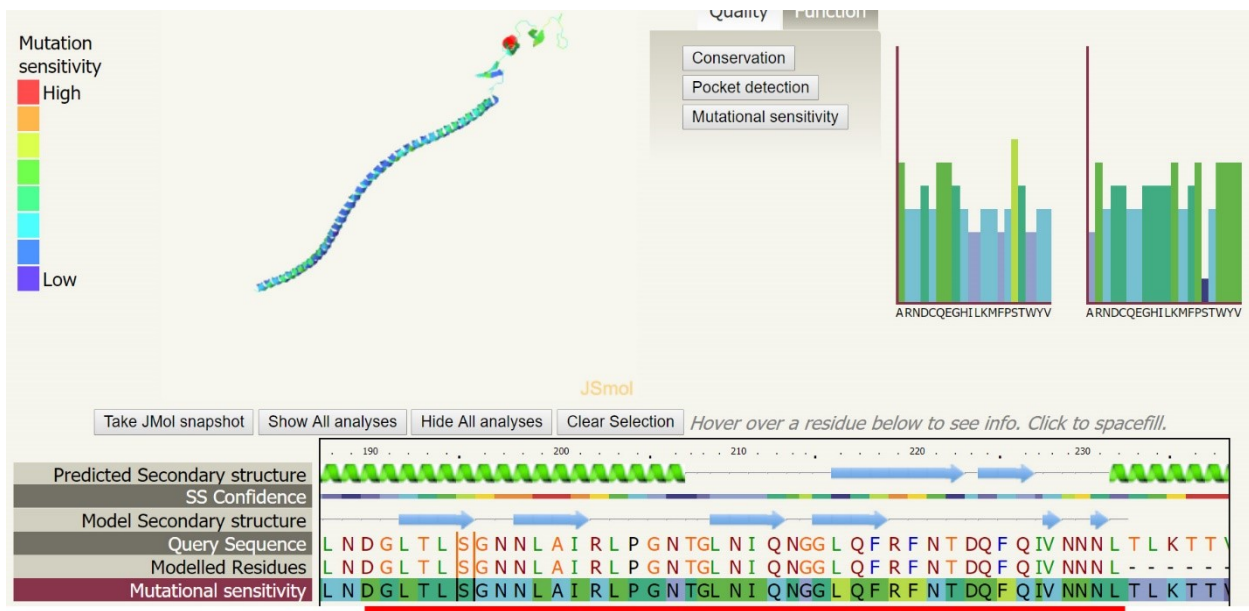


Figure 6- 7. Sigma 1 residues 190-232 are sensitive to mutations, suggesting they are important for $\sigma 1$ functions.

Protein primary structure of the entire $\sigma 1$ is analyzed by Phyre2 (Protein Homology/Analogy Recognition Engine) and the hidden Markov models (HMMs) is used for mutational sensitivity (129,276). Each residue is color-coded and the corresponding color is shown on a mutation sensitivity scale at the top right. Residues 190-232 (underlined with a red line) are very sensitive to mutations relative to other regions of $\sigma 1$, and they are functionally important. Our data show that this region is involved in both viral factory accumulation and virion association.

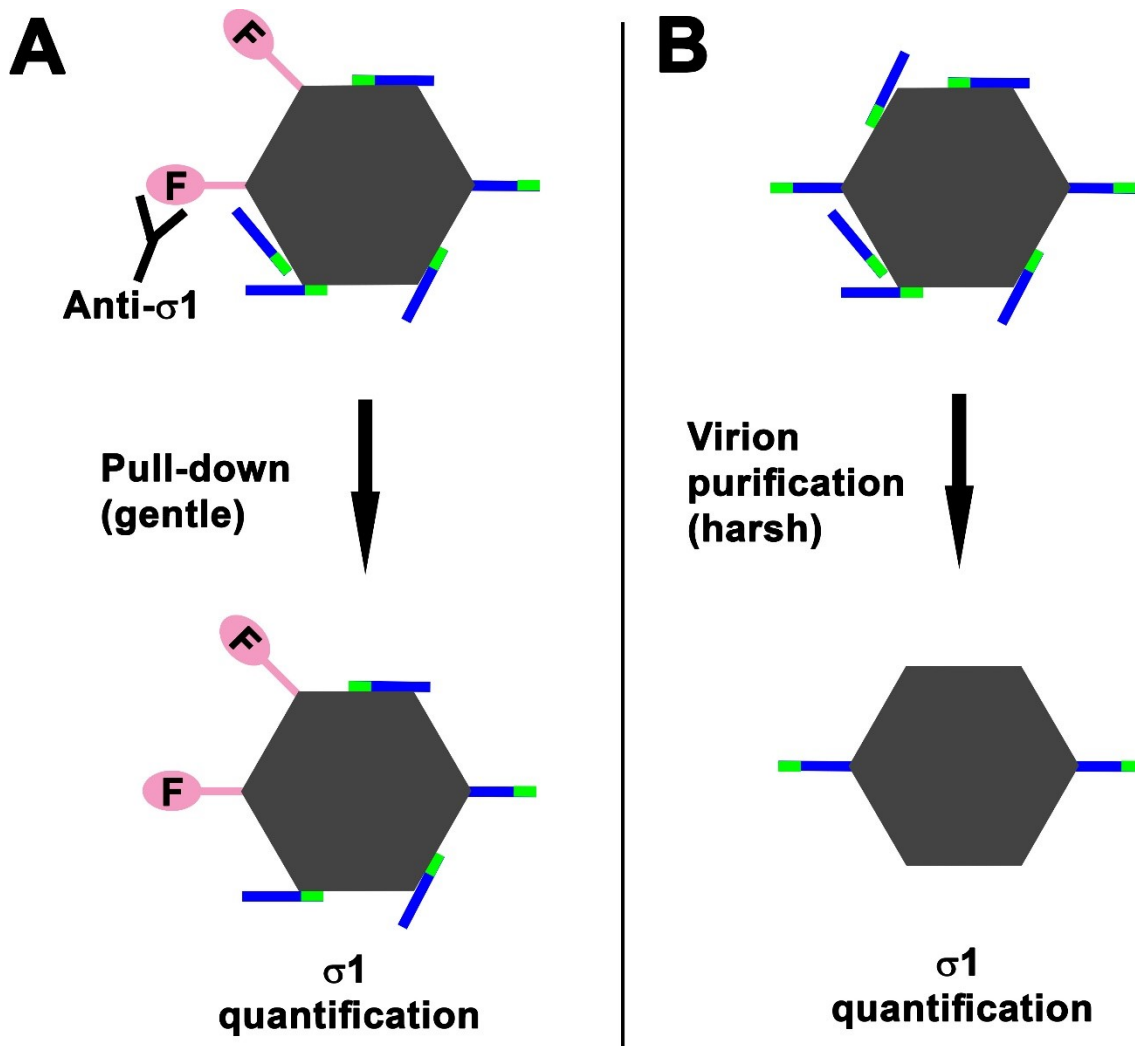


Figure 6- 8. Sigma 1 residues 252-286 promote association with virion but impairs assembly of $\sigma 1$.

Sigma 1 residue 252-286 (represented by the green region) promotes virion association but may impair $\sigma 1$ assembly. **(A)** Transfected $\sigma 1^{1-286}$ proteins associated with virion are pulled down by anti- $\sigma 1$ serum. The pull-down experiments were performed to preserve protein-protein interactions, allowing most $\sigma 1^{1-286}$ proteins to remain on virion during $\sigma 1$ quantification. **(B)** The procedures used to purified virion were rather harsh and caused disassociation of truncated $\sigma 1$.

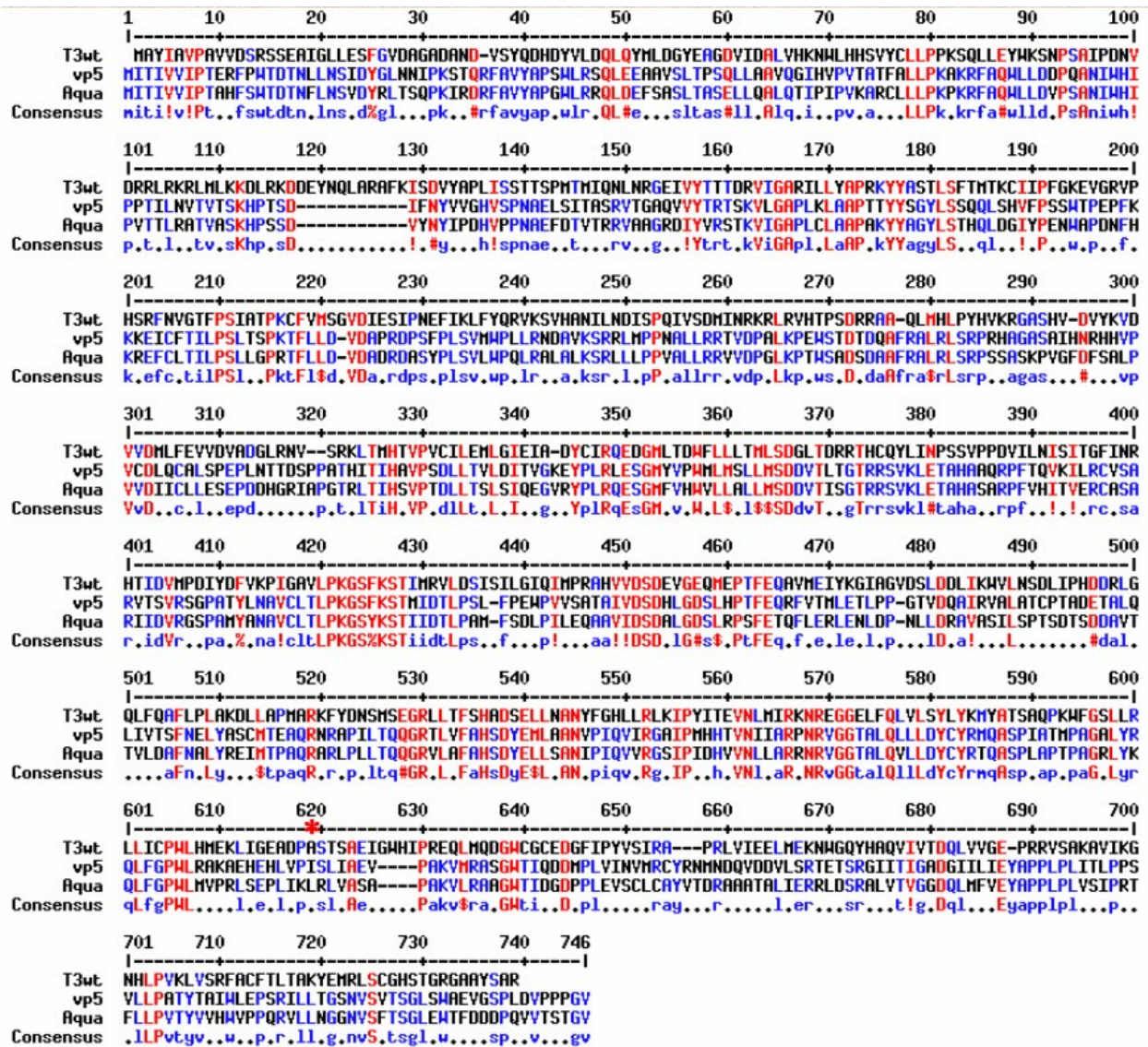


Figure 6- 9. Protein sequence comparison between T3wt m2 and two homologs of VP5.

Sequences of T3wt $\mu 2$ (top sequence), were compared with two subspecies of Aquareovirus homolog VP5. The structure of VP5 has been recently published (Bottom panel) from the middle sequence. The NTPase motifs are well conserved (underlined), but the T3wt residue 612 alanine (the site with an asterisk, and it is replaced by valine in T3v10^{M1}) is located in the C-terminus that is not conserved among the three viruses. Note that, all the sequences have been downshifted when the multiple alignment was performed.

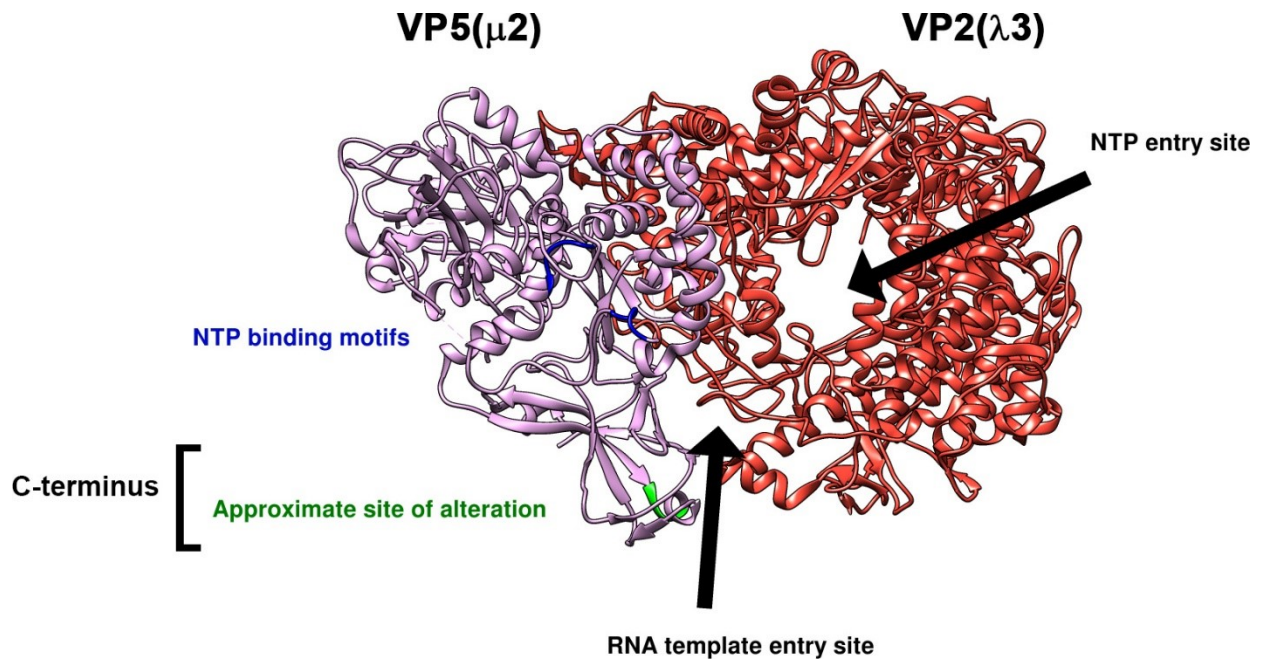


Figure 6- 10. The 3D model showing the transcription complex of Aquareovirus.

A 3D model of the transcription complex composed of the polymerase VP2(λ 3) and its cofactor VP5(μ 2). Due to the high homologous between VP5 and μ 2, a small region of the C-terminus has been highlighted in green to represent the T3wt μ 2 A612V alteration, which is located at the entrance of RNA template entry site, but not in close proximate with the NTP binding motifs. This figure is generated by the software Chimera using the published σ 1 crystal structure (PBD ID: 6GAJ) (267).

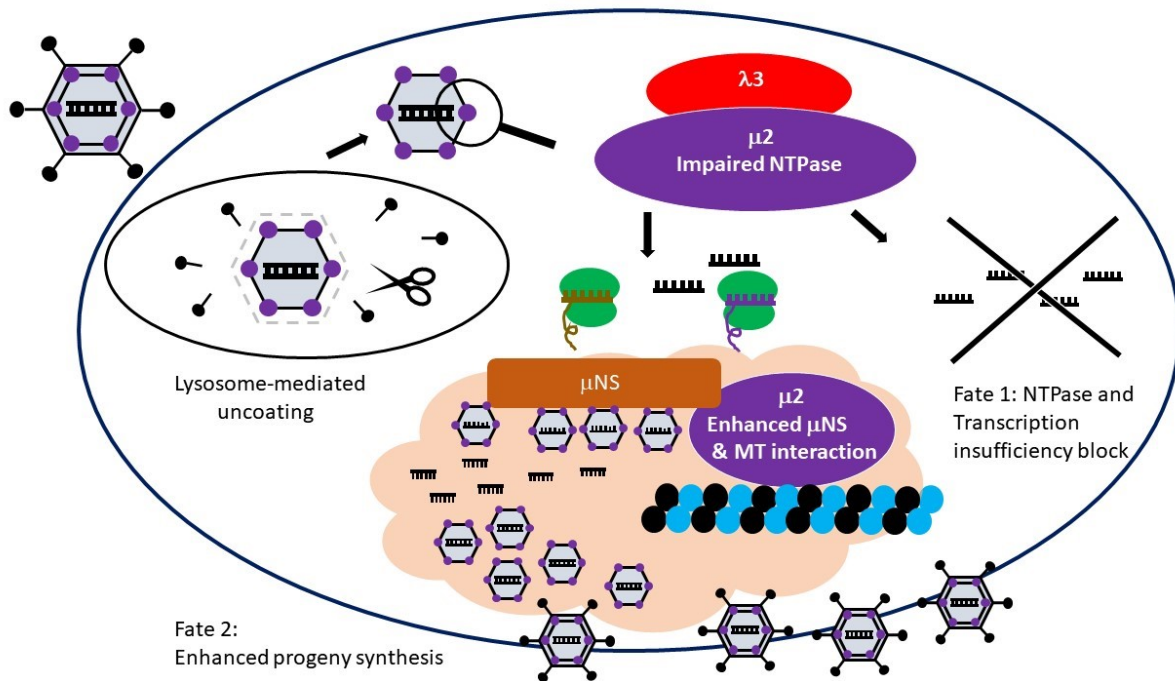


Figure 6- 11. Model: $\mu 2$ A612V promotes reovirus replication in transformed cells.

Reovirus variant T3v10^{M1} has a single amino acid alteration A612V in the previously uncharacterized C-terminus region of $\mu 2$. The alteration does not change the levels of cell-attachment protein $\sigma 1$, and therefore, it binds and uncoats in a similar manner compared to T3wt. As a polymerase cofactor and a major part of the transcriptional complex ($\lambda 3$ - $\mu 2$), the single residue replacement impairs NTPase activities and RNA synthesis via mechanism that is not understood, and this causes ~80% of virions fail to initiate productive infection (producing detectable viral proteins) when cells are exposed to equal cell-bound virion of T3wt or the variant (Fate 1). However, for the virus that is capable of overcoming the transcriptional limitations, T3v10^{M1} $\mu 2$ has 1.5-2 fold increased associations with μNS and microtubule and that directly promotes progeny synthesis by ~ 3-fold in one replication cycle (Fate 2).

REFERENCES

Reference List

1. A.M.Q.King M.J .Adams E.B.Carstens E.J.Lefkowitz. 2012. Virus taxonomy: ninth report of the International Committee on Taxonomy of Viruses. Elsevier (Academic Press).
2. Acs, G., H. Klett, M. Schonberg, J. Christman, D. H. Levin, and S. C. Silverstein. 1971. Mechanism of reovirus double-stranded ribonucleic acid synthesis in vivo and in vitro. *J.Virol.* 8:684-689.
3. Agosto, M. A., T. Ivanovic, and M. L. Nibert. 2006. Mammalian reovirus, a nonfusogenic nonenveloped virus, forms size-selective pores in a model membrane. *Proc.Natl.Acad.Sci.U.S.A* 103:16496-16501. doi:0605835103 [pii];10.1073/pnas.0605835103 [doi].
4. Alain, T., T. S. Kim, X. Lun, A. Liacini, L. A. Schiff, D. L. Senger, and P. A. Forsyth. 2007. Proteolytic disassembly is a critical determinant for reovirus oncolysis. *Mol.Ther.* 15:1512-1521. doi:S1525-0016(16)32446-7 [pii];10.1038/sj.mt.6300207 [doi].
5. Altinoz, M. A., S. Guloksuz, and I. Elmaci. 2017. Rabies virus vaccine as an immune adjuvant against cancers and glioblastoma: new studies may resurrect a neglected potential. *Clin.Transl.Oncol.* 19:785-792. doi:10.1007/s12094-017-1613-6 [doi];10.1007/s12094-017-1613-6 [pii].
6. Amgen Thousand Oaks. BIOLOGICAL LICENSE APPLICATION FOR TALIMOGENE LAHERPAREPVEC. 1-95. 2015.
Ref Type: Report
7. Anderson, J. M. and C. M. Van Itallie. 2009. Physiology and function of the tight junction. *Cold Spring Harb.Perspect.Biol.* 1:a002584. doi:10.1101/cshperspect.a002584 [doi].
8. Angata, T. and A. Varki. 2002. Chemical diversity in the sialic acids and related alpha-keto acids: an evolutionary perspective. *Chem.Rev.* 102:439-469. doi:cr000407m [pii].
9. Atta, M. S., W. L. Irving, R. J. Powell, and I. Todd. 1995. Enhanced expression of MHC class I molecules on cultured human thyroid follicular cells infected with reovirus through induction of type 1 interferons. *Clin.Exp.Immunol.* 101:121-126. doi:10.1111/j.1365-2249.1995.tb02287.x [doi].
10. Attoui, H., P. Biagini, J. Stirling, P. P. Mertens, J. F. Cantaloube, A. Meyer, M. P. de, and L. de, X. 2001. Sequence characterization of Ndelle virus genome segments 1, 5, 7, 8, and 10: evidence for reassignment to the genus Orthoreovirus, family Reoviridae. *Biochem.Biophys.Res.Commun.* 287:583-588. doi:10.1006/bbrc.2001.5612 [doi];S0006-291X(01)95612-8 [pii].
11. Babiss, L. E., R. B. Luftig, J. A. Weatherbee, R. R. Weihing, U. R. Ray, and B. N. Fields. 1979. Reovirus serotypes 1 and 3 differ in their in vitro association with microtubules. *J.Virol.* 30:863-874.

12. Baer, G. S. and T. S. Dermody. 1997. Mutations in reovirus outer-capsid protein sigma3 selected during persistent infections of L cells confer resistance to protease inhibitor E64. *J.Virol.* 71:4921-4928.
13. Bai, Y., P. Hui, X. Du, and X. Su. 2019. Updates to the antitumor mechanism of oncolytic virus. *Thorac.Cancer* 10:1031-1035. doi:10.1111/1759-7714.13043 [doi].
14. Baker, M. L., T. Schountz, and L. F. Wang. 2013. Antiviral immune responses of bats: a review. *Zoonoses.Public Health* 60:104-116. doi:10.1111/j.1863-2378.2012.01528.x [doi].
15. Banerjee, A. C. and W. K. Joklik. 1990. Reovirus protein sigma 1 translated in vitro, as well as truncated derivatives of it that lack up to two-thirds of its C-terminal portion, exists as two major tetrameric molecular species that differ in electrophoretic mobility. *Virology* 179:460-462.
16. Banerjee, S., E. Gusho, C. Gaughan, B. Dong, X. Gu, E. Holvey-Bates, M. Talukdar, Y. Li, S. R. Weiss, F. Sicheri, Y. Sauntharajah, G. R. Stark, and R. H. Silverman. 2019. OAS-RNase L innate immune pathway mediates the cytotoxicity of a DNA-demethylating drug. *Proc.Natl.Acad.Sci.U.S.A* 116:5071-5076. doi:1815071116 [pii];10.1073/pnas.1815071116 [doi].
17. Barton, E. S., J. D. Chappell, J. L. Connolly, J. C. Forrest, and T. S. Dermody. 2001. Reovirus receptors and apoptosis. *Virology* 290:173-180. doi:S0042-6822(01)91160-2 [pii];10.1006/viro.2001.1160 [doi].
18. Barton, E. S., J. L. Connolly, J. C. Forrest, J. D. Chappell, and T. S. Dermody. 2001. Utilization of sialic acid as a coreceptor enhances reovirus attachment by multistep adhesion strengthening. *J.Biol.Chem.* 276:2200-2211. doi:10.1074/jbc.M004680200 [doi];M004680200 [pii].
19. Barton, E. S., J. C. Forrest, J. L. Connolly, J. D. Chappell, Y. Liu, F. J. Schnell, A. Nusrat, C. A. Parkos, and T. S. Dermody. 2001. Junction adhesion molecule is a receptor for reovirus. *Cell* 104:441-451. doi:S0092-8674(01)00231-8 [pii].
20. Bass, D. M., D. Bodkin, R. Dambrauskas, J. S. Trier, B. N. Fields, and J. L. Wolf. 1990. Intraluminal proteolytic activation plays an important role in replication of type 1 reovirus in the intestines of neonatal mice. *J.Virol.* 64:1830-1833.
21. Bassel-Duby, R., M. L. Nibert, C. J. Homcy, B. N. Fields, and D. G. Sawutz. 1987. Evidence that the sigma 1 protein of reovirus serotype 3 is a multimer. *J.Virol.* 61:1834-1841.
22. Bazzoni, G. 2003. The JAM family of junctional adhesion molecules. *Curr.Opin.Cell Biol.* 15:525-530. doi:S0955067403001042 [pii].
23. Berger, A. K. and P. Danthi. 2013. Reovirus activates a caspase-independent cell death pathway. *MBio.* 4:e00178-13. doi:mBio.00178-13 [pii];10.1128/mBio.00178-13 [doi].
24. Bisailon, M., J. Bergeron, and G. Lemay. 1997. Characterization of the nucleoside triphosphate phosphohydrolase and helicase activities of the reovirus lambda1 protein. *J.Biol.Chem.* 272:18298-18303. doi:10.1074/jbc.272.29.18298 [doi].
25. Bisailon, M. and G. Lemay. 1997. Characterization of the reovirus lambda1 protein RNA 5'-triphosphatase activity. *J.Biol.Chem.* 272:29954-29957. doi:10.1074/jbc.272.47.29954 [doi].

26. Blackford, A. N. and R. J. Grand. 2009. Adenovirus E1B 55-kilodalton protein: multiple roles in viral infection and cell transformation. *J.Virol.* 83:4000-4012. doi:JVI.02417-08 [pii];10.1128/JVI.02417-08 [doi].
27. Blank, U., P. Launay, M. Benhamou, and R. C. Monteiro. 2009. Inhibitory ITAMs as novel regulators of immunity. *Immunol.Rev.* 232:59-71. doi:IMR832 [pii];10.1111/j.1600-065X.2009.00832.x [doi].
28. Bodkin, D. K., M. L. Nibert, and B. N. Fields. 1989. Proteolytic digestion of reovirus in the intestinal lumens of neonatal mice. *J.Virol.* 63:4676-4681.
29. Boehme, K. W., K. Hammer, W. C. Tollefson, J. L. Konopka-Anstadt, T. Kobayashi, and T. S. Dermody. 2013. Nonstructural protein sigma1s mediates reovirus-induced cell cycle arrest and apoptosis. *J.Virol.* 87:12967-12979. doi:JVI.02080-13 [pii];10.1128/JVI.02080-13 [doi].
30. Bokiej, M., K. M. Ogden, M. Ikizler, D. M. Reiter, T. Stehle, and T. S. Dermody. 2012. Optimum length and flexibility of reovirus attachment protein sigma1 are required for efficient viral infection. *J.Virol.* 86:10270-10280. doi:JVI.01338-12 [pii];10.1128/JVI.01338-12 [doi].
31. Borsa, J., T. P. Copps, M. D. Sargent, D. G. Long, and J. D. Chapman. 1973. New intermediate subviral particles in the in vitro uncoating of reovirus virions by chymotrypsin. *J.Virol.* 11:552-564.
32. Borsa, J., M. D. Sargent, P. A. Lievaart, and T. P. Copps. 1981. Reovirus: evidence for a second step in the intracellular uncoating and transcriptase activation process. *Virology* 111:191-200. doi:10.1016/0042-6822(81)90664-4 [doi].
33. Bos, J. L. 1989. ras oncogenes in human cancer: a review. *Cancer Res.* 49:4682-4689.
34. Bouvet, M., F. Ferron, I. Imbert, L. Gluais, B. Selisko, B. Coutard, B. Canard, and E. Decroly. 2012. [Capping strategies in RNA viruses]. *Med.Sci.(Paris)* 28:423-429. doi:10.1051/medsci/2012284021 [doi];medsci2012284p423 [pii].
35. Breun, L. A., T. J. Broering, A. M. McCutcheon, S. J. Harrison, C. L. Luongo, and M. L. Nibert. 2001. Mammalian reovirus L2 gene and lambda2 core spike protein sequences and whole-genome comparisons of reoviruses type 1 Lang, type 2 Jones, and type 3 Dearing. *Virology* 287:333-348. doi:10.1006/viro.2001.1052 [doi];S0042-6822(01)91052-9 [pii].
36. Broering, T. J., M. M. Arnold, C. L. Miller, J. A. Hurt, P. L. Joyce, and M. L. Nibert. 2005. Carboxyl-proximal regions of reovirus nonstructural protein muNS necessary and sufficient for forming factory-like inclusions. *J.Virol.* 79:6194-6206. doi:79/10/6194 [pii];10.1128/JVI.79.10.6194-6206.2005 [doi].
37. Broering, T. J., J. Kim, C. L. Miller, C. D. Piggott, J. B. Dinoso, M. L. Nibert, and J. S. Parker. 2004. Reovirus nonstructural protein mu NS recruits viral core surface proteins and entering core particles to factory-like inclusions. *J.Virol.* 78:1882-1892.
38. Broering, T. J., A. M. McCutcheon, V. E. Centonze, and M. L. Nibert. 2000. Reovirus nonstructural protein muNS binds to core particles but does not inhibit their transcription and capping activities. *J.Virol.* 74:5516-5524. doi:10.1128/jvi.74.12.5516-5524.2000 [doi].
39. Broering, T. J., J. S. Parker, P. L. Joyce, J. Kim, and M. L. Nibert. 2002. Mammalian reovirus nonstructural protein microNS forms large inclusions and colocalizes with

- reovirus microtubule-associated protein micro2 in transfected cells. *J.Virol.* 76:8285-8297. doi:10.1128/jvi.76.16.8285-8297.2002 [doi].
40. Bujnicki, J. M. and L. Rychlewski. 2001. Reassignment of specificities of two cap methyltransferase domains in the reovirus lambda 2 protein. *Genome Biol.* 2:RESEARCH0038. doi:10.1186/gb-2001-2-9-research0038 [doi].
 41. Calisher, C. H., J. E. Childs, H. E. Field, K. V. Holmes, and T. Schountz. 2006. Bats: important reservoir hosts of emerging viruses. *Clin.Microbiol.Rev.* 19:531-545. doi:19/3/531 [pii];10.1128/CMR.00017-06 [doi].
 42. Campbell, I. L., L. C. Harrison, R. G. Ashcroft, and I. Jack. 1988. Reovirus infection enhances expression of class I MHC proteins on human beta-cell and rat RINm5F cell. *Diabetes* 37:362-365. doi:10.2337/diab.37.3.362 [doi].
 43. Campbell, J. A., P. Schelling, J. D. Wetzel, E. M. Johnson, J. C. Forrest, G. A. Wilson, M. Aurrand-Lions, B. A. Imhof, T. Stehle, and T. S. Dermody. 2005. Junctional adhesion molecule a serves as a receptor for prototype and field-isolate strains of mammalian reovirus. *J.Virol.* 79:7967-7978. doi:79/13/7967 [pii];10.1128/JVI.79.13.7967-7978.2005 [doi].
 44. Canadian Cancer Society . Canadian Cancer Statistics publication. 2019. Ref Type: Online Source
 45. Carvalho, J., M. M. Arnold, and M. L. Nibert. 2007. Silencing and complementation of reovirus core protein mu2: functional correlations with mu2-microtubule association and differences between virus- and plasmid-derived mu2. *Virology* 364:301-316. doi:S0042-6822(07)00181-X [pii];10.1016/j.virol.2007.03.037 [doi].
 46. Cashdollar, L. W., R. A. Chmelo, J. R. Wiener, and W. K. Joklik. 1985. Sequences of the S1 genes of the three serotypes of reovirus. *Proc.Natl.Acad.Sci.U.S.A* 82:24-28. doi:10.1073/pnas.82.1.24 [doi].
 47. Cauchon, N. S., S. Oghamian, S. Hassanpour, and M. Abernathy. 2019. Innovation in Chemistry, Manufacturing, and Controls-A Regulatory Perspective From Industry. *J.Pharm.Sci.* 108:2207-2237. doi:S0022-3549(19)30092-9 [pii];10.1016/j.xphs.2019.02.007 [doi].
 48. Chakrabarti, A., B. K. Jha, and R. H. Silverman. 2011. New insights into the role of RNase L in innate immunity. *J.Interferon Cytokine Res.* 31:49-57. doi:10.1089/jir.2010.0120 [doi].
 49. Chandran, K., D. L. Farsetta, and M. L. Nibert. 2002. Strategy for nonenveloped virus entry: a hydrophobic conformer of the reovirus membrane penetration protein micro 1 mediates membrane disruption. *J.Virol.* 76:9920-9933. doi:10.1128/jvi.76.19.9920-9933.2002 [doi].
 50. Chandran, K., J. S. Parker, M. Ehrlich, T. Kirchhausen, and M. L. Nibert. 2003. The delta region of outer-capsid protein micro 1 undergoes conformational change and release from reovirus particles during cell entry. *J.Virol.* 77:13361-13375. doi:10.1128/jvi.77.24.13361-13375.2003 [doi].
 51. Chappell, J. D., E. S. Barton, T. H. Smith, G. S. Baer, D. T. Duong, M. L. Nibert, and T. S. Dermody. 1998. Cleavage susceptibility of reovirus attachment protein sigma1 during proteolytic disassembly of virions is determined by a sequence polymorphism in the sigma1 neck. *J.Virol.* 72:8205-8213.

52. Chappell, J. D., V. L. Gunn, J. D. Wetzel, G. S. Baer, and T. S. Dermody. 1997. Mutations in type 3 reovirus that determine binding to sialic acid are contained in the fibrous tail domain of viral attachment protein sigma1. *J.Virol.* 71:1834-1841.
53. Chappell, J. D., A. E. Prota, T. S. Dermody, and T. Stehle. 2002. Crystal structure of reovirus attachment protein sigma1 reveals evolutionary relationship to adenovirus fiber. *EMBO J.* 21:1-11. doi:10.1093/emboj/21.1.1 [doi].
54. Charles M.Deber Tracy A.Stone. Relative role(s) of leucine versus isoleucine in the folding of membrane proteins. e24075 111(1). 2019.
Ref Type: Journal (Full)
55. Charlie Comins ; Guy R.Simpson ; Kate Relph ; Kevin J.Harrington ; Alan Melcher ; Hardev Pandha. *Gene Therapy of Cancer (3rd edition)* . 185-198. 2014.
Ref Type: Online Source
56. Chavakis, T., T. Keiper, R. Matz-Westphal, K. Hersemeyer, U. J. Sachs, P. P. Nawroth, K. T. Preissner, and S. Santoso. 2004. The junctional adhesion molecule-C promotes neutrophil transendothelial migration in vitro and in vivo. *J.Biol.Chem.* 279:55602-55608. doi:M404676200 [pii];10.1074/jbc.M404676200 [doi].
57. Chiang, H. S. and H. M. Liu. 2018. The Molecular Basis of Viral Inhibition of IRF- and STAT-Dependent Immune Responses. *Front Immunol.* 9:3086. doi:10.3389/fimmu.2018.03086 [doi].
58. Chua, K. B., G. Cramer, A. Hyatt, M. Yu, M. R. Tompang, J. Rosli, J. McEachern, S. Cramer, V. Kumarasamy, B. T. Eaton, and L. F. Wang. 2007. A previously unknown reovirus of bat origin is associated with an acute respiratory disease in humans. *Proc.Natl.Acad.Sci.U.S.A* 104:11424-11429. doi:0701372104 [pii];10.1073/pnas.0701372104 [doi].
59. Ciecchonska, M. and R. Duncan. 2014. Reovirus FAST proteins: virus-encoded cellular fusogens. *Trends Microbiol.* 22:715-724. doi:S0966-842X(14)00161-9 [pii];10.1016/j.tim.2014.08.005 [doi].
60. Clarke, P., S. M. Meintzer, S. Gibson, C. Widmann, T. P. Garrington, G. L. Johnson, and K. L. Tyler. 2000. Reovirus-induced apoptosis is mediated by TRAIL. *J.Virol.* 74:8135-8139. doi:10.1128/jvi.74.17.8135-8139.2000 [doi].
61. Clarke, P., S. M. Meintzer, A. C. Spalding, G. L. Johnson, and K. L. Tyler. 2001. Caspase 8-dependent sensitization of cancer cells to TRAIL-induced apoptosis following reovirus-infection. *Oncogene* 20:6910-6919. doi:10.1038/sj.onc.1204842 [doi].
62. Clarke, P., S. M. Meintzer, C. Widmann, G. L. Johnson, and K. L. Tyler. 2001. Reovirus infection activates JNK and the JNK-dependent transcription factor c-Jun. *J.Virol.* 75:11275-11283. doi:10.1128/JVI.75.23.11275-11283.2001 [doi].
63. Cleveland, D. R., H. Zarbl, and S. Millward. 1986. Reovirus guanylyltransferase is L2 gene product lambda 2. *J.Virol.* 60:307-311.
64. Comins, C., L. Heinemann, K. Harrington, A. Melcher, B. J. De, and H. Pandha. 2008. Reovirus: viral therapy for cancer 'as nature intended'. *Clin.Oncol.(R.Coll.Radiol.)* 20:548-554. doi:S0936-6555(08)00252-5 [pii];10.1016/j.clon.2008.04.018 [doi].

65. Connolly, J. L., E. S. Barton, and T. S. Dermody. 2001. Reovirus binding to cell surface sialic acid potentiates virus-induced apoptosis. *J.Virol.* 75:4029-4039. doi:10.1128/JVI.75.9.4029-4039.2001 [doi].
66. Connolly, J. L., S. E. Rodgers, P. Clarke, D. W. Ballard, L. D. Kerr, K. L. Tyler, and T. S. Dermody. 2000. Reovirus-induced apoptosis requires activation of transcription factor NF-kappaB. *J.Virol.* 74:2981-2989.
67. Conry, R. M., B. Westbrook, S. McKee, and T. G. Norwood. 2018. Talimogene laherparepvec: First in class oncolytic virotherapy. *Hum.Vaccin.Immunother.* 14:839-846. doi:10.1080/21645515.2017.1412896 [doi].
68. Coombs, K. M. 1998. Stoichiometry of reovirus structural proteins in virus, ISVP, and core particles. *Virology* 243:218-228. doi:S0042-6822(98)99061-4 [pii];10.1006/viro.1998.9061 [doi].
69. Crowley, L. C., B. J. Marfell, A. P. Scott, and N. J. Waterhouse. 2016. Quantitation of Apoptosis and Necrosis by Annexin V Binding, Propidium Iodide Uptake, and Flow Cytometry. *Cold Spring Harb.Protoc.* 2016. doi:2016/11/pdb.prot087288 [pii];10.1101/pdb.prot087288 [doi].
70. Dales, S. 1963. ASSOCIATION BETWEEN THE SPINDLE APPARATUS AND REOVIRUS. *Proc.Natl.Acad.Sci.U.S.A* 50:268-275. doi:10.1073/pnas.50.2.268 [doi].
71. David M.Underhill. 2006. The many faces of ITAMs. *TRENDS in Immunology* 28:66-73.
72. Day, J. M. 2009. The diversity of the orthoreoviruses: molecular taxonomy and phylogentic divides. *Infect.Genet.Evol.* 9:390-400. doi:S1567-1348(09)00012-4 [pii];10.1016/j.meegid.2009.01.011 [doi].
73. Dell'Angelica, E. C., C. Mullins, S. Caplan, and J. S. Bonifacino. 2000. Lysosome-related organelles. *FASEB J.* 14:1265-1278. doi:10.1096/fj.14.10.1265 [doi].
74. Demidenko, A. A. and M. L. Nibert. 2009. Probing the transcription mechanisms of reovirus cores with molecules that alter RNA duplex stability. *J.Virol.* 83:5659-5670. doi:JVI.02192-08 [pii];10.1128/JVI.02192-08 [doi].
75. Derek C. 2014. Reovirus in cancer therapy: an evidence-based review. *Oncolytic Virotherapy* 3:69-82.
76. Dermody, T. S., M. L. Nibert, R. Bassel-Duby, and B. N. Fields. 1990. A sigma 1 region important for hemagglutination by serotype 3 reovirus strains. *J.Virol.* 64:5173-5176.
77. Desai, S. M., P. B. Sehgal, A. N. Nanavati, and M. V. Shirodkar. 1973. A rabies-induced serum factor inhibiting Rous sarcoma virus in chicks. *J.Gen.Virol.* 19:285-293. doi:10.1099/0022-1317-19-3-285 [doi].
78. Dietrich, M. H., K. M. Ogden, J. M. Long, R. Ebenhoch, A. Thor, T. S. Dermody, and T. Stehle. 2018. Structural and Functional Features of the Reovirus sigma1 Tail. *J.Virol.* 92. doi:JVI.00336-18 [pii];10.1128/JVI.00336-18 [doi].
79. Domingo, E. and J. J. Holland. 1997. RNA virus mutations and fitness for survival. *Annu.Rev.Microbiol.* 51:151-178. doi:10.1146/annurev.micro.51.1.151 [doi].
80. Douville, R. N., R. C. Su, K. M. Coombs, F. E. Simons, and K. T. Hayglass. 2008. Reovirus serotypes elicit distinctive patterns of recall immunity in humans. *J.Virol.* 82:7515-7523. doi:JVI.00464-08 [pii];10.1128/JVI.00464-08 [doi].

81. Drake, J. W. and J. J. Holland. 1999. Mutation rates among RNA viruses. *Proc.Natl.Acad.Sci.U.S.A* 96:13910-13913. doi:10.1073/pnas.96.24.13910 [doi].
82. Dryden, K. A., G. Wang, M. Yeager, M. L. Nibert, K. M. Coombs, D. B. Furlong, B. N. Fields, and T. S. Baker. 1993. Early steps in reovirus infection are associated with dramatic changes in supramolecular structure and protein conformation: analysis of virions and subviral particles by cryoelectron microscopy and image reconstruction. *J.Cell Biol.* 122:1023-1041. doi:10.1083/jcb.122.5.1023 [doi].
83. Duncan, R. 1999. Extensive sequence divergence and phylogenetic relationships between the fusogenic and nonfusogenic orthoreoviruses: a species proposal. *Virology* 260:316-328. doi:10.1006/viro.1999.9832 [doi];S0042-6822(99)99832-X [pii].
84. Duncan, R. and P. W. Lee. 1994. Localization of two protease-sensitive regions separating distinct domains in the reovirus cell-attachment protein sigma 1. *Virology* 203:149-152. doi:S0042-6822(84)71465-6 [pii];10.1006/viro.1994.1465 [doi].
85. Ebert, D. H., J. Deussing, C. Peters, and T. S. Dermody. 2002. Cathepsin L and cathepsin B mediate reovirus disassembly in murine fibroblast cells. *J.Biol.Chem.* 277:24609-24617. doi:10.1074/jbc.M201107200 [doi];M201107200 [pii].
86. Ebert, D. H., J. D. Wetzel, D. E. Brumbaugh, S. R. Chance, L. E. Stobie, G. S. Baer, and T. S. Dermody. 2001. Adaptation of reovirus to growth in the presence of protease inhibitor E64 segregates with a mutation in the carboxy terminus of viral outer-capsid protein sigma3. *J.Virol.* 75:3197-3206. doi:10.1128/JVI.75.7.3197-3206.2001 [doi].
87. Ebnet, K., A. Suzuki, S. Ohno, and D. Vestweber. 2004. Junctional adhesion molecules (JAMs): more molecules with dual functions? *J.Cell Sci.* 117:19-29. doi:10.1242/jcs.00930 [doi];117/1/19 [pii].
88. EDMAN, P. 1949. A method for the determination of amino acid sequence in peptides. *Arch.Biochem.* 22:475.
89. Eichwald, C., M. Ackermann, and M. L. Nibert. 2018. The dynamics of both filamentous and globular mammalian reovirus viral factories rely on the microtubule network. *Virology* 518:77-86. doi:S0042-6822(18)30046-1 [pii];10.1016/j.virol.2018.02.009 [doi].
90. Eichwald, C., J. Kim, and M. L. Nibert. 2017. Dissection of mammalian orthoreovirus micro2 reveals a self-associative domain required for binding to microtubules but not to factory matrix protein microNS. *PLoS.One.* 12:e0184356. doi:10.1371/journal.pone.0184356 [doi];PONE-D-17-07102 [pii].
91. El Mekki, A. A., P. Nieuwenhuysen, G. van der Groen, and S. R. Pattyn. 1981. Characterization of some ungrouped viruses. *Trans.R.Soc.Trop.Med.Hyg.* 75:799-806. doi:10.1016/0035-9203(81)90416-8 [doi].
92. El-Rayes, B. F. and P. M. LoRusso. 2004. Targeting the epidermal growth factor receptor. *Br.J.Cancer* 91:418-424. doi:10.1038/sj.bjc.6601921 [doi];6601921 [pii].
93. Fang, Q., E. K. Seng, Q. Q. Ding, and L. L. Zhang. 2008. Characterization of infectious particles of grass carp reovirus by treatment with proteases. *Arch.Virol.* 153:675-682. doi:10.1007/s00705-008-0048-3 [doi].
94. Fraser, R. D., D. B. Furlong, B. L. Trus, M. L. Nibert, B. N. Fields, and A. C. Steven. 1990. Molecular structure of the cell-attachment protein of reovirus: correlation of

- computer-processed electron micrographs with sequence-based predictions. *J.Virol.* 64:2990-3000.
95. Fujita, T. 2006. *Virology*. Sensing viral RNA amid your own. *Science* 314:935-936. doi:314/5801/935 [pii];10.1126/science.1135756 [doi].
 96. Fukuhara, H., Y. Ino, and T. Todo. 2016. Oncolytic virus therapy: A new era of cancer treatment at dawn. *Cancer Sci.* 107:1373-1379. doi:10.1111/cas.13027 [doi].
 97. Furlong, D. B., M. L. Nibert, and B. N. Fields. 1988. Sigma 1 protein of mammalian reoviruses extends from the surfaces of viral particles. *J.Virol.* 62:246-256.
 98. Gaillard, R. K., Jr. and W. K. Joklik. 1982. Quantitation of the relatedness of reovirus serotypes 1, 2, and 3 at the gene level. *Virology* 123:152-164. doi:10.1016/0042-6822(82)90302-6 [doi].
 99. Garcia, M. A., J. Gil, I. Ventoso, S. Guerra, E. Domingo, C. Rivas, and M. Esteban. 2006. Impact of protein kinase PKR in cell biology: from antiviral to antiproliferative action. *Microbiol.Mol.Biol.Rev.* 70:1032-1060. doi:70/4/1032 [pii];10.1128/MMBR.00027-06 [doi].
 100. Giesen, A., D. Gniel, and C. Malerczyk. 2015. 30 Years of rabies vaccination with Rabipur: a summary of clinical data and global experience. *Expert.Rev.Vaccines.* 14:351-367. doi:10.1586/14760584.2015.1011134 [doi].
 101. Gil, J. and M. Esteban. 2004. Vaccinia virus recombinants as a model system to analyze interferon-induced pathways. *J.Interferon Cytokine Res.* 24:637-646. doi:10.1089/jir.2004.24.637 [doi].
 102. Gilmore, R., M. C. Coffey, G. Leone, K. McLure, and P. W. Lee. 1996. Co-translational trimerization of the reovirus cell attachment protein. *EMBO J.* 15:2651-2658.
 103. Goldberg, D. M., R. Campbell, and A. D. Roy. 1969. Fate of trypsin and chymotrypsin in the human small intestine. *Gut* 10:477-483. doi:10.1136/gut.10.6.477 [doi].
 104. Goldberg, D. M., R. Campbell, and A. D. Roy. 1969. Studies on the binding of trypsin and chymotrypsin by human intestinal mucosa. *Scand.J.Gastroenterol.* 4:217-226.
 105. Golden, J. W., J. A. Bahe, W. T. Lucas, M. L. Nibert, and L. A. Schiff. 2004. Cathepsin S supports acid-independent infection by some reoviruses. *J.Biol.Chem.* 279:8547-8557. doi:10.1074/jbc.M309758200 [doi];M309758200 [pii].
 106. Gollamudi, R., M. H. Ghalib, K. K. Desai, I. Chaudhary, B. Wong, M. Einstein, M. Coffey, G. M. Gill, K. Mettinger, J. M. Mariadason, S. Mani, and S. Goel. 2010. Intravenous administration of Reolysin, a live replication competent RNA virus is safe in patients with advanced solid tumors. *Invest New Drugs* 28:641-649. doi:10.1007/s10637-009-9279-8 [doi].
 107. Gong, J. and M. M. Mita. 2014. Activated ras signaling pathways and reovirus oncolysis: an update on the mechanism of preferential reovirus replication in cancer cells. *Front Oncol.* 4:167. doi:10.3389/fonc.2014.00167 [doi].
 108. Gong, J., E. Sachdev, A. C. Mita, and M. M. Mita. 2016. Clinical development of reovirus for cancer therapy: An oncolytic virus with immune-mediated antitumor activity. *World J.Methodol.* 6:25-42. doi:10.5662/wjm.v6.i1.25 [doi].
 109. Guglielmi, K. M., E. Kirchner, G. H. Holm, T. Stehle, and T. S. Dermody. 2007. Reovirus binding determinants in junctional adhesion molecule-A. *J.Biol.Chem.* 282:17930-17940. doi:M702180200 [pii];10.1074/jbc.M702180200 [doi].

110. Health Canada. 2018-19 Departmental Plan: Health Canada. 2019.
Ref Type: Online Source
111. Hirschman, S. Z. and G. S. Hammer. 1974. Coxsackie virus myopericarditis. A microbiological and clinical review. *Am.J.Cardiol.* 34:224-232. doi:0002-9149(74)90201-X [pii];10.1016/0002-9149(74)90201-x [doi].
112. Hoenig, L. J., A. C. Jackson, and G. M. Dickinson. 2018. The early use of Pasteur's rabies vaccine in the United States. *Vaccine* 36:4578-4581. doi:S0264-410X(18)30623-6 [pii];10.1016/j.vaccine.2018.05.016 [doi].
113. Holm, G. H., J. Zurney, V. Tumilasci, S. Leveille, P. Danthi, J. Hiscott, B. Sherry, and T. S. Dermody. 2007. Retinoic acid-inducible gene-I and interferon-beta promoter stimulator-1 augment proapoptotic responses following mammalian reovirus infection via interferon regulatory factor-3. *J.Biol.Chem.* 282:21953-21961. doi:M702112200 [pii];10.1074/jbc.M702112200 [doi].
114. Honda, K., A. Takaoka, and T. Taniguchi. 2006. Type I interferon [corrected] gene induction by the interferon regulatory factor family of transcription factors. *Immunity.* 25:349-360. doi:S1074-7613(06)00394-3 [pii];10.1016/j.immuni.2006.08.009 [doi].
115. Hu, J. C., R. S. Coffin, C. J. Davis, N. J. Graham, N. Groves, P. J. Guest, K. J. Harrington, N. D. James, C. A. Love, I. McNeish, L. C. Medley, A. Michael, C. M. Nutting, H. S. Pandha, C. A. Shorrocks, J. Simpson, J. Steiner, N. M. Steven, D. Wright, and R. C. Coombes. 2006. A phase I study of OncoVEXGM-CSF, a second-generation oncolytic herpes simplex virus expressing granulocyte macrophage colony-stimulating factor. *Clin.Cancer Res.* 12:6737-6747. doi:12/22/6737 [pii];10.1158/1078-0432.CCR-06-0759 [doi].
116. Huang, C., W. J. Liu, W. Xu, T. Jin, Y. Zhao, J. Song, Y. Shi, W. Ji, H. Jia, Y. Zhou, H. Wen, H. Zhao, H. Liu, H. Li, Q. Wang, Y. Wu, L. Wang, D. Liu, G. Liu, H. Yu, E. C. Holmes, L. Lu, and G. F. Gao. 2016. A Bat-Derived Putative Cross-Family Recombinant Coronavirus with a Reovirus Gene. *PLoS.Pathog.* 12:e1005883. doi:10.1371/journal.ppat.1005883 [doi];PPATHOGENS-D-16-00961 [pii].
117. Hughes, P. J., C. North, P. D. Minor, and G. Stanway. 1989. The complete nucleotide sequence of coxsackievirus A21. *J.Gen.Virol.* 70 (Pt 11):2943-2952. doi:10.1099/0022-1317-70-11-2943 [doi].
118. Irvin, S. C., J. Zurney, L. S. Ooms, J. D. Chappell, T. S. Dermody, and B. Sherry. 2012. A single-amino-acid polymorphism in reovirus protein mu2 determines repression of interferon signaling and modulates myocarditis. *J.Virol.* 86:2302-2311. doi:JVI.06236-11 [pii];10.1128/JVI.06236-11 [doi].
119. Ivanovic, T., S. Boulant, M. Ehrlich, A. A. Demidenko, M. M. Arnold, T. Kirchhausen, and M. L. Nibert. 2011. Recruitment of cellular clathrin to viral factories and disruption of clathrin-dependent trafficking. *Traffic.* 12:1179-1195. doi:10.1111/j.1600-0854.2011.01233.x [doi].
120. James, K. T., B. Cooney, K. Agopsowicz, M. A. Trevors, A. Mohamed, D. Stoltz, M. Hitt, and M. Shmulevitz. 2016. Novel High-throughput Approach for Purification of Infectious Virions. *Sci.Rep.* 6:36826. doi:srep36826 [pii];10.1038/srep36826 [doi].

121. Jan, E., I. Mohr, and D. Walsh. 2016. A Cap-to-Tail Guide to mRNA Translation Strategies in Virus-Infected Cells. *Annu.Rev.Virol.* 3:283-307. doi:10.1146/annurev-virology-100114-055014 [doi].
122. Jeffery, K. J. and C. R. Bangham. 2000. Do infectious diseases drive MHC diversity? *Microbes.Infect.* 2:1335-1341. doi:S1286-4579(00)01287-9 [pii].
123. Jenkins, G. M., A. Rambaut, O. G. Pybus, and E. C. Holmes. 2002. Rates of molecular evolution in RNA viruses: a quantitative phylogenetic analysis. *J.Mol.Evol.* 54:156-165. doi:10.1007/s00239-001-0064-3 [doi].
124. John T.Patton. 2008. *Segmented Double-stranded RNA Viruses: Structure and Molecular Biology.* Caister Academic Press, Bethesda, MD 20892-8026, USA.
125. Joklik, W. K. 1972. Studies on the effect of chymotrypsin on reovirions. *Virology* 49:700-715. doi:10.1016/0042-6822(72)90527-2 [doi].
126. Kaltschmidt, B., C. Kaltschmidt, T. G. Hofmann, S. P. Hehner, W. Droge, and M. L. Schmitz. 2000. The pro- or anti-apoptotic function of NF-kappaB is determined by the nature of the apoptotic stimulus. *Eur.J.Biochem.* 267:3828-3835. doi:ejb1421 [pii];10.1046/j.1432-1327.2000.01421.x [doi].
127. Karin, M. and A. Lin. 2002. NF-kappaB at the crossroads of life and death. *Nat.Immunol.* 3:221-227. doi:10.1038/ni0302-221 [doi];ni0302-221 [pii].
128. Kawai, T. and S. Akira. 2006. Innate immune recognition of viral infection. *Nat.Immunol.* 7:131-137. doi:ni1303 [pii];10.1038/ni1303 [doi].
129. Kelley, L. A., S. Mezulis, C. M. Yates, M. N. Wass, and M. J. Sternberg. 2015. The Phyre2 web portal for protein modeling, prediction and analysis. *Nat.Protoc.* 10:845-858. doi:nprot.2015.053 [pii];10.1038/nprot.2015.053 [doi].
130. Kelly, K., S. Nawrocki, A. Mita, M. Coffey, F. J. Giles, and M. Mita. 2009. Reovirus-based therapy for cancer. *Expert.Opin.Biol.Ther.* 9:817-830. doi:10.1517/14712590903002039 [doi].
131. Kelly, K. R., C. M. Espitia, W. Zhao, E. Wendlandt, G. Tricot, F. Zhan, J. S. Carew, and S. T. Nawrocki. 2015. Junctional adhesion molecule-A is overexpressed in advanced multiple myeloma and determines response to oncolytic reovirus. *Oncotarget.* 6:41275-41289. doi:5753 [pii];10.18632/oncotarget.5753 [doi].
132. Kim, J., J. S. Parker, K. E. Murray, and M. L. Nibert. 2004. Nucleoside and RNA triphosphatase activities of orthoreovirus transcriptase cofactor mu2. *J.Biol.Chem.* 279:4394-4403. doi:10.1074/jbc.M308637200 [doi];M308637200 [pii].
133. Kim, J., X. Zhang, V. E. Centonze, V. D. Bowman, S. Noble, T. S. Baker, and M. L. Nibert. 2002. The hydrophilic amino-terminal arm of reovirus core shell protein lambda1 is dispensable for particle assembly. *J.Virol.* 76:12211-12222. doi:10.1128/jvi.76.23.12211-12222.2002 [doi].
134. Kirchner, E., K. M. Guglielmi, H. M. Strauss, T. S. Dermody, and T. Stehle. 2008. Structure of reovirus sigma1 in complex with its receptor junctional adhesion molecule-A. *PLoS.Pathog.* 4:e1000235. doi:10.1371/journal.ppat.1000235 [doi].
135. Kobayashi, T., L. S. Ooms, J. D. Chappell, and T. S. Dermody. 2009. Identification of functional domains in reovirus replication proteins muNS and mu2. *J.Virol.* 83:2892-2906. doi:JVI.01495-08 [pii];10.1128/JVI.01495-08 [doi].

136. Kohl, C., R. Lesnik, A. Brinkmann, A. Ebinger, A. Radonic, A. Nitsche, K. Muhldorfer, G. Wibbelt, and A. Kurth. 2012. Isolation and characterization of three mammalian orthoreoviruses from European bats. *PLoS.One.* 7:e43106. doi:10.1371/journal.pone.0043106 [doi];PONE-D-12-13747 [pii].
137. Koonin, E. V. 1993. Computer-assisted identification of a putative methyltransferase domain in NS5 protein of flaviviruses and lambda 2 protein of reovirus. *J.Gen.Virol.* 74 (Pt 4):733-740. doi:10.1099/0022-1317-74-4-733 [doi].
138. Kothandaraman, S., M. C. Hebert, R. T. Raines, and M. L. Nibert. 1998. No role for pepstatin-A-sensitive acidic proteinases in reovirus infections of L or MDCK cells. *Virology* 251:264-272. doi:S0042-6822(98)99434-X [pii];10.1006/viro.1998.9434 [doi].
139. KUNZ T.H.AND FENTON A.B. 2003. *Bat Ecology.* University of Chicago Press, Chicago, USA.
140. Larson, S. M., J. B. Antczak, and W. K. Joklik. 1994. Reovirus exists in the form of 13 particle species that differ in their content of protein sigma 1. *Virology* 201:303-311. doi:S0042-6822(84)71295-5 [pii];10.1006/viro.1994.1295 [doi].
141. Lawler, S. E., M. C. Speranza, C. F. Cho, and E. A. Chiocca. 2017. Oncolytic Viruses in Cancer Treatment: A Review. *JAMA Oncol.* 3:841-849. doi:2536204 [pii];10.1001/jamaoncol.2016.2064 [doi].
142. Lee, P. W., E. C. Hayes, and W. K. Joklik. 1981. Protein sigma 1 is the reovirus cell attachment protein. *Virology* 108:156-163. doi:10.1016/0042-6822(81)90535-3 [doi].
143. Lelli, D., A. Moreno, A. Lavazza, M. Bresaola, E. Canelli, M. B. Boniotti, and P. Cordioli. 2013. Identification of Mammalian orthoreovirus type 3 in Italian bats. *Zoonoses.Public Health* 60:84-92. doi:10.1111/zph.12001 [doi].
144. Leone, G., R. Duncan, and P. W. Lee. 1991. Trimerization of the reovirus cell attachment protein (sigma 1) induces conformational changes in sigma 1 necessary for its cell-binding function. *Virology* 184:758-761.
145. Leone, G., R. Duncan, D. C. Mah, A. Price, L. W. Cashdollar, and P. W. Lee. 1991. The N-terminal heptad repeat region of reovirus cell attachment protein sigma 1 is responsible for sigma 1 oligomer stability and possesses intrinsic oligomerization function. *Virology* 182:336-345. doi:0042-6822(91)90677-4 [pii].
146. Leone, G., D. C. Mah, and P. W. Lee. 1991. The incorporation of reovirus cell attachment protein sigma 1 into virions requires the N-terminal hydrophobic tail and the adjacent heptad repeat region. *Virology* 182:346-350. doi:0042-6822(91)90678-5 [pii].
147. Li, X. and Q. Fang. 2013. High-resolution 3D structures reveal the biological functions of reoviruses. *Virol.Sin.* 28:318-325. doi:10.1007/s12250-013-3341-6 [doi].
148. Li, Z., D. Liu, X. Ran, C. Liu, D. Guo, X. Hu, J. Tian, X. Zhang, Y. Shao, S. Liu, and L. Qu. 2016. Characterization and pathogenicity of a novel mammalian orthoreovirus from wild short-nosed fruit bats. *Infect.Genet.Evol.* 43:347-353. doi:S1567-1348(16)30221-0 [pii];10.1016/j.meegid.2016.05.039 [doi].
149. Liang, M. 2018. Oncorine, the World First Oncolytic Virus Medicine and its Update in China. *Curr.Cancer Drug Targets.* 18:171-176. doi:CCDT-EPUB-87188 [pii];10.2174/1568009618666171129221503 [doi].

150. Liemann, S., K. Chandran, T. S. Baker, M. L. Nibert, and S. C. Harrison. 2002. Structure of the reovirus membrane-penetration protein, Mu1, in a complex with its protector protein, Sigma3. *Cell* 108:283-295. doi:S0092867402006128 [pii].
151. Liu, H., D. W. Chang, and X. Yang. 2005. Interdimer processing and linearity of procaspase-3 activation. A unifying mechanism for the activation of initiator and effector caspases. *J.Biol.Chem.* 280:11578-11582. doi:M414385200 [pii];10.1074/jbc.M414385200 [doi].
152. Liu, Y., A. Nusrat, F. J. Schnell, T. A. Reaves, S. Walsh, M. Pochet, and C. A. Parkos. 2000. Human junction adhesion molecule regulates tight junction resealing in epithelia. *J.Cell Sci.* 113 (Pt 13):2363-2374.
153. Lossi, L., C. Castagna, and A. Merighi. 2018. Caspase-3 Mediated Cell Death in the Normal Development of the Mammalian Cerebellum. *Int.J.Mol.Sci.* 19. doi:ijms19123999 [pii];10.3390/ijms19123999 [doi].
154. Luongo, C. L., K. A. Dryden, D. L. Farsetta, R. L. Margraf, T. F. Severson, N. H. Olson, B. N. Fields, T. S. Baker, and M. L. Nibert. 1997. Localization of a C-terminal region of lambda2 protein in reovirus cores. *J.Virol.* 71:8035-8040.
155. Luongo, C. L., K. M. Reinisch, S. C. Harrison, and M. L. Nibert. 2000. Identification of the guanylyltransferase region and active site in reovirus mRNA capping protein lambda2. *J.Biol.Chem.* 275:2804-2810. doi:10.1074/jbc.275.4.2804 [doi].
156. Luzio, J. P., B. M. Mullock, P. R. Pryor, M. R. Lindsay, D. E. James, and R. C. Piper. 2001. Relationship between endosomes and lysosomes. *Biochem.Soc.Trans.* 29:476-480. doi:10.1042/bst0290476 [doi].
157. Luzio, J. P., B. A. Rous, N. A. Bright, P. R. Pryor, B. M. Mullock, and R. C. Piper. 2000. Lysosome-endosome fusion and lysosome biogenesis. *J.Cell Sci.* 113 (Pt 9):1515-1524.
158. Mabrouk, T., C. Danis, and G. Lemay. 1995. Two basic motifs of reovirus sigma 3 protein are involved in double-stranded RNA binding. *Biochem.Cell Biol.* 73:137-145.
159. Mabrouk, T. and G. Lemay. 1994. Mutations in a CCHC zinc-binding motif of the reovirus sigma 3 protein decrease its intracellular stability. *J.Virol.* 68:5287-5290.
160. Mabrouk, T. and G. Lemay. 1994. The sequence similarity of reovirus sigma 3 protein to picornaviral proteases is unrelated to its role in mu 1 viral protein cleavage. *Virology* 202:615-620. doi:S0042-6822(84)71382-1 [pii];10.1006/viro.1994.1382 [doi].
161. MacArthur, M. W. and J. M. Thornton. 1991. Influence of proline residues on protein conformation. *J.Mol.Biol.* 218:397-412. doi:0022-2836(91)90721-H [pii].
162. Madren, J. A., P. Sarkar, and P. Danthi. 2012. Cell entry-associated conformational changes in reovirus particles are controlled by host protease activity. *J.Virol.* 86:3466-3473. doi:JVI.06659-11 [pii];10.1128/JVI.06659-11 [doi].
163. Maginnis, M. S., J. C. Forrest, S. A. Kopecky-Bromberg, S. K. Dickeson, S. A. Santoro, M. M. Zutter, G. R. Nemerow, J. M. Bergelson, and T. S. Dermody. 2006. Beta1 integrin mediates internalization of mammalian reovirus. *J.Virol.* 80:2760-2770. doi:80/6/2760 [pii];10.1128/JVI.80.6.2760-2770.2006 [doi].
164. Maginnis, M. S., B. A. Mainou, A. Derdowski, E. M. Johnson, R. Zent, and T. S. Dermody. 2008. NPXY motifs in the beta1 integrin cytoplasmic tail are required for functional reovirus entry. *J.Virol.* 82:3181-3191. doi:JVI.01612-07 [pii];10.1128/JVI.01612-07 [doi].

165. Mah, D. C., G. Leone, J. M. Jankowski, and P. W. Lee. 1990. The N-terminal quarter of reovirus cell attachment protein sigma 1 possesses intrinsic virion-anchoring function. *Virology* 179:95-103.
166. Mainou, B. A. and T. S. Dermody. 2012. In search of cathepsins: how reovirus enters host cells. *DNA Cell Biol.* 31:1646-1649. doi:10.1089/dna.2012.1868 [doi].
167. Mainou, B. A. and T. S. Dermody. 2012. Transport to late endosomes is required for efficient reovirus infection. *J.Virol.* 86:8346-8358. doi:JVI.00100-12 [pii];10.1128/JVI.00100-12 [doi].
168. Mainou, B. A., P. F. Zamora, A. W. Ashbrook, D. C. Dorset, K. S. Kim, and T. S. Dermody. 2013. Reovirus cell entry requires functional microtubules. *MBio.* 4. doi:mBio.00405-13 [pii];10.1128/mBio.00405-13 [doi].
169. Maratos-Flier, E., M. J. Goodman, A. H. Murray, and C. R. Kahn. 1986. Ammonium inhibits processing and cytotoxicity of reovirus, a nonenveloped virus. *J.Clin.Invest* 78:1003-1007. doi:10.1172/JCI112653 [doi].
170. Marcato, P., M. Shmulevitz, D. Pan, D. Stoltz, and P. W. Lee. 2007. Ras transformation mediates reovirus oncolysis by enhancing virus uncoating, particle infectivity, and apoptosis-dependent release. *Mol.Ther.* 15:1522-1530. doi:6300179 [pii];10.1038/sj.mt.6300179 [doi].
171. Matsuda, T., H. Karube, and A. Aruga. 2018. A Comparative Safety Profile Assessment of Oncolytic Virus Therapy Based on Clinical Trials. *Ther.Innov.Regul.Sci.* 52:430-437. doi:10.1177/2168479017738979 [doi].
172. Mayor, H. D. and L. E. JORDAN. 1965. STUDIES ON REOVIRUS. I. MORPHOLOGIC OBSERVATIONS ON THE DEVELOPMENT OF REOVIRUS IN TISSUE CULTURE. *Exp.Mol.Pathol.* 4:40-50. doi:0014-4800(65)90022-5 [pii].
173. Mellman, I. 1996. Endocytosis and molecular sorting. *Annu.Rev.Cell Dev.Biol.* 12:575-625. doi:10.1146/annurev.cellbio.12.1.575 [doi].
174. Mendez, I. I., L. L. Hermann, P. R. Hazelton, and K. M. Coombs. 2000. A comparative analysis of freon substitutes in the purification of reovirus and calicivirus. *J.Virol.Methods* 90:59-67. doi:S0166093400002172 [pii].
175. Mendez, I. I., S. G. Weiner, Y. M. She, M. Yeager, and K. M. Coombs. 2008. Conformational changes accompany activation of reovirus RNA-dependent RNA transcription. *J.Struct.Biol.* 162:277-289. doi:S1047-8477(08)00019-1 [pii];10.1016/j.jsb.2008.01.006 [doi].
176. Miller, C. L., M. M. Arnold, T. J. Broering, C. E. Hastings, and M. L. Nibert. 2010. Localization of mammalian orthoreovirus proteins to cytoplasmic factory-like structures via nonoverlapping regions of microNS. *J.Virol.* 84:867-882. doi:JVI.01571-09 [pii];10.1128/JVI.01571-09 [doi].
177. Minekus, M., M. Alminger, P. Alvito, S. Ballance, T. Bohn, C. Bourlieu, F. Carriere, R. Boutrou, M. Corredig, D. Dupont, C. Dufour, L. Egger, M. Golding, S. Karakaya, B. Kirkhus, F. S. Le, U. Lesmes, A. Macierzanka, A. Mackie, S. Marze, D. J. McClements, O. Menard, I. Recio, C. N. Santos, R. P. Singh, G. E. Vegarud, M. S. Wickham, W. Weitschies, and A. Brodtkorb. 2014. A standardised static in vitro digestion method suitable for food - an international consensus. *Food Funct.* 5:1113-1124. doi:10.1039/c3fo60702j [doi].

178. Minuk, G. Y., R. W. Paul, and P. W. Lee. 1985. The prevalence of antibodies to reovirus type 3 in adults with idiopathic cholestatic liver disease. *J.Med.Virol.* 16:55-60.
179. Mohamed, A., R. N. Johnston, and M. Shmulevitz. 2015. Potential for Improving Potency and Specificity of Reovirus Oncolysis with Next-Generation Reovirus Variants. *Viruses.* 7:6251-6278. doi:v7122936 [pii];10.3390/v7122936 [doi].
180. Mohamed, A., C. Teicher, S. Haefliger, and M. Shmulevitz. 2015. Reduction of virion-associated sigma1 fibers on oncolytic reovirus variants promotes adaptation toward tumorigenic cells. *J.Virol.* 89:4319-4334. doi:JVI.03651-14 [pii];10.1128/JVI.03651-14 [doi].
181. Mourad Ferhat. 2017. Oncolytic Viruses: The Next Major Breakthrough in Cancer Treatment. *Journal of Human Virology & Retrovirology* 5:00141-00142.
182. Mousavi, S. A., L. Malerod, T. Berg, and R. Kjekken. 2004. Clathrin-dependent endocytosis. *Biochem.J.* 377:1-16. doi:10.1042/BJ20031000 [doi];BJ20031000 [pii].
183. Naglic, T., D. Rihtaric, P. Hostnik, N. Toplak, S. Koren, U. Kuhar, U. Jamnikar-Ciglenecki, D. Kutnjak, and A. Steyer. 2018. Identification of novel reassortant mammalian orthoreoviruses from bats in Slovenia. *BMC.Vet.Res.* 14:264. doi:10.1186/s12917-018-1585-y [doi];10.1186/s12917-018-1585-y [pii].
184. Netherton, C., K. Moffat, E. Brooks, and T. Wileman. 2007. A guide to viral inclusions, membrane rearrangements, factories, and viroplasm produced during virus replication. *Adv.Virus Res.* 70:101-182. doi:S0065-3527(07)70004-0 [pii];10.1016/S0065-3527(07)70004-0 [doi].
185. Nibert, M. L., J. D. Chappell, and T. S. Dermody. 1995. Infectious subvirion particles of reovirus type 3 Dearing exhibit a loss in infectivity and contain a cleaved sigma 1 protein. *J.Virol.* 69:5057-5067.
186. Nibert, M. L., T. S. Dermody, and B. N. Fields. 1990. Structure of the reovirus cell-attachment protein: a model for the domain organization of sigma 1. *J.Virol.* 64:2976-2989.
187. Nibert, M. L. and J. Kim. 2004. Conserved sequence motifs for nucleoside triphosphate binding unique to turreted reoviridae members and coltivirus. *J.Virol.* 78:5528-5530. doi:10.1128/jvi.78.10.5528-5530.2004 [doi].
188. Noble, S. and M. L. Nibert. 1997. Core protein mu2 is a second determinant of nucleoside triphosphatase activities by reovirus cores. *J.Virol.* 71:7728-7735.
189. Novoa, R. R., G. Calderita, R. Arranz, J. Fontana, H. Granzow, and C. Risco. 2005. Virus factories: associations of cell organelles for viral replication and morphogenesis. *Biol.Cell* 97:147-172. doi:BC20040058 [pii];10.1042/BC20040058 [doi].
190. O'Shea, T. J., P. M. Cryan, A. A. Cunningham, A. R. Fooks, D. T. Hayman, A. D. Luis, A. J. Peel, R. K. Plowright, and J. L. Wood. 2014. Bat flight and zoonotic viruses. *Emerg.Infect.Dis.* 20:741-745. doi:10.3201/eid2005.130539 [doi].
191. Odegard, A. L., K. Chandran, X. Zhang, J. S. Parker, T. S. Baker, and M. L. Nibert. 2004. Putative autocleavage of outer capsid protein micro1, allowing release of myristoylated peptide micro1N during particle uncoating, is critical for cell entry by reovirus. *J.Virol.* 78:8732-8745. doi:10.1128/JVI.78.16.8732-8745.2004 [doi];78/16/8732 [pii].

192. Olland, A. M., J. Jane-Valbuena, L. A. Schiff, M. L. Nibert, and S. C. Harrison. 2001. Structure of the reovirus outer capsid and dsRNA-binding protein sigma3 at 1.8 Å resolution. *EMBO J.* 20:979-989. doi:10.1093/emboj/20.5.979 [doi].
193. Ooms, L. S., W. G. Jerome, T. S. Dermody, and J. D. Chappell. 2012. Reovirus replication protein mu2 influences cell tropism by promoting particle assembly within viral inclusions. *J.Virol.* 86:10979-10987. doi:JVI.01172-12 [pii];10.1128/JVI.01172-12 [doi].
194. Organ, E. L. and D. H. Rubin. 1998. Pathogenesis of reovirus gastrointestinal and hepatobiliary disease. *Curr.Top.Microbiol.Immunol.* 233:67-83.
195. Parker, J. S., T. J. Broering, J. Kim, D. E. Higgins, and M. L. Nibert. 2002. Reovirus core protein mu2 determines the filamentous morphology of viral inclusion bodies by interacting with and stabilizing microtubules. *J.Virol.* 76:4483-4496.
196. Paul, R. W., A. H. Choi, and P. W. Lee. 1989. The alpha-anomeric form of sialic acid is the minimal receptor determinant recognized by reovirus. *Virology* 172:382-385. doi:10.1016/0042-6822(89)90146-3 [doi].
197. Pearse, B. M. 1976. Clathrin: a unique protein associated with intracellular transfer of membrane by coated vesicles. *Proc.Natl.Acad.Sci.U.S.A* 73:1255-1259. doi:10.1073/pnas.73.4.1255 [doi].
198. Phelps, K. L., L. Hamel, N. Alhmoud, S. Ali, R. Bilgin, K. Sidamonidze, L. Urushadze, W. Karesh, and K. J. Olival. 2019. Bat Research Networks and Viral Surveillance: Gaps and Opportunities in Western Asia. *Viruses.* 11. doi:v11030240 [pii];10.3390/v11030240 [doi].
199. Phillips, M. B., J. D. Stuart, R. M. Rodriguez Stewart, J. T. Berry, B. A. Mainou, and K. W. Boehme. 2018. Current understanding of reovirus oncolysis mechanisms. *Oncolytic.Virother.* 7:53-63. doi:10.2147/OV.S143808 [doi];ov-7-053 [pii].
200. Poggioli, G. J., C. Keefer, J. L. Connolly, T. S. Dermody, and K. L. Tyler. 2000. Reovirus-induced G(2)/M cell cycle arrest requires sigma1s and occurs in the absence of apoptosis. *J.Virol.* 74:9562-9570.
201. Pol, J., G. Kroemer, and L. Galluzzi. 2016. First oncolytic virus approved for melanoma immunotherapy. *Oncoimmunology.* 5:e1115641. doi:10.1080/2162402X.2015.1115641 [doi];1115641 [pii].
202. Prajapati, R. S., M. Das, S. Sreeramulu, M. Sirajuddin, S. Srinivasan, V. Krishnamurthy, R. Ranjani, C. Ramakrishnan, and R. Varadarajan. 2007. Thermodynamic effects of proline introduction on protein stability. *Proteins* 66:480-491. doi:10.1002/prot.21215 [doi].
203. Pritchard, L. I., K. B. Chua, D. Cummins, A. Hyatt, G. Crameri, B. T. Eaton, and L. F. Wang. 2006. Pulau virus; a new member of the Nelson Bay orthoreovirus species isolated from fruit bats in Malaysia. *Arch.Virol.* 151:229-239. doi:10.1007/s00705-005-0644-4 [doi].
204. Prota, A. E., J. A. Campbell, P. Schelling, J. C. Forrest, M. J. Watson, T. R. Peters, M. Aurrand-Lions, B. A. Imhof, T. S. Dermody, and T. Stehle. 2003. Crystal structure of human junctional adhesion molecule 1: implications for reovirus binding. *Proc.Natl.Acad.Sci.U.S.A* 100:5366-5371. doi:10.1073/pnas.0937718100 [doi];0937718100 [pii].

205. Ramanathan, A., G. B. Robb, and S. H. Chan. 2016. mRNA capping: biological functions and applications. *Nucleic Acids Res.* 44:7511-7526. doi:gkw551 [pii];10.1093/nar/gkw551 [doi].
206. Reinisch, K. M., M. L. Nibert, and S. C. Harrison. 2000. Structure of the reovirus core at 3.6 Å resolution. *Nature* 404:960-967. doi:10.1038/35010041 [doi].
207. Reiter, D. M., J. M. Frierson, E. E. Halvorson, T. Kobayashi, T. S. Dermody, and T. Stehle. 2011. Crystal structure of reovirus attachment protein sigma1 in complex with sialylated oligosaccharides. *PLoS.Pathog.* 7:e1002166. doi:10.1371/journal.ppat.1002166 [doi];PPATHOGENS-D-11-00490 [pii].
208. Rodgers, S. E., E. S. Barton, S. M. Oberhaus, B. Pike, C. A. Gibson, K. L. Tyler, and T. S. Dermody. 1997. Reovirus-induced apoptosis of MDCK cells is not linked to viral yield and is blocked by Bcl-2. *J.Virol.* 71:2540-2546.
209. ROSEN, L., H. E. EVANS, and A. SPICKARD. 1963. Reovirus infections in human volunteers. *Am.J.Hyg.* 77:29-37.
210. Rubin, D. H. 1987. Reovirus serotype 1 binds to the basolateral membrane of intestinal epithelial cells. *Microb.Pathog.* 3:215-219. doi:0882-4010(87)90098-2 [pii].
211. SABIN, A. B. 1959. Reoviruses. A new group of respiratory and enteric viruses formerly classified as ECHO type 10 is described. *Science* 130:1387-1389.
212. Sborov, D. W., G. J. Nuovo, A. Stiff, T. Mace, G. B. Lesinski, D. M. Benson, Jr., Y. A. Efebera, A. E. Rosko, F. Pichiorri, M. R. Grever, and C. C. Hofmeister. 2014. A phase I trial of single-agent reolysin in patients with relapsed multiple myeloma. *Clin.Cancer Res.* 20:5946-5955. doi:1078-0432.CCR-14-1404 [pii];10.1158/1078-0432.CCR-14-1404 [doi].
213. Schauer R. 1982. *Sialic Acids: Chemistry, Metabolism, and Function*. Springer-Verlag Wien, Austria.
214. Schauer, R. 2000. Achievements and challenges of sialic acid research. *Glycoconj.J.* 17:485-499.
215. Schiff, L. A. a. B. N. F. 2019. Reoviruses and their replication, p. 1275-1306. In: B.N.Fields and D.M.Knipe (ed.), *Fields Virology*. Raven Press, New York.
216. Schlee, M. and G. Hartmann. 2016. Discriminating self from non-self in nucleic acid sensing. *Nat.Rev.Immunol.* 16:566-580. doi:nri.2016.78 [pii];10.1038/nri.2016.78 [doi].
217. Schonberg, M., S. C. Silverstein, D. H. Levin, and G. Acs. 1971. Asynchronous synthesis of the complementary strands of the reovirus genome. *Proc.Natl.Acad.Sci.U.S.A* 68:505-508. doi:10.1073/pnas.68.2.505 [doi].
218. Schuberth-Wagner, C., J. Ludwig, A. K. Bruder, A. M. Herzner, T. Zillinger, M. Goldeck, T. Schmidt, J. L. Schmid-Burgk, R. Kerber, S. Wolter, J. P. Stumpel, A. Roth, E. Bartok, C. Drosten, C. Coch, V. Hornung, W. Barchet, B. M. Kummerer, G. Hartmann, and M. Schlee. 2015. A Conserved Histidine in the RNA Sensor RIG-I Controls Immune Tolerance to N1-2'O-Methylated Self RNA. *Immunity.* 43:41-51. doi:S1074-7613(15)00259-9 [pii];10.1016/j.immuni.2015.06.015 [doi].
219. Sei, S., J. K. Mussio, Q. E. Yang, K. Nagashima, R. E. Parchment, M. C. Coffey, R. H. Shoemaker, and J. E. Tomaszewski. 2009. Synergistic antitumor activity of oncolytic reovirus and chemotherapeutic agents in non-small cell lung cancer cells. *Mol.Cancer* 8:47. doi:1476-4598-8-47 [pii];10.1186/1476-4598-8-47 [doi].

220. Seliger, L. S., K. Zheng, and A. J. Shatkin. 1987. Complete nucleotide sequence of reovirus L2 gene and deduced amino acid sequence of viral mRNA guanylyltransferase. *J.Biol.Chem.* 262:16289-16293.
221. Senzer, N. N., H. L. Kaufman, T. Amatruda, M. Nemunaitis, T. Reid, G. Daniels, R. Gonzalez, J. Glaspy, E. Whitman, K. Harrington, H. Goldsweig, T. Marshall, C. Love, R. Coffin, and J. J. Nemunaitis. 2009. Phase II clinical trial of a granulocyte-macrophage colony-stimulating factor-encoding, second-generation oncolytic herpesvirus in patients with unresectable metastatic melanoma. *J.Clin.Oncol.* 27:5763-5771. doi:JCO.2009.24.3675 [pii];10.1200/JCO.2009.24.3675 [doi].
222. Shah, P. N. M., M. L. Stanifer, K. Hohn, U. Engel, U. Haselmann, R. Bartenschlager, H. G. Krausslich, J. Krijnse-Locker, and S. Boulant. 2017. Genome packaging of reovirus is mediated by the scaffolding property of the microtubule network. *Cell Microbiol.* 19. doi:10.1111/cmi.12765 [doi].
223. Shatkin, A. J. and G. W. Both. 1976. Reovirus mRNA: transcription and translation. *Cell* 7:305-313. doi:0092-8674(76)90159-8 [pii];10.1016/0092-8674(76)90159-8 [doi].
224. Shatkin, A. J. and J. D. Sipe. 1968. RNA polymerase activity in purified reoviruses. *Proc.Natl.Acad.Sci.U.S.A* 61:1462-1469. doi:10.1073/pnas.61.4.1462 [doi].
225. Shatkin, A. J., J. D. Sipe, and P. Loh. 1968. Separation of ten reovirus genome segments by polyacrylamide gel electrophoresis. *J.Virol.* 2:986-991.
226. Shepard, D. A., J. G. Ehnstrom, and L. A. Schiff. 1995. Association of reovirus outer capsid proteins sigma 3 and mu 1 causes a conformational change that renders sigma 3 protease sensitive. *J.Virol.* 69:8180-8184.
227. Sherry, B. 2009. Rotavirus and reovirus modulation of the interferon response. *J.Interferon Cytokine Res.* 29:559-567. doi:10.1089/jir.2009.0072 [doi].
228. Sherry, B. and B. N. Fields. 1989. The reovirus M1 gene, encoding a viral core protein, is associated with the myocarditic phenotype of a reovirus variant. *J.Virol.* 63:4850-4856.
229. Sherry, B., J. Torres, and M. A. Blum. 1998. Reovirus induction of and sensitivity to beta interferon in cardiac myocyte cultures correlate with induction of myocarditis and are determined by viral core proteins. *J.Virol.* 72:1314-1323.
230. Shmulevitz, M. and R. Duncan. 2000. A new class of fusion-associated small transmembrane (FAST) proteins encoded by the non-enveloped fusogenic reoviruses. *EMBO J.* 19:902-912. doi:10.1093/emboj/19.5.902 [doi].
231. Shmulevitz, M., S. A. Gujar, D. G. Ahn, A. Mohamed, and P. W. Lee. 2012. Reovirus variants with mutations in genome segments S1 and L2 exhibit enhanced virion infectivity and superior oncolysis. *J.Virol.* 86:7403-7413. doi:JVI.00304-12 [pii];10.1128/JVI.00304-12 [doi].
232. Shmulevitz, M., L. Z. Pan, K. Garant, D. Pan, and P. W. Lee. 2010. Oncogenic Ras promotes reovirus spread by suppressing IFN-beta production through negative regulation of RIG-I signaling. *Cancer Res.* 70:4912-4921. doi:0008-5472.CAN-09-4676 [pii];10.1158/0008-5472.CAN-09-4676 [doi].
233. Silverstein, S. C., J. K. Christman, and G. Acs. 1976. The reovirus replicative cycle. *Annu.Rev.Biochem.* 45:375-408. doi:10.1146/annurev.bi.45.070176.002111 [doi].

234. Skehel, J. J. and W. K. Joklik. 1969. Studies on the in vitro transcription of reovirus RNA catalyzed by reovirus cores. *Virology* 39:822-831. doi:0042-6822(69)90019-1 [pii].
235. Skup, D. and S. Millward. 1980. mRNA capping enzymes are masked in reovirus progeny subviral particles. *J.Virol.* 34:490-496.
236. Skup, D., H. Zarbl, and S. Millward. 1981. Regulation of translation in L-cells infected with reovirus. *J.Mol.Biol.* 151:35-55. doi:0022-2836(81)90220-5 [pii];10.1016/0022-2836(81)90220-5 [doi].
237. Snigdha, S., E. D. Smith, G. A. Prieto, and C. W. Cotman. 2012. Caspase-3 activation as a bifurcation point between plasticity and cell death. *Neurosci.Bull.* 28:14-24. doi:10.1007/s12264-012-1057-5 [doi].
238. Snyder, A. J. and P. Danthi. 2018. Cleavage of the C-Terminal Fragment of Reovirus mu1 Is Required for Optimal Infectivity. *J.Virol.* 92. doi:JVI.01848-17 [pii];10.1128/JVI.01848-17 [doi].
239. Stanifer, M. L., C. Kischnick, A. Rippert, D. Albrecht, and S. Boulant. 2017. Reovirus inhibits interferon production by sequestering IRF3 into viral factories. *Sci.Rep.* 7:10873. doi:10.1038/s41598-017-11469-6 [doi];10.1038/s41598-017-11469-6 [pii].
240. STANLEY, N. F., D. C. DORMAN, and J. PONSFORD. 1953. Studies on the pathogenesis of a hitherto undescribed virus (hepato-encephalomyelitis) producing unusual symptoms in suckling mice. *Aust.J.Exp.Biol.Med.Sci.* 31:147-159.
241. Stebbing, R. E., S. C. Irvin, E. E. Rivera-Serrano, K. W. Boehme, M. Ikizler, J. A. Yoder, T. S. Dermody, and B. Sherry. 2014. An ITAM in a nonenveloped virus regulates activation of NF-kappaB, induction of beta interferon, and viral spread. *J.Virol.* 88:2572-2583. doi:JVI.02573-13 [pii];10.1128/JVI.02573-13 [doi].
242. Stoeckel, J. and J. G. Hay. 2006. Drug evaluation: Reolysin--wild-type reovirus as a cancer therapeutic. *Curr.Opin.Mol.Ther.* 8:249-260.
243. Strong, J. E., G. Leone, R. Duncan, R. K. Sharma, and P. W. Lee. 1991. Biochemical and biophysical characterization of the reovirus cell attachment protein sigma 1: evidence that it is a homotrimer. *Virology* 184:23-32.
244. Strong, J. E., D. Tang, and P. W. Lee. 1993. Evidence that the epidermal growth factor receptor on host cells confers reovirus infection efficiency. *Virology* 197:405-411. doi:S0042-6822(83)71602-8 [pii];10.1006/viro.1993.1602 [doi].
245. Sturzenbecker, L. J., M. Nibert, D. Furlong, and B. N. Fields. 1987. Intracellular digestion of reovirus particles requires a low pH and is an essential step in the viral infectious cycle. *J.Virol.* 61:2351-2361.
246. Subudhi, S., N. Rapin, and V. Misra. 2019. Immune System Modulation and Viral Persistence in Bats: Understanding Viral Spillover. *Viruses.* 11. doi:v11020192 [pii];10.3390/v11020192 [doi].
247. Sugano, Y., M. Takeuchi, A. Hirata, H. Matsushita, T. Kitamura, M. Tanaka, and A. Miyajima. 2008. Junctional adhesion molecule-A, JAM-A, is a novel cell-surface marker for long-term repopulating hematopoietic stem cells. *Blood* 111:1167-1172. doi:blood-2007-03-081554 [pii];10.1182/blood-2007-03-081554 [doi].
248. SusanPayne. 2017. *Viruses.* Academic Press, Texas, United States.

249. Taguchi, S., H. Fukuhara, Y. Homma, and T. Todo. 2017. Current status of clinical trials assessing oncolytic virus therapy for urological cancers. *Int.J.Urol.* 24:342-351. doi:10.1111/iju.13325 [doi].
250. Tai, J. H., J. V. Williams, K. M. Edwards, P. F. Wright, J. E. Crowe, Jr., and T. S. Dermody. 2005. Prevalence of reovirus-specific antibodies in young children in Nashville, Tennessee. *J.Infect.Dis.* 191:1221-1224. doi:JID33615 [pii];10.1086/428911 [doi].
251. Tan, Y. F., C. L. Teng, K. B. Chua, and K. Voon. 2017. Pteropine orthoreovirus: An important emerging virus causing infectious disease in the tropics? *J.Infect.Dev.Ctres.* 11:215-219. doi:10.3855/jidc.9112 [doi].
252. Thirukkumaran, C. and D. G. Morris. 2015. Oncolytic Viral Therapy Using Reovirus. *Methods Mol.Biol.* 1317:187-223. doi:10.1007/978-1-4939-2727-2_12 [doi].
253. Traving, C. and R. Schauer. 1998. Structure, function and metabolism of sialic acids. *Cell Mol.Life Sci.* 54:1330-1349. doi:10.1007/s000180050258 [pii];10.1007/s000180050258 [doi].
254. Tyler, K. L., M. K. Squier, S. E. Rodgers, B. E. Schneider, S. M. Oberhaus, T. A. Grdina, J. J. Cohen, and T. S. Dermody. 1995. Differences in the capacity of reovirus strains to induce apoptosis are determined by the viral attachment protein sigma 1. *J.Virol.* 69:6972-6979.
255. Tyler, K. O. M. 1998. *Reoviruses I : Structure, Proteins, and Genetics.* Springer-Verlag Berlin Heidelberg.
256. Uehara, A., C. W. Tan, S. Mani, K. B. Chua, Y. S. Leo, D. E. Anderson, and L. F. Wang. 2019. Serological evidence of human infection by bat orthoreovirus in Singapore. *J.Med.Virol.* 91:707-710. doi:10.1002/jmv.25355 [doi].
257. Valentine, R. C. and H. G. Pereira. 1965. Antigens and structure of the adenovirus. *J.Mol.Biol.* 13:13-20. doi:S0022-2836(65)80076-6 [pii];10.1016/s0022-2836(65)80076-6 [doi].
258. Varki A, C. R. E. J. 2009. *Essentials of Glycobiology.* 2nd edition. Cold Spring Harbor Laboratory Press, New York, USA.
259. Varki, A. 2007. Glycan-based interactions involving vertebrate sialic-acid-recognizing proteins. *Nature* 446:1023-1029. doi:nature05816 [pii];10.1038/nature05816 [doi].
260. Varki, A. 2008. Sialic acids in human health and disease. *Trends Mol.Med.* 14:351-360. doi:S1471-4914(08)00133-0 [pii];10.1016/j.molmed.2008.06.002 [doi].
261. Varki, N. M. and A. Varki. 2007. Diversity in cell surface sialic acid presentations: implications for biology and disease. *Lab Invest* 87:851-857. doi:3700656 [pii];10.1038/labinvest.3700656 [doi].
262. Vidal, L., H. S. Pandha, T. A. Yap, C. L. White, K. Twigger, R. G. Vile, A. Melcher, M. Coffey, K. J. Harrington, and J. S. DeBono. 2008. A phase I study of intravenous oncolytic reovirus type 3 Dearing in patients with advanced cancer. *Clin.Cancer Res.* 14:7127-7137. doi:14/21/7127 [pii];10.1158/1078-0432.CCR-08-0524 [doi].
263. Vojtek, A. B. and C. J. Der. 1998. Increasing complexity of the Ras signaling pathway. *J.Biol.Chem.* 273:19925-19928.
264. Walter, C. and Frieden. E. 1963. THE PREVALENCE AND SIGNIFICANCE OF THE PRODUCT INHIBITION OF ENZYMES. *Adv.Enzymol.Relat Subj.Biochem.* 25:167-274.

265. Wang, L., S. Fu, L. Cao, W. Lei, Y. Cao, J. Song, Q. Tang, H. Zhang, Y. Feng, W. Yang, and G. Liang. 2015. Isolation and identification of a natural reassortant mammalian orthoreovirus from least horseshoe bat in China. *PLoS One*. 10:e0118598. doi:10.1371/journal.pone.0118598 [doi];PONE-D-14-38857 [pii].
266. Wang, L. F. and D. E. Anderson. 2019. Viruses in bats and potential spillover to animals and humans. *Curr Opin Virol*. 34:79-89. doi:S1879-6257(18)30107-X [pii];10.1016/j.coviro.2018.12.007 [doi].
267. Wang, X., F. Zhang, R. Su, X. Li, W. Chen, Q. Chen, T. Yang, J. Wang, H. Liu, Q. Fang, and L. Cheng. 2018. Structure of RNA polymerase complex and genome within a dsRNA virus provides insights into the mechanisms of transcription and assembly. *Proc Natl Acad Sci U S A* 115:7344-7349. doi:1803885115 [pii];10.1073/pnas.1803885115 [doi].
268. Webb, H. E. and C. E. Smith. 1970. Viruses in the treatment of cancer. *Lancet* 1:1206-1208. doi:S0140-6736(70)91790-3 [pii];10.1016/s0140-6736(70)91790-3 [doi].
269. Wei, D., J. Xu, X. Y. Liu, Z. N. Chen, and H. Bian. 2018. Fighting Cancer with Viruses: Oncolytic Virus Therapy in China. *Hum Gene Ther*. 29:151-159. doi:10.1089/hum.2017.212 [doi].
270. Weiss, S., P. W. Dabrowski, A. Kurth, S. A. J. Leendertz, and F. H. Leendertz. 2017. A novel Coltivirus-related virus isolated from free-tailed bats from Cote d'Ivoire is able to infect human cells in vitro. *Virol J*. 14:181. doi:10.1186/s12985-017-0843-0 [doi];10.1186/s12985-017-0843-0 [pii].
271. Wolf, J. L., D. H. Rubin, R. Finberg, R. S. Kauffman, A. H. Sharpe, J. S. Trier, and B. N. Fields. 1981. Intestinal M cells: a pathway for entry of reovirus into the host. *Science* 212:471-472. doi:10.1126/science.6259737 [doi].
272. Wong, A. H., P. K. Cheng, M. Y. Lai, P. C. Leung, K. K. Wong, W. Y. Lee, and W. W. Lim. 2012. Virulence potential of fusogenic orthoreoviruses. *Emerg Infect Dis*. 18:944-948. doi:10.3201/eid1806.111688 [doi].
273. Wu, X., T. G. Smith, and C. E. Rupprecht. 2011. From brain passage to cell adaptation: the road of human rabies vaccine development. *Expert Rev Vaccines*. 10:1597-1608. doi:10.1586/erv.11.140 [doi].
274. Xu, W. and K. M. Coombs. 2009. Conserved structure/function of the orthoreovirus major core proteins. *Virus Res*. 144:44-57. doi:S0168-1702(09)00115-4 [pii];10.1016/j.virusres.2009.03.020 [doi].
275. Yang, X. L., B. Tan, B. Wang, W. Li, N. Wang, C. M. Luo, M. N. Wang, W. Zhang, B. Li, C. Peng, X. Y. Ge, L. B. Zhang, and Z. L. Shi. 2015. Isolation and identification of bat viruses closely related to human, porcine and mink orthoreoviruses. *J Gen Virol*. 96:3525-3531. doi:10.1099/jgv.0.000314 [doi].
276. Yates, C. M., I. Filippis, L. A. Kelley, and M. J. Sternberg. 2014. SuSPect: enhanced prediction of single amino acid variant (SAV) phenotype using network features. *J Mol Biol*. 426:2692-2701. doi:S0022-2836(14)00225-3 [pii];10.1016/j.jmb.2014.04.026 [doi].
277. Yeung, M. C., D. Lim, R. Duncan, M. S. Shahrabadi, L. W. Cashdollar, and P. W. Lee. 1989. The cell attachment proteins of type 1 and type 3 reovirus are differentially

- susceptible to trypsin and chymotrypsin. *Virology* 170:62-70. doi:10.1016/0042-6822(89)90352-8 [doi].
278. Yin, P., M. Cheang, and K. M. Coombs. 1996. The M1 gene is associated with differences in the temperature optimum of the transcriptase activity in reovirus core particles. *J.Virol.* 70:1223-1227.
279. Yin, P., N. D. Keirstead, T. J. Broering, M. M. Arnold, J. S. Parker, M. L. Nibert, and K. M. Coombs. 2004. Comparisons of the M1 genome segments and encoded mu2 proteins of different reovirus isolates. *Virol.J.* 1:6. doi:1743-422X-1-6 [pii];10.1186/1743-422X-1-6 [doi].
280. Yoneyama, M., W. Suhara, and T. Fujita. 2002. Control of IRF-3 activation by phosphorylation. *J.Interferon Cytokine Res.* 22:73-76. doi:10.1089/107999002753452674 [doi].
281. Yue, Z. and A. J. Shatkin. 1997. Double-stranded RNA-dependent protein kinase (PKR) is regulated by reovirus structural proteins. *Virology* 234:364-371. doi:S0042-6822(97)98664-5 [pii];10.1006/viro.1997.8664 [doi].
282. Zarbl, H., K. E. Hastings, and S. Millward. 1980. Reovirus core particles synthesize capped oligonucleotides as a result of abortive transcription. *Arch.Biochem.Biophys.* 202:348-360. doi:0003-9861(80)90437-3 [pii].
283. Zarbl, H., D. Skup, and S. Millward. 1980. Reovirus progeny subviral particles synthesize uncapped mRNA. *J.Virol.* 34:497-505.
284. Zeller, H. G., N. Karabatsos, C. H. Calisher, J. P. Digoutte, C. B. Cropp, F. A. Murphy, and R. E. Shope. 1989. Electron microscopic and antigenic studies of uncharacterized viruses. III. Evidence suggesting the placement of viruses in the family Reoviridae. *Arch.Virol.* 109:253-261.
285. Zhang, L., M. A. Agosto, T. Ivanovic, D. S. King, M. L. Nibert, and S. C. Harrison. 2009. Requirements for the formation of membrane pores by the reovirus myristoylated micro1N peptide. *J.Virol.* 83:7004-7014. doi:JVI.00377-09 [pii];10.1128/JVI.00377-09 [doi].
286. Zhang, X., Y. Ji, L. Zhang, S. C. Harrison, D. C. Marinescu, M. L. Nibert, and T. S. Baker. 2005. Features of reovirus outer capsid protein mu1 revealed by electron cryomicroscopy and image reconstruction of the virion at 7.0 Angstrom resolution. *Structure.* 13:1545-1557. doi:S0969-2126(05)00271-6 [pii];10.1016/j.str.2005.07.012 [doi].
287. Zhang, X., S. B. Walker, P. R. Chipman, M. L. Nibert, and T. S. Baker. 2003. Reovirus polymerase lambda 3 localized by cryo-electron microscopy of virions at a resolution of 7.6 A. *Nat.Struct.Biol.* 10:1011-1018. doi:10.1038/nsb1009 [doi];nsb1009 [pii].
288. Zhao, X., C. Chester, N. Rajasekaran, Z. He, and H. E. Kohrt. 2016. Strategic Combinations: The Future of Oncolytic Virotherapy with Reovirus. *Mol.Cancer Ther.* 15:767-773. doi:1535-7163.MCT-15-0695 [pii];10.1158/1535-7163.MCT-15-0695 [doi].
289. Zhou, P., M. Tachedjian, J. W. Wynne, V. Boyd, J. Cui, I. Smith, C. Cowled, J. H. Ng, L. Mok, W. P. Michalski, I. H. Mendenhall, G. Tachedjian, L. F. Wang, and M. L. Baker. 2016. Contraction of the type I IFN locus and unusual constitutive expression of IFN-alpha in bats. *Proc.Natl.Acad.Sci.U.S.A* 113:2696-2701. doi:1518240113 [pii];10.1073/pnas.1518240113 [doi].

290. Zhu, B., C. Yang, H. Liu, L. Cheng, F. Song, S. Zeng, X. Huang, G. Ji, and P. Zhu. 2014. Identification of the active sites in the methyltransferases of a transcribing dsRNA virus. *J.Mol.Biol.* 426:2167-2174. doi:S0022-2836(14)00158-2 [pii];10.1016/j.jmb.2014.03.013 [doi].
291. Zurney, J., T. Kobayashi, G. H. Holm, T. S. Dermody, and B. Sherry. 2009. Reovirus mu2 protein inhibits interferon signaling through a novel mechanism involving nuclear accumulation of interferon regulatory factor 9. *J.Virol.* 83:2178-2187. doi:JVI.01787-08 [pii];10.1128/JVI.01787-08 [doi].
292. Zust, R., L. Cervantes-Barragan, M. Habjan, R. Maier, B. W. Neuman, J. Ziebuhr, K. J. Szretter, S. C. Baker, W. Barchet, M. S. Diamond, S. G. Siddell, B. Ludewig, and V. Thiel. 2011. Ribose 2'-O-methylation provides a molecular signature for the distinction of self and non-self mRNA dependent on the RNA sensor Mda5. *Nat.Immunol.* 12:137-143. doi:ni.1979 [pii];10.1038/ni.1979 [doi].